

MAMMALIAN AND VIRAL PROTEASE INHIBITORS

A Dissertation By

Dengfeng Dou

B. S., Sichuan University, P. R. China, 1998

Submitted to the Department of Chemistry
and the faculty of the Graduate School of
Wichita State University
in partial fulfillment of
the requirements for the degree of
Doctor of Philosophy

May 2010

© Copyright 2010 by Dengfeng Dou

All Rights Reserved

MAMMALIAN AND VIRAL PROTEASE INHIBITORS

The following faculty members have examined the final copy of this dissertation for form and content, and recommend that it be accepted in partial fulfillment of the requirement for the degree of Doctor of Philosophy with a major in Chemistry.

William C. Groutas, Committee Chair

Dennis H. Burns, Committee Member

Kandatege Wimalasena, Committee Member

Michael Van Stipdonk, Committee Member

Lop-Hing Ho, Committee Member

Accepted for the College of Liberal Arts and Sciences

William D. Bischoff, Dean

Accepted for the Graduate School

J. David McDonald, Dean

DEDICATION

To my parents, parents-in-law, my wife,
my son, my brother, and dear friends

ACKNOWLEDGMENTS

I would like to express my deepest thanks to my research advisor, Dr. William C. Groutas for his tremendous guidance, encouragement, kindness and support throughout my graduate studies and research at Wichita State University. His wisdom and enthusiasm have introduced me to a new dimension of medicinal chemistry and enhanced my research interest and understanding in this area. All the time I have spent with him is deserved to be memorized in my life.

I would also like to thank my committee members, Dr. Burns, Dr. Wimalasena, Dr. Van Stipdonk and Dr. Ho, for their great advice and support during my graduate study.

Sincere thanks go to Dr. Gerald H. Lushington at University of Kansas for his help with the computational studies and Dr. Eichhorn and his group for X-ray crystal structure determination. I also want to thank Dr. R. Pad Padmanabhan of Georgetown University Medical Center for the wonderful collaboration with West Nile virus and Dengue virus inhibitor evaluation. Equal thanks go to Dr. Talaty for his help in organic reaction mechanisms and nomenclature and Dr. Alliston, Swathi Mohan, Yi Li, and Guijia He for the biochemical studies and all the help from current and former group members during my graduate studies. I especially want to thank my friend, Zhong Lai, for introducing me to this research group and his constant help during the years.

Special thanks go to my parents, parents-in-law for their love and support. My deepest thanks go to my wife, Guijia He, not only for her love, patience, and encouragement, but also for her contribution in this work. I am also extremely grateful to my lovely son, Qi Dou, for all the love and happiness he brought to me. Finally, I owe my sincere gratitude to all my friends for their help in English and friendship.

ABSTRACT

Chronic Obstructive Pulmonary Disease (COPD) is currently the fourth leading cause of death in the US. COPD is a multi-factorial disorder characterized by an oxidant/antioxidant imbalance, inflammation, a protease/antiprotease imbalance and apoptosis. This dissertation describes a general strategy for the design, synthesis and biochemical evaluation of dual function inhibitors which could potentially interrupt the above disorder, thereby enhancing the treatment of COPD. An example of this type inhibitor based on the 1,2,5-thiadiazolidin-3-one scaffold has been proven effective against both human neutrophil elastase (HNE) and caspase-1, two key enzymes responsible for elastin degradation and inflammation, respectively. In addition, an X-ray crystal structure and a high resolution mass spectrum of inhibitor bonded HNE have proven the proposed mechanism of HNE inactivation. Furthermore, simple reversible competitive inhibitors of COPD-related enzymes (HNE and proteinase 3) have also been designed, synthesized and evaluated biochemically.

West Nile virus and Dengue virus are recognized as a major health threat that affects millions of people worldwide. However, there is currently no treatment or vaccine available for the virus infection. This dissertation describes the design, synthesis and biochemical evaluation of reversible competitive inhibitors of both West Nile virus and Dengue virus NS2B-NS3 protease. Combinatorial chemistry and click chemistry methods have been used in the design of the protease inhibitor and the identified hit was optimized using computational programs (AutoDock4 and SYBYL). Several more hits were identified during the optimization and further development could potentially lead to very potent inhibitors of NS2B-NS3 protease with good pharmacokinetics and oral bioavailability.

TABLE OF CONTENTS

Chapter	Page
1. INTRODUCTION.....	1
1.1 Introduction to the Proteases.....	1
1.1.1 Proteases and Diseases.....	1
1.1.1.1 Mammalian Proteases and Diseases.....	1
1.1.1.2 Viral Proteases and Diseases.....	3
1.1.2 Proteases as Targets in Drug Discovery.....	4
1.1.3 The Nomenclature and Classification of Proteases.....	4
1.1.3.1 Proteases and Proteolytic Reactions.....	4
1.1.3.2 Protease Terminology.....	5
1.1.3.3 Substrate Specificity of Proteases.....	6
1.1.3.4 Classification of Proteases.....	8
1.1.3.4.1 Classification Based on Chemical Mechanism.....	8
1.1.3.4.2 Classification of Proteases by IUBMB.....	9
1.1.3.4.3 The Barrett & Rawlings Classification of Proteases.....	11
1.2 Chronic Obstructive Pulmonary Disease (COPD) and Related Proteases.....	12
1.2.1 Overview of COPD.....	12
1.2.2 Oxidant/Antioxidant Imbalance.....	15
1.2.3 Apoptosis Related to COPD.....	15
1.2.4 Inflammation and Related Proteases.....	17
1.2.5 Protease/Anti-Protease Imbalance.....	19
1.2.5.1 Neutrophil Derived Serine Proteases.....	20
1.2.5.1.1 Overall Structures.....	20
1.2.5.1.2 Mechanism of Catalysis.....	22
1.2.5.1.3 Substrate Specificity in Proteolysis.....	24
1.2.5.1.4 Roles in Human Diseases.....	28
1.2.5.2 Granzyme B.....	31
1.2.5.3 COPD Related Matrix Metalloproteinases.....	32
1.3 West Nile Virus/Dengue Virus and Related Proteases.....	34
1.3.1 Overview of West Nile and Dengue Viruses.....	34
1.3.2 Flavivirus Life Cycle.....	35
1.3.3 The Flaviviral NS2B-NS3 Protease.....	36
1.3.3.1 Overview of NS2B-NS3 Protease Structure.....	37
1.3.3.2 The Flaviviral Active Site.....	40
1.3.3.3 Substrate Specificity of WNV and DENV NS2B-NS3 Proteases.....	40
1.4 Protease Inhibition.....	43
1.4.1 Classification of Protease Inhibitors.....	43
1.4.2 Non-covalent Inhibitors.....	44
1.4.2.1 Competitive Inhibitors.....	45
1.4.2.2 Mixed-type Inhibitors.....	45

TABLE OF CONTENTS (continued)

Chapter	Page
1.4.2.3	Examples of Non-covalent Inhibitors.....46
1.4.3	Transition-State Analog inhibitors.....49
1.4.4	Mechanism-based Inhibitors and Acylating Agents.....56
2.	RESEARCH GOALS.....63
2.1	Development of Inhibitors for COPD Related Targets.....63
2.2	Development of Competitive Inhibitors for WNV/DENV NS2B-NS3 Protease.....64
2.3	Strategies and Methodologies.....65
3.	DUAL FUNCTIONAL INHIBITORS OF COPD-RELEVANT SERINE PROTEASES.....67
3.1	Inhibitor Design Rationale.....67
3.2	Results and Discussions72
3.2.1	Synthesis of Dual Function Inhibitors72
3.2.1.1	Synthesis of the 1, 2, 5-Thiadiazolidin-3-One 1, 1 Dioxide Scaffold.....72
3.2.1.2	Synthesis of Caspases-1 Inhibitor A10.....73
3.2.1.3	Synthesis of MMP-12 inhibitor A14.....74
3.2.1.4	Synthesis of Dual Function Inhibitor by Simple Alkylation...75
3.2.1.5	Synthesis of HNE/MMP-12 Dual Function Inhibitor Using Acid/Amine Coupling.....76
3.2.1.5.1	Amine Synthesis.....77
3.2.1.5.2	Acid/Amine Coupling and Ester Formation.....77
3.2.2	Biochemical Investigation on P1 and R2 Substitutions.....78
3.2.3	X-ray Crystallographic Studies/Mechanism of Action of I.....80
3.2.4	HNE/Caspase-1 Dual Function Inhibitor.....84
3.2.5	HNE/MMP-12 Dual Function Inhibitor.....89
3.3	Conclusions and Future Directions.....90
3.4	Experimental.....91
3.4.1	General.....91
3.4.2	Representative Synthesis.....91
3.4.3	Enzyme Assays and Inhibition Studies.....103
3.4.3.1	Progress Curve Method.....103
3.4.3.2	Human Neutrophil Elastase.....104
3.4.3.3	Human Neutrophil Proteinase 3.....105
3.4.3.4	Computational Method.....105
3.4.3.5	HPLC Analysis.....106

TABLE OF CONTENTS (continued)

Chapter	Page
4. UTILIZATION OF THE 1, 2, 3, 5-THIATRIAZOLIDIN-3-ONE 1, 1-DIOXIDE SCAFFOLD IN THE DESIGN OF POTENTIAL INHIBITORS OF HUMAN LEUKOCYTE PROTEINASE 3	107
4.1 Inhibitor Design Rationale.....	107
4.2 Synthesis of Inhibitors	110
4.2.1 Synthesis of 2,3-Diethyl 1, 2, 3, 5-Thiatriazolidin-3-One 1,1-Dioxide B1.....	110
4.2.2 Synthesis of Compound B4 and B7.....	111
4.2.3 Synthesis of Compound B10a~e.....	113
4.2.4 Synthesis of Compound B13a~i.....	115
4.2.5 Synthesis of Potential Transition State Analogs B13k-m.....	118
4.3 Results and Discussion	119
4.3.1 Biochemical Studies	119
4.3.2 Molecular Modeling Studies.....	121
4.4 Experimental	123
4.4.1 Synthesis	123
4.4.2 Enzyme Assays and Inhibition Studies.....	137
4.4.3 Computational Method.....	138
4.4.4 X-ray Crystallography.....	138
5. 1,2,5-THIADIAZOLIDINE 1,1-DIOXIDE-BASED COPD-RELATED PROTEASE INHIBITORS.....	141
5.1 Inhibitor Design Rationale.....	141
5.2 Results and Discussion	145
5.2.1 Synthesis	145
5.3 Conclusions and Future Plans.....	149
5.4 Experimental.....	150
6. POTENTIAL WEST NILE VIRUS/DENGUE NS2B-NS3 PROTEASE INHIBITORS BASED ON THE 1-OXO-1, 2, 3, 4-TETRAHYDROISOQUINOLINE AND 1-OXO-1, 2-DIHYDROISOQUINOLINE SCAFFOLDS.....	155
6.1 Inhibitor Design Rationale.....	155
6.2 Results and Discussions	156
6.2.1 Synthesis	156
6.2.2 Biochemical Studies.....	160
6.2.3 Molecular Modeling Studies.....	163
6.3 Experimental	164
6.3.1 Synthesis	164

TABLE OF CONTENTS (continued)

Chapter	Page
6.3.2 Biochemical Studies.....	174
6.3.3 Molecular Modeling Studies.....	174
7. WEST NILE VIRUS/DENGUE VIRUS NS2B-NS3 PROTEASE INHIBITORS BASED ON THE 2-MERCAPTOQUINAZOLIN-4(3H)-ONE SCAFFOLD.....	176
7.1 Inhibitor Design Rationale.....	176
7.2 Results and Discussions	177
7.2.1 Synthesis	177
7.2.2 Biological Studies.....	180
7.2.3 Computational Studies.....	181
7.3 Conclusions.....	184
7.4 Experimental	184
7.4.1 Synthesis	184
7.4.2 Biochemical Studies.....	190
7.4.3 Computational Studies.....	190
8. CONCLUSIONS.....	192
REFERENCES.....	194

LIST OF TABLES

Table	Page
1.1	Examples of Mammalian Proteases of Clinical Relevance.....2
1.2	Examples of Viral Proteases of Clinical Relevance.....3
1.3	The Classification of Proteases by IUBMB.....10
1.4	Substrate Specificity of Neutrophil-Derived Serine Proteases.....27
1.5	Enzyme Active-site Residues Involved in Substrate Recognition.....28
1.6	Biological Functions of Elastase, Proteinase 3 and Cathepsin G.....29
1.7	Protease Transition State Analog Inhibitor Templates.....50
1.8	Selected Type I Transition State Analog Inhibitors.....52
1.9	Representative Serine Protease Mechanism-based Inhibitors and Acylating Agents.....58
1.10	Representative Acyclic Acylating Agents of Serine Protease.....61
3.1	Selected Caspase-1 Inhibitors and MMP-12 Inhibitors.....71
4.1	Amine Inputs.....110
4.2	Amide Derivatives.....113
4.3	List of Compound B10a~e.....114
4.4	Summary of Triazole Compounds.....117
4.5	X-ray Data Collection and Structure Solution Parameters for compound B13a.....140
5.1	Crystal Data and Structure Refinement Parameters for C8.....147
6.1	Crystal Data and Structure Refinement Parameters for D5.....158
6.2	Amine Inputs.....160
6.3	Summary of Inhibitor VI.....162
7.1	Chloromethyl Triazole Inputs.....179

LIST OF TABLES (continued)

Table	Page
7.2 2-Mercaptoquinazolin-4(3H)-One Scaffold Based Inhibitors.....	179

LIST OF FIGURES

Figure	Page
1.1 The Hydrolysis Reaction Catalyzed by Proteases.....	5
1.2 General Substrate and Substrate Binding Sites for Proteases.....	6
1.3 Preference for Amino Acids in Substrate Binding Sites.....	7
1.4 Schematic Presentation of Chronic Obstructive Pulmonary Disease as A Multi-factorial Disease.....	13
1.5 Trends in Age–Standardized Death Rates for the Six Leading Causes in The United States, 1970 to 2020	14
1.6 Comparison of Primary Structures of Human Neutrophil Elastase (HNE), Proteinase 3 (Pr3) and Cathepsin G (Cat G)	21
1.7 Tertiary Structures of Human Neutrophil Elastase, Proteinase 3 and Cathepsin G.....	21
1.8 Catalytic Mechanism of Serine Proteases.....	22
1.9 Schematic Representation of the Flaviviral Polyprotein, with the Cleavage Sites Processed by NS2B-NS3pro Indicated by Arrows.....	36
1.10 WNV NS2B/NS3pro Showing the Location of Important Cofactor Residues.....	38
1.11 Stereoview of Two Conformations of the NS2B Cofactor.....	39
1.12 Alignment of Recombinant NS3-NS2B Protease-Cofactor Sequences for Dengue and West Nile Viruses.....	42
1.13 Substrate-like Non-covalent Inhibitors of Thrombin.....	47
1.14 Patented Potent Human Neutrophil Elastase Non-covalent Inhibitors.....	48
1.15 Dengue Virus Protease Inhibitors.....	49
1.16 Peptide-derived Transition State Analog Inhibitors of HIV Protease Used in AIDS Therapies.....	54
1.17 An Example of Structure Optimization Leading Potency and Oral Bioavailability Improvement.....	55

LIST OF FIGURES (continued)

Figure	Page
1.18 Kinetic Scheme for Simple Competitive and Slow-binding Inhibition.....	56
1.19 Schematic Mechanism of Serine Protease Inactivation by Mechanism-based Inhibitor and Acylating Agents.....	57
1.20 Schematic Mechanism of HNE Inactivation by Sulfonyloxy Succinimide.....	59
1.21 Kinetic Scheme for Mechanism-Based Inhibitor and Acylating Agents.....	62
3.1 HNE Mechanism-Based Inhibitors.....	67
3.2 Mechanism-Based Inhibitors Docked into the HNE Active Site.....	68
3.3 Postulated Mechanism of Protease Inactivation by Inhibitor I.....	69
3.4 Dual Function Inhibitor Design Rationale.....	70
3.5 Time-Dependent Loss of Enzymatic Activity with A15.....	79
3.6 Progress Curves for the Inhibition of Human Neutrophil Elastase (HNE) by Inhibitor A15.....	80
3.7 Stereoview of the Active Site Region in An Omit Fo - Fc Map of the Refined Protein-Inhibitor Complex.....	81
3.8 Three-Dimensional Surface of the Active Site of HNE with Modified Inhibitor A16..	82
3.9 High Resolution Mass Spectra of HNE and HNE-Inhibitor Complex.....	83
3.10 Time-Dependent Loss of Enzymatic Activity with A16.....	85
3.11 Progress Curves for the Inhibition of Human Neutrophil Elastase (HNE) by Inhibitor A16.....	85
3.12 Progress Curves for the Inhibition of Caspase-1 by Dual Inhibitor A16.....	86
3.13 HPLC Monitoring of Caspase-1 Inhibitor Release.....	87
3.14 Dual Function Inhibitors and HNE Enzyme Active Site Interactions.....	88
3.5 Time-Dependent Loss of Enzymatic Activity with A18.....	90

LIST OF FIGURES (continued)

Figure	Page
4.1 Pr 3 Inhibitor Design Rationale.....	107
4.2 Structure-based Pr 3 Inhibitor Design.....	109
4.3 Mercury Drawing of Compound B13a.....	116
4.4 Mechanism of Transition State Inhibitor.....	118
4.5 Inhibitory Activity of Selected Compounds Against Human Neutrophil Elastase and Proteinase 3.	121
4.6 Molecular Simulation of Compound B13g bound to Pr3 active site.....	122
5.1 Design of Non-Covalent Inhibitor (IV).....	141
5.2 Predicted HNE/Pr 3 Non-covalent Inhibitors.....	143
5.3 Non-covalent Inhibitors and HNE/Pr 3 Interactions.....	144
5.4 ORTEP Drawing of Compound C8 Showing the 30% Thermal Ellipsoids.....	147
5.5 Postulated Mechanism for the Formation of Compound C8.....	149
6.1 WNV/DENV NS2B-NS3 Protease Inhibitor Design.....	156
6.2 Mercury Drawing of Compound D5.....	158
6.3 Predicted Binding of Energy-Minimized Compound D14j Docked to the Binding Site of WNV Protease	164
7.1 Design of Non-Covalent Inhibitors.....	177
7.2 Percent Inhibition of Selected Inhibitor E3 and E7 against WNV and DENV NS2B-NS3 Proteases	180
7.3 Predicted Binding of Energy-Minimized Compounds Docked to the Binding Site of WNV NS2B-NS3 Protease	183
7.4 Predicted Binding of Energy-Minimized Compounds Docked to the Binding Site of DENV NS2B-NS3 Protease	184

LIST OF SCHEMES

Scheme	Page
3.1 Synthesis of the 1, 2, 5-Thiadiazolidin-3-One 1, 1 Dioxide scaffold.....	72
3.2 Synthesis of the Caspases-1 Inhibitor.....	74
3.3 Synthesis of the MMP-12 Inhibitor.....	75
3.4 Synthesis of Dual Function Inhibitors.....	76
3.5 Synthesis of Hydroxamine Intermediate.....	77
3.6 Synthesis of Dual Function Inhibitors.....	78
4.1 Synthesis of Template B1.....	110
4.2 Synthesis of Compound III.....	111
4.3 Synthesis of Compound III.....	112
4.4 Synthesis of Compound III.....	114
4.5 Synthesis of Triazole Compound III.....	115
4.6 Synthesized Triazole Library.....	116
4.7 Synthesis of Triazole Compound III.....	119
5.1 Synthesis of HNE/Pr 3 Non-covalent Inhibitors.....	146
5.2 Proposed Synthesis of Non-covalent Inhibitors.....	150
6.1 Synthesis of 1-Oxo-1,2,3,4-Tetrahydro-Isoquinoline Scaffold.....	157
6.2 Synthesis of Reversible Inhibitor VI.....	159
6.3 Synthesis of 1-Oxo-1, 2-Dihydroisoquinoline Based Inhibitors.....	161
7.1 Synthesis of WNV/DENV NS2B-NS3 Inhibitors.....	178

LIST OF ABBREVIATIONS AND TERMS

Arg	Arginine	IL-1 β	Interleukin-1beta
Ala	Alanine	IUBMB	The international union of biochemistry and molecular Biology
AIDS	Acquired immunodeficiency syndrome		
Asp	Aspartic acid	K _M	Michaelis-Menten constant
AMC	Aminomethylcoumarin	KO	Knock-out
Boc	<i>tert</i> -Butyloxycarbonyl	Leu	Leucine
BACE	β -Secretase	Lys	Lysine
Cat G	Cathepsin G	MMP12	Macrophage metalloelastase 12
Cbz	Carbobenzyloxy	NMM	N-methylmorpholine
COPD	Chronic obstructive pulmonary disease	Nva	Norvaline
Cys	Cysteine	P	Product
DCB	2,6-Dichlorobenzyloxy	PCC	Pyridinium chlorochromate
DDQ	2,3-Dichloro-5,6- dicyanobenzoquinone	PDE	Phosphodiesterase
DENV	Dengue virus	Phe	Phenylalanine
DIBAL	Diisobutylaluminium hydride	Pro	Proline
DMSO	Dimethyl sulfoxide	Pr 3	Proteinase 3
DNA	Deoxyribonucleic acid	pNA	<i>p</i> -Nitroaniline
E	Enzyme	S	Substrate
EI	Enzyme-inhibitor complex	SARS	Severe acute respiratory syndrome
ES	Enzyme-substrate complex	[S]	Substrate concentration
FRET	Förster resonance energy transfer	SBzl	Thiobenzyl
Gly	Glycine	Ser	Serine
GzmB	Granzyme B	THF	Tetrahydrofuran
HEPES	4-(2-Hydroxyethyl)-1-perazine-ethanesulfonic acid	TEA	Triethylamine
		TS	Transition state
His	Histidine	TSA	Transition state analog
HIV	Human immunodeficiency virus	Tris	Tris(hydroxymethyl)aminomethane
HNE	Human neutrophil elastase	1/ <i>v</i>	Reciprocal of velocity
I	Inhibitor	Val	Valine
[I]	Inhibitor concentration	WHO	World health organization
IBCF	Isobutyl chloroformate	WNV	West Nile virus
ICE	Interleukin-1beta converting enzyme	α 1-ACT	α 1-Antichymotrypsin
Ile	Isoleucine	α 1-PI	α 1-Proteinase inhibitor

CHAPTER 1

INTRODUCTION

1.1 Introduction to the Proteases

The enormous variety of biochemical reactions that comprise life are nearly all mediated by a remarkable array of biological catalysts known as enzymes. Enzymes catalyze reactions involved in all facets of cellular life: metabolism (the production of cellular building blocks and energy from food sources); biosynthesis (how cells make new molecules); detoxification (the breakdown of toxic foreign chemicals) and information storage (the process of deoxyribonucleic acid (DNA)) [1]. Proteases (also known as proteolytic enzymes or proteinases) refer to a group of enzymes whose catalytic function is to hydrolyze peptide bonds in proteins. Proteases account for about 2% of the human genome, 1-5% of genomes of infectious organisms and other forms of life [2-3]. Proteases form one of the largest and more important groups of enzymes and are involved in numerous important physiological processes including protein turnover, digestion, blood coagulation and wound healing, fertilization, cell differentiation and growth, cell signaling, immune response and apoptosis [4].

1.1.1 Proteases and Diseases

1.1.1.1 Mammalian Proteases and Diseases

Mammalian proteases are responsible for the degradation of proteins in all living organisms, where proteins are at the center of action in all biological processes and are continuously synthesized and degraded. Proteases are ordinarily highly regulated by endogenous protein inhibitors [5-9], however, uncontrolled, unregulated, or undesired proteolysis can lead to many disease states including emphysema, stroke, viral infections, cancer, Alzheimer's disease,

inflammation, arthritis and etc (selected proteases and related diseases are shown in Table 1.1).

Table 1.1 Examples of Mammalian Proteases of Clinical Relevance

Protease	Related diseases
Neutrophil elastase [10]	Chronic pulmonary obstructive disease(COPD), emphysema, cystic fibrosis, asthma, chronic bronchitis, adult respiratory distress syndrome (ARDS) and rheumatoid arthritis
Proteinase 3 [11]	Wegener's granulomatoss, inflammation, pulmonary emphysema, cystic fibrosis
Cathepsin G [12]	Inflammation, asthma, tumors
Granzyme B [13]	Cancer, diabetes, chronic inflammation
Thrombin [14]	Blood coagulation/bleeding, cancer, inflammation, thrombosis
Factor Xa [15]	Blood coagulation, fibrosis, cancer
Urokinase [16]	Cancer, fibrocarcinoma, Idiopathic pulmonary fibrosis (IPF)
Dipeptidyl peptidase IV [17]	Diabetes
Chymase [18]	Cardiovascular disease, heart failure, asthma
Tryptase [12d,19]	Inflammation, asthma
Matriptase [12d,20]	Cancer, asthma
Proteasome [21]	Cancer, muscular atrophy, inflammation
Caspases [22]	Inflammation, apoptosis, differentiation, Alzheimer's disease, Parkinson's disease, Huntington's disease
Cathepsin K [23]	Bone resorption, bone tumor
Renin [24]	Hypertension, diabetes mellitus
Plasmemepsins [25]	Malaria
BACE [26]	Alzheimer's disease
Angiotensin-converting enzyme (ACE) [27]	Hypertension, Alzheimer's disease
Matrix Metalloproteinase [28]	Lung cancer, pleural effusions, chronic obstructive pulmonary disease(COPD), asthma, acute respiratory distress syndrome and interstitial lung diseases, multiple sclerosis cancer, arthritis, fibrosis, chronic liver disease, viral heart disease, skin aging
TNF- α convertase (TACE) [29]	Cancer, stroke, arthritis, Crohn's disease, multiple sclerosis, Alzheimer's disease

1.1.1.2 Viral Proteases and Diseases

With the announcement of "As of 27 December 2009, worldwide more than 208 countries and overseas territories or communities have reported laboratory confirmed cases of pandemic influenza H1N1 2009, including at least 12,220 deaths." from World Health Organization (WHO) on Dec 30, 2009 [30], viral infection has become a real global threat. Viral infection is not only associated with serious public diseases like Swine flu, AIDS, SARS, ebola and avian influenza [31], but is also associated with common human diseases including common cold, liver cancer, chickenpox, cold sores and etc. Viral proteases are key enzymes involved in virus maturation [32], and thus have been intensively studied (some viral proteases and related diseases are shown in Table 1.2).

Table 1.2 Examples of Viral Proteases of Clinical Relevance

Protease	Related diseases
HIV protease [33]	HIV/AIDS
Hepatitis C Virus protease [34]	Progressive liver injury, cirrhosis and liver cancer
Hepatitis A Virus 3C protease [35]	Liver acute infectious disease
Norovirus protease [36]	Acute gastroenteritis
Dengue Virus NS2B-NS3 protease [37]	Dengue fever
West Nile Virus NS2B-NS3 protease [38]	Encephalitis
Rhinovirus 3C protease [39]	Common cold
Cytomegalovirus protease [40]	Retinitis
Herpes simplex virus protease [32,41]	Oral lesions, genital herpes
Varicella zoster virus protease [42]	Chickenpox, shingles
Epstein-Barr virus protease [42]	Lymphoproliferative disease

1.1.2 Proteases as Targets in Drug Discovery

Proteases fulfill multiple roles in human disease (such as cancer, AIDS, sepsis, Crohn's disease, rheumatoid arthritis, traumatic brain injury, amyotrophic lateral sclerosis (ALS), cardiovascular conditions, inflammatory, pulmonary, periodontal diseases and etc) and considerable interest has been expressed in the design and development of synthetic inhibitors of disease-related proteases [43-48]. There are several FDA approved protease inhibitors on the market. Tritace[®] (Ramipril), Vasotec[®] (Enalapril), Accupril[®] (Quinapril), Monopril[®] (Fosinopril), and Lotensin[®] (Benzapril) are substrate mimetic Angiotensin-converting Enzyme inhibitors used to treat cardiovascular diseases [49,50]. Novastan[®] (Argatroban) is a thrombin inhibitor for prophylaxis or treatment of thrombosis in patients with heparin-induced thrombocytopenia (HIT) [49,51]. Januvia[®] (Sitagliptin) is a DPP-4 dipeptidyl peptidase enzyme inhibitor for treating Type II Diabetes [49,52]. There are numerous inhibitors of the HIV proteases and this approach has been one of the principal means for treating Autoimmune Immunodeficiency Syndrome (AIDS) [49,53]. A recent review on "protease inhibitors in the clinic" has summarized many more proteases inhibitors in clinical development [3a].

1.1.3 The Nomenclature and Classification of Proteases

1.1.3.1 Proteases and Proteolytic Reactions

Proteases hydrolyze peptide bonds between amino acids in proteins and peptides (shown in Figure 1.1). Although they catalyze the same type reaction, there exists a huge number of proteases to hydrolyze the specific substrates in the precise environment. Up to September 2009, there are 2,415 different proteases have been recognized by *MEROPS* database (the *MEROPS* database is an information resource for peptidases and the proteins that inhibit them found at the

Wellcome Trust Sanger Institute, Cambridge CB10 1SA, UK) [54] and 570 human proteases were identified according to The Mammalian Degradome Database (<http://degradome.uniovi.es/>) [55].

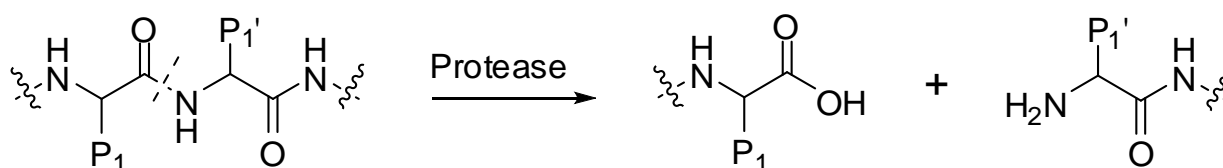


Figure 1.1 The Hydrolysis Reaction Catalyzed by Proteases

1.1.3.2 Protease Terminology [7,56]

Proteases are macromolecules with a number of atoms and side chains, which form tremendous number of possibilities in shape and charges on their surfaces and/or inside the protein. A protease recognizes its peptide substrate based on its backbone conformation, amino acid sequence and location of the amide bonds being cut. The protease substrate binds to a protease with a complementary fashion in size, shape and electro statics. A nomenclature of protease and substrate proposed by Schechter and Berger in 1967 is commonly used to number the active site of a protease. According to this nomenclature, the amino acid residues of protease substrates are considered relative to the site of backbone cleavage (Figure 1.2). Those residues N-terminal to the cleavage site are said to be on the P side, and those residues C-terminal to the cleavage site are said to be on the P' side. Immediately N-terminal to the cleavage site is residue P₁, and moving further N-terminally are residues P₂, P₃, P₄, and so on. Immediately C-terminal to the cleavage site is residue P₁', and moving further C-terminally are residues P₂', P₃', P₄', and so on. Thus, the protease cleaves the amide bond that links residue P₁ and P₁' (Figure 1.2, red amide group).

Proteases contain binding pockets for substrate residues (Figure 1.2). Those pockets that bind to the P side of the substrate are called S pockets, and those pockets that bind to the P' side of the substrate are called S' pockets. The protease pocket that interacts directly with the P1 residue of the substrate is called S1, and protease pockets that bind to residues P2, P3, P4, and so on are called, respectively, S2, S3, S4, and so forth. The protease pocket that interacts directly with the P1' residue of the substrate is called S1', and protease pockets that bind to residues P2', P3', P4', and so on are called, respectively, S2', S3', S4', and so forth. Thus, the residues involved in catalysis are located between the S1 and S1' pockets. The character of these pockets dictates the degree of specificity of the protease (i.e., whether it will cleave only one particular sequence of amino acid residues, a wide variety of substrates, or somewhere in between).

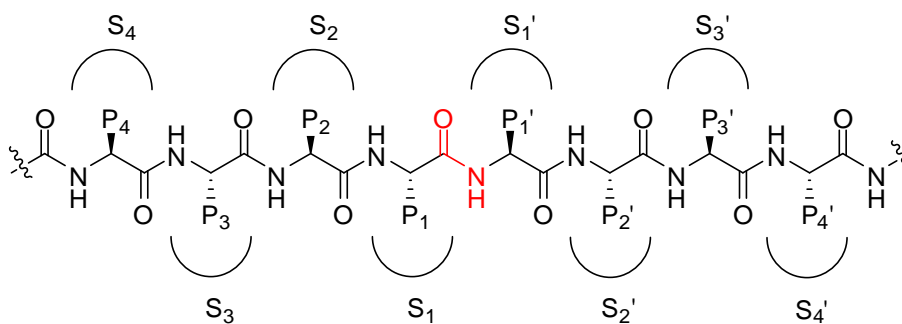


Figure 1.2 General Substrate and Substrate Binding Sites for Proteases. The scissile amide functionality is in red. Moving left from the cleavage site are residues P1, P2, P3, P4, etc. Moving right from the cleavage site are residues P1', P2', P3', P4', etc. Corresponding binding pockets on the protease for these residues are S1, S2, S3, S4, etc., on the left side and S1', S2', S3', S4', etc., on the right.

1.1.3.3 Substrate Specificity of Proteases

A protease has multiple subsites in the active site, but the subsites are not equally important. Short peptides (up to 8 amino acid residues) are commonly used to map the active sites of proteases and Rawlings et al. has demonstrated the importance of these subsites in

Figure 1.3 [54]. Apparently the S1 pocket is the most important binding site in terms of substrate recognition, therefore complementary with S1 pocket was the basis of protease inhibitor design.

The S1' pocket is recognized as the second important binding site which provides the highest

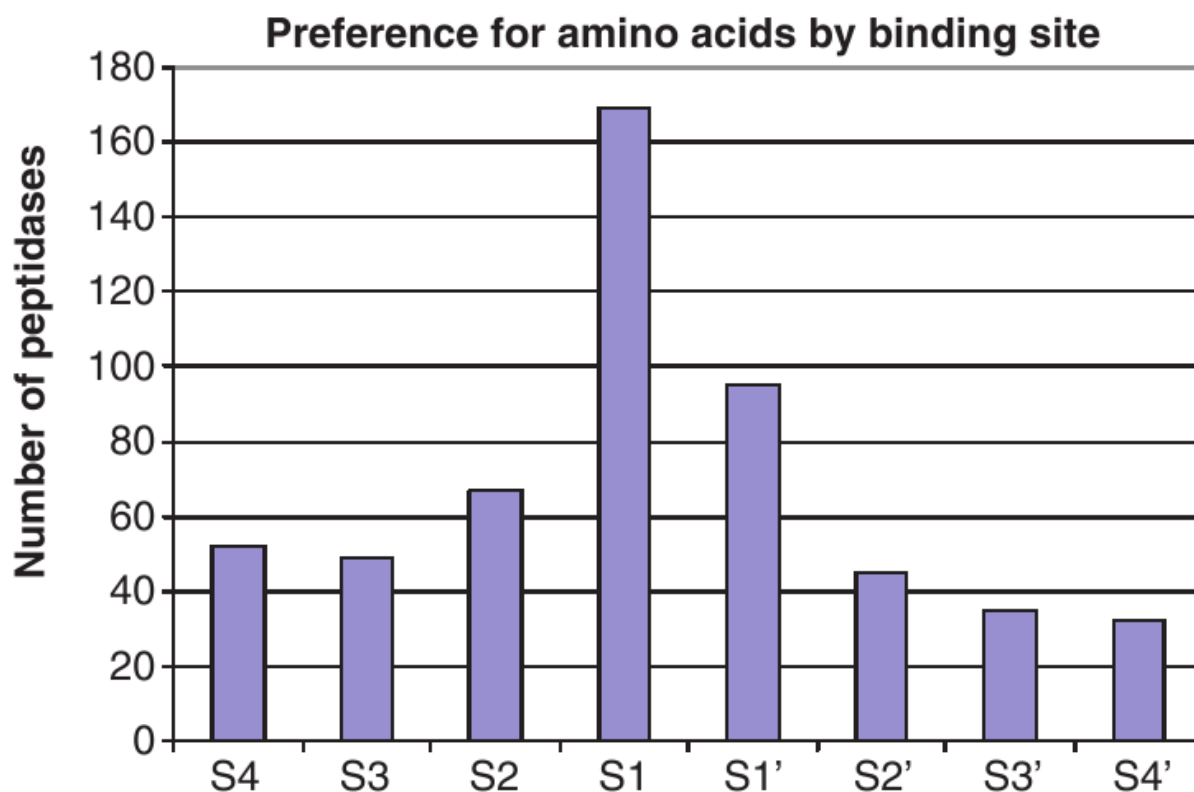


Figure 1.3 Preference for Amino Acids in Substrate Binding Sites. The bar chart shows the number of peptidases showing a preference for one or two amino acids for each substrate binding site S4–S4'. Of the 312 peptidase with 10 or more known substrate cleavages, 202 show a preference and are included in the figure. A count is made whenever an amino acid occurs in one binding pocket in 40% or more of the substrates. There are 15 peptidases that have a preference for two amino acids in a binding pocket: walleye dermal sarcoma virus retropepsin (A02.063, Asn or Gln in S2), sapovirus 3C-like peptidase (C24.003, Glu or Gln in S1), SARS coronavirus picornain 3C-like peptidase (C30.005, Gly or Gln in S1), peptidyl-peptidase Acer (M02.002, Gly or Pro in S1), vimelysin (M04.010, Phe or Leu in S1), carboxypeptidase M (M14.006, Arg or Lys in S1'), carboxypeptidase U (M14.009, Arg or Lys in S1'), dactylisin (M9G.026, Leu or Phe in S1'), chymase (S01.140, Phe or Tyr in S1), trypsin alpha (S01.143, Lys or Arg in S1), trypsin 1 (S01.151, Lys or Arg in S1), plasmin (S01.233, Lys or Arg in S1), flavivirin (S07.001, Lys or Arg in S2), dipeptidyl aminopeptidase A (S09.005, Ala or Pro in S1) and kumamolisin (S53, 004, Glu or Gly in S3). Many peptidases show a preference in more than one binding pocket. There are 13 peptidases with a preference for all eight binding pockets, another 13 with a preference in seven, five peptidases in six, three in five, eight in four, 24 in three, 47 in two and 89 in only one.[54]

affinity to substrate along with the S1 pocket. The rest of the subsites also contribute to binding specificity.

1.1.3.4 Classification of Proteases

A landmark in the development of any field of study is the appearance of a sound system of nomenclature and classification for the objects with which it deals. Both nomenclature and classification are vitally important for information-handling. A good system also serves to highlight important questions and thus prompts new discoveries. Three major criteria have been employed in grouping peptidases and they are preferentially based on: (a) the chemical mechanism of catalysis; (b) the details of the reaction catalyzed, and (c) the similarity of molecular structure and homology [54]. These three classification methods are described in detail below.

1.1.3.4.1 Classification Based on Chemical Mechanism

In 1960, Hartley initiated a sequence of developments that has now provided the peptidase community with the very useful concept of catalytic type [57]. Depending on the mechanisms used in the catalysis, proteases are currently classified into six groups: serine proteases, threonine proteases, cysteine proteases, aspartic proteases, metalloproteases and glutamic proteases. Such assignments are widely used for obvious reasons. For example, serine proteases contain a serine residue that acts as the nucleophile at the heart of the catalytic site. The threonine and glutamic acid peptidases are very small groups and were not described until 1995 and 2004, respectively. The other four classes of proteases have been intensively studied for both their catalytic mechanisms and proteolytic specificity. Among these classes, cysteine proteases, metallo-proteases and serine proteases form the majority of the protease subclasses [54,58].

The system of catalytic types has great strengths, but it also has limitations that need to be recognized. Each type of peptidase includes many very different molecular structures and catalytic mechanisms. Moreover, they are by no means all homologues of each other, so an expression like "the serine peptidase family" has little meaning.

1.1.3.4.2 Classification of Proteases by IUBMB (based on the details of the reaction catalyzed) [59]

The term "peptidase" has been recommended by The International Union of Biochemistry and Molecular Biology (IUBMB) to describe a subset of peptide bond hydrolases with code E.C.3.4. "Proteases" is a widely used as synonymous to peptidase. According to *Enzyme Nomenclature* from IUBMB (1992), all peptides fall into two major categories: the endopeptidases and exopeptidases. The endopeptidases, which cleave peptide bonds at points within the protein, are often called proteinases in the literature. The exopeptidases, which remove amino acids sequentially from either the N- or C-terminus, include aminopeptidases, dipeptidases, dipeptidyl-peptidases and tripeptidyl-peptidases, peptidyl-dipeptidases, serine-type carboxypeptidases, metallo-carboxypeptidases, cysteine-type carboxypeptidases and *omega* peptidases. The nomenclature does not include glutamic acid peptidase, which was found in 2004. The IUBMB protease/peptidase classification is shown in Table 1.3.

According to this classification, every peptidase is assigned a unique four-number code. The codes of proteases that will be focused on in this dissertation are shown below: Human neutrophil elastase: EC 3.4.21.37; Proteinase-3: EC 3.4.21.76; Matrix metalloproteinase-12: EC 3.4.24.65; West Nile virus NS2B-NS3 protease: EC 3.4.21.91; Dengue virus NS2B-NS3 protease: EC 3.4.21.91.

This classification system in Enzyme Nomenclature has been used for several decades and provides a practical approach for the characterization of new peptidases, without having any structure information about them. *Enzyme Nomenclature* of peptidases depends primarily on the reaction catalyzed, but it fails to recognize the structural relationship between peptidases. In 1993, Neil D. Rawlings and Alan J. Barrett proposed another classification of proteases focused on the relationship between structure and function.

Table 1.3 The Classification of Proteases by IUBMB

Exopeptidases -cleave near the N- or C-termini of peptides and proteins
EC 3.4.11 Aminopeptidases
EC 3.4.13 Dipeptidases
EC 3.4.14 Dipeptidyl-peptidases and tripeptidyl-peptidases
EC 3.4.15 Peptidyl-dipeptidases
EC 3.4.16 Serine-type carboxypeptidases
EC 3.4.17 Metallo carboxypeptidases
EC 3.4.18 Cysteine-type carboxypeptidases
EC 3.4.19 Omega peptidases
Endopeptidases -cleave internal peptide bonds in peptides and proteins
EC 3.4.21 Serine endopeptidases
EC 3.4.22 Cysteine endopeptidases
EC 3.4.23 Aspartic endopeptidases
EC 3.4.24 Metallo endopeptidases
EC 3.4.25 Threonine endopeptidases
EC 3.4.99 Endopeptidases of unknown catalytic mechanism

1.1.3.4.3 The Barrett & Rawlings Classification of Proteases (based on the similarity of molecular structure and homology) [60,61]

The Barrett & Rawlings classification which is based on molecular structure and homology is the newest classification (proposed in 1993) and it depends on the availability of data for amino acid sequences and three-dimensional structures in quantities that were realized only in the early 1990s. In this system, peptidases are assigned to families and the families are grouped in clans (these terms are described below in detail). From 1999, a peptidase database, *MEROPS* was launched by Rawlings & Barrett and the classification is also known as “*MEROPS* classification”.

The term *family* is used to describe a group of peptidases each of which can be proved to be homologous to the type example. The homology is shown by a significant similarity in amino acid sequence either to the type example itself, or to another protein that has been shown to be homologous to the type example, and thus a member of the family. The relationship must exist in the peptidase unit at least. A family can contain a single peptidase if no homologues are known, and a single gene product such as a virus polyprotein can contain more than one peptidase, each assigned to a different family. Each family is identified by a letter representing the catalytic type of the peptidases (S, C, T, A, G, M or U, for serine, cysteine, threonine, aspartic, glutamic, metallo- or unknown, respectively) and a unique number, e.g. S1, M1. Some families are divided into subfamilies because there is evidence of a very ancient divergence within the family, e.g. S1A, S1B.

A *clan* contains all the modern-day peptidases that have arisen from a single evolutionary origin of peptidases. It represents one or more families that show evidence of their evolutionary relationship by their similar tertiary structures, or when structures are not available, by the order

of catalytic-site residues in the polypeptide chain and often by common sequence motifs around the catalytic residues. Each clan is identified with two letters, the first representing the catalytic type of the families included in the clan (with the letter "P" being used for a clan containing families of more than one of the catalytic types serine, threonine and cysteine). Some families cannot yet be assigned to clans, and when a formal assignment is required, such a family is described as belonging to clan A-, C-, M-, S-, T- or U-, according to the catalytic type. Some clans are divided into subclans because there is evidence of a very ancient divergence within the clan, for example MA(E), the gluzincins, and MA(M), the metzincins.

The full information about families and clans for *MEROPS* classification can be found from the following linkages, http://merops.sanger.ac.uk/cgi-bin/family_index?type=P, and http://merops.sanger.ac.uk/cgi-bin/clan_index?type=P. The MEROPS Ids of proteases included in this dissertation are shown below: human neutrophil elastase S01.131, proteinase-3: S01.134, Matrix metalloproteinase-12: M10.009, West Nile virus NS2B-NS3 protease: S07.001, Dengue virus NS2B-NS3 protease: S07.001.

1.2 Chronic Obstructive Pulmonary Disease (COPD) and Related Proteases

1.2.1 Overview of COPD

Chronic Obstructive Pulmonary Disease (COPD) is not one single disease but an umbrella term used to describe chronic lung diseases (including chronic bronchitis and emphysema, Figure 1.4) that cause limitations in lung airflow. The most common symptoms of COPD are breathlessness, excessive sputum production, and a chronic cough. However, COPD is not just simply a "smoker's cough", but an under-diagnosed, life threatening lung disease that may progressively lead to death. According to the latest WHO estimates (2007), currently 210

million people have COPD and 3 million people died of COPD in 2005. WHO predicts that COPD will become the third leading cause of death worldwide by 2030 (the trends in the leading causes of death in the United States between 1970 and 2002 are shown in Figure 1.5) [62].

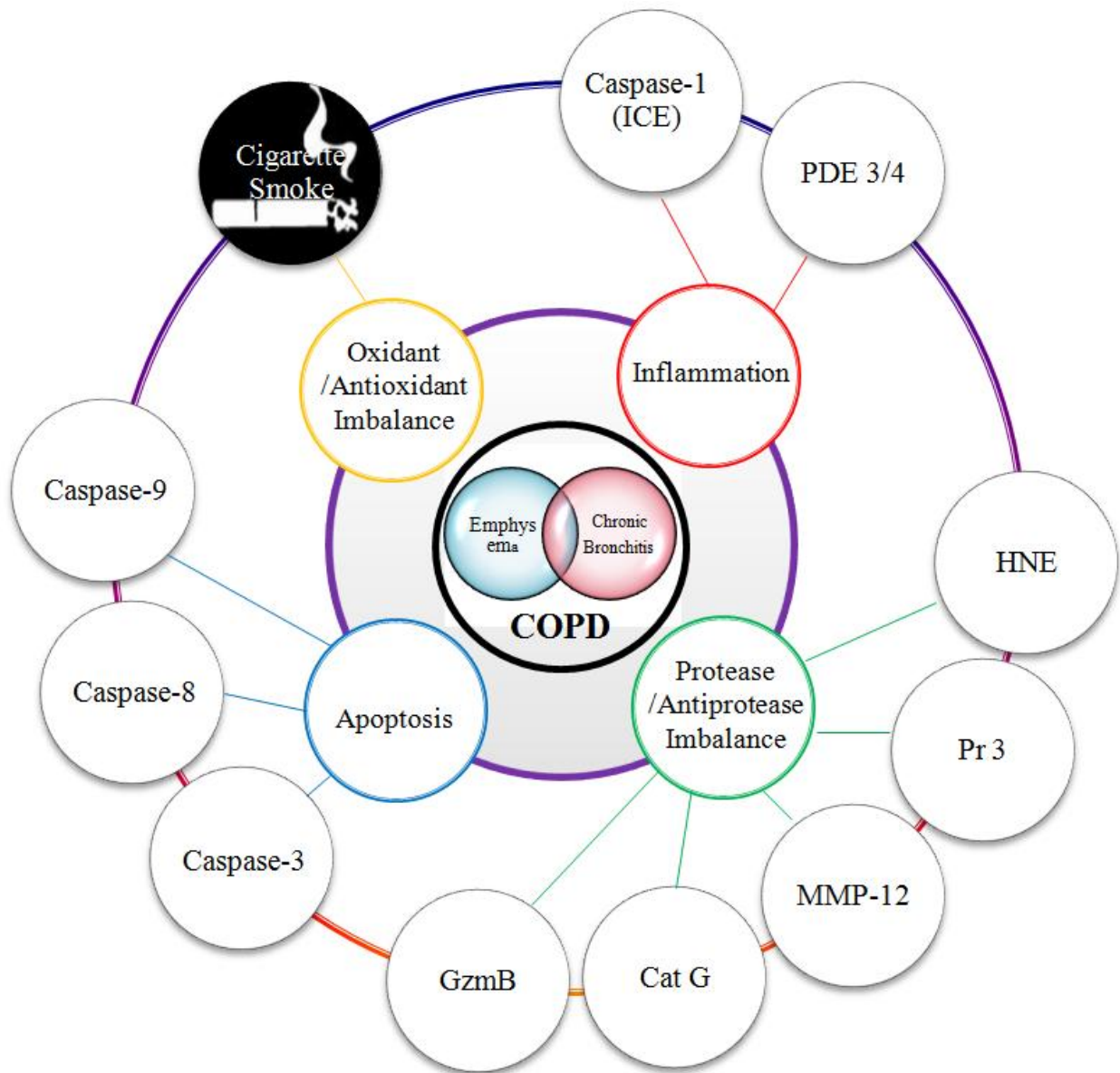


Figure 1.4 Schematic Presentation of Chronic Obstructive Pulmonary Disease as A Mutli-factorial Disease.

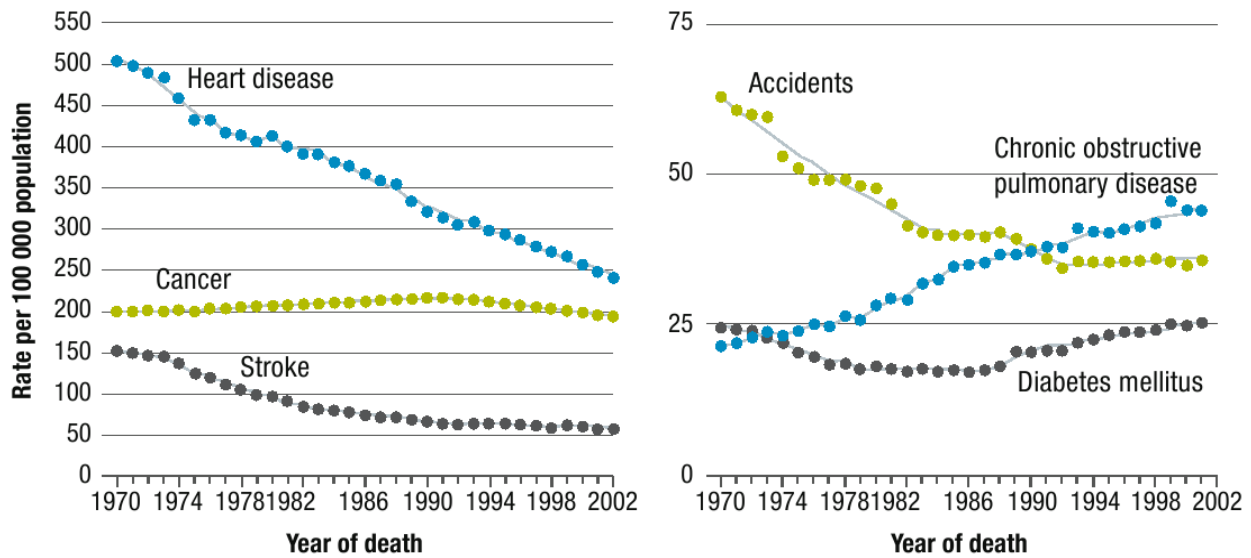


Figure 1.5 Trends in Age-Standardized Death Rates for the Six Leading Causes in the United States, 1970 to 2020.

COPD is characterized by an oxidant/antioxidant imbalance [63,64], alveolar septal cell apoptosis [65,66], chronic inflammation [63,67], and a protease/antiprotease imbalance where an excess of proteolytic enzymes (serine, cysteine proteases and MMPs) is not counterbalanced by a similar rise of protease inhibitors [68,69] (shown in Figure 1.4). The molecular mechanisms which underline the initiation and progression of the disorder are poorly understood. Furthermore, the precise role and actions of the proteases involved in COPD are not fully delineated, consequently there is a need for a better definition of which proteases and protease actions are of importance in COPD pathogenesis [70].

1.2.2 Oxidant/Antioxidant Imbalance

Cigarette smoking introduces noxious gases and particles, which are known to form reactive oxygen species (ROS) such as superoxide anion, hydrogen peroxide, and hydroxyl radicals [63,70]. Oxidative stress in the lung arises when ROS overwhelm antioxidant defense (oxidant and antioxidant imbalance shifts in favor of oxidants), and then ROS readily react with proteins, lipids and DNA resulting a number of pathological consequences [64,71-72]. A primary consequence of oxidant stress is lipid peroxidation, or the oxidative degeneration of lipids caused by a free radical chain reaction. If the free radical reaction is not quenched, it can permanently damage cell membranes, ultimately leading to cell death [71]. ROS can act directly or indirectly on proteins to cause oxidation of the polypeptide backbone peptide cleavage, protein-protein cross linking, or amino acid side chain modifications [71,73]. This includes the inactivation of antiproteases (such as α_1 -antitrypsin and secretory leukocyte protease inhibitor) or activation of metalloproteases by oxidants, resulting in a protease/antiprotease imbalance in the lungs [74-76]. Without protection from α_1 -antitrypsin, the alveolar matrix is susceptible to destruction by neutrophil elastase, which can eventually lead to emphysema [68-69]. Over-expression of matrix metalloproteases may contribute to the pathogenesis of tissue destructive processes associated with lung inflammation and disease [77]. Oxidative stress also stimulates molecular pathways and signaling mechanisms resulting in increased gene expression, production of proinflammatory cytokines, influx of inflammatory leukocytes and subsequent enhanced inflammation in the lung [78].

1.2.3 Apoptosis Related to COPD

Apoptosis is the process of programmed cell death that may occur in multicellular

organisms and is likely a contributor to the pathogenesis of COPD, particularly in irreversible tissue destruction such as emphysema [65,66]. The first data demonstrating the presence of apoptotic cells in the lungs of patients with COPD did not begin to appear until relatively recently [79]. Apoptosis is a tightly regulated mechanism of cell death which allows the elimination of unwanted, damaged or infected cells. At present, there are three different pathways that are involved in the regulation of apoptosis. Different caspases (cysteine proteases with an important function in the regulation of apoptosis) are involved in these different pathways [66]. The first pathway, ligand-death-receptor pathway, is active in response to extracellular signals: death factors trigger apoptosis by binding on death receptors, which recruit procaspase-8 [66,80]. After cleavage the mature caspase-8 then directly activates caspase-3 (caspase-3 is one of apoptosis executors) [81,82]. The second pathway, the mitochondrial intrinsic pathway, responds to physical and chemical stress signals: mitochondria release cytochrome C, which together with apoptotic protease activating factor-1 and caspase-9 form the apoptosome complex [66,83-85], resulting in the activation of caspase-9 which then activates caspase-3 and initiates the execution of apoptosis [81,86]. In the third pathway, the endoplasmatic reticulum pathway, caspase-12 is activated in response to stress signals (such as hypoxia) and converge further downstream into activation of caspase-3 [66]. In addition, noncaspase proteases such as granzyme B and the deprivation of survival signals such as growth factors also induce apoptosis by means of caspase-3 activation and mitochondrial release of cytochrome C, respectively [87-89].

As mentioned before, apoptosis interacts with all of the other three pathways including chronic inflammation, protease/antiprotease imbalance and oxidative stress. It has been proved that apoptosis of alveolar wall or endothelial cells is sufficient to cause pulmonary emphysema,

even without the accumulation of inflammatory cells. However, in the lungs of COPD patients, there is an impressive influx of inflammatory cells and interactions between inflammatory and apoptotic mechanisms most likely take place [66]. Uncontrolled proteolytic reactions in the lungs can induce apoptosis. Neutrophil elastase-cleavage of the phosphatidylserine receptor on macrophages results in impaired clearance of apoptotic cells and sustained inflammation [90]. The basal membrane contains signals for cell survival and loss of these survival signals (as a consequence of degradation of the basement membrane by matrix metalloproteinases) can induce apoptosis [66]. Apoptosis may also be affected by direct proteolysis of death-inducing signals [66,91]. In a rat model of emphysema induced by VEGFR blockade, Tudor et al. demonstrated that apoptosis predominated in the lung in areas of oxidative stress and that experimental blockade of apoptosis markedly reduced the expression of markers of oxidative stress [66,92]. Other experiments, in turn, have shown that mice with impaired expression of antioxidant genes have increased numbers of apoptotic alveolar septal cells and develop early and extensive emphysema in response to cigarette smoke [93]. Apoptosis obviously plays very important roles in the pathogenesis of COPD.

1.2.4 Inflammation and Related Proteases

Inflammation is a coordinated immune response to harmful stimuli that appear during infections or after tissue damage. COPD related inflammation is mostly caused by cigarette smoking or air pollution [94] and oxidative stress in the lungs introduced by smoking or inhaling noxious gases results in increased gene expression and production of pro-inflammatory cytokines [78,95]. This in turn causes both influx and activation of inflammatory leukocytes [78]. As a result, chronic inflammation in COPD is characterized by an accumulation of neutrophils,

macrophages, B-cells, lymphoid aggregates and CD8⁺ T-cells, particularly in the small airways [96], and in addition, increased IL-6, IL-1 β , TNF- α , GRO- α , MCP-1, and IL-8 levels are found in COPD patient sputum [97]. The degree of inflammation increases with the severity of disease [96]. In people who have smoked, lung inflammation continues for many years after smoking cessation [94]. Currently, phosphodiesterases and interleukin-1-beta convertase are believed to be promising therapeutic targets for preventing inflammation and their inhibitors are under investigation.

The phosphodiesterase (PDE) enzyme family contains eleven PDEs, which hydrolyze cyclic adenosine monophosphate (cAMP) and cyclic guanosine monophosphate (cGMP) (cAMP and cGMP are second messengers that regulate a number of critical cellular processes including airway smooth muscle relaxation and the release of inflammatory mediators [98]) to inactive 5'AMP and 5'GMP respectively, and thus inhibition of PDEs represents a potential mechanism by which cellular processes can be modulated [99]. PDE 4 is the primary cAMP-hydrolyzing enzyme in inflammatory and immune cells (macrophages, eosinophils, neutrophils) [100]. In these cells, the inhibition of PDE 4 leads to increased cAMP levels, down-regulating the inflammatory response [97,101]. Because PDE 4 is also expressed in airway smooth muscle and, in vitro, PDE 4 inhibitors relax lung smooth muscle, selective PDE 4 inhibitors are being developed for treating COPD [97]. Interestingly, dual PDE3/4 inhibitors appear to give enhanced mucociliary clearance and broad anti-inflammatory and bronchodilatory activity [99].

Cytokine interleukin-1 (IL-1) has been invoked in the pathophysiology of a variety of inflammatory and immune lung diseases including asthma, pulmonary hypertension, pulmonary fibrosis, and granuloma formation [102,103]. In the interleukin-1 family, IL-1 β and IL-18 are key cytokines responsible for chronic inflammation and immunoregulation, respectively and are

unregulated by gene expression, synthesis, secretion, receptor association and maturation via interleukin converting enzyme (ICE, which now is called caspase-1) [104-107]. Caspase-1 cleaves the biologically inactive pro-IL-1 β and pro-IL-18, releasing the biologically active mature IL-1 β and pro-IL-18 [104,105]. Since its discovery, caspase-1 has been considered a therapeutic target for the modulation of inflammation. Caspase-1 inhibitors will be reviewed (vide infra) and examples are listed in Table 3.1.

1.2.5 Protease/Anti-Protease Imbalance

Proteases play a key role in the lung in health and disease. In the healthy lung, proteases fulfill basic homeostatic roles and regulate processes such as regeneration and repair [10a]. The levels and activities of proteases are ordinarily tightly regulated by endogenous protein inhibitors, however, when this balance is compromised lung damage can occur [10-13,22,28]. Past observations have shown that: 1) a genetic deficiency of α_1 -proteinase inhibitor (α_1 -PI), the major inhibitor of neutrophil elastase in the lower respiratory tract, is associated with earlyonset, severe panlobular pulmonary emphysema [108]; 2) instillation of papain (a cysteine protease with elastin-degrading activity) into rat lungs results in progressive emphysema [109]; and 3) proteases including porcine pancreatic elastase, neutrophil elastase and proteinase 3 (Pr 3), have been shown to degrade lung elastin and enlarge airspaces when instilled into the lungs of experimental animals [110-112], the protease/antiprotease imbalance hypothesis was formulated. The hypothesis states that inhalation of cigarette smoke (or other pollutants) leads to the recruitment of inflammatory cells into the lungs which release various proteases that exceed the protease inhibitor defense of the lung. Uncontrolled proteases degrade the extracellular matrix (ECM) protein components of the alveolar walls leading to destruction and loss of the alveolar

walls and airspace enlargement [113]. Chronic inflammatory lung diseases are associated with higher-than-normal levels of proteases [10a]. The proteases implicated in the pathogenesis of COPD include serine proteases, metalloproteases and cysteine proteases. Serine proteases and MMPs are believed to play the most important role in extracellular proteolysis [113].

1.2.5.1 Neutrophil Derived Serine Proteases

Human neutrophil elastase, proteinase 3 and cathepsin G are the three major serine proteases stored in the primary (azurophil) granules of polymorphonuclear neutrophils (PMNs) [114,115]. Their traditional functions are ingesting and killing bacteria, therefore they are providing a primary line of defense against bacterial infection [115]. However, the higher-than-normal level of these proteases is able to activate specifically pro-inflammatory cytokines including interleukin-1 beta and TNF-alpha and lead to the activation of different receptors including epidermal growth factor receptor and proteinase-activated receptors [114]. Neutrophil serine proteases might therefore be important regulators of the inflammatory innate immune response and are interesting targets for new therapeutic approaches against inflammatory disorders [114].

1.2.5.1.1 Overall Structures

Human neutrophil elastase (HNE: EC3.4.21.37), proteinase 3 (Pr 3: EC3.4.21.76) and cathepsin G (Cat G: EC3.4.21.20) belong to chymotrypsin family. HNE, Pr 3 and Cat G are homologous proteases that have evolved from a common ancestor by gene duplication and are quite distinct from the main branches of the chymotrypsin superfamily of serine proteases [116]. The overall structures of these three enzymes are very similar (the amino acid sequence of

HNE has 57% identity to those of Pr 3 and 37% identity to those of Cat G (Figure 1.5). Their activities depend upon a catalytic triad composed of His57, Asp102 and Ser195 which are widely separated in the primary sequence (Figure 1.6) but are brought together at the active site of the enzymes in their tertiary structures (Figure 1.7) [115]. In general, the HNE active site has hydrophobic S and S'. Pr 3 has similar S subsites but the S' subsites are more polar than HNE. The overall active site of Cat G has more positive charges on the S' pockets.

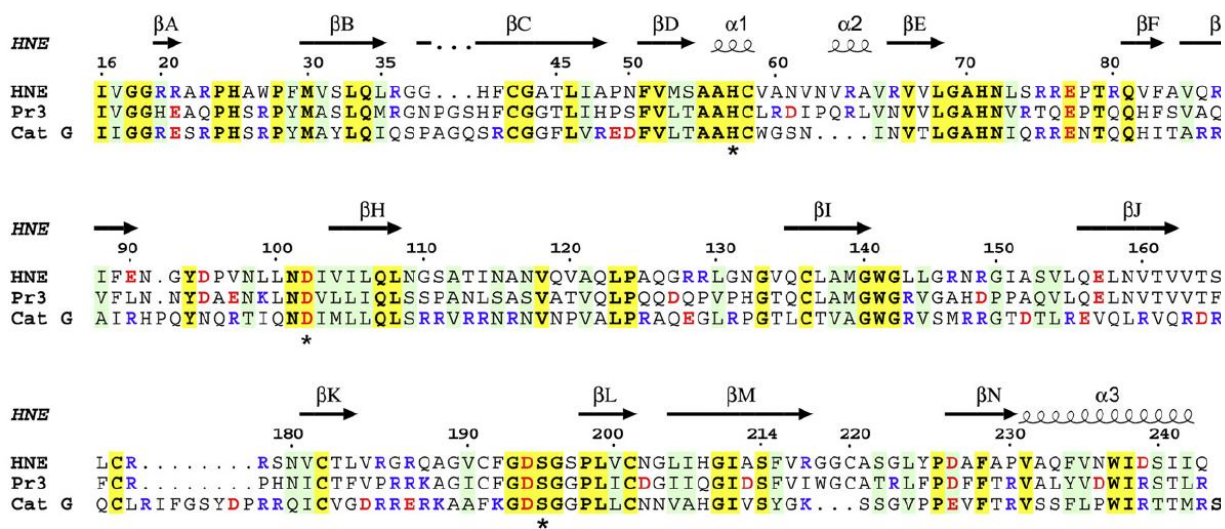


Figure 1.6 Comparison of Primary Structures of Human Neutrophil Elastase (HNE), Proteinase 3 (Pr 3) and Cathepsin G (Cat G) [115].

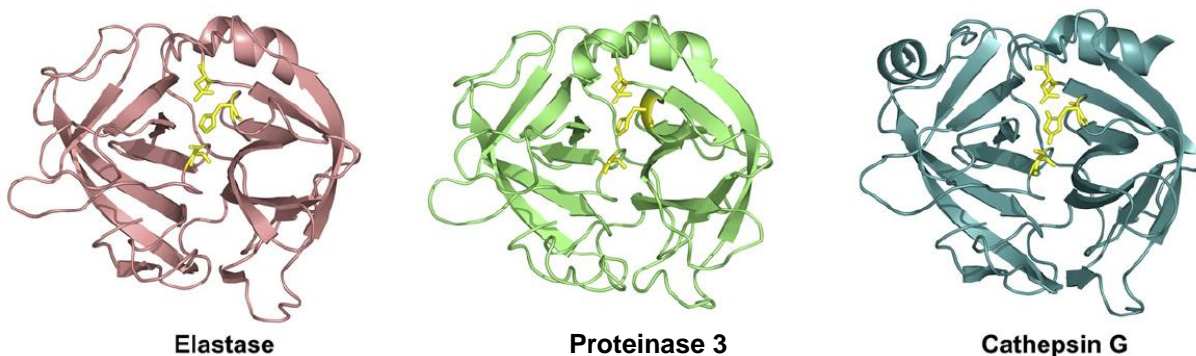


Figure 1.7 Tertiary Structures of Human Neutrophil Elastase, Proteinase 3 and Cathepsin G. His57, Asp102 and Ser195 are shown in yellow at the active sites of the enzyme 3D structures [115].

1.2.5.1.2 Mechanism of Catalysis

The catalytic mechanism of serine proteases has been extensively studied, both by kinetic methods in solution and by NMR [117] and X-ray crystallography [118]. Additional evidence of transition state of proteolysis was published recently by Nunez's group [119]. The general catalytic mechanism of serine proteases is shown in Figure 1.8.

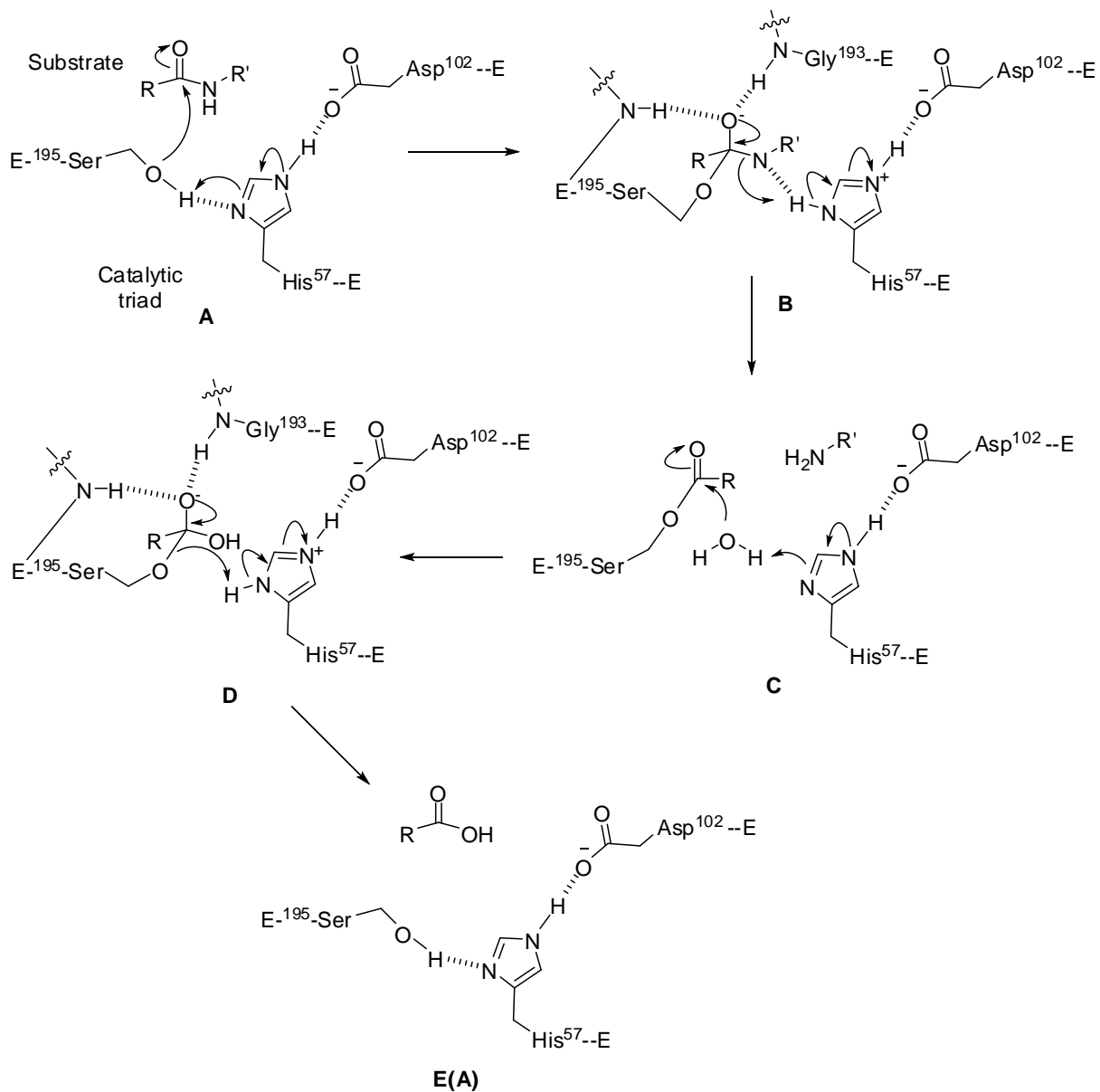


Figure 1.8 Catalytic Mechanism of Serine Proteases

Catalysis proceeds in two steps: acylation and deacylation. In the first step (acylation step) an acyl enzyme intermediate is formed between the substrate and the side chain of the active site serine. Formation of this covalent complex proceeds through a negatively charged tetrahedral transition state intermediate, and then the peptide bond is cleaved [120]. In the second step (deacylation step) the newly formed ester linkage in the acyl enzyme complex is hydrolyzed by a water molecule. The deacylation step also proceeds through a negatively charged tetrahedral transition state intermediate, which then releases the remaining peptide fragment and restores the active site of enzyme, completing the catalytic cycle [120].

Structurally, serine proteases rely on their oxyanion hole and catalytic triad to perform these reactions. The oxyanion hole consists of two back bone amide groups from Gly193 and Ser195 that form hydrogen bonds to the negatively charged carbonyl oxygen of the tetrahedral transition state intermediates. Such hydrogen bonding stabilizes the transition states involving the acylation and deacylation steps, and thus plays a critical role in catalysis. The catalytic triad in the serine proteases of the chymotrypsin family is formed by the side chains of three conserved residues mentioned **1.2.5.1.1**: His57, Asp102 and Ser195. Each amino acid in the triad performs a specific task in the catalysis. The O^γ of Ser195 is the nucleophile, which attacks the scissile carbonyl carbon (hence named serine proteases) and becomes part of the newly formed ester linkage in the acyl enzyme complex. The His57 residue functions as a general base and a general acid during the course of catalysis. The general base catalysis is involved in the formation of the tetrahedral transition state intermediates, where the imidazole group of His57 functions as a general base to subtract the proton from the O^γ of Ser195 in the acylation step or from a water molecule in the deacylation step, facilitating the nucleophilic attack. This newly protonated imidazole then provides a general acid catalysis to assist the collapse of the

tetrahedral transition state intermediates by transferring its proton to the leaving group (the scissile amide N in the acylation step and the O^γ of Ser195 in the deacylation step). Such behavior of His57 is called “proton shuttle”. During catalysis, His 57 is involved in a direct interaction with the substrate, so a slight movement of the imidazole group may be required for its function. The carboxyl group of Asp102 serves to orient the imidazole ring in an appropriate fashion to function as an acid-base catalyst and also provides an appropriate electrostatic environment for stabilizing the tetrahedral intermediates. [115,120]

1.2.5.1.3 Substrate Specificity in Proteolysis

The activity of proteolytic enzymes is generally measured by the release of a chromophore (such as 4-nitroanilide) or a fluorophore (such as coumarylamide) covalently attached to a peptide moiety that confers S pocket specificity. Recently, Forster Resonance Energy Transfer (FRET) technology which relies on the distance-dependent transfer of energy from a donor molecule to an acceptor molecule was introduced to protease substrates. Specifically, a FRET-based substrate uses a fluorescent donor moiety on one terminus and a quenching acceptor molecule on the other terminus, separated by a peptide containing the protease cleavage sequence. Upon cleavage, the fluorescence of the donor is recovered and can be continuously monitored. FRET-based substrate allows its sequence extend on both sides of the cleavage site, giving more information on the specificity of proteases, especially on S' binding sites. The enzyme activity of HNE, Pr3 and Cat G has been investigated using protein substrates such as the oxidized insulin B chain, and synthetic chromogenic/fluorogenic peptide substrates (4-nitroanilide, thioesters, coumarylamide, FRET) [115].

HNE hydrolyzes the B chain of oxidized insulin at the C-terminus of small residues like

Val, Ala, Ser and Cys [121]. The activity of HNE depends greatly on the length of substrates, suggesting that it has an extended substrate binding site [121]. The substrate preference and extended binding site have been confirmed using synthetic substrates and the crystal structure of the HNE-OMTKY-III complex, respectively [122]. Consequently, HNE substrate specificity depends not only on the nature of the P1 amino acid, as in many serine proteases, but also on secondary interactions with the S and S' subsites. The S2 subsite has a preference for medium-size, hydrophobic side chains (such as proline) and the same is true for the S3 and S4 subsites that preferentially accommodate Ala residues at P3 and P4 [115]. The favorable effect of S'-P' interaction on HNE is mainly due to the occupancy of S1' [123]. There is evidence showing that other S' subsites beyond S1' have no significant effect on catalysis by HNE [124,125].

Both analysis of the peptides generated from oxidized insulin B chain and synthetic substrates by Pr 3 reveal that the preference of Pr 3 for small hydrophobic amino acids like Cys, Ala, Val and Norval [126]. The presence of an Ile at position 190 of the Pr 3 sequence instead of a Val in HNE, and of an Asp at position 213 instead of an Ala reduces the size of the S1 pocket and accounts for the preference of Pr 3 for amino acids smaller than those accommodated in the S1 pocket of HNE that include Ile, Leu, and Norleu [127]. The deep, polar S2 subsite in Pr 3, due to Lys99, preferentially accommodates a negatively charged P2 residue [124]. Pr 3 accommodates small hydrophobic residues at position P4 as a result of the replacement of Arg217 in HNE by an Ile residue in Pr 3. Residue 217, together with Trp218, probably contributes to the P4/P5 specificity [128]. Most conventional peptide substrates having a chromogenic or fluorogenic group on their P1 residue are cleaved much more slowly by Pr 3 than by HNE. The fact that C-terminal elongation of FRET substrates greatly increases the catalytic activity of Pr 3, but not that of HNE suggests that S' subsites are important for substrate

binding and/or hydrolysis [125,127]. The specificities of subsites S5 to S3' investigated kinetically and by molecular dynamic simulations show that subsites S2, S1', and S2' are the main determinants of Pr 3 specificity [124,128]. Pr 3 has a negatively charged residue at position 61 in the vicinity of the S1' subsite, but HNE does not. As a consequence, Pr 3 prefers a positively charged P1' residue, whereas HNE has no preference at that position [124]. This emphasizes the importance of the S1' subsite for Pr 3 specificity, even though an electrostatic interaction at S1' in the Pr 3 active site is not a prerequisite for substrate binding, explaining why Pr 3 can also accommodate small hydrophobic residue at position P1' [115]. The presence of a positively charged residue at position 143 in the vicinity of the S2' subsite of Pr 3, but not in HNE, is essential for discriminating between HNE and Pr 3 activities [124,125]. Any type of residue at P3' is accepted by Pr 3 and improves the specificity constant by favoring substrate stabilization, but this is not the case for HNE. In summary, the S2, S1', S2', and S3' subsites are the main determinants of the substrate specificity of Pr 3, and account for its difference from HNE. A consensus sequence for Pr 3 substrates may therefore be deduced that extends from P2 to P3' and includes negative, small hydrophobic, positive, negative and positive residues from P2 to P3' respectively, a sequence that is not recognized by HNE [124,128].

Cat G accommodates both large, hydrophobic P1 residues (Phe, Leu, Met) and positive Lys or Arg residues due to the presence of a Glu residue at the bottom of its S1 subsite [129]. Like many other chymotrypsin-like enzymes, Cat G has a marked preference for a Pro at P2. Most of commonly used chromogenic (pNA) and/or fluorogenic (MCA) Cat G substrates have a Pro-Phe pair at P2-P1 [130-132]. There are no obvious binding determinants for the P3 side chain, although Lys192 has been suggested to favor the accommodation of acidic residues [129]. Cat G does not accept a Pro residue in its S3 subsite because it would interfere with the anti-

parallel β sheet structure formed between a section of the extended substrate binding site and the peptide chain of the substrate [133]. The primary specificity of Cat G has not been completely elucidated using synthetic substrates, but modeling studies suggest that the Ser40 in Cat G forms a hydrogen bond with a P1' Ser in the substrate [132]; which provides a structural basis for the preference of this residue at P1'. The side chain of Arg41 might favor the accommodation of an acidic residue at P2' and possibly interfere with the P3' specificity [132].

Summarized substrate specificities for HNE, Pr 3 and Cat G are shown in Table 1.4, and the amino acid residues involved in substrate recognition for these three enzymes are shown in Table 1.5.

Table 1.4 Substrate Specificity of Neutrophil-Derived Serine Proteases

Enzyme	P3	P2	P1	P1'	P2'
HNE	Ala	Pro	Leu, Ile, norLue,Ala, Val,Ser	N.S.	N.S.
Pr 3	Ala	Pro	Cys, Ala, Val, norVal	Lys	Asp
Cat G	Ala	Pro	Phe, Leu, Met, Lys, Arg	Ser	N.C.E.

N.S.: Not Significant; N.C.E.: Not completely elucidated.

Table 1.5 Enzyme Active-site Residues Involved in Substrate Recognition

Enzyme	S3	S2	S1	S1'	S2'
HNE	Val216 Phe192	His57 Leu99 Phe215	Val190 Phe192 Ala213 Val216 Phe218	His57 Phe41	Leu143 Ile151
Pr 3	Val216 Phe192	His57 Leu99 Phe215	Val190 Phe192 Ala213 Val216	His57 Phe41	Leu143 Ile151
Cat G	Gly216 Lys192	His57 Ile99 Tyr215	Ala190 Lys192 Val213 Gly216	His57 Arg41	Arg143 Gly151

1.2.5.1.4 Roles in Human Diseases

Neutrophil-derived serine proteases elastase, proteinase 3 and cathepsin G are implicated in a variety of infectious inflammatory diseases, including lung diseases (COPD, acute respiratory distress syndrome, cystic fibrosis, and ischemic-reperfusion injury) and in non-infectious inflammatory processes such as glomerulonephritis, arthritis, and bullous pemphigoid [10-12,134,135]. The main biological functions of these three enzymes have been summarized by Korkmaz et al. and are shown in Table 1.6.

In these neutrophil-derived proteases, HNE occupies the most important position at the apex of a specific protease hierarchy. HNE has a number of important intrinsic proteolytic properties (Table 1.6) and there is strong evidence to support the destructive actions of HNE (HNE breaks down elastin, a protein in connective tissue that is elastic and is responsible for resuming tissue shape after stretching and contracting) as the main pathogenic mechanism in

Table 1.6 Biological Functions of Elastase, Proteinase 3 and Cathepsin G [115]

Elastase	Proteinase 3
Degradation of ECM components	Degradation of ECM components
Degradation of plasma proteins	Bactericidal properties
Bactericidal properties	Cleavage of inflammatory mediators
Cleavage of inflammatory mediators	Platelet activation
Cleavage of receptors	Induction of endothelial cells, apoptosis
Cleavage of lung surfactant	Negative feedback regulation of granulopoiesis
Activation of lymphocytes and platelets	Target of auto-antibodies in Wegener's granulomatosis
Activation of proteases	
Inactivation of endogenous inhibitors	
Cytokines and chemokines induction	
Induction of airway submucosal gland secretion	
	Cathepsin G
	Degradation of ECM components
	Degradation of plasma proteins
	Bactericidal properties
	Cleavage of receptors
	Cleavage of inflammatory mediators
	Conversion of angiotensin I to angiotensin II
	Platelet activation
	Induction of airway submucosal gland secretion

emphysema associated with severe α 1-antitrypsin (also called α 1-PI) deficiency, as α 1-antitrypsin is the main inhibitor of neutrophil elastase [108]. In this deficiency, anti-elastase protection in the lung interstitium and alveolar space is markedly decreased to about 15-20% of normal levels [68]. Due to this destructive damage to the lungs, patients with emphysema usually experience difficulty in breathing, coughing, wheezing and excess mucus production. Further evidence of the importance of HNE in emphysema was confirmed by intra-tracheal injection of

HNE in experimental animals inducing emphysema [111, 136]. Even without severe genetic α 1-antitrypsin deficiency, cigarette smoke may induce the overproduction of HNE in the lungs and reduction of α 1-antitrypsin activity, causing this protease/antiprotease imbalance [137,138]. Other than its intrinsic proteolytic properties, HNE can also directly control the inducible expression and biological properties of other pulmonary proteases. For example, HNE regulates expression of cathepsin B and MMP-2 in alveolar macrophages [139] and also activates proMMP-2, MMP-6 and MMP-9 [140-142]. Thus, HNE also behaves as a proinflammatory mediator in addition to being a protease. In certain circumstances, HNE also controls signalling mechanisms regulating innate immunity (reviewed by Greene et al.) [10a]. Its pluripotency distinguishes it as a unique factor controlling many aspects of infection and inflammation in the lung.

Proteinase 3 is the major target antigen of the anti-neutrophil cytoplasmic autoantibodies (c-ANCA) produced in Wegener's granulomatosis (WG) [143]. Blood neutrophils from patients with active WG bear greater amounts of Pr 3 on their cell membranes than do neutrophils from healthy individuals because of the ongoing inflammatory process. The Pr 3 exposed on the cell surface is directly accessible to circulating c-ANCA, which results in complete activation of polymorphonuclear neutrophils [144]. In addition, α 1-antitrypsin deficiency positively correlated with the severity of vasculitis in WG patients suggests that Pr 3 is a biological target of α 1-antitrypsin [145,146]. Pr 3 also has a proapoptotic function through the proteolytic activation of procaspase-3 to active caspase [147], as well as the direct cleavage of NF- κ B and p21 [148-150].

Cathepsin G, which makes up approximately 20% of the azurophilic granule proteins of neutrophils [151], has many important roles in neutrophil function during inflammatory

processes, including degradation of extracellular matrix components and cytokines, modulation of integrin clustering on neutrophils, and direct chemoattraction of T cells and other leukocytes (reviewed by Shimoda et al.) [152]. The activity of cathepsin G is primarily regulated by α 1-antichymotrypsin (also called α 1-ACT). α 1-ACT is very effective inhibitor of cathepsin G in solution phase, but efficiency can be greatly reduced in the presence of ionic surfaces like DNA and heparin. The reason is that because both Cat G and HNE are very basic proteins and bind negatively charged molecules with high affinity, causing the phase separation of Cat G/HNE from α 1-ACT/ α 1-PI due to the inability of the inhibitor to bind these ionic surfaces [153]. Partitioning of these proteases from their endogenous inhibitors could explain the tissue damage associated with many chronic inflammatory disorders because they are protected from inhibitors by anionic macromolecules present in cell debris [154-156].

1.2.5.2 Granzyme B

Similar to neutrophil-derived serine proteases, granzyme B (also called GzmB), a serine protease which shares the same catalytic mechanism as all serine proteases) is another potent protease and dysregulation of its expression or activity could potentially contribute to extracellular matrix (ECM) destruction and parenchymal remodeling if it is released in the absence of perforin and subsequently accumulates extracellularly [88]. While the majority of GzmB is released unidirectionally towards target cells, GzmB can also be released non-specifically, escaping into the extracellular environment [157,158]. The effect on non-targeted cells may be due in part to the failure of endogenous GzmB inhibition mechanisms, including the lack of counteraction by proteinase inhibitor 9 (PI-9), a human serpin (serine protease inhibitor) shown to directly inhibit GzmB activity *in vitro* [159-161]. Without perforin-mediated delivery

of GzmB to target cells, the non-specifically released GzmB accumulates in the extracellular milieu, leading to tissue destruction and parenchymal remodeling [88]. Importantly, GzmB is capable of cleaving ECM proteins, specifically, vitronectin, fibronectin, laminin, proteoglycan and maybe elastin fibres [158,162,163]. Although the amount of non-specifically released GzmB may be small, it is sufficient to elicit matrix remodeling in chronic inflammatory states [88]. Fragments of the ECM generated by proteolysis have been shown to possess chemotactic properties and contribute to chronic inflammation (reviewed by Ngan et al) [88], thus causing emphysema. Perpetuity of inflammation may result as a consequence of the infiltration of inflammatory cells importing additional GzmB [88]. GzmB also facilitates its direct involvement in COPD as a pro-apoptotic mediator in the absence of perforin [164].

1.2.5.3 COPD Related Matrix Metalloproteinases

Matrix metalloproteinases (MMPs) are a large family of zinc-dependent neutral endopeptidases involved in the degradation of ECM components, and thus they play a crucial role in the homeostasis of normal tissue remodeling [43,165-167]. The activity of MMPs is controlled and finely balanced at many levels: RNA transcription, protein translation, secretion, localization, activation of zymogen, inhibition by endogenous proteins, and degradation [165]. Overexpression of MMPs results in an imbalance between the activity of MMPs and endogenous inhibitors of MMPs, TIMPs (Tissue Inhibitor of Metalloproteinases), leading to tissue degradation and consequently facilitating a variety of pathological disorders, including arthritis, cancer and COPD [43,165].

MMP-12 plays a predominant role in the pathogenesis of chronic lung injury, particularly in emphysema. The production of MMP-12 results from macrophage activation and resident cells

synthesis (epithelial cells, smooth muscle cells and endothelial cells) along alveolar wall of lungs [165]. As suggested by its trivial name, metalloelastase, MMP-12 is clearly the most active MMP to degrade elastin [168] although it can cleave many of the other components of the extracellular matrix [165]. The pathology of COPD is associated with an airway inflammatory process characterized by an accumulation of inflammatory cells such as macrophages and neutrophils. There is a positive correlation between the number of macrophages in the alveolar walls and the mild-to-moderate emphysema status in patients with COPD [169]. *In vitro* studies on alveolar macrophages collected from COPD patients have shown their ability to degrade more elastin than macrophages collected from healthy volunteers [170]. The number of MMP-12-expressing macrophages and staining intensity are higher in BAL samples from COPD patients than in control subjects. Enhanced MMP-12 activity is also detected in BAL fluids from patients with COPD in comparison with control subjects [167]. In animal model, MMP-12 knock-out (KO) mice subjected to a 6-month cigarette smoke do not have increased numbers of macrophages in their lungs and do not develop emphysema. A monthly intratracheal instillation of monocyte chemoattractant protein-1 into the lungs of MMP-12 smoked-exposed KO do not develop air space enlargement in response to smoke exposure. These data seem to suggest that MMP-12 is sufficient for the development of emphysema that results from chronic inhalation of cigarette [171]. However, in an acute model of smoke exposure, neutrophils, desmosine and hydroxyproline, markers for elastin and collagen breakdown, respectively, were examined in BAL fluids from MMP-12 KO mice and wild-type mice 24 h after smoke exposure. None of these markers could be detected in MMP-12 KO mice, suggesting that acute smoke-induced connective tissue breakdown, the initial step towards emphysema, requires both neutrophils and MMP-12 and that the neutrophil influx is dependent on the presence of MMP-12 [172].

As a general mechanism, the substrate binds to the active site of MMP-12, and interacts with the catalytic zinc ion through carbonyl group of the scissile peptide bond while the peptide group is hydrogen bonded to the carbonyl carbon atom of Ala182 and then the peptide substrate is finally hydrolyzed [173].

1.3 West Nile Virus/Dengue Virus and Related Proteases

1.3.1 Overview of West Nile and Dengue Viruses

West Nile virus (WNV) and Dengue virus (DENV) are members of *Flaviviruses* genus, which belong to the *Flaviviridae* family [174]. WNV and DENV are recognized as major health threats that affect millions of people worldwide. West Nile virus (WNV, first isolated in 1937 from the blood of a woman with a febrile illness who lived in the West Nile region of Uganda), an emerging mosquito-borne human pathogen, is now found throughout Africa, Europe, Central Asia and most recently, in North America [175]. WNV is the cause of severe neurological disease and fatalities, particularly among the elderly, with more than 900 fatalities and an estimated 280,000 infections in humans. In the US, there are several hundreds registered deaths and thousands reported cases each year according to Centers of Disease Control and Prevention [176]. Typical symptoms of WNV infection include fever, rashes, and myalgia; however, occasionally more severe and potentially fatal symptoms develop, including acute encephalitis and fulminant hepatitis [177]. The dengue viruses, also transmitted through mosquitoes as WNV, are reported to infect over 50 million people each year, and with more than half the world's population living in areas at risk of infection [178,179]. There are four serotypes of dengue, DEN-1, DEN-2, DEN-3, and DEN-4 [180], and the infection severity ranges from the self-limiting dengue fever (DF) to the more serious dengue hemorrhagic fever (DHF) and dengue

shock syndrome (DSS), with reported ranges of 1-5% to 10-30% of cases resulting in death, respectively [179]. Although human life is at the risk of these two viruses infection, there is currently no effective vaccine available for the diseases [181,182], and thus the alternative strategy of chemotherapeutic development has become imperative.

1.3.2 Flavivirus Life Cycle

Flaviviruses are small, enveloped viruses [178-180]. Enveloped virions are composed of a lipid bilayer surrounding a nucleocapsid, which consists of a single-stranded, positive-sense 11 kb genome RNA complexed with multiple copies of a small, basic capsid protein. Binding and uptake involve receptor-mediated endocytosis via cellular receptors specific for viral envelope proteins [183]. After attachment to the cell surface, the low pH of the endosomal pathway induces fusion of the virion envelope with cellular membranes. Following uncoating of the nucleocapsid, the RNA genome is released into the cytoplasm [183,184]. The genomic viral RNA serves as mRNA and can thus be directly translated – as a single open reading frame – by the host cell translation machinery into a single polyprotein precursor. This polyprotein is cleaved co- and post-translationally into three structural (C-prM-E) and seven non-structural proteins (NS1-NS2A-NS2B-NS3-NS4A-NS4B-NS5) (Figure 1.8) [178-181,184]. Both the viral NS2B-NS3 enzyme and cellular proteases take part in this process which involves both *cis*- and *trans*-cleavage events [178,184]. Once the viral polymerase NS5 has been synthesized and released from the polyprotein precursor, the viral RNA can be transcribed into the complementary minus strand RNA, which is then transcribed back into a positive strand. A dsRNA transient intermediate is thus formed during this process that must be separated into its individual strands in order to give access to the NS5 polymerase for further rounds of viral

genome replication. The NS3 protein which physically associates with the NS5 polymerase appears to play an essential role in the viral life cycle since mutagenesis studies showed that impairment of the proteolytic activity led to a defective genome unable to produce infectious viral particles [178,184].

1.3.3 The Flaviviral NS2B-NS3 Protease

The Flavivirus encoded full-length NS3 protein is a long multi-functional protein, which contains a chymotrypsin-like serine protease (NS3pro) in the N-terminal and a helicase (NS3hel) in the C-terminal (shown in Figure 1.9) [174,178,184]. Heterologously expressed NS3 protease domain (NS3pro) or NS3 full-length (NS3 FL) has the tendency to form aggregates, and is inactive as a protease [184]. The NS2B protein, which is located in the polypeptide precursor immediately upstream of the NS3pro domain, functions as the cofactor for NS3pro [174,178,184]. The NS2B-NS3pro cleaves the NS2B-NS3 linkage in *cis* and the composition and length of the NS2B-NS3 linker seems not to be important for protease activity toward external substrates [174]. NS3pro cleaves internal linkages within NS2A and the capsid protein C, as well

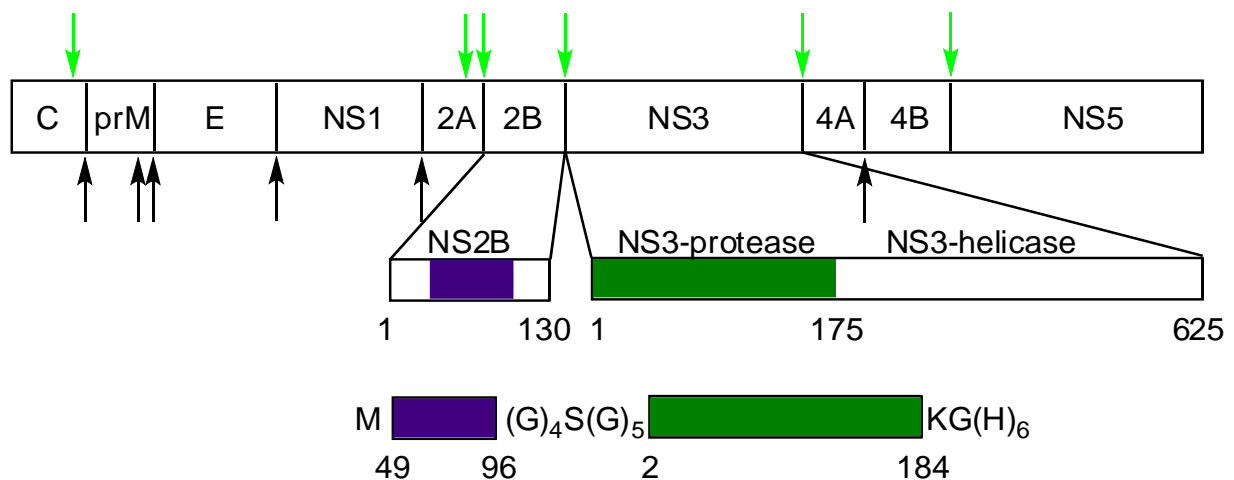


Figure 1.9 Schematic Representation of the Flaviviral Polyprotein, with the Cleavage Sites Processed by NS2B-NS3pro Indicated by Arrows. [184]

as the boundaries between NS2A/NS2B, NS2B/NS3, NS3/NS4A, NS4A/NS4B, and NS4B/NS5. Mutations in the NS3pro cleavage sites in the polyprotein precursor abolish viral infectivity, suggesting that small molecule inhibition of NS3pro may be an effective antiviral strategy [174,185].

1.3.3.1 Overview of NS2B-NS3 Protease Structure

The WNV NS2B-NS3 protease is a two-component protease (shown in Figure 1.10) and the inhibitor-free DENV NS2B-NS3pro structure is overall very similar to the inhibitor free WNV structure [174]. The cofactor domain NS2B wraps around the NS3 protease domain like a belt and the central hydrophobic sequence of NS2B constrains the flexibility of NS3 and force it to adopt the active conformation [38b]. The comparisons between the crystal structures of the NS2B-NS3 proteases of DEN2 and WNV with those of DEN2 NS3pro alone reveal that NS3 undergoes substantial rearrangement in the presence of the NS2B cofactor [38b,174]. The crystal structure of WNV NS2B-NS3pro-aldehyde inhibitor complex (2FP7) shows that the C terminus of the cofactor domain forms part of the active site [38b]. This explains why, in the absence of NS2B, NS3 is unable to interact properly with substrates extending beyond the S1 site and is thus inactive.

In addition, there is evidence showing that NS2B-NS3pro exhibits two alternative, productive and nonproductive, conformations for both WNV and DENV (shown in Figure 1.11) [174]. In the nonproductive conformation, substrate- or inhibitor-free conformation, the N-terminal residues of NS2B remain associated with the N-terminal β -barrel of NS3pro, the C-terminal residues of NS2B extend into the solvent and do not form part of the C-terminal β -barrel. In the productive conformation, inhibitor-bound conformation, these C-terminal residues

form part of the substrate-binding cleft with residue NS2B interacting directly with P2 of the inhibitor [38b]. Along with the fact that the nonproductive conformation of the oxyanion hole is energetically favored in the absence of substrate, an “induced fit” mechanism was proposed by Aleshin et al. [174]. Such a requirement of these interactions for catalysis raises the possibility of designing allosteric inhibitors that interfere with the NS2B fold rather than directly targeting the catalytic triad of NS3pro.

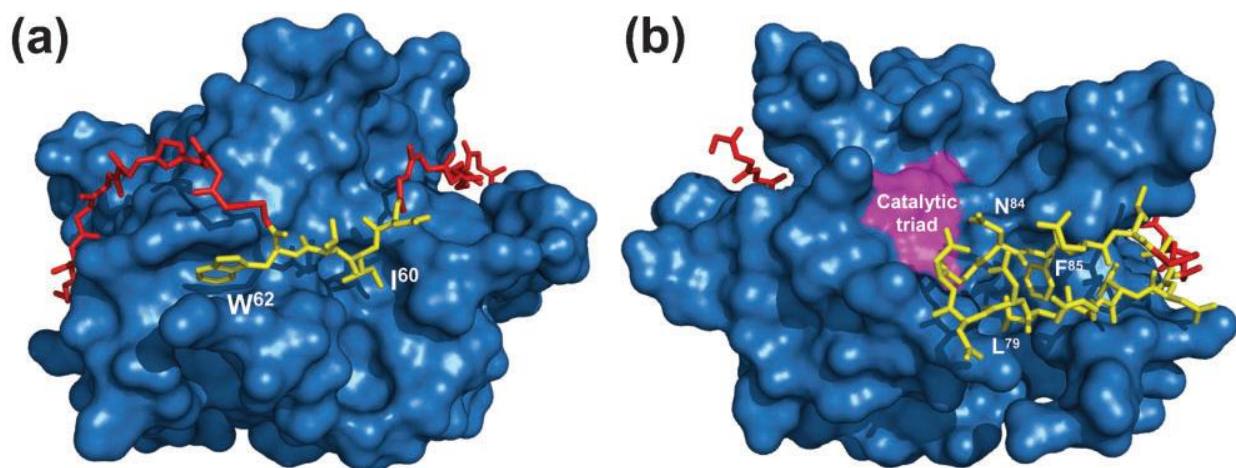


Figure 1.10 WNV NS2B-NS3pro Showing the Location of Important Cofactor Residues. The NS3 protease is shown as a solid surface in blue with the catalytic triad highlighted in (b) in magenta. The polypeptide backbone of the cofactor domain is shown in red with the polypeptide backbone and side chains of sites identified as important for proteolytic activity shown in yellow. (a) Site 1, NS2B59–62 and (b) site 2, NS2B75–87. [38b]

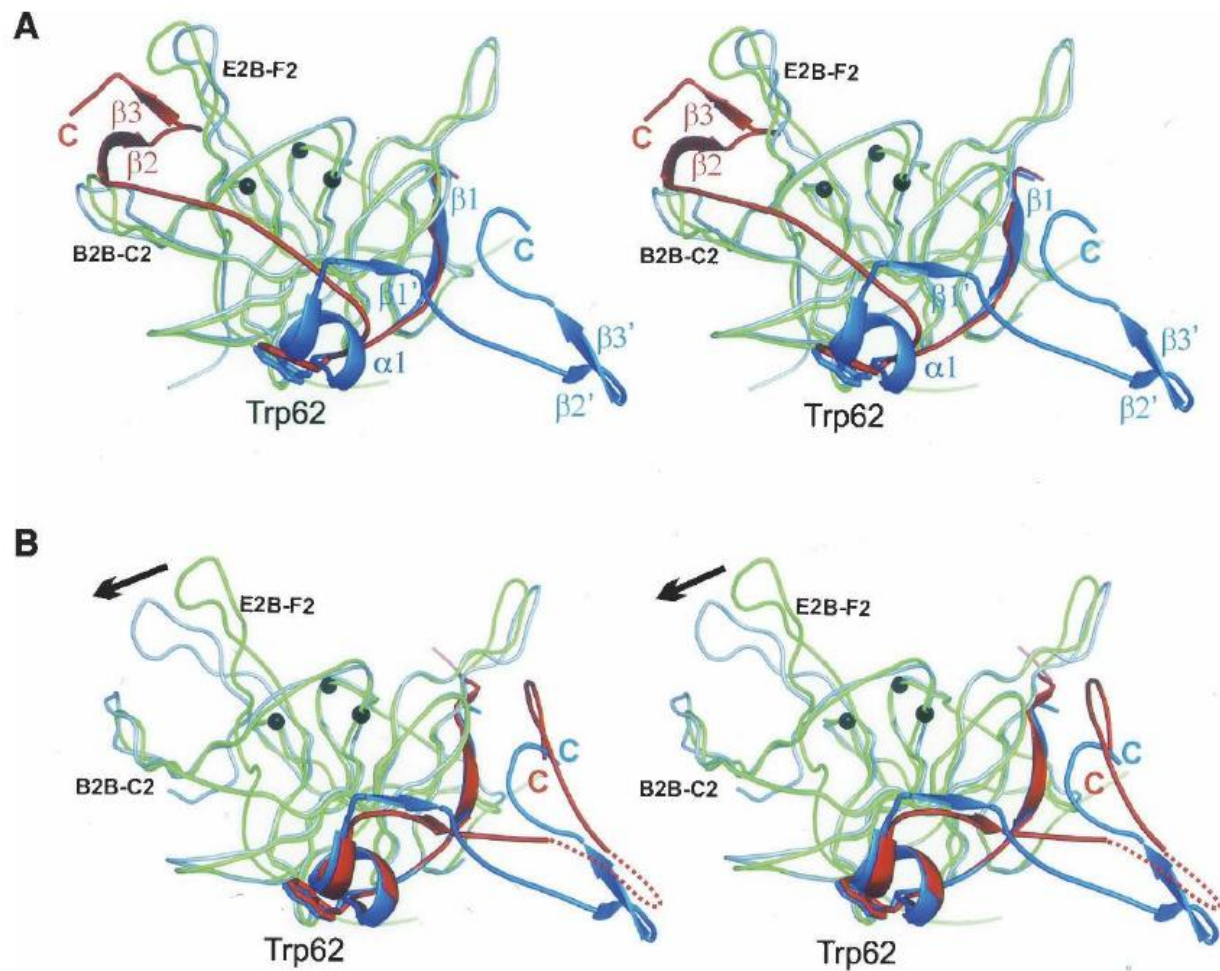


Figure 1.11 Stereoview of Two Conformations of the NS2B Cofactor. (A) Superposition of WNV NS2B-NS3 proteases: substrate-free (green and blue) and aprotinin-bound (gray and red). The secondary elements of NS2B unique to the substrate-free ($\alpha 1$ and $\beta 1'$) and the substrate-bound ($\beta 2$ and $\beta 3$) structures, as well as the alternative C termini are indicated. The point of departure (Trp62) for the two NS2B elements is labeled and shown as a stick model. The elements $\beta 2'$ and $\beta 3'$ in the substrate-free structure are stabilized by crystal contacts. Active site residues are shown as black circles. (B) Superposition of substrate-free DENV (gray and red) and WNV (green and blue) NS2B-NS3pro. The collapse of the E2B-F2B loop observed in DENV is indicated by the arrow. [174]

1.3.3.2 The Flaviviral Active Site

As aforementioned, WNV and DENV are chymotrypsin-like serine proteases. The active site of chymotrypsin-like serine proteases includes three conserved elements: (1) A classic His-Asp-Ser catalytic triad (His51, Asp75, and Ser135 in both WNV and DENV), whose precise arrangement in space is required to enhance the nucleophilicity of the serine hydroxyl group; (2) the “oxyanion hole,” which stabilizes the developing negative charge on the scissile peptide carbonyl oxygen in the transition state; and (3) the substrate binding β -strands E2 and B1, which help to position the substrate in the active site. In the ground state of the active protease, the Ser hydroxyl H-bonds to the His imidazole, which in turn H-bonds to the Asp carboxyl group [174]. The typical serine catalytic mechanism is shown in Figure 1.8.

1.3.3.3 Substrate Specificity of WNV and DENV NS2B-NS3 Proteases

WNV and DENV NS2B-NS3 proteases are highly homologous (53% sequence identity, 79% sequence similarity within the 184 residues of NS3pro and conserved catalytic residues His51, Asp75, and Ser135 and oxyanion residue Gly133. (Figure 1.12) [187]); they have similar but distinct substrate specificities [174,188]. The aprotinin-bound WNV X-ray structure mimics a classic Michaelis–Menten complex, allowing for an authentic and complete view of the enzyme–substrate pre-cleavage complex. It is strongly supported that WNV and related flaviviral proteases have a requirement for basic residues at both the P1 and P2 positions of their substrates [174,188-189]. The P2 side chain (Lys/Arg) interacts both directly with Asn84 of NS2B and indirectly with a negatively charged surface created by the invading hairpin of NS2B, including Asp80 and Asp82. NS2B binding also helps to define the S1 pocket in WNV protease, by changing the conformation of NS3 residues 116–132, such that Asp129 is introduced into the

base of the pocket, where it can salt-bridge with the P1 Lys/Arg [174,188]. Although both fluorogenic substrates and aldehyde inhibitors of WNV and DENV proteases suggest their preferences of Lys and Nle at P3 and P4, respectively [184,189], the significant interactions of viral NS2B-NS3 proteases are restricted to P2-P2' [188]. The S1' pocket in WNV NS2B-NS3pro comprises a cavity between strand B1 and the helical turn (residues 50–53) following strand C1 and is lined on one side by the catalytic histidine and on the other by an invariant Gly37. In comparison of WNV and DENV NS2B-NS3pro, WNV protease has a strong preference for Gly at both P1' and P2' positions [174,188], whereas the DENV protease could accommodate a number of amino acid residues, including the bulky hydrophobic tryptophan, phenylalanine and tyrosine residue at P1' and P2', especially if a glycine residue is present at one of the these two substrate positions [188]. The P1' preference of WNV protease may correlate with the presence of a Thr residue at position 132 of NS3 rather than the Pro residue found in DENV. The Thr side chain makes a H-bond with the main-chain C=O of the P1' residue, which is flanked on one side by a short H-bond between the P2' main-chain nitrogen and the C=O of Ala36 and on the other side by the P1 C=O that occupies the oxyanion hole [174].

```

Histidine Tag                               NS2B CoFactor (40 residues)
WNV MRGSHHHHHHG STDMWIERTADISWESDAEITGSSSERVDVRLDDDGNGFQLMNDPGAPWK
DEN MRGSHHHHHHG SADLELERAADVKWEDQAEISGSSPILSITISEDGMSIKNEEEEQTL
********** *::: ***:***:.*.:***:*** ::: ::** .::: *:

Linker 1                                       NS3protease (184 residues)                    50
WNV GGGSGGGG GGVLWDTPSPKEYKKGDTTGGVYRIMTRGLLGSYQAGAGVMVEGVFHTLW
DEN GGGSGGGG AGVLWDVPSPPPVGKAELEDGAYRIKQKGI LGYSQIGAGVYKEGTFHTMW
********** .***** .*** *.: *.*** *:*** * **** ** .*** .*

                                                                    110
WNV HTTKGAALMSGEGRLDPYWGSVKEDRLCYGGPWKLQHKWNGQDEVQMIIVVEPGKNVKNVR
DEN HVTRGAVLMHNGKRIEPSWADVKKDLISYGGGWKLEGEWKEGEEVQVLALEPGKNPRAVQ
*.*** .*** . *.: * ..*** .* ..*** *** .: * ..*** .: *** .: ***** .: *

                                                                    170
WNV TKPGVFKTPEGEIGAVTLDFPTGTSGSPIVDKNGDVIGLYNGVIMPNGSYISAIVQGKR
DEN TKPGLFKTNAGTIGAVSLDFSPGTSGSPIIDKKGKVGLYNGVVTRSGAYVSAIAQTEK
**** .*** * **** .*** .***** .*** .* .***** .: *** .*** .* ::

                                                                    ^
                                                                    184
WNV MDEPIPAGFEPEML
DEN SIEDNPE-IEDDIFR
* * : * :::

```

Figure 1.12 Alignment of Recombinant NS3-NS2B Protease-Cofactor Sequences for Dengue and West Nile Viruses. Alignment shows catalytic residues Ser135 (S), Asp75 (D), His51 (H) in bold, oxyanion residue Gly 133 (G). 40 residue cofactor domain of NS2B (underlined) as defined for Dengue type 4 virus (^); exact amino acid match (*), high chemical similarity (:), low chemical similarity (.), insertion/deletions (), and residues (italics) incorporated in construct design. Alignment is numbered from the first residue of the protease domain. [187]

1.4 Protease Inhibition

Because of the important roles proteases play in human disease, inhibition of proteases has been the focus of intense and ongoing investigations and many protease inhibitors are used in the clinic. Over 1500 crystal structures of proteases have been deposited in the Protein Data Bank. A number of protease inhibitors have been found to display promising therapeutic activity in early clinical trials for viral and parasitic infections; cancer; inflammatory, immunological, and respiratory conditions; cardiovascular and degenerative disorders [10b]. Many of them have been developed further and are currently either in development or have been launched to the market. The most successful example of protease inhibitors is HIV-1 protease inhibitors. To date approximately 8 drugs have been launched and 13 candidates are in clinical trials for the treatment of AIDS [10b].

Protease inhibitors include synthetic organic compounds and many naturally occurred products (including proteins and herbal extracts). As a matter of fact, protein inhibitors have been extensively studied using X-ray crystal structures of protease-ligand complexes, providing critical information in protease inhibitor design and development. On the other hand, the active ingredients isolated from herbal extracts are highly diverse and complex in their structures and they are commonly modified to improve stability and bioavailability.

1.4.1 Classification of Protease Inhibitors

Structurally, the protease inhibitors can be classified into protein-based inhibitors, peptide-based inhibitors and heterocyclic inhibitors. According to their inhibitory kinetics, they can be classified as reversible or irreversible inhibitors; however, the most informative approach for classifying protease inhibitors is through their mechanism of action, which eventually

determines their kinetic behavior during inhibition. The mechanism of action used by protease inhibitors includes non-covalent inhibition, transition-state analog inhibition, mechanism-based inhibition, and affinity labeling. Affinity labels contain a highly reactive group and serve as alkylating agents, such as halomethyl ketones, diazomethyl ketones, acyloxymethyl ketones, epoxides, aziridine derivatives, vinyl sulfones and azodicarboxamides. These functional groups are highly reactive with nucleophilic atoms present in enzymes and therefore lack of selectivity and quite toxic. They are mainly used in characterizing proteases. Mechanism-base inhibitors contain specific recognition elements and the reactive functional group is generated during catalysis, avoiding nonspecific reactions with the enzyme. Non-covalent inhibitors and transition-state inhibitors are favored in drug discovery because of their reversibility, which significantly lowers the toxicity of the drugs. However, developing reversible inhibitors require much more effective contact between inhibitors and proteases, which is often more challenging.

1.4.2 Non-covalent Inhibitors

As suggested by their name, non-covalent inhibitors do not bond covalently to proteases during inactivation and can be easily removed by dialysis. Interactions between these inhibitors and their proteases are mainly ionic, hydrogen bonds, hydrophobic interactions, cation- π interactions and complementarity. According to the effect of varying the concentration of the enzyme's substrate on the inhibitor, non-covalent inhibitors can be further divided to four groups: competitive inhibitors, uncompetitive inhibitors, mixed inhibitors, and non-competitive inhibitors. Among these four groups, competitive inhibitors and mixed inhibitors are discussed in detail.

1.4.2.1 Competitive Inhibitors

For competitive inhibitors, the substrate and inhibitor can not bind to the protease at the same time. This usually results from the inhibitor having an affinity for the active site of a protease where the substrate also binds. The substrate and inhibitor compete for access to the enzyme's active site. This type of inhibition can be overcome by using high concentrations of substrate. Competitive inhibitors are often similar in structure to the substrate and most protein inhibitors belong to this group (with few exceptions). Many natural protein inhibitors are highly effective against a variety of serine proteases, however they are not considered as drugs because they are non-human proteins, which can induce an immunogenic response.

Although protein inhibitors are infrequently used in drug development, the protease-inhibitor complexes are well studied [10b]. Because a protein inhibitor typically occupies the active site of the protease in a substrate-like fashion, therefore the enzyme-inhibitor complex gives the most direct evidence on how the substrate binds, especially on the prime subsites of proteases, providing the most accurate information for structure based inhibitor design. The X-ray crystal structure of the third domain of the turkey ovomucoid inhibitor bound to HNE (pdb code: 1ppf) [190] and aprotinin-bound WNV NS2B-NS3 protease (pdb code: 2ijo) [174] were solved in 1986 and 2007, respectively. These two X-ray crystal structures are the foundation of the design of reversible competitive inhibitors in this dissertation.

1.4.2.2 Mixed-type Inhibitors

In mixed inhibition, the inhibitor can bind to the enzyme at the same time as the enzyme's substrate. However, the binding of the inhibitor affects the binding of the substrate, and vice versa. This type of inhibition can be reduced, but not overcome by increasing concentrations

of substrate. Although it is possible for mixed-type inhibitors to bind in the active site, this type of inhibition generally results from an allosteric effect where the inhibitor binds to a different site on an enzyme. Inhibitor binding to this allosteric site changes the conformation of the enzyme so that the affinity of the substrate for the active site is reduced. Flaviviral proteases have a unique cofactor wrapping around NS3 through hydrophobic interactions, and the cofactor's functions are stabilization of NS3 protease and formation of part of the active sites. Therefore the interruption of these hydrophobic interactions can reduce the activity of two-component protease. As shown in Figure 1.11, WNV and Dengue have two conformations, productive and non-productive conformations. The C-terminal of non-productive conformation is free from the active site and flowing into the solvent, which provides a chance for designing inhibitors that target the NS2B-NS3 binding, therefore behaving as an allosteric inhibitor.

1.4.2.3 Examples of Non-covalent Inhibitors

Obviously, by mimicking protease substrates or the partial protein inhibitor structure which occupies the active site of protease can result in potent inhibitors. However, the peptide back bone can be degraded by many other enzymes in the body, especially in the stomach. In order to prevent hydrolysis and improve bioavailability, further modifications are required in the substrate mimicking. For example, clinically approved (in Japan) thrombin inhibitor *Argatroban* (K_i 39 nM) [10b] mimics the thrombin substrate at P1 residue. By changing the P2 and P' residues it becomes an inhibitor (Figure 1.13). Apparently, a greater structure similarity of the inhibitor with the substrate will result in a more potent inhibitor. Tucker et al. have reported several extremely potent inhibitors (potency range from 0.0025 to 0.1 nM) of thrombin [191], in which all of them mimic the P1-P3 residues (the general structure of these compounds are shown

in Figure 1.13). Interestingly, by varying the substitution of these inhibitors, the bioavailability and pharmacokinetics can be improved without significant loss of potency [191]. A similar strategy has been widely used in non-covalent inhibitor design.

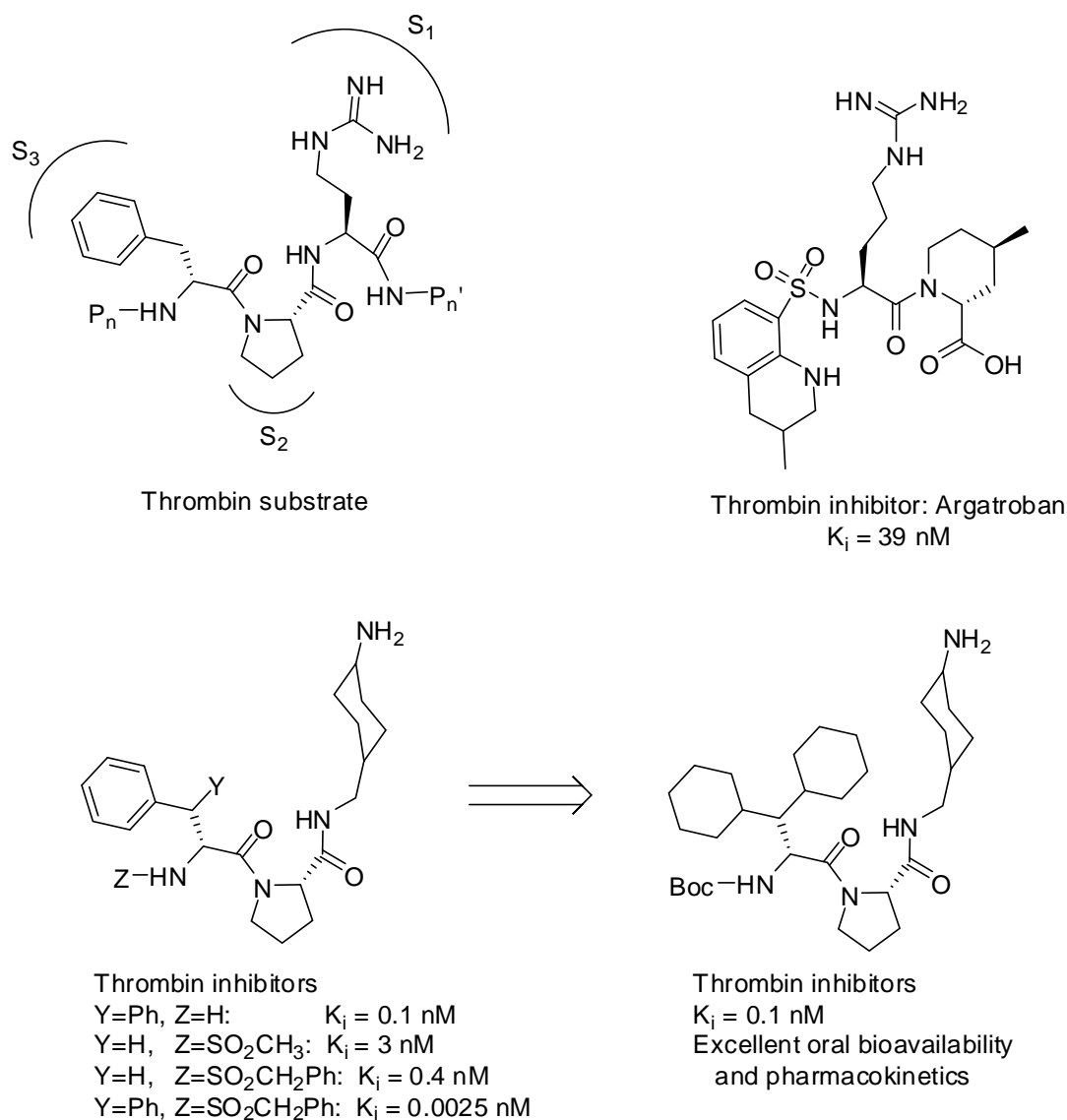


Figure 1.13 Substrate-like Non-covalent Inhibitors of Thrombin.

For COPD related proteases, there are some non-peptide inhibitors with low nanomolar inhibition constants (K_i) that have been patented by several pharmaceutical companies. Their

structures are shown in Figure 1.14 [192a]. According to these patents, these are effective inhibitors of HNE that are potentially useful for treatment of acute or chronic inflammatory [192a]. Several synthetic small molecular weight protein inhibitors (MW: 6-11kDa), such as DX-890(EPI-HNE-4), recombinant α 1-antitrypsin (rAAT), elafin and secretory leukocyte protease inhibitor (SLPI) have been developed and actively researched in consideration of establishing a protease/antiprotease balance in COPD [192a]. More importantly, cyclotides (macrocylic cysteine knotted microprotein composed of 26-37 amino acids) have been found to be low nanomolar inhibitors for serine proteases, such as HNE and β -tryptase, with exceptional rigidity, thermal stability and enzymatic resistance [192b]. As stated earlier, COPD is a multi-factorial disorder, which involves many enzymes, therefore, there is still a need for the development of effective competitive inhibitors against Pr3 and other proteases related to COPD.

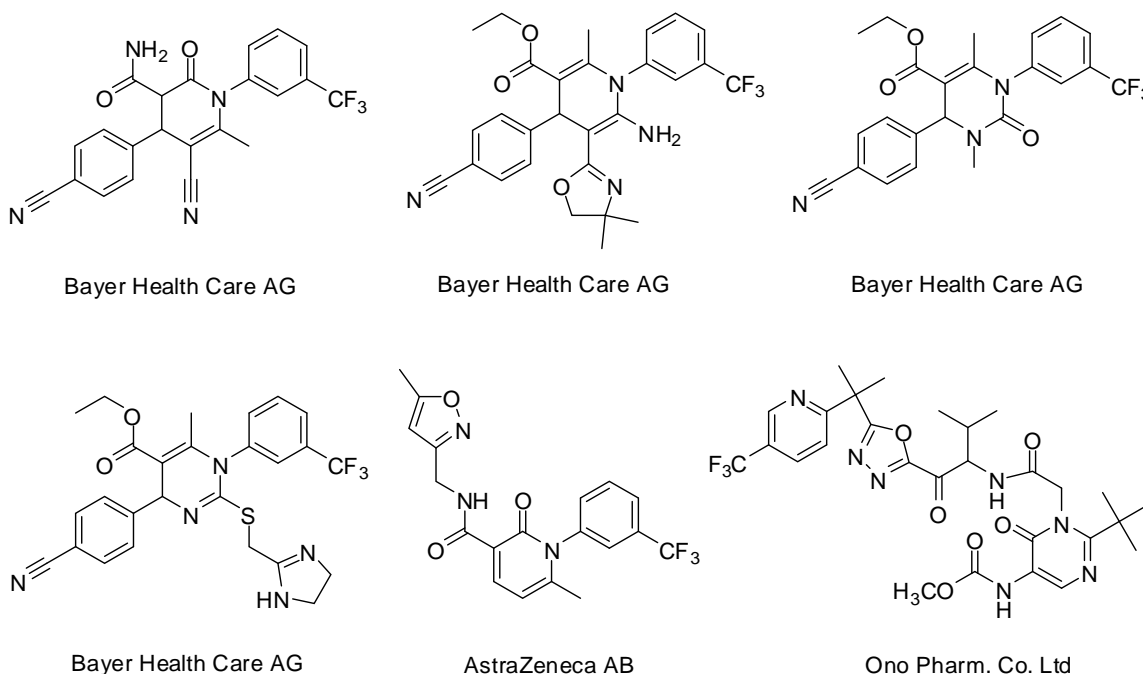


Figure 1.14 Patented Potent Human Neutrophil Elastase Non-covalent Inhibitors.

Several noncompetitive DENV NS2B-NS3 protease inhibitors with K_i 's or ED_{50} 's in the

4-30 micromolar range have been reported recently (shown in Figure 1.15) [193]. At first glance, they are drug-like molecules (small molecular weight, rigid structure and good aqueous solubility), however, these inhibitors are not sufficiently good drug candidates because of synthetic tractability and potentially poor pharmacokinetic properties. Therefore there is a remaining need to develop small organic molecules with the following properties: chemically robust and a versatile structure capable of optimizing the potency, physical properties and other drug-like parameters.

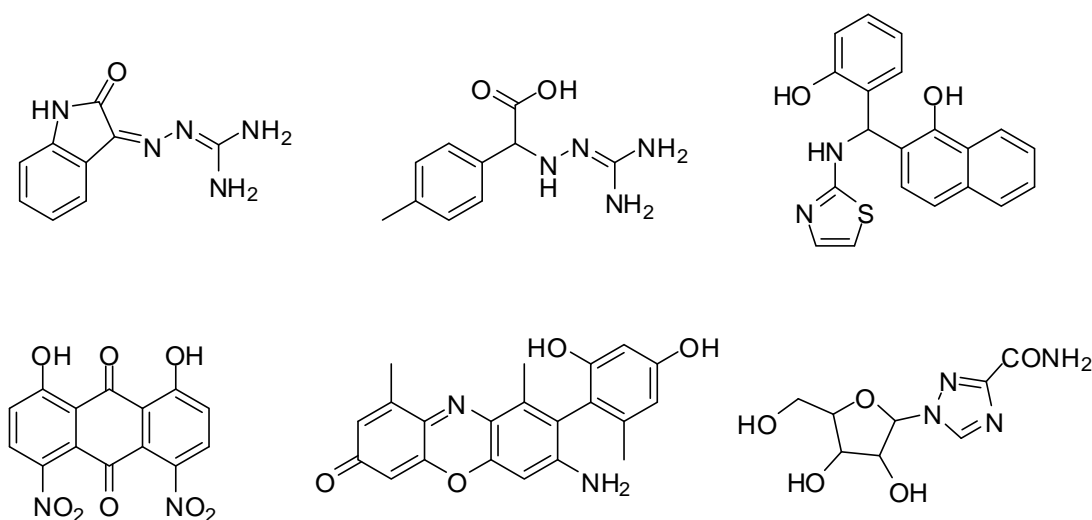
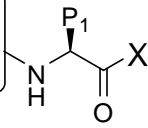
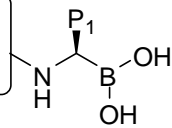
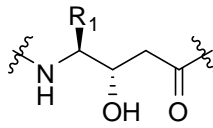
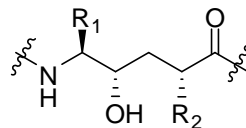
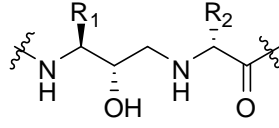
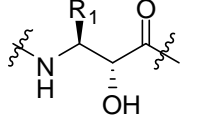
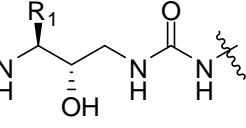
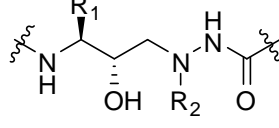
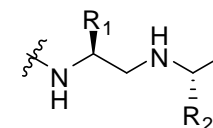
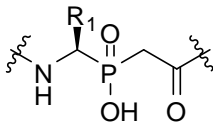


Figure 1.15 Dengue Virus Protease Inhibitors

1.4.3 Transition-State Analog Inhibitors

“An enzyme must bind the altered substrate in the transition state more tightly than it binds the substrate in the ground state” forms the transition-state theory of enzymatic catalysis [194]. This theory underlines the design of “transition-state analog inhibitors (TSA)”. There are two tetrahedral transition states involved in serine protease catalysis: acylation step and deacylation step. A number of functional groups are employed in the design of transition state analogs and the general structures are summarized in Table 1.7.

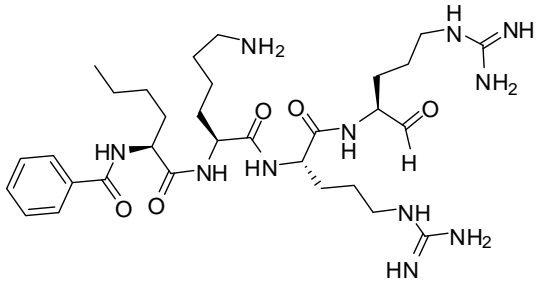
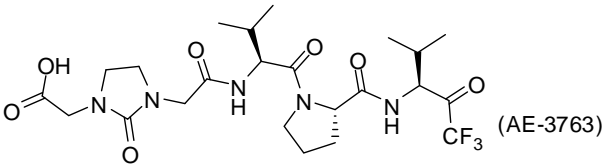
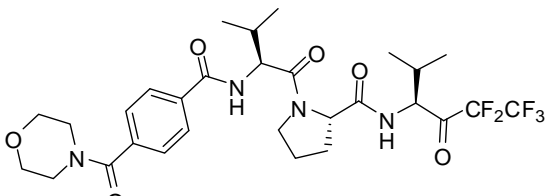
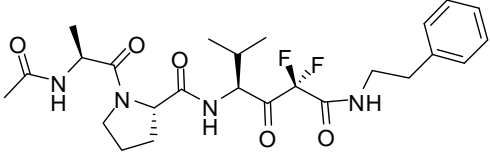
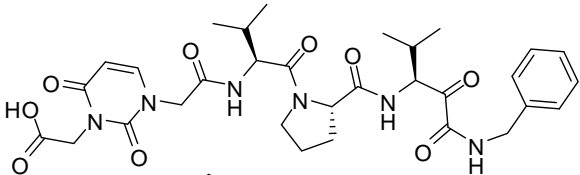
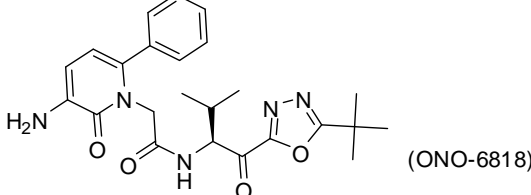
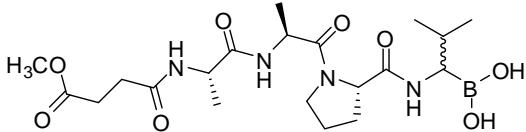
Table 1.7 Protease Transition State Analog Inhibitor Templates

<p>Type I</p>	<div style="display: flex; align-items: center;"> <div style="border: 1px solid black; padding: 5px; margin-right: 10px;">S pockets Recognition Elements</div>  <div style="margin-left: 20px;"> <p>X = H, CF₃, CF₂CF₃, Heterocycle, CF₂-S_n' recognition elements C(=O)-Y-S_n' recognition elements (Y = O, NH, CH₂)</p> </div> </div> <div style="display: flex; align-items: center;"> <div style="border: 1px solid black; padding: 5px; margin-right: 10px;">S pockets Recognition Elements</div>  </div>
<p>Type II [201]</p>	<div style="display: flex; justify-content: space-around; align-items: center;"> <div style="border: 1px solid black; padding: 5px;">S_n-S₂ pockets Recognition Elements</div> <div style="text-align: center;">Z</div> <div style="border: 1px solid black; padding: 5px;">S₂'-S_n' pockets Recognition Elements</div> </div> <p>Z:</p> <div style="display: grid; grid-template-columns: repeat(3, 1fr); gap: 10px;"> <!-- Statine (Sta) --> <div style="text-align: center;">  <p>Statine (Sta)</p> </div> <!-- Hydroxyethylene --> <div style="text-align: center;">  <p>Hydroxyethylene</p> </div> <!-- Hydroxyethylamine --> <div style="text-align: center;">  <p>Hydroxyethylamine</p> </div> <!-- alpha-Hydroxy-beta-amino acid --> <div style="text-align: center;">  <p>α-Hydroxy-β-amino acid</p> </div> <!-- Hydroxyethylurea --> <div style="text-align: center;">  <p>Hydroxyethylurea</p> </div> <!-- Hydroxyethylhydrazine --> <div style="text-align: center;">  <p>Hydroxyethylhydrazine</p> </div> <!-- Reduced Amide --> <div style="text-align: center;">  <p>Reduced Amide</p> </div> <!-- Phosphonic --> <div style="text-align: center;">  <p>Phosphonic</p> </div> </div>

Type I TSA involves mainly the S (and S') pockets recognition elements and an activated carbonyl group or a boronic acid. These are commonly used in designing serine protease,

cysteine protease, and threonine protease inhibitors where the enzyme nucleophilic group interacts with the inhibitor. In serine proteases, peptidyl aldehydes react with serine oxygen to form a reversible covalent adduct, a hemiacetal. The hemiacetal hydroxyl group interacts with the oxyanion hole and the peptide sequence only interacts with S pockets of the enzyme active site in this adduct because of the nature of peptidyl aldehydes. This adduct is considered as the transition state analog of the deacylation step. Peptidyl aldehyde inhibitors have often been used in the crystallographic study of serine proteases (such as WNV NS2B-NS3 protease-Bz-Nle-Lys-Arg-Arg-H complex, pdb code: 2fp7) [195] and enzyme active site mapping via peptidyl aldehyde inhibitor SAR studies [189]. Peptidyl ketones have the advantage of interacting with both S subsites and S' subsites of serine proteases. However the corresponding ketal adduct formed by an ordinary ketone and serine protease is much less stable than the one resulting from an aldehyde. Increasing the stability of ketone-enzyme adducts, which parallels the potency of the inhibitors, has been achieved by using electron-withdrawing groups to increase the electrophilicity of the ketone group in peptidyl ketone inhibitors. Activated ketones, such as α -fluoroketones [196-198], α -diketones [199], α -ketoesters [196], α -ketoamides [196], α -ketoheterocycles [192a,196], have been successfully used in the design of serine protease inhibitors. Boronic acids have also been found to function as potent transition state analog inhibitors [200]. Selected type I transition state inhibitors are listed in Table 1.8.

Table 1.8 Selected Type I Transition State Analog Inhibitors

Structure	Target Protease	References
	<p>WNV/Dengue 3 NS2B-NS3 Protease</p>	<p>[195]</p>
 <p>(AE-3763)</p>	<p>Human Neutrophil Elastase</p>	<p>[196]</p>
	<p>Human Neutrophil Elastase</p>	<p>[197]</p>
	<p>Porcine Pancreatic Elastase</p>	<p>[198]</p>
	<p>Human Neutrophil Elastase</p>	<p>[196]</p>
 <p>(ONO-6818)</p>	<p>Human Neutrophil Elastase</p>	<p>[192]</p>
	<p>Human Neutrophil Elastase</p>	<p>[200]</p>

In Type II TSA, the specific protease substrate dipeptidyl cleavage sites are replaced with

various structures that mimic the enzyme catalytic transition state hybridization. These replacements usually involve changing the sp² scissile carbonyl to an sp³ hydroxymethyl, phosphonic, or methylene group and the inhibitor binding relays on the rest of the active site recognition [201]. One structural feature present in most tight-binding aspartic protease inhibitors is a critical hydroxyl group that replaces a water molecule present in the active site. This hydroxyl group forms hydrogen bonds to the catalytically active aspartates in HIV protease complexes with all hydroxyethylamine inhibitors being the most frequently studied structures in protein data bank and therefore it has been supposed necessary for tight-binding of aspartic protease inhibitors [202]. Type II TSA are also used in the design of inhibitors of other aspartic proteases, such as renin and β -secretase transition state analogs [10b,201]. Very few first generation peptide-based aspartic protease inhibitors have proved clinically useful due to limited oral bioavailability [201]. However, after extensive modification, several HIV protease inhibitors have been launched as AIDS therapeutics (Figure 1.16) [10b,201].

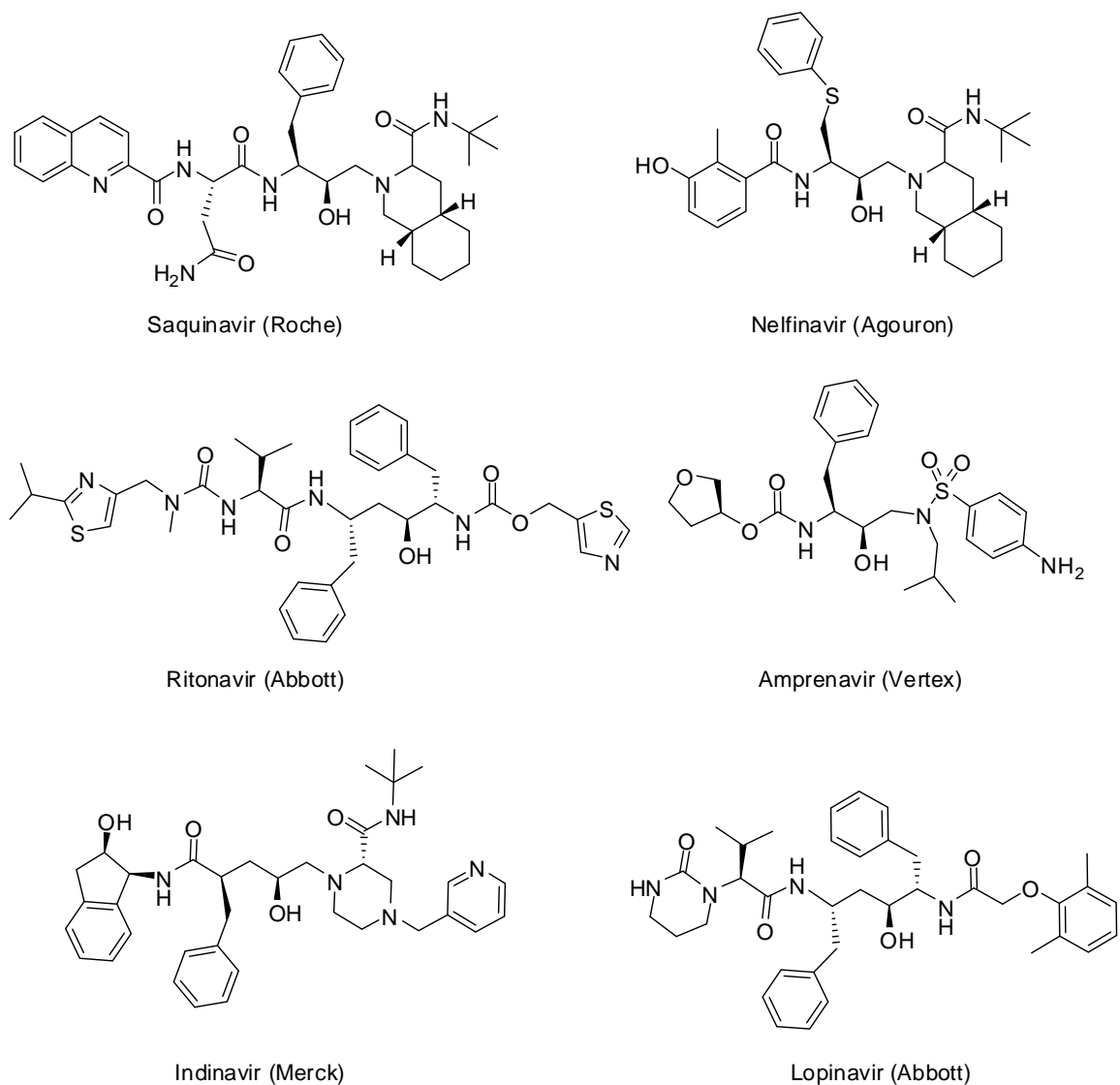


Figure 1.16 Peptide-derived Transition State Analog Inhibitors of HIV Protease Used in AIDS Therapies [10b,201].

Structurally, all proteases have their own preferences for substrates, however the first generation peptide-based transition state analogs, in general, show low selectivity against specific proteases. In addition, these peptide-based transition state analogs have poor oral bioavailability and pharmacokinetics because of their peptide-like nature. In some cases, however, selectivity, bioavailability, and pharmacokinetics (in animal model) have been improved by extensive optimization of the recognition elements and/or formation of macrocycles

of these transition state inhibitors. For example, ketoamide derived macrocyclic inhibitors of HCV NS3 protease are more potent and have much better oral pharmacokinetics in rats than their parent generation (Figure 1.17) [203]. For COPD related serine proteases, several transition state analogs (AE-3763, ONO-6816) of HNE are currently under clinical investigation [192,196]. WNV/DENV peptidyl aldehydes are mostly used for mapping the active sites and crystallographic studies [189,195] and none of them has reached clinical trials.

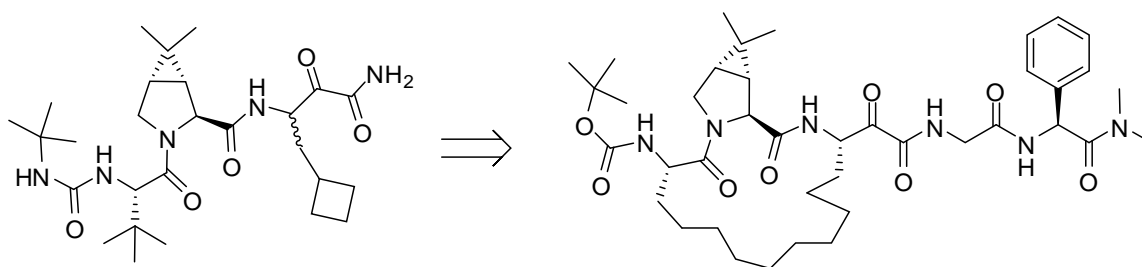


Figure 1.17 An Example of Structure Optimization Leading to Potency and Oral Bioavailability Improvement.

While most of the transition state analog inhibitors exert competitive inhibition with rapid steady state kinetics (Figure 1.18 a), more potent inhibitors of this class may have slow-binding behavior [204]. In such cases, the inhibition undergoes a two-step binding mechanism in which the first step is a simple, rapid equilibrium binding of inhibitor to enzyme to form an encounter complex (EI), and the second step is a slow isomerization of the enzyme to form a higher affinity complex (EI*) (Figure 1.18 b) [204,205]. Two mechanisms have been proposed to explain the slow-binding behavior of transition state analog inhibitors: a) inhibitor binding at an enzyme active site requires the slow expulsion of a tightly bound water molecule and the high affinity of EI complex manifests its slow dissociation; b) there are two conformations for either enzyme or inhibitor in solution, and only one of the conformations is capable of high-affinity interactions

between enzyme and inhibitor [205]. As mentioned earlier, both West Nile and Dengue virus NS2B-NS3 proteases have two conformations. Only the productive conformation binds to the substrate effectively because the NS2B cofactor forms part of the active site (Figure 1.11) [174]. It is possible that an NS2B-NS3 protease TSA inhibitor which mimics the substrate only binds to the productive conformation tightly, therefore showing slow-binding inhibition.

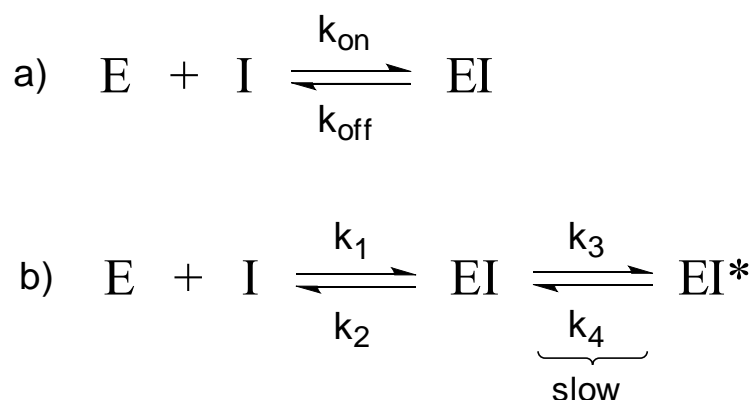


Figure 1.18 Kinetic Scheme for Simple Competitive and Slow-binding Inhibition

1.4.4 Mechanism-based Inhibitors and Acylating Agents

Mechanism-based inhibitors (also called suicide inhibitors) utilize the catalytic machinery of their target protease for inhibition [206]. This class of inhibitors are recognized as substrates and react with their target proteases to form stable enzyme-inhibitor complexes in the process of enzymatic catalysis, leading to the termination of the catalytic cycle. A more specific definition of mechanism-based inhibition is Silverman's definition: a mechanism-based inhibitor is defined as an unreactive compound, whose structure resembles that of either the substrate or product of the target enzyme, and which undergoes a catalytic transformation by the enzyme to form a

reactive species (Figure 1.19, product of step I) that, prior to release from the active site, inactivates the enzyme (Figure 1.19, product of step II) [207]. This definition classifies heterocyclic inhibitors that can form “double-hit” complexes with proteases as mechanism-based inhibitors, while those that form only stable acyl enzyme complexes with a protease as “acylating agents”. Mechanism inhibitors refer to the inhibitors which can form “double-hit” enzyme-inhibitor complexes in this dissertation.

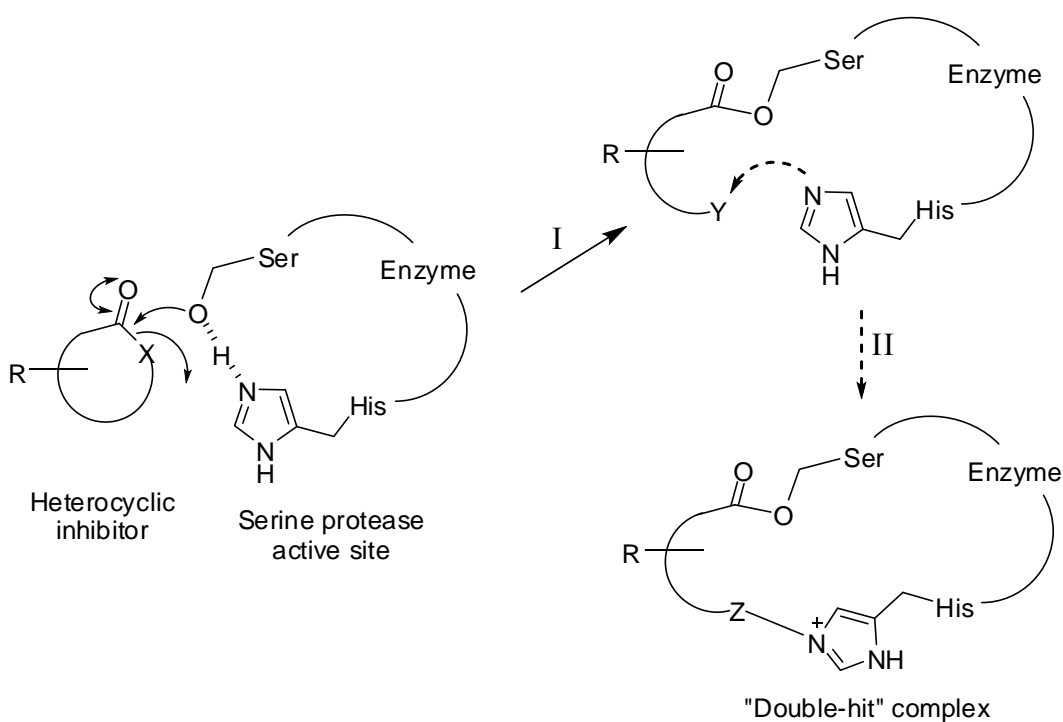
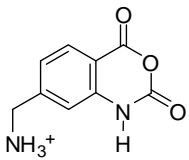
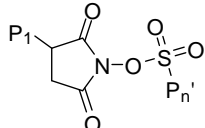
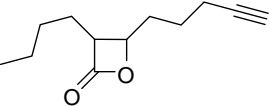
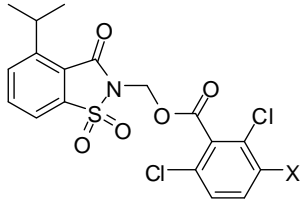
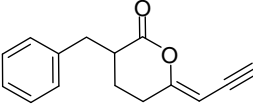
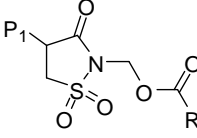
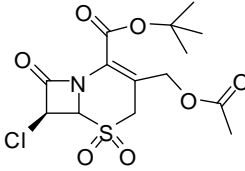
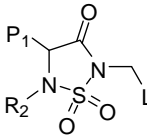
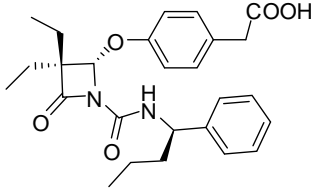


Figure 1.19 Schematic Mechanism of Serine Protease Inactivation by Mechanism-based Inhibitor and Acylating Agents.

A large number of mechanism-based serine protease inhibitors have been reported in the literature. In principle, many heterocyclic inhibitors can serve as mechanism inhibitors, but whether they behave as mechanism inhibitors or acylating agents depends on the experiment

evidence. This can be achieved by determining the X-ray crystal structure [208], high resolution mass spectrum [208] and ^{13}C labeling of inactive enzyme [209]. From an inhibitor design point of view, both mechanism-based inhibitors and acylating agents share many common structure features. Cyclic anhydrides [210], lactones [211,212], lactams [213,214], sulfonyloxy N-hydroxysuccinimides [209], and sulfonamides [215-217] are frequently used as the templates in the design of mechanism-based inhibitors and cyclic acylating agents of serine proteases. Representative mechanism-based inhibitor and acylating agents are listed in Table 1.9.

Table 1.9 Representative Serine Protease Mechanism-based Inhibitors and Acylating Agents

Structure	Target	Ref.	Structure	Target	Ref.
	Thrombin, Trypsin	[210]		α -CT, HNE	[209]
	Caseinolytic protein protease	[211]		HNE	[215]
	HNE	[212]		HNE, Cat G	[216]
	HNE	[213]		HNE, Pr 3	[217]
	HNE	[214]			

Most heterocyclic serine protease inhibitors inhibit their targets by first acylating the active site oxygen, then unmasking a latent inhibitory functionality to hinder the deacylation step (“double-hit”). An example of mechanism-based HNE inhibitor employing such an inhibitory strategy is illustrated in Figure 1.20 [209]. Human neutrophil elastase first catalyzes the ring-opening of the succinimide with its Ser195 acylated by the inhibitor, followed by a Lossen rearrangement with formation of an electrophilic isocyanate. The His57 imidazole is then acylated by the isocyanate, resulting in a “double-hit” enzyme-inhibitor complex.

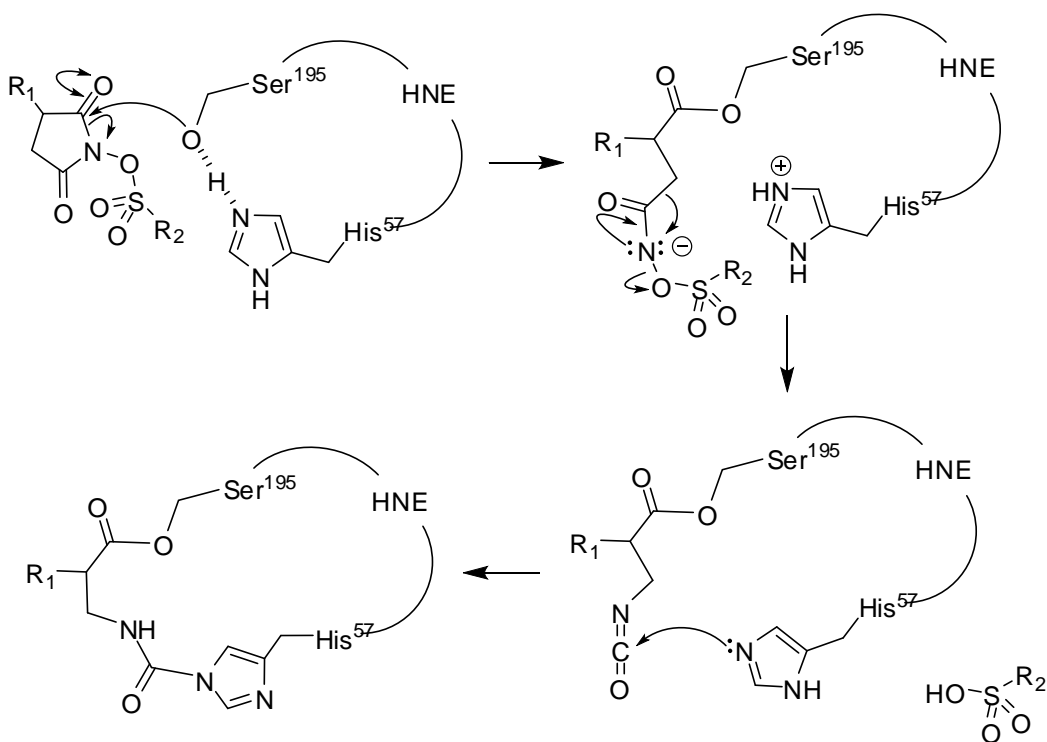
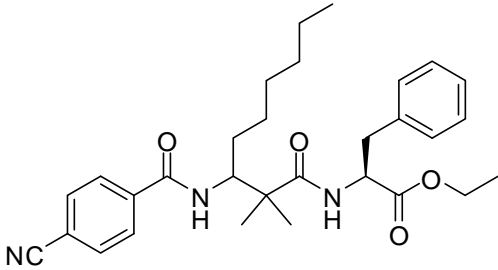
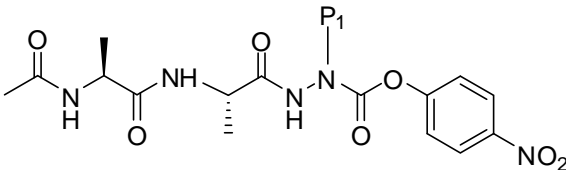
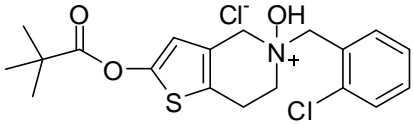
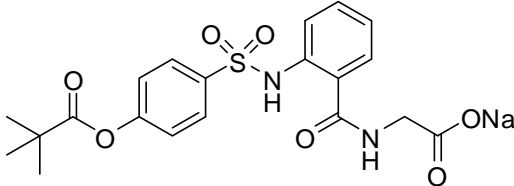
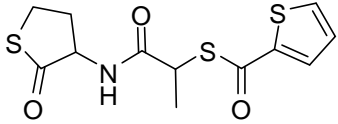


Figure 1.20 Schematic Mechanism of HNE Inactivation by Sulfonyloxy Succinimide.

Examples of acyclic acylating agents include symmetric anhydrides [218], azapeptides [219] and esters [218,220] (Table 1.10). Symmetric anhydrides are too reactive for use in *in vivo* studies [218] and are usually modified to ester to improve the stability. Acyclic acylating agents

are commonly believed to lack selectivity in protease family [218], yet there are several examples which show a high preference towards specific protease. The inhibitory preference of azapeptide inhibitors can be altered to selectively inhibit only either HNE or PPE by varying the size of P1 substitution in very high efficiency and used for HNE and PPE titration [219]. SR26831 is a very selective inhibitor of HNE over pepsin, collagenase, trypsin, α -chymotrypsin, factor Xa, plasmin, kallikrein, cathepsins B, C, D and G and thrombin [220]. The other two similar HNE inhibitors, Silvestat sodium hydrate (ONO-5046) and Midesteine (MR-889), with good stability and specificity to HNE have been considered as most promising drug candidates for the treatment of COPD [192a]. Specifically, *Sivelestat* has been launched in Japan in 2002 to treat acute lung injury associated with systemic inflammatory response syndrome and *Midesteine* is currently in pre-registration for the treatment of COPD in Italy [10b]. All these acylating agents act as substrates for HNE, forming a stable complex, thereby potently and selectively inhibiting its hydrolytic process. In the first step, the catalytic site Ser195 hydroxyl group of HNE attacks the reactive carbonyl carbon of the inhibitor, followed by the formation of a tetrahedral intermediate. Following this, the tetrahedral intermediate collapses and forms a relatively stable acyl-enzyme complex, thus potently inactivating HNE [192a].

Table 1.10 Representative Acyclic Acylating Agents of Serine Protease

Structure	Target	Reference
	HNE, Cat G α -CT	[218]
	HNE, PPE	[219]
 <p>SR26831</p>	HNE	[220]
 <p>Sivelestat sodium hydrate (ONO-5046)</p>	HNE	[192]
 <p>Midesteine (MR-889)</p>	HNE	[192]

Heterocyclic mechanism-based inhibitors and acylating agents generally have higher specificity than other classes of inhibitors, which is largely due to their structural rigidity. These “drug-like” mechanism-based inhibitors or acylating agents with high selectivity are expected to be favorable drug candidates, however, only very few β -lactams [214,215] and acylating agents [192] are orally active and are currently in clinical trials or have been launched in some countries. The main issue with these classes of inhibitors is lack of chemical stability or *in vivo* stability.

The kinetics behavior of mechanism-based inhibitor and acylating agents is similar (shown in Figure 1.21). Enzymes inhibited by these inhibitors can regain their activity very slowly. Potent inhibitors of this kind can lead to virtually stoichiometric inhibition. Enzyme activity can be inhibited completely using very low concentrations. Kinetics studies of such potent inhibitors use the progress curve method. Compared to slow-binding inhibitors, mechanism-based inhibitors have much rapid inactivation rate and require much lower concentration to achieve the same inhibition.

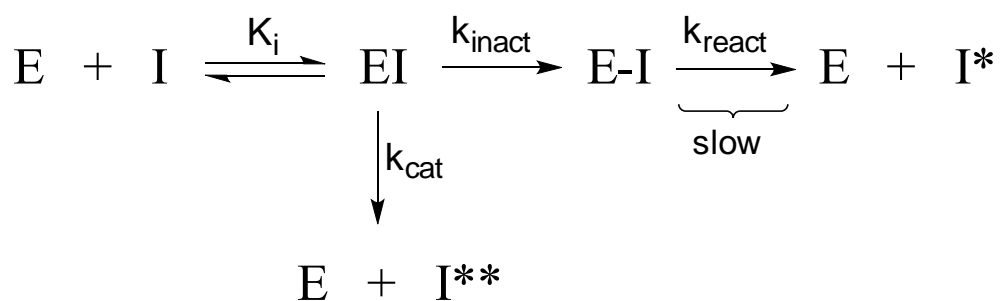


Figure 1.21 Kinetic Scheme for Mechanism-Based Inhibitors and Acylating Agents

CHAPTER 2

RESEARCH GOALS

2.1 Development of Inhibitors for COPD Related Targets

COPD is a multi-factorial disorder which involves the interplay of multiple events and mediators, including an oxidant/antioxidant imbalance, apoptosis, a protease/antiprotease imbalance and chronic inflammation. The molecular mechanisms which underline initiation and progression of the disorder are currently poorly understood, however, an array of proteases (HNE, Pr 3, Cat G, granzyme B, Caspases, MMPs) are believed to contribute to the pathophysiology of the disorder. Specific enzyme inhibitors are being extensively studied against individual enzymes, however, the multi-factorial nature of COPD suggests that multi-functional molecules designed to disrupt the aforementioned cycle of events by inhibiting more than one enzyme or target may be more effective in alleviating the disorder (Figure 1.4).

Mechanism-based inhibitors against HNE have been extensively investigated in our group [216, 217] and the various templates used primarily reflected the preferences of HNE subsites, mainly on S pockets. These inhibitors have revealed that HNE can tolerate fairly large groups in the primary subsite (S1), and also in the recognition element projecting toward the primed subsites of these HNE inhibitors are released during the enzyme inactivation process. This opens an opportunity for the design of inhibitors which incorporate a second known inhibitor against other targets to HNE inhibitor template(s), serving as multi-functional inhibitors. These multi-functional inhibitors could potentially serve as a drug delivery system for inhibitors which have poor pharmacokinetics. For example, MMPs usually employ a hydroxamic acid moiety which is difficult to deliver to the target enzymes due to poor selectivity. However, no multi-functional molecules against proteases have been reported so far.

HNE and Pr 3 are neutrophil-derived serine proteases which play an important role in COPD. The substrate specificity of these two enzymes has been fully explored. HNE mechanism-based inhibitors/acylating agents are highly efficient and specific toward the target enzyme, but the chemical and/or in vivo instability and high reactivity increase the potential clinical risk, which limits their practical use in the clinic. Six reversible heterocyclic inhibitors developed in pharmaceutical companies have been recently patented as potent HNE inhibitors (Chapter 1), however, clinical studies with these inhibitors remain unclear. Several transition state analogs of HNE have been reported, but the peptide nature of the majority of these inhibitors limits their advance to clinical use. In addition, currently no non-covalent inhibitor or transition state inhibitor against Pr 3 has been reported. Consequently, our goal is to develop novel heterocyclic “drug-like” molecules which serve as *reversible* inhibitors for HNE and Pr3. The design of small heterocyclic organic molecules which only rely on non-covalent interactions to achieve inhibition is a challenging task.

2.2 Development of Competitive Inhibitors for WNV/DENV NS2B-NS3 Protease

The X-ray crystal structures of WNV NS2B-NS3 protease-peptide inhibitor complex and NS2B-NS3 pro-aprotinin complex have been reported at the protein data bank (pdb code: 2fp7 and 2ijo), however the development of WNV NS2B-NS3 protease reversible inhibitors has not been successful. Peptide-based aldehyde inhibitors are only used for crystal structure determination and in probing subsites. The high reactivity and the requirement for multiple positive charges and peptide backbone exclude them from clinical use due to low selectivity, poor permeability and lack of oral bioavailability. In contrast, small heterocyclic organic molecules have many advantages for the design of WNV NS2B-NS3 protease inhibitors: a) these

“drug-like” molecules are chemically robust; b) stable to metabolism; c) easy to optimize the pharmacokinetics; d) good oral bioavailability and etc. No potent heterocyclic reversible competitive inhibitors have been reported thus.

The X-ray crystal structures of WNV NS2B-NS3 protease and NS2B-NS3 pro-aprotinin complex also revealed that there are two conformations, productive and nonproductive conformations, for this two-component protease (shown in Figure 1.11). The interface between the NS2B and NS3 proteins relies primarily on hydrophobic interactions, which can interact with relatively hydrophobic molecules that behave as allosteric inhibitors. Although both protease substrates and peptide inhibitors suggest a preference for the presence of multiple basic substitutions, the X-ray crystal structure of a tetra-peptide inhibitor bound to WNV protease show that the hydrophobic part of Lys and Arg may also contribute the inhibitor binding. The core of the active site is fairly hydrophobic and therefore having multiple basic substitutions is not strictly required in the design of WNV protease inhibitor.

DENV NS2B-NS3 protease shares a very similar active site geometric complementarity and substrate specificity with WNV NS2B-NS3 protease, and it is also a two-component with NS2B as a cofactor. Accordingly, the same strategy is applied in the design of inhibitors of DENV NS2B-NS3 protease.

2.3 Strategies and Methodologies

The enzyme inhibitor design described in this dissertation is based on the published SAR of mechanism-based inhibitors of HNE, and X-ray crystal structures of the protein inhibitor-enzymes complexes for HNE and NS2B-NS3 protease of WNV and DENV. The following strategies and methodologies have been used in these studies:

- a) Use a structure-based approach to design novel inhibitor templates;
- b) Use combinatorial chemistry and click chemistry approaches to explore the affinity and specificity of these novel inhibitors for their target enzymes;
- c) Conduct kinetic and structure-activity relationship studies for the novel classes of inhibitors in order to search for a rational approach for optimizing the potency of the inhibitors of serine proteases;
- d) Use molecular simulations to fine tune the design strategies in structural optimization.

Inhibitor design is also under the guidance of Lipinski's Rule of Five [221]: no more than 5 hydrogen bond donors, no more than 10 hydrogen bond acceptors, molecular weight under 500 Daltons, and $\log P$ of less than 5.

CHAPTER 3

DUAL FUNCTION INHIBITORS OF COPD-RELEVANT SERINE PROTEASES

3.1 Inhibitor Design Rationale

A large number of 1, 2, 5-thiadiazolidin-3-one 1, 1 dioxides derivatives developed in our group have been found to function as potent mechanism-based inhibitors against COPD related serine proteases, in particular HNE (general structure (I) and representative HNE mechanism-based inhibitors are shown in Figure 3.1) [216,217,222]. Molecular modeling studies have shown that all of these inhibitors bind similarly to the active site of HNE with hydrophobic P₁ residue (mainly isobutyl and benzyl) nestled at the S1 pocket which is defined by the main chains of Phe192 and Phe215, and the side chains of Val190, Val216 and Phe192. Either a benzyl or a

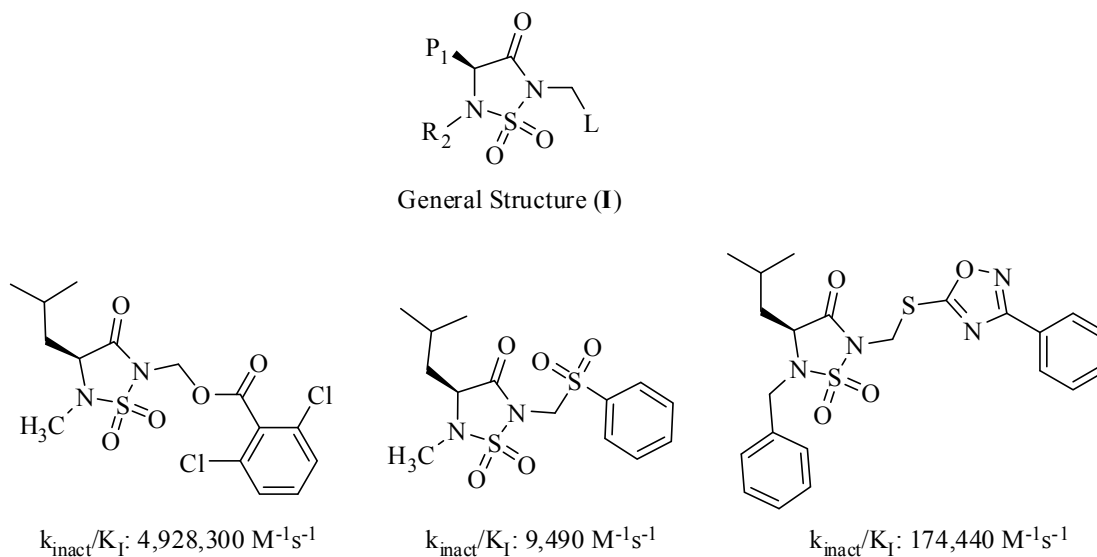


Figure 3.1 HNE Mechanism-Based Inhibitors

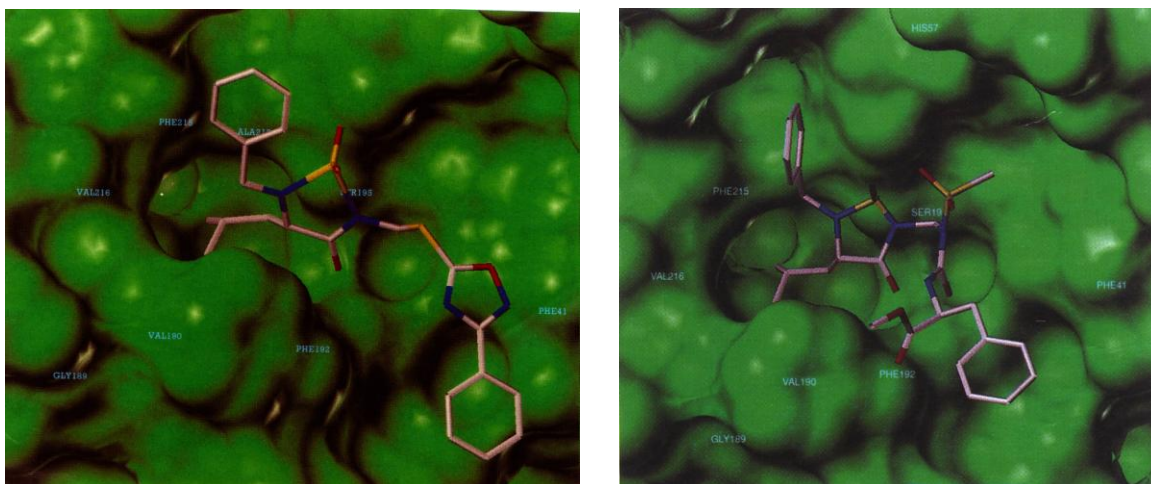


Figure 3.2 Mechanism-Based Inhibitors Docked into the HNE Active Site.

methyl group at R₂ interacts with the S₂ pocket of HNE (shown in Figure 3.2). The presence of -L^{\prime} serves as a leaving group which drives the inactivation of the enzyme (a postulated mechanism is shown in Figure 3.3)[217]. NMR studies using a double ¹³C labeled mechanism-based inhibitor based on scaffold (I) strongly supported the proposed mechanism of enzyme inactivation [217]. More importantly, optimal inhibition of HNE is attained when the leaving group has a low pK_a, such as a carboxylic acid. High inhibition was also observed when a range of structurally diverse leaving groups -L^{\prime} (accommodated in the S' subsites) was used [217]. The lack of specificity in the S' subsites of HNE can be exploited in the design of the inhibitor II by replacing -L^{\prime} with a second inhibitor (Figure 3.4).

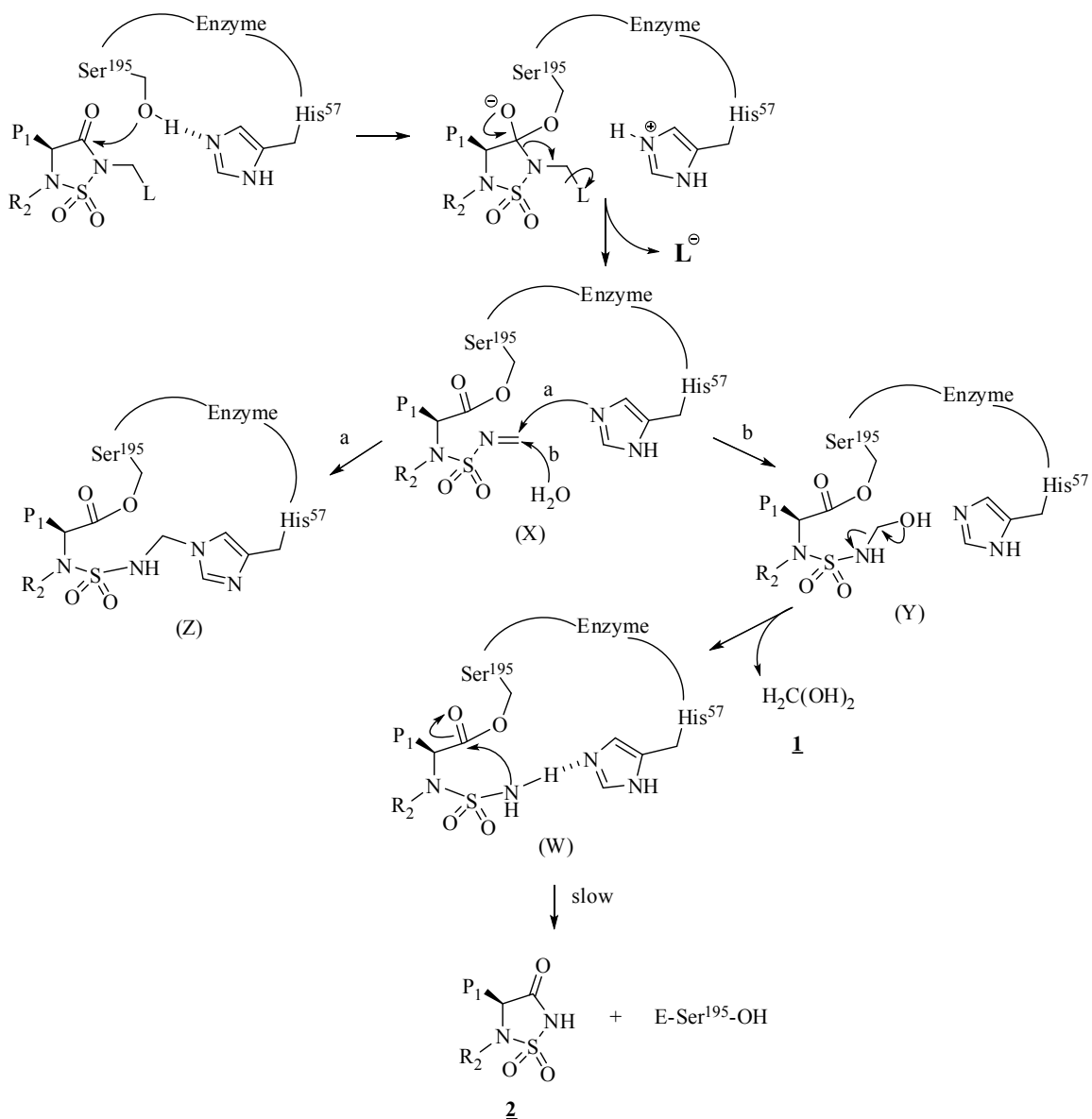
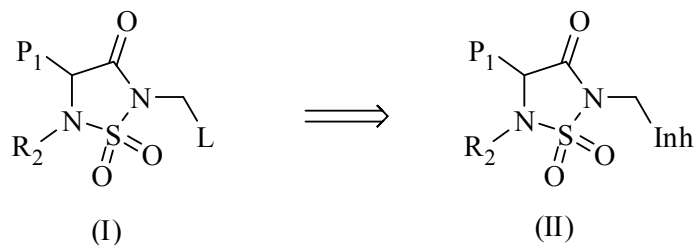


Figure 3.3 Postulated Mechanism of Protease Inactivation by Inhibitor I

Based on the above observations, we speculated that the replacement of leaving group $-L$ with an inhibitor, such as a caspase inhibitor (Asp side chain is used in P1 residue) or MMP-12 inhibitor, would result in a dual function inhibitor (Figure 3.4), which could potentially inhibit both HNE and caspase(s) or both HNE and MMP-12, thereby inhibiting elastin degradation, apoptosis and inflammation.



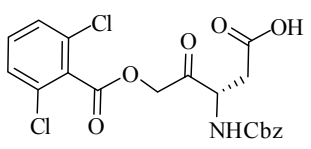
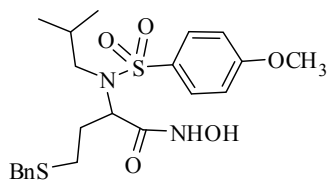
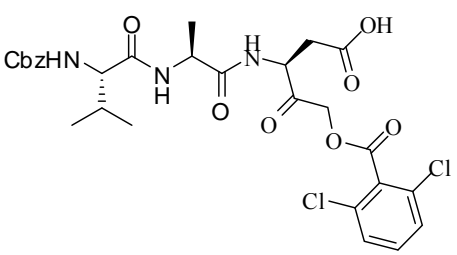
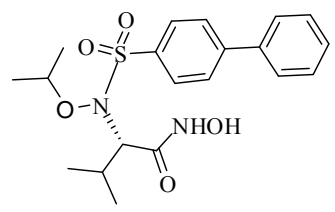
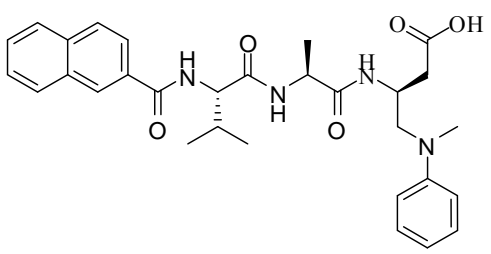
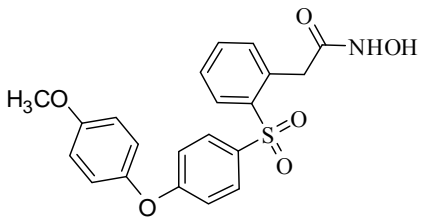
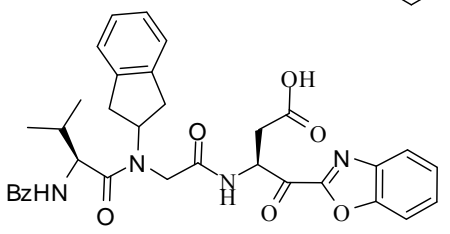
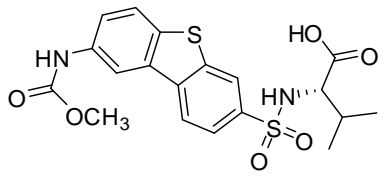
L: leaving group; Inh: second inhibitor

Figure 3.4 Dual Function Inhibitor Design Rationale

In COPD, caspase-1 is believed to be a pro-inflammatory enzyme which prefers an aspartic acid residue at P₁ position (selected caspase-1 inhibitors are shown in Table 3.1) [223-225]. If the leaving group “L” is replaced by a caspase-1 inhibitor, the resulting inhibitor would be expected to inhibit both HNE and caspase-1, thus regulating both elastase activity and inflammation. MMP-12 is another important enzyme that is involved lung connecting tissue degradation. The majority of potent MMP-12 inhibitors are hydroxamic acids (selected MMP-12 inhibitors are shown in **Table 3.1**) [226-228]. Likewise, these hydroxamic acids can also be used to replace the leaving group “L” and the resulting dual function inhibitors, in principle, would inhibit both HNE and MMP-12, thereby inhibiting elastin degradation more effectively. Hydroxamic acid inhibitors usually have shortcomings associated with selectivity and difficulty of delivery. We envisaged that dual function inhibitor(s) may improve the selectivity and delivery problems since the MMP-12 inhibitor will be released in the site where MMP-12 accumulates. Since both HNE and MMP-12 are important in lung tissue degradation, we reasoned that it would be more efficacious in ameliorating lung injury by using a dual functional inhibitor. This dissertation is focused on establishing proof of concept, therefore a simple caspase-1 inhibitor and a more synthetically accessible MMP-12 inhibitor were used for dual function inhibitor studies. Such a strategy can be used to construct more complex inhibitors with a carboxylic acid or hydroxamic

acid as part of the inhibitor structure, which are common for caspases and MMP inhibitors, respectively.

Table 3.1 Selected Caspase-1 Inhibitors and MMP-12 Inhibitors

Caspase-1 Inhibitor	Reference	MMP-12 Inhibitor	Reference
	[1]		[4]
	[1]		[5]
	[2]		[5]
	[3]		[6]

Pr 3 has very similar primary substrate specificity as HNE (Table 1.5) with the S1 pocket slightly smaller than HNE; therefore a slightly smaller hydrophobic substitution (*n*-propyl) was used as the P₁ residue. As a result, the dual function inhibitor with *n*-propyl at P1 residue would potentially inhibit HNE, Pr3 and the third enzyme. Mechanism-based inhibitor I covalently modifies the active site serine residue (Ser 195), the bound enzyme regains activity rapidly when

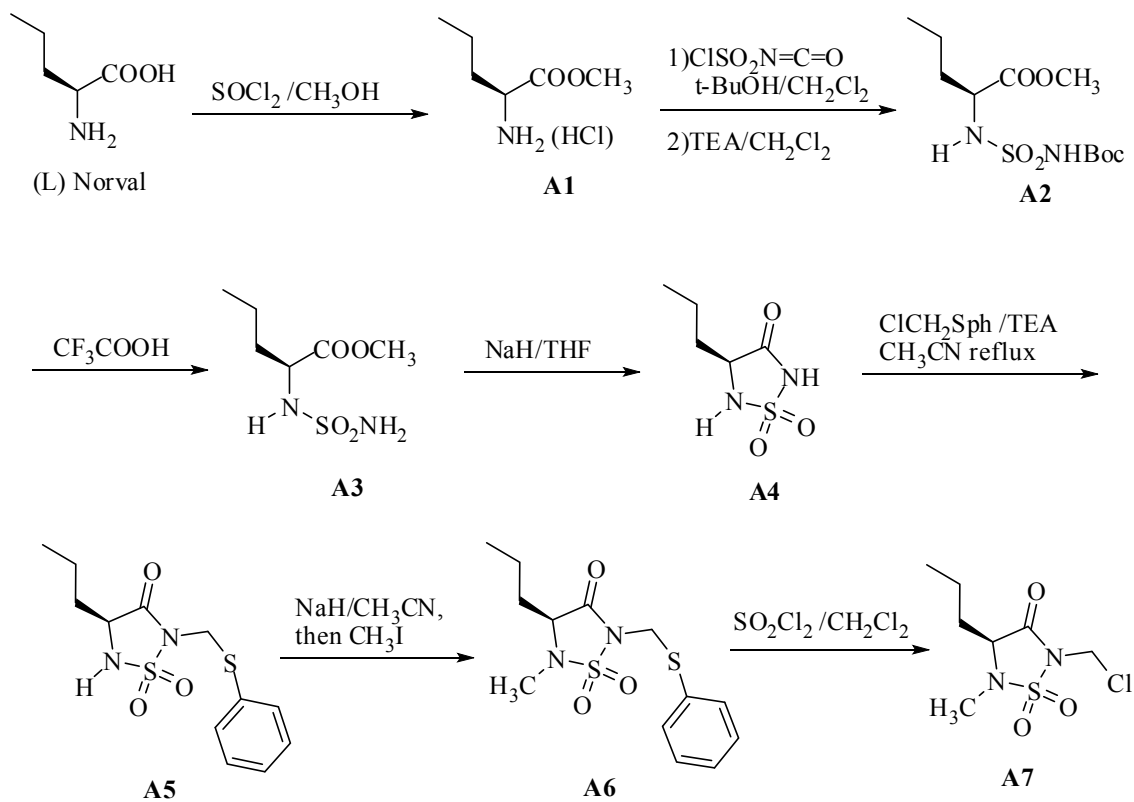
the R₂ substitution is benzyl group whereas an optimal stability of the resulting enzyme-inhibitor acyl complex(es) was observed when a methyl substitution at R₂ was used [217]. Based on the above considerations, an *n*-propyl and a methyl group were used at P₁ and R₂ substitutions, respectively.

3.2 Results and Discussions

3.2.1 Synthesis of Dual Function Inhibitors

3.2.1.1 Synthesis of the 1, 2, 5-Thiadiazolidin-3-One 1, 1 Dioxide Scaffold

The key intermediate **A7** was readily prepared via treatment of (L)-norvaline with thionyl chloride in methanol, and the resulting methyl ester hydrochloride salt **A1** was reacted with tert-butyl chlorosulfonylcarbamate, freshly prepared by adding *tert*-butanol into chlorosulfonyl

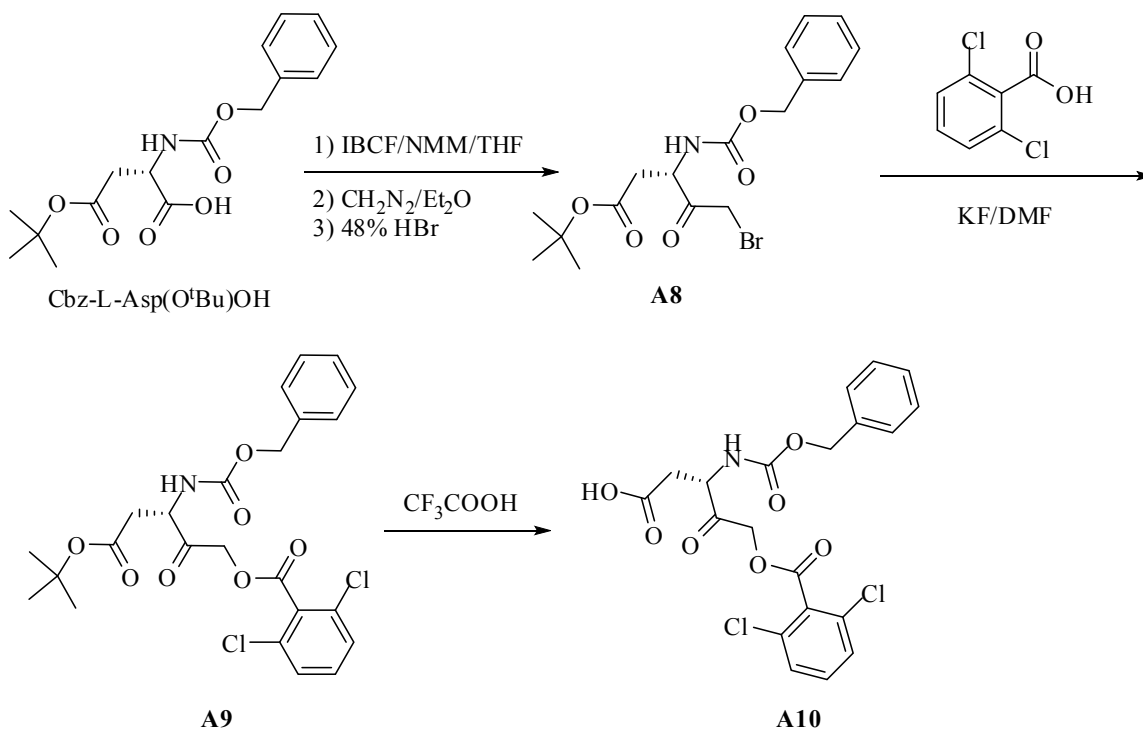


Scheme 3.1 Synthesis of the 1, 2, 5-Thiadiazolidin-3-One 1, 1 Dioxide Scaffold

isocyanate in the presence of TEA, to give compound **A2**. The Boc protection was then removed with trifluoroacetic acid, followed by a cyclization using NaH in THF, yielding a cyclic compound **A4**. The compound **A4** was forwarded to final chloromethyl compound **A7** via an alkylation with chloromethyl phenyl sulfide in the presence of TEA, followed by methylation with iodomethane after compound **A5** was treated with NaH in acetonitrile. Finally, the phenylthio group was replaced with chloride using sulfuryl chloride (Scheme 3.1).

3.2.1.2 Synthesis of Caspase-1 Inhibitor **A10**

Representative caspase-1 inhibitors are shown in Table 3.1. A simple amino acid-based caspase-1 (ICE) affinity label Z-Asp-CH₂DCB (DCB = (2,6-dichlorobenzoyl)oxy) has been shown to rapidly inactivate caspase-1 with a $k_{\text{obs}}/[\text{I}]$ of $7,100 \text{ M}^{-1}\text{s}^{-1}$. Much higher activity was obtained when two additional amino acids were attached to the N-terminal of this inhibitor (Z-Val-Ala-Asp-CH₂DCB has a $k_{\text{obs}}/[\text{I}]$ of $406,700 \text{ M}^{-1}\text{s}^{-1}$). More recently, potent non-covalent inhibitors and transition state analogs of caspase-1 have also been reported. In this dissertation, Z-(L)-Asp-CH₂DCB was used as a model in the investigation of dual function inhibitors. Z-(L)-Asp-CH₂DCB was prepared according to the literature [223]. The synthetic scheme is shown in Scheme 3.2. Briefly, Z-(L)-Asp(O^tBu)OH was activated using isobutyl chloroformate in the presence of N-methylmorpholine followed by treatment with diazomethane to form the diazoketone which was then treated with 48% hydrobromic acid to give bromomethyl ketone **A8**. The bromine was replaced by a 2,6-dichlorobenzoyl group using 2,6-dichloro-benzoic acid in the presence of potassium fluoride in DMF. The final product **A10** was obtained by removal of tert-butyl ester using trifluoroacetic acid.

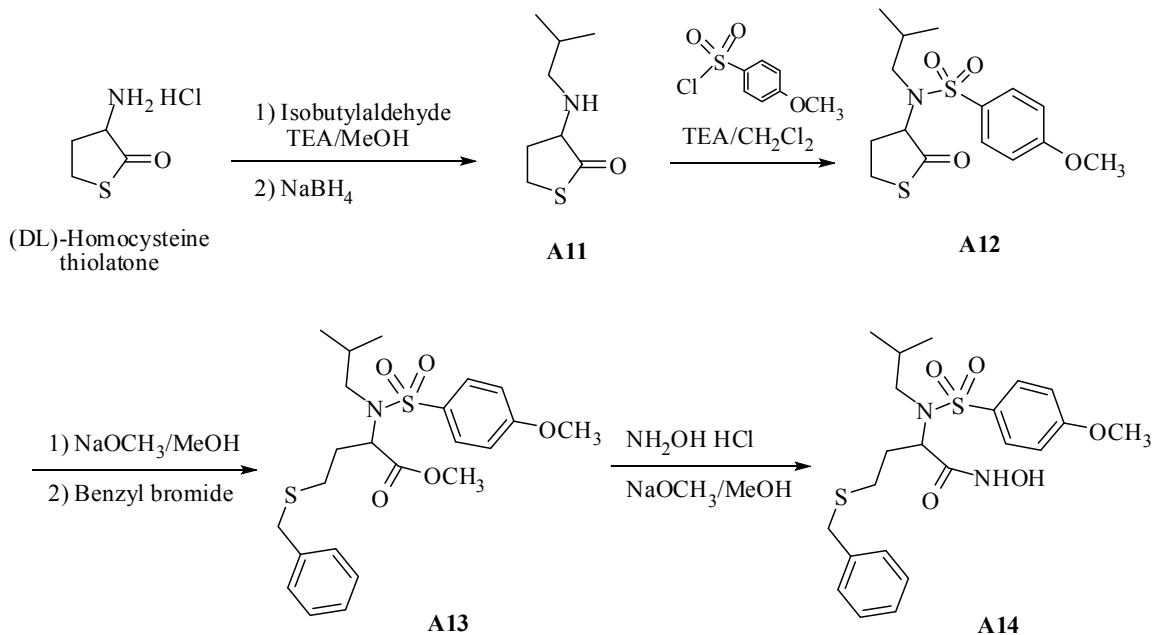


Scheme 3.2 Synthesis of Caspase-1 Inhibitor

3.2.1.3 Synthesis of MMP-12 inhibitor A14

As previously mentioned, the majority of MMP inhibitors are hydroxamic acids and several examples are shown in Table 3.1. It should be noted that an inhibitor with a carboxylate-chelating group has been developed recently which also showed potent inhibition toward MMP-12 (Table 3.1). The first MMP-12 inhibitor listed in Table 3.1 was chosen because it is synthetically more accessible. This inhibitor was synthesized according to the procedure of Hanessian et al. (shown in Scheme 3.3) [226]. (DL)-homocysteine thiolactone was treated with isobutyl aldehyde in the presence of triethylamine followed by reduction with sodium borohydride to give compound **A11**, which was coupled with 4-methoxyphenyl sulfonyl chloride. The resulting product **A12** was subjected to ring opening with sodium methoxide followed by alkylation with benzyl bromide. Finally, the methyl ester was transformed to the

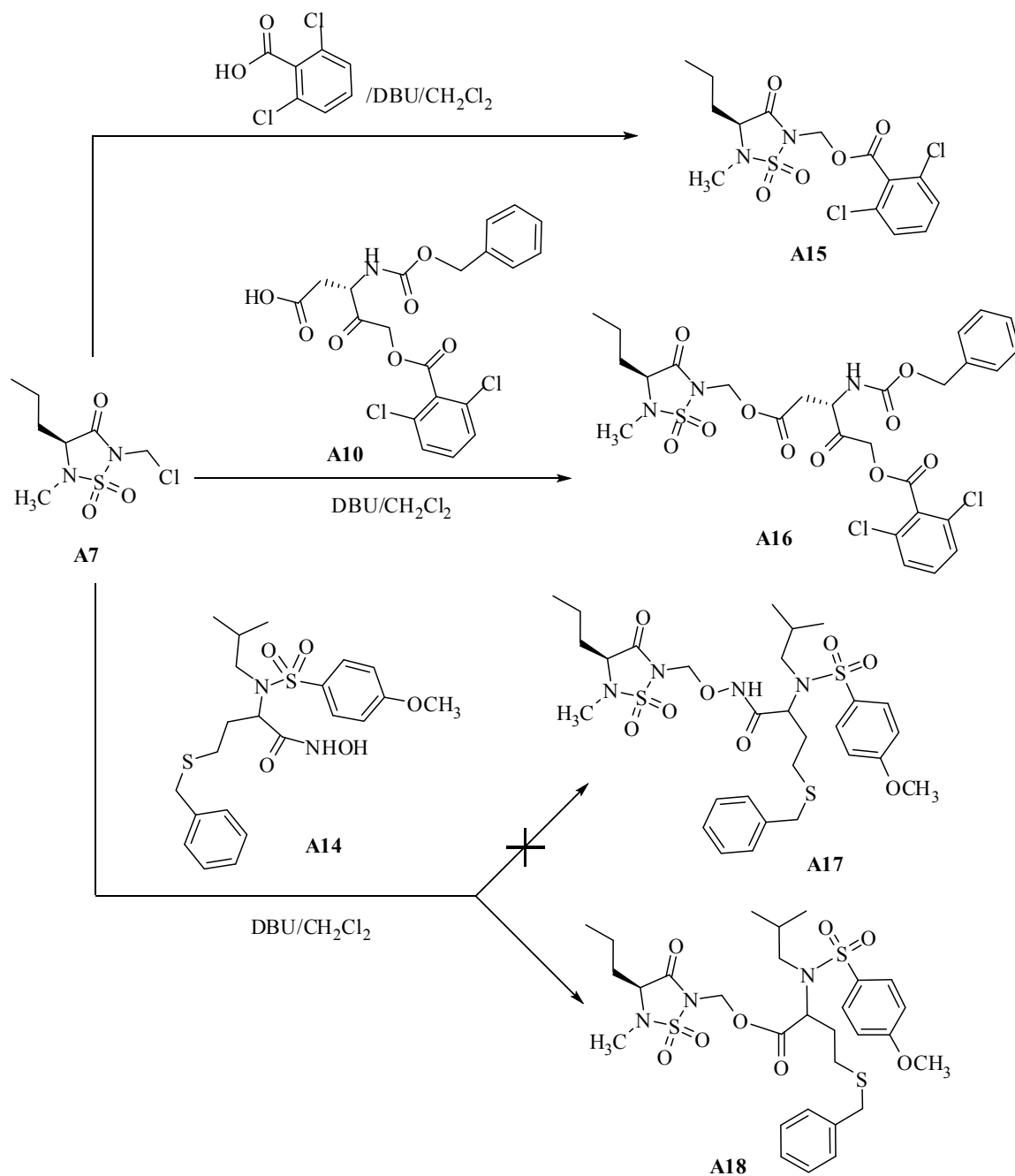
hydroxamic acid using hydroxylamine hydrochloride in the presence of sodium methoxide.



Scheme 3.3 Synthesis of MMP-12 Inhibitor

3.2.1.4 Synthesis of Dual Function Inhibitor by Simple Alkylation

The preparation of dual function inhibitors is shown in Scheme 3.4. Generally, the anion was generated using DBU followed by addition of chloromethyl compound **A7**. In order to confirm the feasibility of replacement of P₁, R₂ residues with *n*-propyl, methyl groups and the mechanism of action in the inactivation of HNE, a simple 2,6-dichlorobenzoate was first used to replace the leaving group P^- . Unexpectedly, the reaction of **A14** yielded a compound **A18**, whose structure was confirmed using high resolution mass spectrometry and an alternative method shown in **3.2.1.5**.



Scheme 3.4 Synthesis of Dual Function Inhibitors

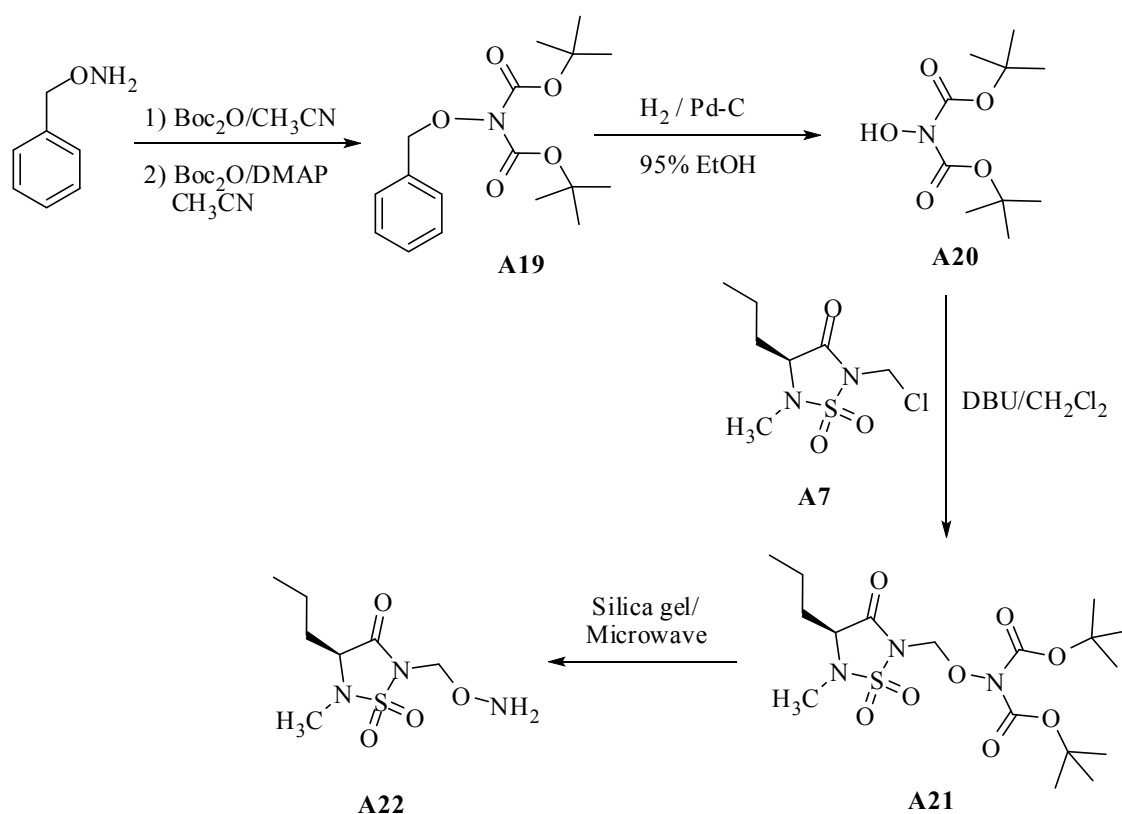
3.2.1.5 Synthesis of HNE/MMP-12 Dual Function Inhibitor Using Acid/Amine Coupling

To overcome the difficulty in the O-alkylation of **A14**, an alternative procedure was used. The amino intermediate and the corresponding acid were prepared and the target compound **A17**

was synthesized using a typical acid/amine coupling (shown in Scheme 3.5, Scheme3.6).

3.2.1.5.1 Amine Synthesis

O-Benzyl hydroxylamine was treated with di-tert-butyl dicarbonate in the presence of DMAP, yielding a di-N-Boc protected amide **A19**. The benzyl group was removed by catalytic hydrogenation followed by alkylation with **A7** yielded compound **A21**, which was then deprotected using microwave/silica gel (Scheme 3.5)

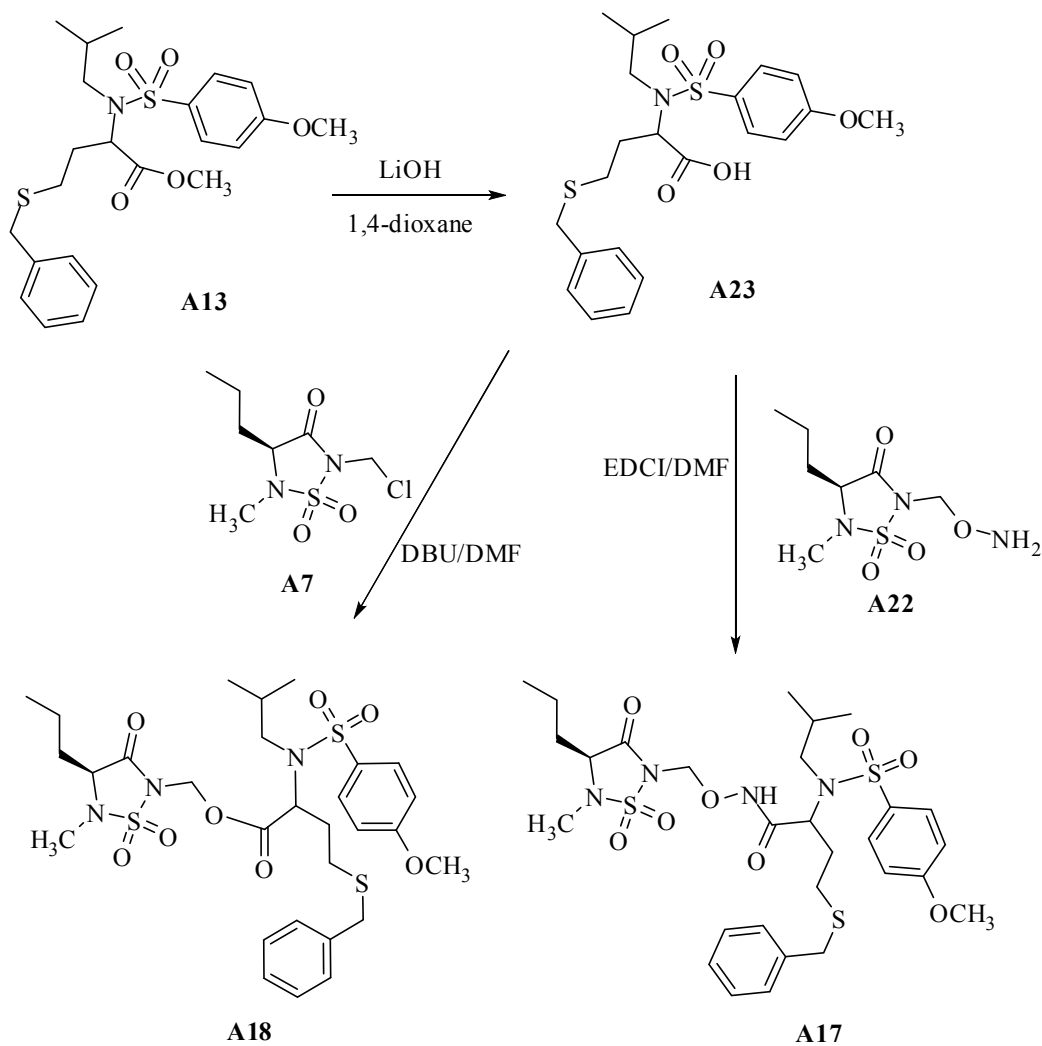


Scheme 3.5 Synthesis of Hydroxamine Intermediate

3.2.1.5.2 Acid/Amine Coupling and Ester Formation

Acid **A23** was readily prepared by hydrolyzing **A13** using lithium hydroxide aqueous dioxane. The acid was used in an alkylation to confirm the structure of the product obtained

earlier (Scheme 3.4). The designed dual function inhibitor was synthesized by a standard acid/amine coupling using EDCI (shown in Scheme 3.6).



Scheme 3.6 Synthesis of Dual Function Inhibitors

3.2.2 Biochemical Investigation on P₁ and R₂ Substitutions

Incubation of inhibitor A15 with HNE led to rapid, time-dependent, irreversible loss of enzymatic activity (Figure 3.5). The bimolecular rate constant k_{inact}/K_i , an index of inhibitor

potency, was determined using the progress curve method [217] and found to be $8.9 \times 10^6 \text{ M}^{-1}\text{s}^{-1}$ (Figure 3.6). The k_{on} and k_{off} values were $24,290 \text{ M}^{-1}\text{s}^{-1}$ and $1.33 \times 10^{-4} \text{ s}^{-1}$, respectively, yielding

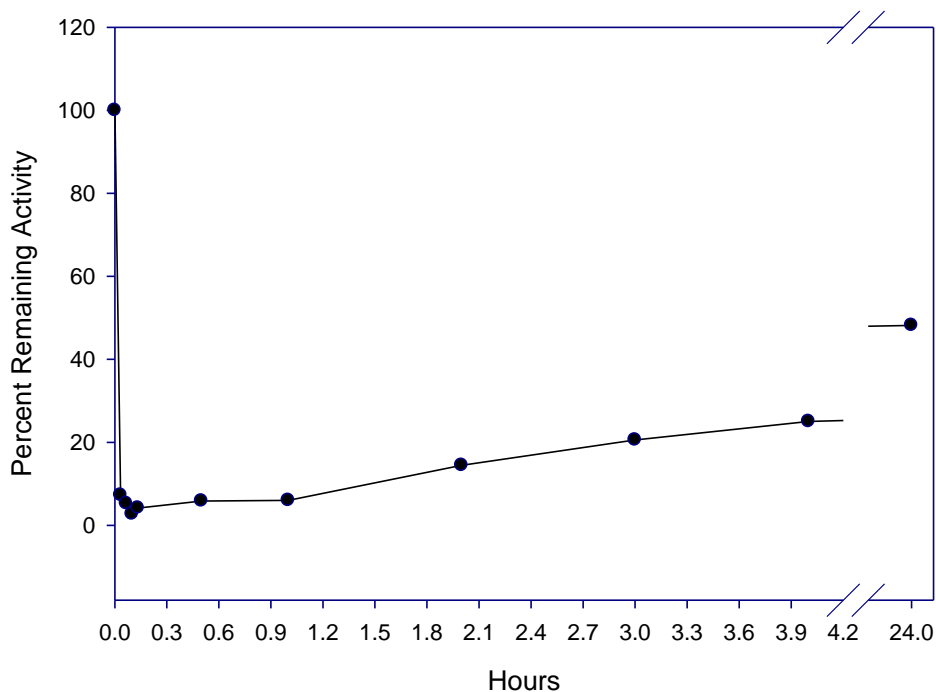


Figure 3.5 Time-Dependent Loss of Enzymatic Activity with A15. Percent remaining activity versus time plot obtained by incubating inhibitor A15 (700 nM) with human neutrophil elastase (700 nM) in 0.1 M HEPES buffer containing 0.5 M NaCl, pH 7.25, and 1% DMSO. Aliquots were withdrawn at different time intervals and assayed for enzymatic activity using MeOSuc-AAPV p-NA by monitoring the absorbance at 410 nm.

an apparent inhibition constant (K_i) of 5.47 nM [208]. These values compare very favorably with “gold standard” inhibitors of HNE reported in the literature. Compound A15 was also found to inhibit human leukocyte proteinase 3 ($k_{\text{obs}}/[I]$ $3020 \text{ M}^{-1} \text{ s}^{-1}$), however, it was devoid of any inhibitory activity toward human leukocyte cathepsin G and human thrombin at an $[I]/[E]$ ratio of 250 and a 30 min incubation time. Interestingly, incubation of A15 with bovine trypsin led to time-dependent inactivation of the enzyme despite the absence of a basic P_1 residue in the inhibitor.

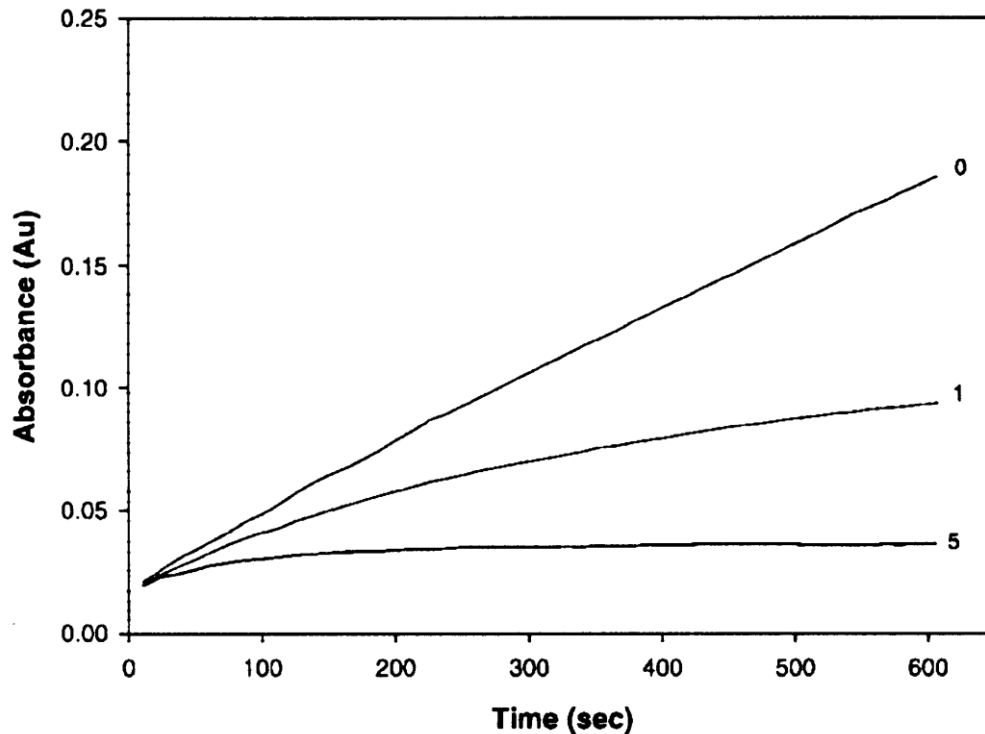


Figure 3.6 Progress Curves for the Inhibition of Human Neutrophil Elastase (HNE) by Inhibitor A15. Absorbance was monitored at 410 nm for reaction solutions containing 10 nM HNE, 105 μ M MeOSuc-AAPV *p*-nitroanilide, and the inhibitor at the indicated inhibitor to enzyme ratios in 0.1 M HEPES buffer containing 0.5 M NaCl, pH 7.25, and 2.5% DMSO. The temperature was maintained at 25 $^{\circ}$ C, and reactions were initiated by the addition of enzyme.

3.2.3 X-ray Crystallographic Studies/Mechanism of Action of I

The precise mechanism of action of this class of mechanism-based serine protease inhibitors has been in question due to a lack of relevant structural information. Although earlier studies [217] using a 13 C-labeled derivative of **I** (P_1 = benzyl, R_2 = methyl, L = SO_2Ph) led to the isolation and characterization of two low molecular weight products **1** and **2** (P_1 = benzyl, R_2 = methyl), which suggested that path b (Figure 3.3) was operative, definitive evidence in support of the mechanism shown in Figure 3.3 was lacking. Thus, a crystal structure of a derivative of **I** with human neutrophil elastase was obtained to determine its mode of binding and to establish unequivocally the mechanism of action of **I**. It was initially envisioned that the structure of the

enzyme–inhibitor complex would reveal whether formation of intermediate **X** would subsequently lead to enzyme–inhibitor complex **Z** via Michael addition of the imidazole of His57 to the sulfonyl imine conjugated system in **X** (“double hit” mechanism) or whether **X** would undergo Michael addition with water to yield species **Y** that then collapses to form acyl enzyme **W**.

Quite unexpectedly the X-ray crystal structure obtained by soaking crystals of HNE with inhibitor **A15** was determined to be that of intermediate **X** (Figure 3.7). The enzyme-inhibitor complex shows the oxygen of the active site serine (Ser195) to be covalently bound to the

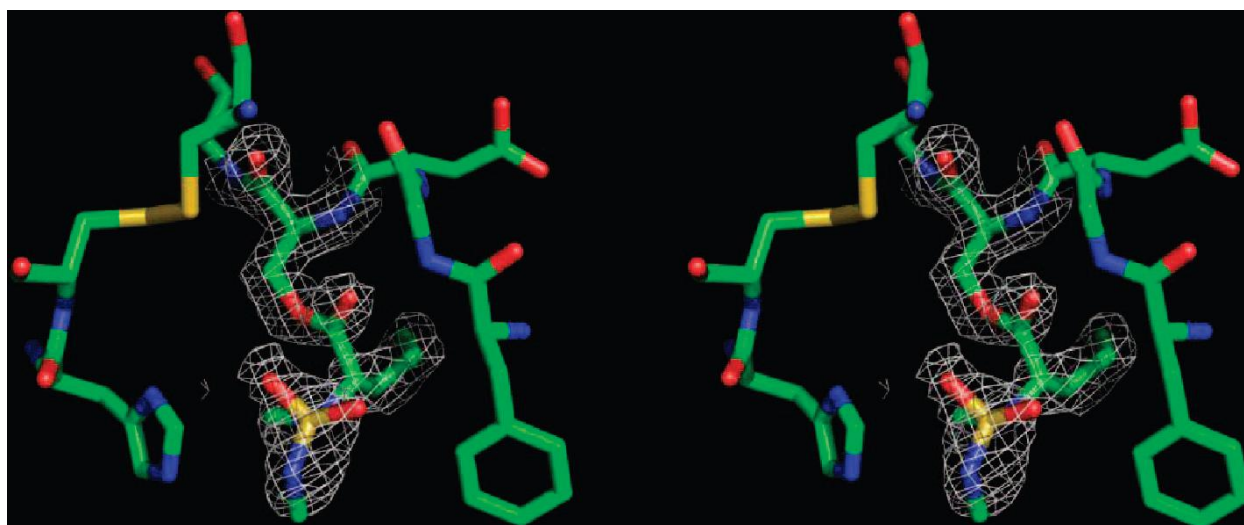


Figure 3.7 Stereoview of the Active Site Region in An Omit $F_o - F_c$ Map of the Refined Protein-Inhibitor Complex, where the inhibitor and Ser 195 have been excluded from the structure factor calculation. The map was contoured at 3.0 times the standard deviation. Parts of the refined structure are included. The carbonyl carbon of modified inhibitor **I** is shown to be covalently bound to the O_γ of Ser195.

carbonyl carbon of the inhibitor. The distance of the sp^2 -hybridized carbon to the nearest imidazole nitrogen of His57 is 3.577 Å, which is too far to be covalently bonded to the carbon, ruling out species **Z**. Figure 3.7 also shows that the 2,6-dichlorobenzoate group is absent in the enzyme-inhibitor complex in accordance with the proposed mechanism of action (Figure 3.3). The hydrophobic *n*-propyl group occupies a pocket (S_1) formed by the main chains of Phe192

and Phe215, and the side chains of Val190, Val216, and Phe192, with which it engages in multiple hydrophobic interactions. The $\text{SO}_2\text{NH}=\text{CH}_2$ is located between the side chains of His57 and Phe192 with one of the oxygen atoms forming a hydrogen bond with His57. A surface representation of the HNE active site cleft with the docked inhibitor is shown in Figure 3.8.

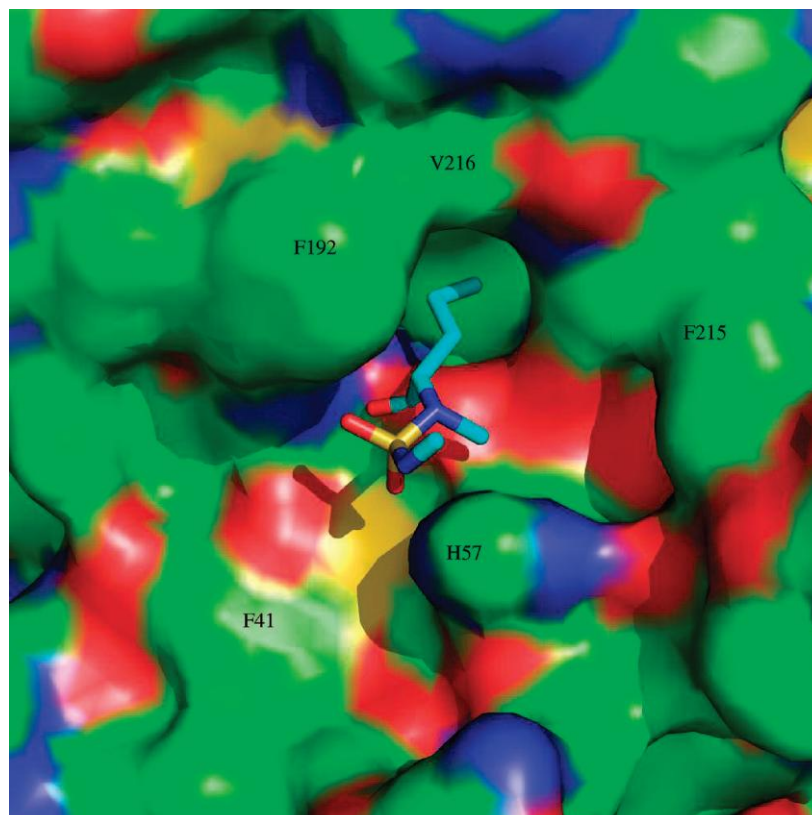


Figure 3.8 Three-Dimensional Surface of the Active Site of HNE with Modified Inhibitor A16 Bound to the Active Site Cleft and the *N*-Propyl Group Nestled into the S1 Subsite.

Interestingly, when crystals of complex **X** were re-examined after a significant time lapse, the modified inhibitor was found to be no longer bound to the enzyme. Specifically, the inhibitor had been completely “processed” by the enzyme. This indicates that the interaction of **A15** with HNE proceeds through multiple states of inactivated enzyme complexes that have variable stability. This is consistent with previous observations [217], where the addition of excess hydroxylamine

to the totally inactivated HNE-inhibitor **I** (P_1 = isobutyl, R_2 = methyl, L = SO_2Ph) adducts lead to incomplete regain in enzymatic activity.

The nature of species **X** was further probed using ESI-MS. The mass spectra of a sample of unreacted HNE and the HNE-inhibitor **A15** derived complex are shown in Figure 3.9. The mass spectrum of unreacted HNE shows two major peaks at 24522.2 and 25195.7, [208] while the HNE-**A15** complex shows an increase in mass of the two major components of 204 amu. The ESI-MS data support the conclusion, based on the X-ray structure, that the inhibited form of the enzyme is structure **X** and not structure **Y**, which would require a mass shift of 222.

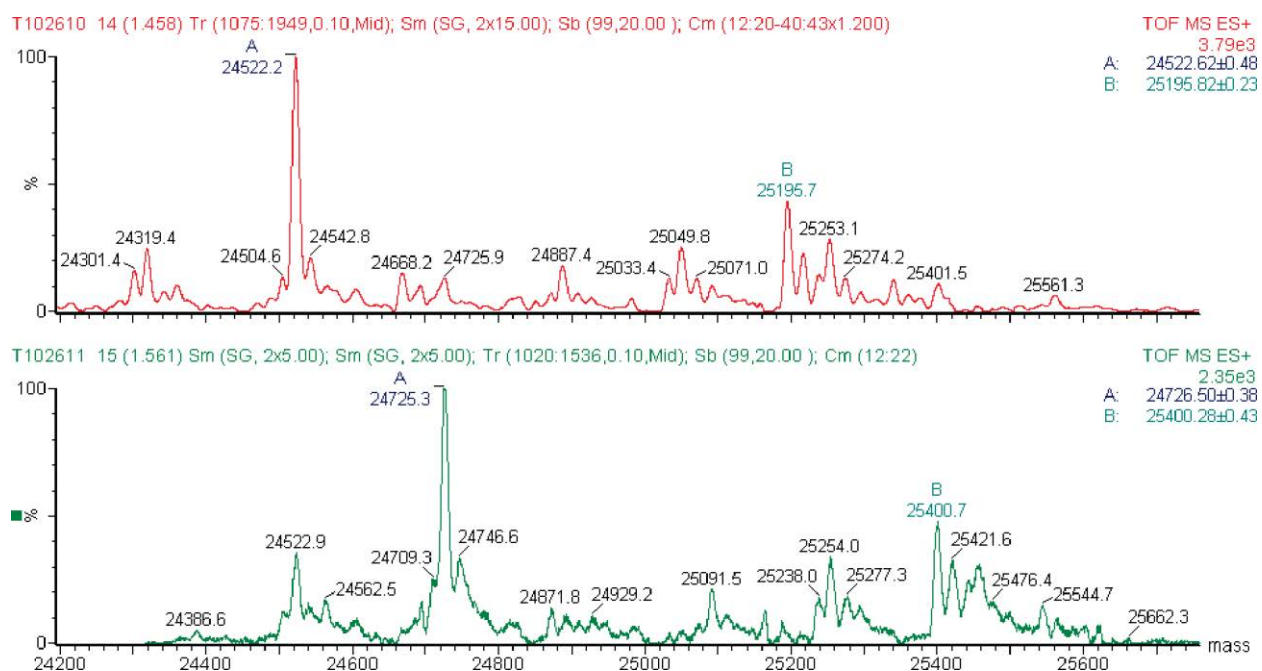


Figure 3.9 High Resolution Mass Spectra of HNE and HNE-Inhibitor Complex. (a) Derived mass spectrum of HNE (top). (b) Derived mass spectrum of the HNE-inhibitor complex (bottom).

Taken together, the available data indicate that inhibitor **A15** inactivates HNE via a mechanism that involves the initial formation of a relatively stable acyl enzyme that incorporates in its structure a conjugated sulfonyl imine functionality. Subsequent slow reaction with water

leads to the formation of one or more acyl enzymes of variable stability (i.e., structures **Y** and **W**) that eventually hydrolyze to regenerate active enzyme, as well as some low molecular weight products.

3.2.4 HNE/Caspase-1 Dual Function Inhibitor

Incubation of HNE/Caspase-1 Dual function inhibitor **A16** with HNE led to rapid, time-dependent, irreversible loss of enzymatic activity (Figure 3.10). The bimolecular rate constant k_{inact}/K_I , an index of inhibitor potency, was determined using the progress curve method and found to be $24,705 \text{ M}^{-1}\text{s}^{-1}$ (Figure 3.11). Compound **A16** was also screened against human leukocyte proteinase 3, however, it was devoid of any inhibitory activity toward human leukocyte proteinase 3 at an $[I]/[E]$ ratio of 250 and a 30 min incubation time. Again incubation of **A16** with bovine trypsin showed time-dependent inactivation of the enzyme.

The caspase-1 inhibitor **A10** is an affinity label of caspase-1 [223], therefore the rate of inactivation of caspase-1 by caspase-1 inhibitor **A10** generated from HNE inactivation by compound **A16** was determined by the progress curve method (Figure 3.12). The release of caspase-1 inhibitor **A10** from **A16** was also monitored using HPLC (Figure 3.13). Both results have showed that the release of caspase-1 inhibitor **A10** from compound **A16** was rapid in the presence of HNE.

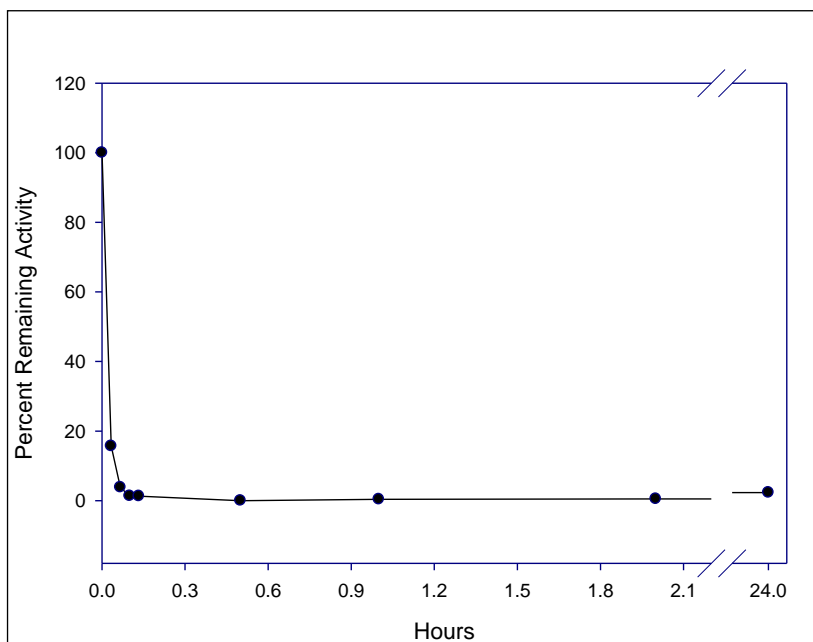


Figure 3.10 Time-Dependent Loss of Enzymatic Activity with A16. Percent remaining activity versus time plot obtained by incubating inhibitor A16 (10.5 μM) with human neutrophil elastase (700 nM) in 0.1 M HEPES buffer containing 0.5 M NaCl, pH 7.25, and 1% DMSO. Aliquots were withdrawn at different time intervals and assayed for enzymatic activity using MeOSuc-AAPV p-NA by monitoring the absorbance at 410 nm.

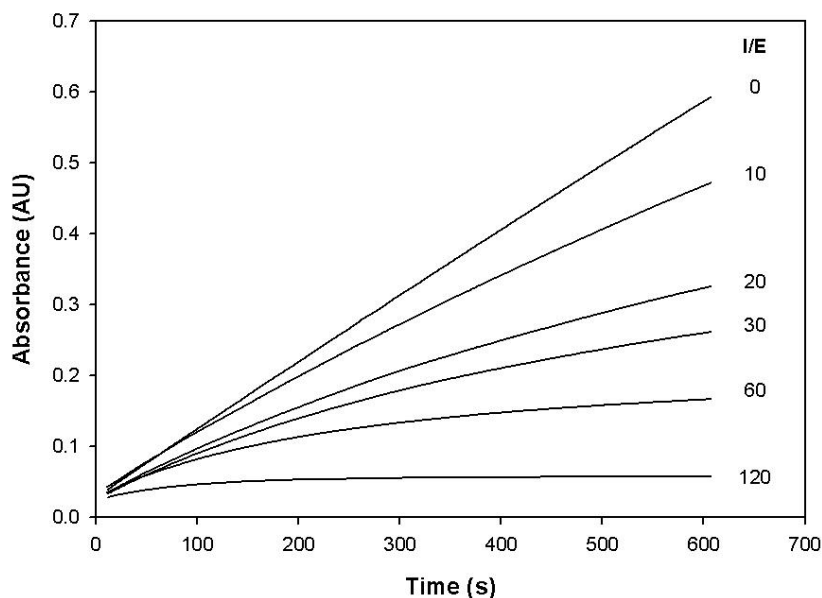


Figure 3.11 Progress Curves for the Inhibition of Human Neutrophil Elastase (HNE) by Inhibitor A16. Absorbance was monitored at 410 nm for reaction solutions containing 10 nM HNE, 105 μM MeOSuc-AAPV p-nitroanilide, and the inhibitor at the indicated inhibitor to enzyme ratios in 0.1 M HEPES buffer containing 0.5 M NaCl, pH 7.25, and 2.5% DMSO. The temperature was maintained at 25 $^{\circ}\text{C}$, and reactions were initiated by the addition of enzyme.

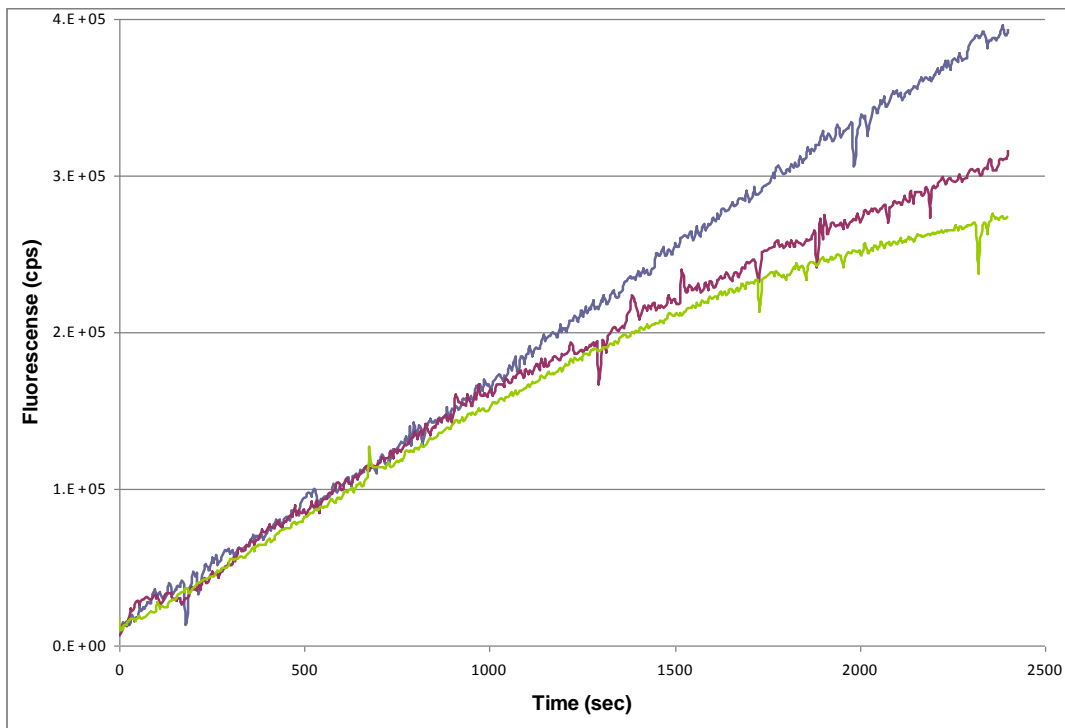


Figure 3.12 Progress Curves for the Inhibition of Caspase-1 by Dual Inhibitor A16 after Incubation with HNE for 2 min. The fluorescence emission at 460 nm (excited at 380 nm) was monitored for reaction solutions containing 4 nM caspase-1, 46 μ M Ac-YVAD-AMC, and the inhibitor at the indicated inhibitor to enzyme ratios in 10 mM Tris buffer containing 1mM DTT, 0.1% CHAPS, pH 7.5, and 4% DMSO. The temperature was maintained at 37 $^{\circ}$ C, and reactions were initiated by the addition of enzyme. Blue line: **A16**:HNE:Caspase-1 = 0:0:1 (Hydrolysis control); red line: **A16**:HNE:Caspase-1 = 200:20:1; green line: **A16**:HNE:Caspase-1 = 400:40:1.

A molecular modeling simulation was also performed using AutoDock4. As expected, inhibitor **A16** was found to bind to the HNE active site as inhibitor **A15**. Specifically, the n-propyl residue nestled in the S1 hydrophobic pocket and the hydrophobic leaving group/caspase-1 inhibitor occupies the S' subsites which is exposed to the solvent. The reason that **A16** showed no inhibition against Pr 3 is that the S' subsites of Pr 3 are more polar than HNE, but relatively hydrophobic and large caspase-1 inhibitor **A10** is not complementary to Pr 3 primary subsites in electro statics and size. A comparison of docking results is shown in Figure 3.14 A-B.

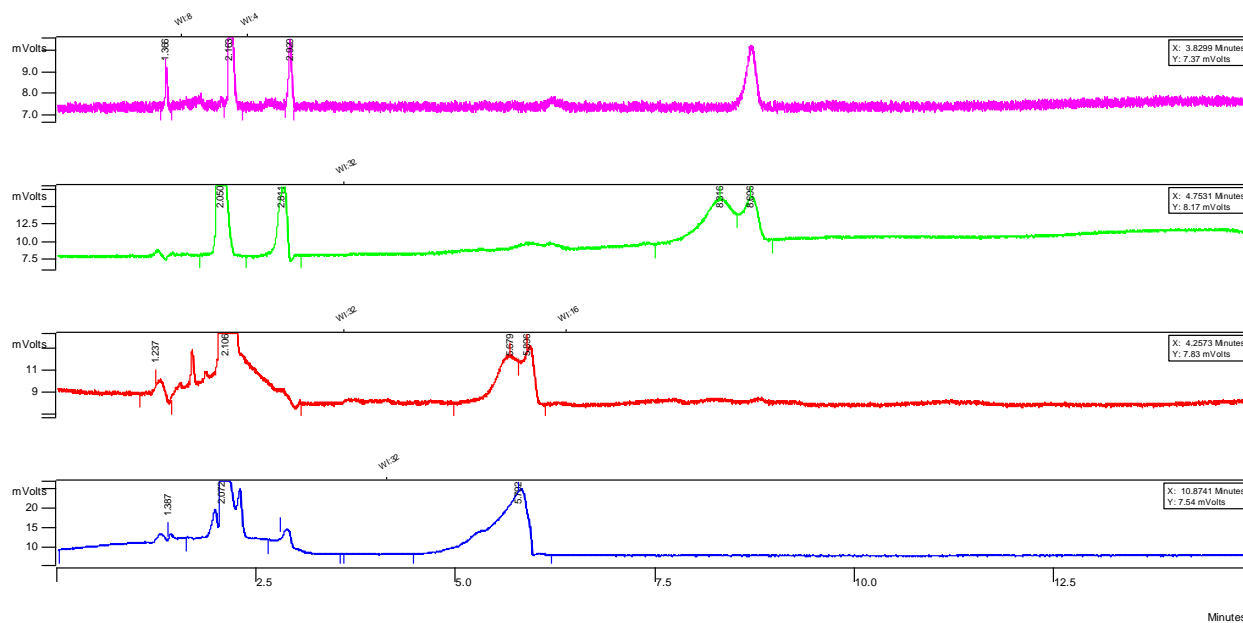


Figure 3.13 HPLC Monitoring of Caspase-1 Inhibitor Release. 5 μM of each sample was injected to Kinetex column (Phenomenex, 2.6 μ , C18, 100 \AA), the mobile phase was using 1:1 water and acetonitrile at 1 mL/min flow rate and the absorbance at 254 nm was recorded for 15 min. Purple line: dual function inhibitor **A16** at 0.5 mM; green line: **A16** at 5 mM without treatment of HNE; red line: 15 min after **A16** mixed with HNE; blue line: caspase-1 inhibitor **A10**.

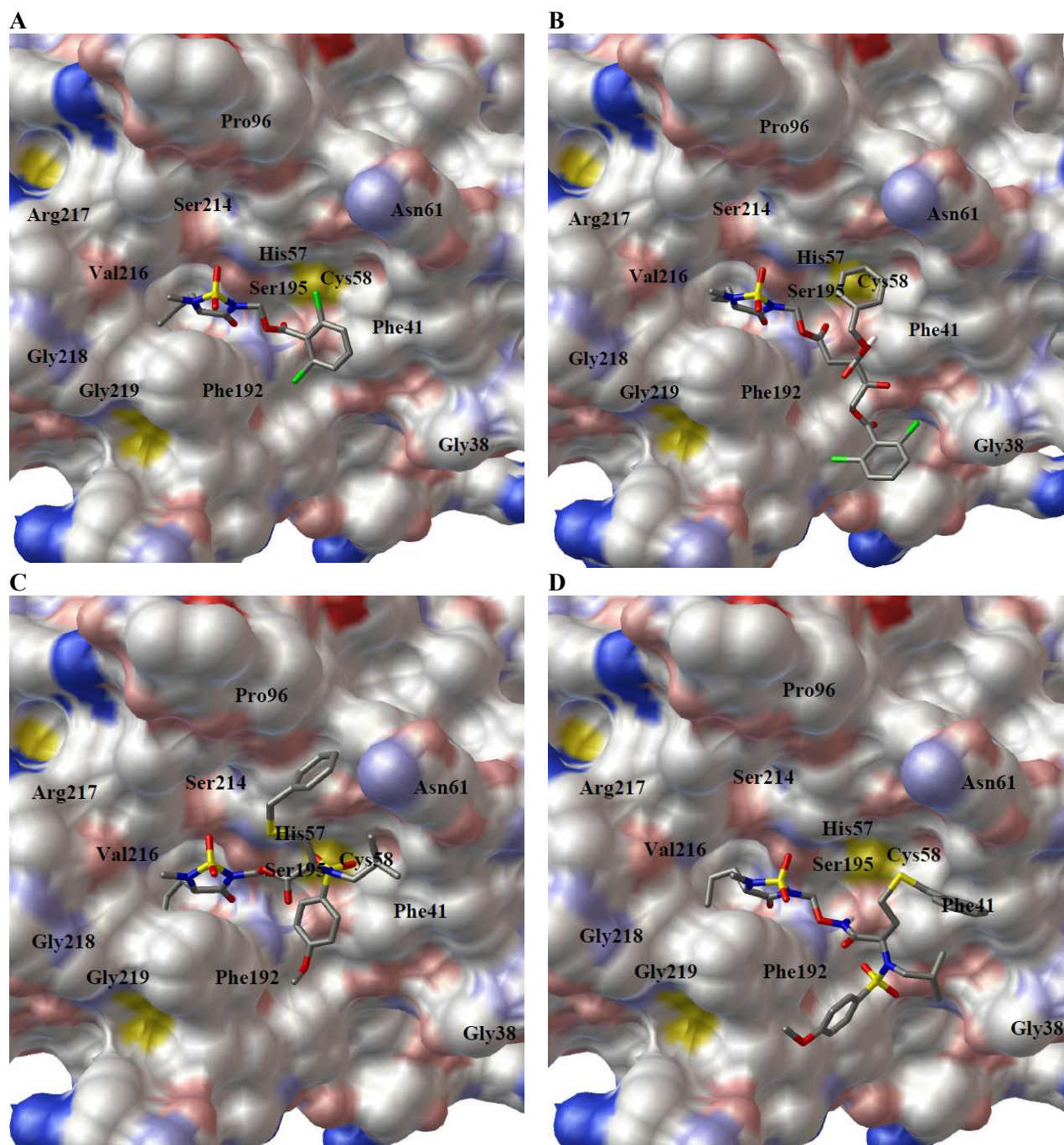


Figure 3.14 Dual Function Inhibitors and HNE Enzyme Active Site Interactions. The molecular docking simulations were performed using Autodock4.0 (The Scripps Research Institute); the receptor model was prepared from HNE-OMTKY3 complex (pdb code:1ppf), stripped of all water molecules and OMTKY3 ligand; the inhibitors were constructed in SYBYL 8.0 and were structurally optimized to default convergence thresholds using the Tripos Force Field and Gasteiger-Marsili partial atomic charges. The ligands are colored by their atom type and the enzyme surface is colored using David Goodsell colors. (A) Compound **A15** bound to the HNE enzyme active site; (B) Compound **A16** bound to the HNE enzyme active site; (C) Compound **A18** bound to the HNE enzyme active site; (D) Compound **A17** bound to the HNE enzyme active site.

3.2.5 HNE/MMP-12 Dual Function Inhibitor

Both the desired HNE/MMP-12 dual function inhibitor **A17** and unexpected compound **A18** were screened against HNE. Unfortunately inhibitor **A17** did not show potent inhibition toward HNE, however, compound **A18** showed potent inhibition against HNE. The inhibition was time-dependent and the 24 h remaining activity is shown in Figure 3.15. Compounds **A17** and **A18** were also docked into HNE active site using AutoDock4 (Figure 3.14 C-D). It appears that both have favorable interactions with HNE active sites with the P₁ residue n-propyl nestled in the S1 pocket, the carbonyl group is positioned in the similar fashion which is readily attacked by HNE active site serine (Ser195), the leaving group/MMP-12 inhibitor are both hydrophobic and interact with the S' subsites of HNE. The possible reason causing the low inhibition of **A17** against HNE is due to the high pKa value of the hydroxamic acid (~8.8) whereas the acid has a pKa of 4.7. The pKa of the leaving group(s) has a profound effect on the inactivation of HNE. This finding is consistent with previous observations [217]. It should be noted that the S' subsites of HNE has an extreme tolerance to accommodate a variety of structural diverse substitutions, which potentially allows many structurally diverse inhibitors to replace leaving group -L".

The excellent inhibition of **A18** provided further support for the idea that a carboxylic acid MMP-12 inhibitor to form a dual function HNE/MMP-12 could result in a promising dual function inhibitor for both HNE and MMP-12. Several potent carboxylic acid MMP-12 inhibitors have been reported recently [228,229], including the ones listed in Table 3.1.

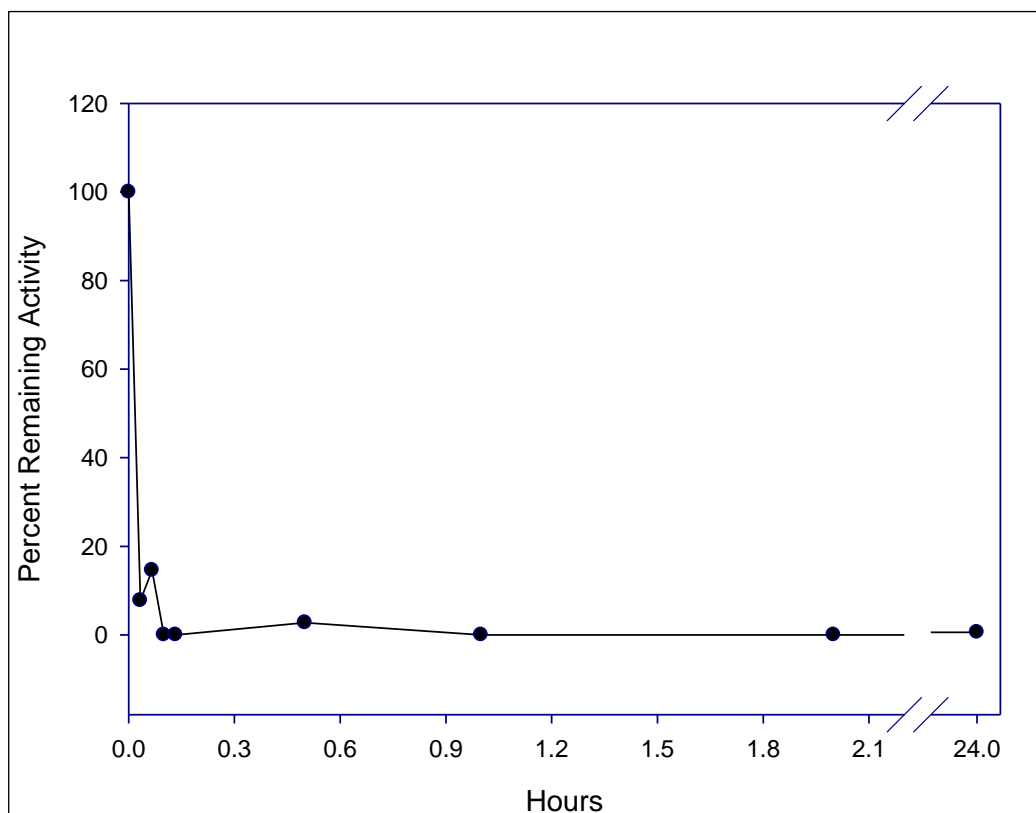


Figure 3.15 Time-dependent Loss of Enzymatic Activity with A18. Percent remaining activity versus time plot obtained by incubating inhibitor A18 (3.5 μM) with human neutrophil elastase (700 nM) in 0.1 M HEPES buffer containing 0.5 M NaCl, pH 7.25, and 1% DMSO. Aliquots were withdrawn at different time intervals and assayed for enzymatic activity using MeOSuc-AAPV p-NA by monitoring the absorbance at 410 nm.

3.3 Conclusions and Future Directions

These studies have demonstrated that dual function inhibitors of COPD relevant proteases can be designed and synthesized. Furthermore, inhibitors of this type (**A16**) capable of disrupting two or more pathogenic processes involved in COPD could potentially be more efficacious in the treatment of the disease than simple protease inhibitors. Future plans on COPD dual function inhibitors will focus on replacing the leaving group with potent reversible inhibitor or transition state analogs which contain a carboxylic acid as part of the molecule.

3.4 Experimental

3.4.1 General

The ^1H spectra were recorded on a Varian XL-300 or XL-400 NMR spectrometer. A Hewlett–Packard diode array UV–vis spectrophotometer was used in the in vitro evaluation of the inhibitors. Human neutrophil elastase, proteinase 3 and Boc-Ala-Ala-Nva thiobenzyl ester were purchased from Elastin Products Company, Owensville, MO. Caspase-1 human, methoxysuccinyl Ala-Ala-Pro-Val p-nitroanilide and 5,5'-dithio-bis(2-nitrobenzoic acid) were purchased from Sigma Chemicals, St. Louis, MO. Ac-Trp-Val-Ala-Asp-AMC was purchased from AnaSpec Inc., Fremont, CA. Reagents and solvents were purchased from various chemical suppliers (Aldrich, Acros Organics, TCI America, and Bachem). Silica gel (230-450 mesh) used for flash chromatography was purchased from Sorbent Technologies (Atlanta, GA). Melting points were determined on a Mel-Temp apparatus and are uncorrected. Thin layer chromatography was performed using Analtech silica gel plates. The TLC plates were visualized using iodine and/or UV light. HPLC was performed on a Varian ProStar 210 system equipped with a Kinetex C-18 column (Phenomenex, 2.6 μ , 100 Å, 4.6 cm \times 20 cm). The high resolution mass spectra were performed by the Mass Spectrometry Lab at the University of Kansas, Lawrence, KS.

3.4.2 Representative Synthesis

(S)-Methyl 2-aminopentanoate hydrochloride A1: Thionyl chloride (27.87 g; 234 mmol) was added dropwise to dry methanol (85 mL) cooled in an ice-salt bath. L-Norvaline hydrochloride (25.00 g; 213 mmol) was added in small portions. The ice-salt bath was then removed and the reaction mixture was heated to 40 °C for 2 h using a water bath. The reaction mixture was stirred

for 2 h and the solvent was removed on the rotary evaporator, leaving a solid residue which was treated with ethyl ether (100 mL) and collected by suction filtration. The white solid **A1** (34.17 g; 96% yield) was dried in a desiccator and used in the next step without further purification. m.p. 109-110 °C, ¹H NMR (CDCl₃): δ 0.96-1.02 (t, 3H), 1.43-1.68 (m, 2H), 1.80-1.95 (m, 1H), 2.00-2.15 (m, 1H), 3.80 (s, 3H), 4.05-4.15 (m, 1H), 8.82 (bs, 2H).

(S)-Methyl 2-(N-(tert-butoxycarbonyl)sulfamoylamino)pentanoate A2: A solution of N-chlorosulfonyl isocyanate (28.73 g; 203 mmol) in dry methylene chloride (140 mL) was cooled in an ice-water bath and a solution of t-butyl alcohol (15.05 g; 203 mmol) in dry methylene chloride (60 mL) was added dropwise with stirring. The mixture was stirred for another 15 min at 0 °C and the resulting mixture was added dropwise to a solution of **A1** (34.17 g; 203 mmol) and triethylamine (41.08 g; 406 mmol) in dry methylene chloride (200 mL) kept in an ice-water bath. The ice-water bath was removed and the mixture was stirred at room temperature overnight. The reaction mixture was then washed with 5% aqueous HCl (2×100 mL) and brine (100 mL). The organic layer was dried over anhydrous sodium sulfate, the drying agent was filtered off, and the solvent was removed in vacuo to give **A2** (82.23 g; 100% yield) as a white solid, m.p. 127-128 °C. ¹H NMR (CDCl₃): δ 0.94-0.98 (t, 3H), 1.38-1.46 (m, 2H), 1.48 (s, 9H), 1.63-1.81 (m, 2H), 3.77 (s, 3H), 4.15-4.20 (m, 1H).

(S)-Methyl 2-(sulfamoylamino)pentanoate A3: Compound **A2** (62.99 g; 203 mmol) was dissolved in trifluoroacetic acid (200 mL) and the reaction mixture was stirred at room temperature overnight. Excess trifluoroacetic acid was removed using a rotary evaporator and the residue was taken up in ethyl acetate (500 mL) and washed with saturated sodium bicarbonate (5×150 mL) and brine (150 mL). The organic layer was dried over anhydrous sodium sulfate, the drying agent was filtered off, and the solvent was removed in vacuo leaving **A3** (33.28 g; 78%

yield) as a white solid, m.p. 53-55 °C. ¹H NMR (CDCl₃): δ 0.92-1.00 (t, 3H), 1.40-1.48 (m, 2H), 1.60-1.72 (m, 1H), 1.73-1.82 (m, 1H), 3.80 (s, 3H), 4.04-4.11 (m, 1H).

(S)-4-Propyl-1,2,5-thiadiazolidin-3-one 1,1-dioxide A4: A solution of compound **A3** (33.28 g; 158 mmol) in dry THF (300 mL) was kept in an ice-water bath and treated portion-wise with 60% w/w sodium hydride (9.48 g; 237 mmol) under nitrogen. The reaction mixture was stirred at room temperature overnight. The solvent was removed and the residue was dissolved in cold water (150 mL). The pH was adjusted to 7 with 6 M HCl, the starting material was extracted once with ethyl acetate (150 mL), and the aqueous layer was acidified with 6 M HCl to pH 1. The product was extracted with ethyl acetate (3×150 mL) and the combined organic extracts were dried over anhydrous sodium sulfate. The drying agent was filtered off and the solvent was removed on a rotary evaporator, leaving product **A4** (28.36 g; 100% yield), as a yellow oil. ¹H NMR (DMSO-d₆): δ 0.93-1.00 (t, 3H), 1.43-1.58 (m, 2H), 1.72-1.84 (m, 1H), 1.86-1.98 (m, 1H), 4.20-4.25 (m, 1H), 5.60 (bs, 1H), 7.97 (bs, 1H).

(S)-2-[(Phenylsulfanyl)methyl]-4-propyl-1,2,5-thiadiazolidin-3-one 1,1-dioxide A5: To a solution of compound **A4** (5.33 g; 30 mmol) in 45 mL dry acetonitrile was added triethylamine (3.03 g; 30 mmol) and chloromethyl phenyl sulfide (5.70 g; 36 mmol). The reaction mixture was refluxed overnight. The solvent was removed and the residue was taken up with 150 ml ethyl acetate. The organic solution was washed with 5% HCl (3×30mL), saturated NaHCO₃ (3×30mL) and brine (30 mL). The organic layer was dried and the drying agent was filtered. The solvent of filtrate was removed and the crude product was purified using flash chromatography (silica gel/ethyl acetate/hexanes) to give product **A5** (7.31 g; 81% yield), as a colorless oil. ¹H NMR (CDCl₃): δ 0.93-0.96 (t, 3H), 1.40-1.48 (m, 2H), 1.64-1.75 (m, 1H), 1.82-1.92 (m, 1H), 4.05-4.13 (m, 1H), 4.96 (s, 2H), 7.28-7.35 (m, 3H), 7.52-7.56 (m, 2H).

(S)-5-Methyl-2-[(phenylsulfanyl)methyl]-4-propyl-1,2,5-thiadiazolidin-3-one 1,1-dioxide

A6: To a chilled solution of compound **A5** (4.51 g; 15 mmol) in 15 ml acetonitrile, was added NaH (60%w/w; 0.72 g; 18 mmol). After 30 min stirring under N₂, iodomethane (2.55 g; 18 mmol) was added and the reaction was allowed to warm to room temperature for overnight. The solvent was removed and the residue was taken up with 50 mL CH₂Cl₂. The organic layer was washed with 5% HCl (3x20mL), saturated NaHCO₃ (3x20mL) and brine (20 mL). The organic layer was dried and the drying agent was filtered. The solvent of filtrate was removed to give product **A6** (4.25 g; 90% yield), as a colorless oil. ¹H NMR (CDCl₃): δ 0.86-0.94 (t, 3H), 1.20-1.50 (m, 2H), 1.65-1.92 (m, 2H), 2.83 (s, 3H), 3.75-3.77 (t, 1H), 4.98 (s, 2H), 7.28-7.35 (m, 3H), 7.52-7.56 (m, 2H).

(S)-2-(Chloromethyl)-5-methyl-4-propyl-1,2,5-thiadiazolidin-3-one 1,1-dioxide A7:

To a solution of compound **A6** (4.25 g; 13.5 mmol) in 40 ml CH₂Cl₂ chilled in an ice-bath was added sulfonyl chloride (3.7 g; 27 mmol) dropwise. The reaction mixture was stirred at room temperature for 3 h. CH₂Cl₂ 150 mL was added to the reaction mixture and the organic solution was washed with saturated NaHCO₃ (3x50mL) and brine (50 mL). The organic layer was dried and the drying agent was filtered. The solvent of filtrate was removed and the crude product was purified using flash chromatography (silica gel/ethyl acetate/hexanes) to give product **A7** (1.97 g; 61% yield), as a white solid, m.p.52-53 °C. ¹H NMR (CDCl₃): δ 0.95-1.00 (t, 3H), 1.30-1.60 (m, 2H), 1.78-2.05 (m, 2H), 2.92 (s, 3H), 3.89-3.93 (t, 1H), 5.37 (s, 2H).

(S)-Tert-butyl 3-(benzyloxycarbonylamino)-5-bromo-4-oxopentanoate A8:

To a solution of L-Cbz-Asp(O-tBu)-OH (8.08g; 25 mmol) in 120 dry THF was added N-Methylmorpholine (NMM, 2.78 G; 27.5 mmol) at 0 °C under N₂, followed by isobutyl chloroformate (3.41 g; 25 mmol). 15

min later, the precipitate was filtered off and the filtrate was added to a pre-cooled freshly made ethereal solution of diazomethane* (64~69 mmol) in portions with occasional swirling. The resulting mixture was kept in the hood overnight. Evaporation of the solvent and excess diazomethane left a yellow oil. The oily product was dissolved in 48% aqueous HBr (4.21 g; 25 mmol) and diethyl ether (80 mL) with vigorous stirring. The ethereal layer was extracted with water (5×15 mL) to remove acid, then the organic layer was dried over anhydrous sodium sulfate. The drying agent was removed and the filtrate was concentrated to give a crude product as a yellow oil **A8** (8.7 g; 87% yield). ¹H NMR (CDCl₃): δ 1.61 (s, 9H), 2.72-3.01 (m, 2H), 4.20 (s, 2H), 4.72-4.80 (m, 1H), 5.15 (s, 2H), 5.89-5.98 (d, 1H), 7.28-7.40 (m, 5H).

* **Preparation of diazomethane:** In a 500 mL distilling flask were placed a solution of 6 g KOH in 10 mL of water, 35 mL carbitol (2(2-ethoxyethoxy)ethanol), 10 mL diethyl ether and a "Teflon"-coated stir bar. An addition funnel (250 mL) was attached and adjusted so that the stem was just above the surface of the solution in the distilling flask. A solution of p-tolylsulfonylmethylnitrosamide (Diazald) (21.5 g; 100 mmol) in 125 mL of diethyl ether was placed in the addition funnel. The distilling flask was heated in a water-bath at 70-75 °C, the stirrer was started and the Diazald solution was added at a regular rate during 15-20 min. As soon as all the Diazald had been added, 100 mL additional diethyl ether was added through the dropping funnel at the previous rate until the distillate is colorless. The distillate was then ready for further use.

(S)-3-(benzyloxycarbonylamino)-5-tert-butoxy-2,5-dioxopentyl 2,6-dichlorobenzoate A9: To a suspension of dry KF (2.38 g; 41 mmol) in 18 mL DMF was added 2,6-dichlorobenzoic acid (3.59 g; 18.8 mmol) and compound **A8** (6.27 g; 15.7 mmol) successively. The reaction was stirred at room temperature overnight. The solvent was removed and the residue was taken up

with 150 mL ethyl acetate. The organic layer was washed with brine (3x50 mL), and then dried over anhydrous sodium sulfate. The drying agent was filtered off and the filtrate was concentrated. The crude product was purified using flash chromatography (silica gel/ethyl acetate/hexanes) to give product **A9** (4.30 g; 62% yield), as a colorless oil. ¹H NMR (CDCl₃): δ 1.61 (s, 9H), 2.72-3.01 (m, 2H), 4.68-4.75 (m, 1H), 5.12-5.25 (m, 4H), 6.02-6.06 (d, 1H), 7.28-7.40 (m, 8H).

(S)-3-(benzyloxycarbonylamino)-5-(2,6-dichlorobenzoyloxy)-4-oxopentanoic acid A10:

Compound **A9** (4.3 g; 9.74 mmol) was treated with 25%(v/v) TFA in methylene chloride at room temperature for 2 h. The solvent was removed and the residue was taken up with 100 mL ethyl acetate. The organic layer was washed with saturated NaHCO₃ (30 mL) and brine (30 mL). The organic layer was dried over anhydrous sodium sulfate. The drying agent was removed and the filtrate was concentrated to give compound **A10** as a colorless oil (3.6 g; 96% yield). ¹H NMR (CDCl₃): δ 2.70-2.82 (dd, 1H), 3.00-3.12 (dd, 1H), 4.60-4.70 (q, 1H), 4.80-5.05 (dd, 2H), 5.16 (s, 2H), 5.70 (bs, 1H), 7.30-7.40 (m, 8H).

(RS)-3-(Isobutylamino)dihydrothiophen-2(3H)-one A11: A solution of (DL) homocysteine thiolatone hydrochloride (61.6 g; 400 mmol) in dry methanol (500 mL) was cooled in an ice-bath and then treated with isobutylaldehyde (61.0 g; 800 mmol) with stirring. After stirring for 15 min, triethylamine (60.7 g; 600 mmol) was added, and the ice-bath was removed and the reaction mixture was stirred at room temperature overnight. The reaction was again placed in an ice-bath and sodium borohydride (30.3 g; 800 mmol) was added in small portions over a period of 50 min. The reaction mixture was stirred for an additional 3 h at 0 °C. The solvent was removed on the rotary evaporator and the residue was taken up with 150 mL water and 200 mL ethyl acetate. The organic layer was separated and the aqueous layer was extracted with an additional 200 mL

ethyl acetate. The combined organic layers were dried over anhydrous sodium sulfate and the drying agent was filtered. The solvent was removed and the crude product was purified using flash chromatography (silica gel/ethyl acetate/hexanes) to give product **A11** as a yellow oil (37.30 g; 54% yield). $^1\text{H NMR}$ (CDCl_3): δ 0.92-0.98 (d, 6H), 6.65-6.82 (m, 2H), 0.93-2.06 (m, 1H), 2.39-2.58 (ddd, 2H), 2.50-2.60 (m, 1H), 3.23 (m, 1H), 3.23-3.41 (ddd, 2H).

(RS)-N-isobutyl-4-methoxy-N-(2-oxotetrahydrothiophen-3-yl)benzenesulfonamide A12: A solution of compound **A11** (16.62 g; 96 mmol) in 90 ml methylene chloride was added to a 250 ml round bottom flask, and then triethylamine (10.7 g; 106 mmol) was added in an ice-bath. After 10 min stirring, a solution of 4-methoxybenzene-1-sulfonyl chloride (21.8 G; 106 mmol) in 20 ml methylene chloride was added dropwise. The ice bath was then removed and the reaction was stirred overnight at room temperature. Upon reaction completion, 300 mL methylene chloride was added the reaction mixture was transferred to a separatory funnel. The organic layer was washed with brine (150 mL), 5% HCl (2×150 mL), and then brine (150 mL). The organic solution was dried and the drying agent was filtered off. The solvent was removed and the crude product was purified using flash chromatography (silica gel/ethyl acetate/hexanes) to give product **A12** as a white solid (16.0 g; 49% yield), m.p. 91-92 °C. $^1\text{H NMR}$ (CDCl_3): δ 0.80-0.88 (t, 6H), 1.78-1.92 (m, 1H), 2.32-2.50 (m, 2H), 2.71-3.02 (ddd, 2H), 3.18-3.37 (m, 2H), 3.83 (s, 3H), 4.60-4.66 (q, 1H), 6.95-7.00 (d, 2H), 7.77-7.82 (d, 2H).

(RS)-Methyl 4-(benzylthio)-2-(N-isobutyl-4-methoxyphenylsulfonamido)butanoate A13: Place dry methanol (50 ml) in 100 ml round bottom flash, then Na (1.33 g; 57.4 mmol) was added. A solution of compound **A12** (12.92 g; 37.6 mmol) in dry methanol was warmed to about 50 °C and added to the above sodium methoxide solution. The reaction was stirred for 30 min before benzyl bromide (12.9 g; 75.6 mmol). The resulting mixture was stirred at room

temperature overnight. The solvent was removed on the rotary evaporator (below 40 °C) and the residue was extracted with 300 mL ethyl acetate. The organic layer was washed with 100 mL brine and dried over anhydrous sodium sulfate. The drying agent and solvent were removed and the crude product was purified using flash chromatography (silica gel/ethyl acetate/hexanes) to give product **A13** as a yellow oil (7.3 g; 42% yield). ¹H NMR (CDCl₃): δ 0.80-0.86 (dd, 6H), 1.80-1.95 (m, 2H), 2.15-2.25 (m, 1H), 2.41-2.48 (m, 2H), 2.80-3.34 (ddd, 2H), 3.54 (s, 3H), 3.68 (s, 2H), 3.85 (s, 3H), 4.49-4.53 (t, 1H), 6.94-6.97 (d, 2H), 7.20-7.32 (m, 5H), 7.96-7.99 (d, 2H).

(RS)-4-(Benzylthio)-N-hydroxy-2-(N-isobutyl-4-methoxyphenylsulfonamido)butanamide

A14: Compound **A13** (7.3 g; 15.7 mmol) was dissolved in 45 mL methanol. To this solution was added hydroxylamine hydrochloride (2.25 g; 31.4 mmol), followed by the addition of sodium methoxide, freshly prepared from sodium (1.09 g; 47.4 mmol) dissolved in methanol (30 mL). The reaction mixture was stirred at room temperature overnight. The solvent was removed and 150 mL 5% HCl was added, which was extracted with ethyl acetate (3×200 mL). The combined organic layers were dried and the drying agent was filtered off. The solvent was removed and the crude product was purified using flash chromatography (silica gel/ethyl acetate/hexanes) to give product **A14** as a colorless oil (4.2 g; 57% yield). ¹H NMR (CDCl₃): δ 0.80-0.92 (dd, 6H), 1.38-1.50 (m, 1H), 1.83-2.23 (m, 4H), 2.82-3.16 (ddd, 2H), 3.40-3.56 (dd, 2H), 3.84 (s, 3H), 4.33-4.38 (t, 1H), 6.95-6.99 (d, 2H), 7.18-7.33 (m, 5H), 7.72-7.76 (d, 2H), 8.02 (bs, 1H), 9.43 (bs, 1H).

Compound A15: Compound **A7** (0.48 g; 2 mmol) was dissolved in 10 mL dry acetone and NaI (0.33 g; 2.2 mmol) was added. The reaction was stirred at room temperature for 10 h, and the precipitate was filtered using a small silica gel column (the silica gel was washed with 10 mL CH₂Cl₂). The combined organic layers were evaporated to dryness and the residue was re-

dissolved in 10 mL CH₂Cl₂. To the above solution was added 2,6-dichlorobenzoic acid (0.42 g; 2.2 mmol), followed by DBU (0.33 g; 2.2 mmol). The resulting mixture was stirred at room temperature overnight. The solvent was removed and 40 mL ethyl acetate was added. The organic solution was washed with 5% HCl (20mL) and brine (20 mL). The organic layer was dried over anhydrous sodium sulfate and the drying agent was filtered off. The solvent was removed and the crude product was purified using flash chromatography (silica gel/ethyl acetate/hexanes) to give product **A15** (0.39 g; 49% yield), as a colorless oil. ¹H NMR (CDCl₃): δ 0.91-1.00 (t, 3H), 1.30-1.60 (m, 2H), 1.78-2.02 (m, 2H), 2.91 (s, 3H), 3.89-3.95 (t, 1H), 5.84-5.95 (dd, 2H), 7.25-7.35 (m, 3H).

Compound A16: Compound **A7** (0.96 g; 4 mmol) was dissolved in 20 mL dry acetone and NaI (0.66 g; 4.4 mmol) was added. The reaction was stirred at room temperature for 10 h, and the precipitate was filtered using a small silica gel column (the silica gel was washed with 10 mL CH₂Cl₂). The combined organic layers were evaporated to dryness and the residue was re-dissolved in 10 mL CH₂Cl₂. To the above solution was added compound **A10** (1.70 g; 4.4 mmol), followed by DBU (0.66 g; 4.4 mmol). The resulting mixture was stirred at room temperature overnight. The solvent was removed and 60 mL ethyl acetate was added. The organic solution was washed with 5% HCl (20mL) and brine (20 mL). The organic layer was dried and the drying agent was filtered. The solvent of filtrate was removed and the crude product was purified using flash chromatography (silica gel/ethyl acetate/methylene chloride/hexanes) to give product **A16** (0.59 g; 25% yield), as a colorless oil. ¹H NMR (CDCl₃): δ 0.88-0.98 (t, 3H), 1.25-1.56 (m, 2H), 1.68-2.00 (m, 2H), 2.82 (s, 3H), 2.90-3.20 (m, 2H), 3.80-3.88 (m, 1H), 4.71-4.79 (m, 1H), 5.09-5.20 (m, 4H), 5.57-5.75 (m, 2H), 5.98-6.05 (t, 1H), 7.28-7.40 (m, 8H); HRMS (ESI) calculated for C₂₇H₂₉Cl₂N₃O₁₀SNa [M+Na]⁺ 680.0848, found 680.0847.

Syntheses of compound A17, A18 were intentionally placed after A23.

Di-*tert*-butyl (benzyloxy)imidodicarbonate A19: A solution of O-benzylhydroxylamine (2.32 g; 18.8 mmol) in 15 mL acetonitrile was added a solution of di-*tert*-butyl dicarbonate (4.5 g; 20.7 mmol) in 15 mL acetonitrile under an ice-bath over 20 min. The reaction mixture was stirred at 0 °C for 1 h and then allowed to warm up to room temperature slowly with stirring overnight. Thin layer chromatography (TLC) monitoring indicated all O-benzylhydroxylamine was consumed and the mono-Boc-O-benzylhydroxylamine intermediate was formed. To the reaction mixture was added a solution of di-*tert*-butyl dicarbonate (6.7 g; 31 mmol) in acetonitrile (15 mL), followed by a solution of 4-dimethylaminopyridine (DMAP) (0.20 g; 1.64 mmol) in 3 mL acetonitrile. The reaction mixture was then stirred at 40 °C until TLC indicating the complete conversion of the intermediate N-Boc-O-benzylhydroxylamine (about 2 h). The reaction mixture was evaporated to dryness and the residue was re-dissolved in 30 mL ethyl acetate. The organic layer was washed with a mixture of 1M phosphate buffer (pH 7, 15 mL) and saturated sodium chloride (8 mL). The organic layer was then dried over anhydrous sodium sulfate. The drying agent was filtered off and the solvent was removed, leaving the crude product as a yellow solid **A19** (4.7 g; 78%), m.p. 73-75 °C. ¹H NMR (CDCl₃): δ 1.56 (s, 18H), 4.91 (s, 2H), 7.36-7.44 (m, 5H).

Di-*tert*-butyl hydroxyimidodicarbonate A20: A suspension of compound **A19** (2.0 g; 6.19 mmol) in 95% ethanol was added Pd-C (10%, 0.1 g). The reaction mixture was shaken at 20 Psi hydrogen gas for 2 h and the TLC showed total disappearance of compound **A19**. The catalyst was filtered using Celite and the filtrate was pumped to dryness, yielding a white solid **A20** (1.35 g; 93%), m.p. 75-77 °C. ¹H NMR (CDCl₃): δ 1.53 (s, 18H).

(S)-Di-tert-butyl [(5-methyl-1,1-dioxido-3-oxo-4-propyl-1,2,5-thiadiazolidin-2-yl)methoxy]-imidodicarbonate A21: To a solution of compound **A7** (0.96 g; 4 mmol) in 20 mL dry acetone was added sodium iodide (0.68 g; 4.4 mmol), and the resulting mixture was stirred at room temperature overnight. The white sodium chloride precipitate was filtered by a small column packed with dry silica gel, and the column was washed with 20 mL methylene chloride. The combined organic solutions were evaporated to dryness and the residue was dissolved 20 mL methylene chloride. To this solution was added premixed solution of compound **A19** (0.92 g; 4 mmol) and 1,8-Diazabicyclo[5.4.0]undec-7-ene (DBU) (0.68 g; 4.4 mmol). The resulting mixture was stirred at room temperature overnight. Methylene chloride (40 mL) was added and the organic solution was washed with brine (2 x 60mL), saturated NaHCO₃ (2 x 60mL), and then brine (60 mL). The organic layer was then dried over anhydrous sodium sulfate. The drying agent was filtered off and the solvent was removed, leaving the crude product as a yellow solid. The crude product was purified using flash chromatography (silica gel/ethyl acetate/hexanes) to give product **A21** as a colorless oil (1.2 g; 68%). ¹H NMR (CDCl₃): δ 0.96-1.00 (t, 3H), 1.40-1.60 (m, 2H), 1.53 (s, 18H), 1.78-2.03 (m, 2H), 2.96 (s, 3H), 3.82-3.86 (t, 1H), 5.29-5.44 (dd, 2H).

(S)-2-[(Aminoxy)methyl]-5-methyl-4-propyl-1,2,5-thiadiazolidin-3-one 1,1-dioxide A22: To a solution of compound **A21** (1.0 g; 2.3 mmol) in 25 mL methylene chloride was added dry silica gel (10 g). The mixture was pumped to dryness on a rotary evaporator connected to an oil pump. The silica gel adsorbed with compound **A20** was spread on a flat crystallization dish. The silica gel was placed into a 500 W microwave oven and the sample was microwaved for 14 min. TLC showed the starting material had disappeared and the silica gel became yellow-colored. The silica gel was washed with methanol (3×20 mL) on a small Büchner funnel and the filtrate was

concentrated to a small volume. The crude product was purified using flash chromatography (silica gel/ethyl acetate/hexanes) to give product **A22** as a yellow oil (0.34 g; 68%). ^1H NMR (CDCl_3): δ 0.89-1.00 (t, 3H), 1.24-1.60 (m, 2H), 1.62-1.85 (m, 2H), 2.53 (s, 3H), 2.77-2.90 (d, 1H), 4.36-4.45 (t, 1H), 4.72-5.35 (dd, 2H), 6.06 (bs, 1H).

(RS)-4-(Benzylthio)-2-(N-isobutyl-4-methoxyphenylsulfonamido)butanoic acid A23:

Compound **A13** (1.9 g; 4 mmol) was dissolved in a mixture of 10 mL 1,4-dioxane and 7 mL 6 N NaOH at room temperature and the reaction was stirred overnight. The mixture was adjusted to pH 7 using 5% HCl and then the solvent was removed. The residue was added 5 mL water and acidified to pH 2 using 6 N HCl, then extracted with ethyl acetate (2 x 25 mL). The combined organic extracts were dried over anhydrous sodium sulfate. The drying agent and solvent were removed and then the crude product was purified using flash chromatography (silica gel/ethyl acetate/hexanes) to give product **A23** as a yellow oil (1.4 g; 72%). ^1H NMR (CDCl_3): δ 0.80-0.88 (m, 6H), 1.80-1.96 (m, 2H), 2.22-2.37 (m, 2H), 2.40-2.45 (t, 2H), 2.85-3.05 (ddd, 2H), 3.64 (s, 2H), 3.82 (s, 3H), 4.40-4.46 (t, 1H), 6.95-6.99 (d, 2H), 7.22-7.35 (m, 5H), 7.77-7.81 (d, 2H).

Compound 17: Compound **A23** (0.65 g; 1.43 mmol) was dissolved in 8 mL DMF, 1-ethyl-3-(3-dimethylaminopropyl) carbodiimide (EDCI) (0.46 g; 2.4 mmol) was added and the reaction was stirred for 15 min. Then compound **A22** (0.34 g; 1.43 mmol) was added, followed by triethylamine (0.20 mL; 1.44 mmol) and the reaction was stirred at room temperature overnight. The solvent was removed and the residue was taken up with 50 mL ethyl acetate and 30 mL brine. The organic layer was separated and washed with additional 30 mL brine. The organic layer was dried over anhydrous sodium sulfate and the drying agent and solvent were removed. The crude product was purified using flash chromatography (silica gel/ethyl acetate/hexanes) to give product **A17** as a colorless oil (0.25 g; 26% yield). ^1H NMR (CDCl_3): δ 0.80-1.02 (m, 9H),

1.35-1.54 (m, 2H), 1.76-2.00 (m, 5H), 2.23-2.55 (m, 2H), 2.62-2.68 (d, 3H), 2.83-3.23 (m, 2H), 3.63-3.68 (d, 2H), 3.83-3.90 (d, 3H), 4.33-4.41 (m, 1H), 4.47-4.67 (m, 2H), 5.20-5.38 (m, 2H), 5.48-5.56 (d, 1H), 6.95-7.01 (dd, 2H), 7.20-7.34 (m, 5H), 7.72-7.78 (dd, 2H).

Compound 18: To a solution of compound **A23** (0.45 g; 1 mmol) in 3 mL DMF was added DBU (0.15 g; 1 mmol). The reaction was stirred at room temperature for 30 min and compound **A7** (0.24 g; 1 mmol) in 3 mL DMF was added. The resulting mixture was stirred overnight. DMF was removed under vacuum and the residue was taken up with 50 mL ethyl acetate. The organic layer was washed with 5% HCl (15 mL), saturated NaHCO₃ (15 mL) and then brine (15 mL). The organic layer was dried over anhydrous sodium sulfate and the drying agent and solvent were removed. The crude product was purified using flash chromatography (silica gel/ethyl acetate/hexanes) to give product **A18** as a colorless oil (0.25 g; 38% yield). ¹H NMR (CDCl₃): δ 0.78-1.00 (m, 9H), 1.23-1.40 (m, 1H), 1.21-1.38 (m, 1H), 1.78-2.00 (m, 4H), 2.20-2.30 (m 1H), 2.47-2.52 (t, 2H), 2.80-3.10 (ddd, 2H), 3.85 (s, 3H), 3.70 (s, 2H), 3.85 (s, 3H), 4.56-4.60 (m, 1H), 5.35-5.60 (ddd, 2H), 6.95-7.00 (d, 2H), 7.20-7.34 (m, 5H), 7.75-7.80 (d, 2H); HRMS (ESI) calculated for C₂₉H₄₁N₃O₈S₃Na [M+Na]⁺ 678.1953, found 678.1974.

3.4.3 Enzyme Assays and Inhibition Studies

3.4.3.1 Progress Curve Method [217]

The apparent second-order inactivation rate constant ($k_{inact}/K_I \text{ M}^{-1} \text{ s}^{-1}$) was determined in duplicate. Typical progress curves for the hydrolysis of MeOSuc-AAPV-pNA by HNE in the presence of inhibitor are shown in Figure 3.3. Control curves in the absence of inhibitor were linear. The release of p-nitroaniline was continuously monitored at 410 nm. The pseudo first-order rate constants (k_{obs}) for the inhibition of HNE by inhibitor as a function of time were

determined according to Eq. 3.1, where A is the absorbance at 410 nm, v_o is the reaction velocity at $t = 0$, v_s is the final steady-state velocity, k_{obs} is the observed first-order rate constant, and A_o is the absorbance at $t = 0$. The k_{obs} values were obtained by fitting the A versus t data to Eq. 3.1 using nonlinear regression analysis (SigmaPlot, Jandel Scientific). The second order rate constants ($k_{inact}/K_I \text{ M}^{-1} \text{ s}^{-1}$) were then determined by calculating $k_{obs}/[I]$ and then correcting for the substrate concentration using Eq. 3.2. The apparent second-order rate constants ($k_{inact}/K_I \text{ M}^{-1} \text{ s}^{-1}$) were determined in duplicate.

$$A = v_s t + \{(v_o - v_s)(1 - e^{-k_{obs}t})/k_{obs}\} + A_o \quad \text{Eq. 3.1}$$

$$k_{obs}/[I] = (k_{inact}/K_I) [1 + [S]/K_m] \quad \text{Eq. 3.2}$$

3. 4.3.2 Human Neutrophil Elastase

HNE was assayed by mixing 10 μL of a 70 μM enzyme solution in 0.05 M sodium acetate/0.5 M NaCl buffer, pH 5.5, 10 μL dimethyl sulfoxide and 980 μL of 0.1 M HEPES buffer containing 0.5 M NaCl, pH 7.25, in a thermostated cuvette. A 100 μL aliquot was transferred to a thermostated cuvette containing 880 μL 0.1 M HEPES/0.5 M NaCl buffer, pH 7.25, and 20 μL of a 70 μM solution of MeOSuc-Ala-Ala-Pro-Val p-nitroanilide, and the change in absorbance was monitored at 410 nm for 60 s. In a typical inhibition run, 10 μL of inhibitor (3.5 mM) in dimethyl sulfoxide was mixed with 10 μL of 70 μM enzyme solution and 980 μL 0.1 M HEPES/0.5M NaCl buffer, pH 7.25, and placed in a constant temperature bath. Aliquots (100 μL) were withdrawn at different time intervals and transferred to a cuvette containing 20 μL of MeOSuc-Ala-Ala-Pro-Val p-nitroanilide (7 mM) and 880 μL 0.1 M HEPES/0.5M NaCl buffer. The absorbance was monitored at 410 nm for 60 s. HNE remaining activity was determined using % remaining activity = $(v/v_o) \times 100$ and is the average of duplicate or triplicate determinations.

3. 4.3.3 Human Neutrophil Proteinase 3

Twenty microliters of 32.0 mM 5,5'-dithio-bis(2-nitrobenzoic acid) in dimethyl sulfoxide and 10 μ L of a 3.45 μ M solution of human proteinase 3 in 0.1 M phosphate buffer, pH 6.50 (final enzyme concentration: 34.5 nM) were added to a cuvette containing a solution of 940 μ L 0.1 M HEPES buffer, pH 7.25, containing 0.5 M NaCl, 10 μ L 862.5 μ M inhibitor in dimethyl sulfoxide (final inhibitor concentration: 8.62 μ M) and 20 μ L 12.98 mM Boc-Ala-Ala-NVa-SBzl and the change in absorbance was monitored at 410 nM for 2 min. A control (hydrolysis run) was also run under the same conditions by adding 5,5'-dithio-bis(2-nitrobenzoic acid) in dimethyl sulfoxide and 10 μ L of a 3.45 μ M solution of human proteinase 3 in 0.1 M phosphate buffer, pH 6.50 (final enzyme concentration: 34.5 nM) to a cuvette containing a solution of 940 μ L 0.1 M HEPES buffer, pH 7.25, containing 0.5 M NaCl, 10 μ L dimethyl sulfoxide and 20 μ L 12.98 mM Boc-Ala-Ala-NVa-SBzl and the change in absorbance was monitored at 410 nM for 2 min. Pr 3 remaining activity was determined using $\% \text{ remaining activity} = (v/v_0) \times 100$ and is the average of duplicate or triplicate determinations.

3. 5.4.4 Computational Method

Molecular docking simulations were performed via Autodock4 program (the Scripps Research Institute) [230]. All structures of compounds **A15-A18** were constructed in SYBYL8 [231] and structurally optimized to default convergence thresholds using the Tripos Force Field [232] and Gasteiger–Marsili partial atomic charges [233]. Receptor model of HNE was prepared using the 1PPF [190] crystal structures. This structure was protonated in AutoDock4, stripped of all water molecules and bound ligand, and electrostatically represented with Gasteiger-Marsili charges.

3. 4.3.5 HPLC Analysis

A typical HPLC analysis for compounds **A10** and **A16** was performed on a varian ProStar 210 system equipped with a Kinetex C-18 column (Phenomenex, 2.6 μ , 100 Å, 4.6cm \times 20 cm). A constant 1:1 ratio of acetone/water mobile phase at 1.0 mL/min flow rate was used and the column was not thermally controlled. A 5 μ L injection was used for all samples and the absorbance at 254 nm was recorded for 15 min. Pure caspase-1 inhibitor and dual function inhibitor in ethyl acetate were first confirmed by NMR before the injections. The specific concentrations used for injection are indicated in Figure 3.13. For monitoring the release of caspase-1 inhibitor **A10** from dual function inhibitor **A16**, compound **A16** was first incubated with HNE at assay buffer for 2 min, an equal amount of ethyl acetate was used to extract the released **A10** and remaining **A16**. The organic solvent was rapidly removed at room temperature by oil pump (about 3 min), and the residue was re-dissolved in ethyl acetate at a similar concentration as the standard. A control sample without treatment of HNE was used.

CHAPTER 4

UTILIZATION OF THE 1, 2, 3, 5-THIATRIAZOLIDIN-3-ONE 1, 1-DIOXIDE SCAFFOLD IN THE DESIGN OF POTENTIAL INHIBITORS OF HUMAN LEUKOCYTE PROTEINASE 3

4.1 Inhibitor Design Rationale

The biochemical rationale underlying the design of inhibitor (III) was based on the following considerations: (a) in previous studies [216-217,222] we have demonstrated that the heterocyclic scaffold (I) (1,2,5-thiadiazolidin-3-one 1, 1-dioxide) (**Figure 4.1**) is a highly versatile peptidomimetic that embodies a structural motif that renders the platform capable of binding to the active site of HNE and related chymotrypsin-like serine proteases in a substrate-like fashion, orienting recognition elements R_1 and R_2 toward the S_n subsites and R_3 toward the S_n' subsites. Specifically, R_1 is accommodated at the primary substrate specificity subsite S_1 and its nature determines which subclass of serine proteases (neutral, basic, or acidic) will be inhibited, resulting in optimal enzyme selectivity; (b) the encouraging results obtained with scaffold (I) suggested that it could serve as a prototype structure for the design of related scaffolds [235], providing additional opportunities in terms of improving pharmacological and

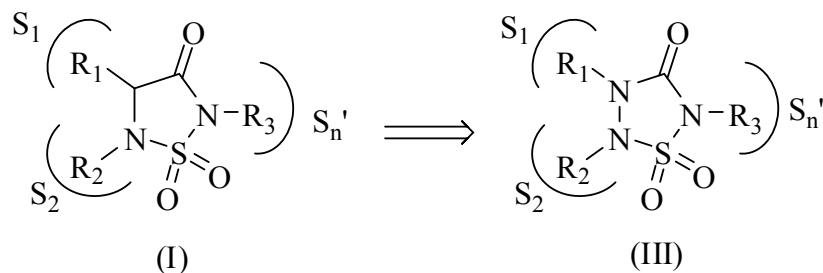


Figure 4.1 Pr 3 Inhibitor Design Rationale.

physicochemical properties. Thus, it was reasoned that a functionalized surrogate scaffold (III) embellished with appropriate recognition elements could provide a structural framework for the

rational design of non-covalent inhibitors of Pr 3 and related serine proteases. It was anticipated that the replacement of the α -carbon in scaffold (I) with nitrogen would decrease significantly the electrophilicity of the C=O carbon [236] and lead to a chemically robust ring system (III) that retained the substrate-like characteristics of (I) (Figure 4.1); (c) Pr 3 shows a strong preference for small aliphatic P₁ residues (ethyl, n-propyl) [237], while HNE prefers medium size P₁ alkyl groups (isopropyl/n-propyl or isobutyl/n-butyl). This is because the size of the S₁ subsite in Pr 3 is smaller due to the replacement of Val190 (HNE) by Ile (Pr 3) [238]. Unlike HNE, S'₁-P' interactions beyond S'₁ increase significantly the catalytic efficiency of Pr 3 [239], suggesting that S'_n interactions play an important role in substrate specificity [240]. Furthermore, the substitution of Leu143 (HNE) by Arg143 (Pr 3) and the presence of Asp61 in Pr 3 make the S'₁-S'₃ subsites of Pr 3 more polar [238]. Based on the aforementioned considerations, as well as modeling studies using the X-ray crystal structure of Pr 3 [238], it was envisaged that an entity based on scaffold (II) with attached recognition elements that can potentially interact with the S'_n subsites of the enzyme may function as non-covalent inhibitors of Pr 3. Thus, the S'_n subsites of Pr 3 were initially explored via the construction of focused libraries based on (II).

Based on the initial assumption that inhibitor (III) would bind to the active site of Pr 3 as inhibitor (I), a ring nitrogen substitution (ethyl) was chosen that is congruent with the primary substrate specificity (S₁) of Pr 3 and a diversity of amides and polar substituted triazoles were initially utilized to probe the S' subsites via combinatorial and click chemistry methods, respectively. From a synthetic point of view, several structurally diverse (in size and polarity) substituted α -hydroxy acids generated from α -amino acids can be coupled to the ring using the Mitsunobu reaction. This amino acid substitutions should allow further exploration of the S'₂-S'₃ subsites by coupling the acid group with a variety of amines (Figure 4.2a, Table 4.1).

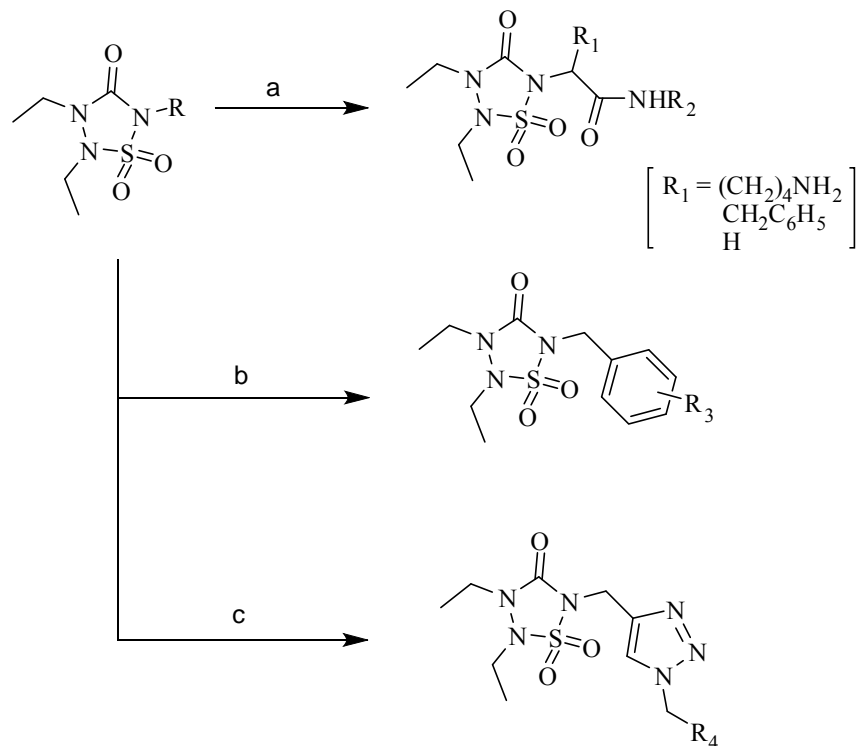
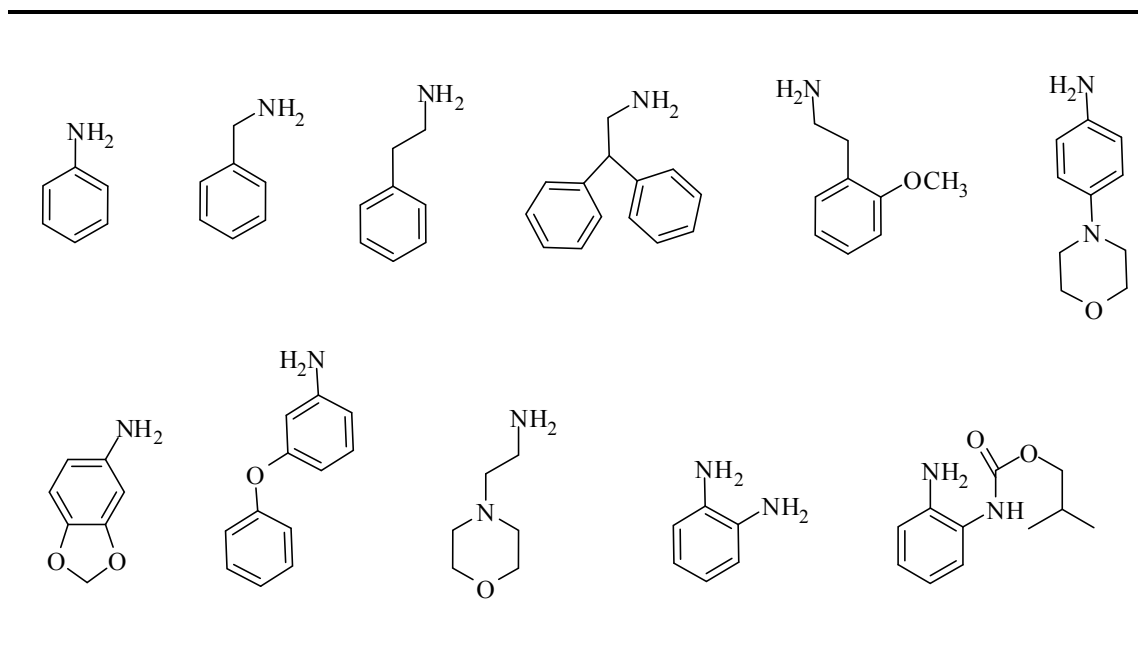


Figure 4.2 Structure-based Pr 3 Inhibitor Design.

An alternative amino functional group which can further extend the inhibitor structure was introduced by coupling of amino benzyl alcohol using Mitsunobu reaction (Figure 4.2b). The advantage of introducing an amino group is that the structural extension has the capability to project in different directions. Ideally, the inhibitor component projecting toward the S' subsites utilizing meta-substituted phenyl derivatives with a carboxyl group that could potentially interact with the Arg 241 side chain located in the vicinity of the S2' subsite of the enzyme. Furthermore, a focused library of structurally-diverse electron-rich compounds having multiple sites capable of interacting with the S' subsites of Pr 3 can be generated using click chemistry, after an alkyne is linked to the scaffold by either S_N2 reaction or Mitsunobu reaction (Figure 4.2c).

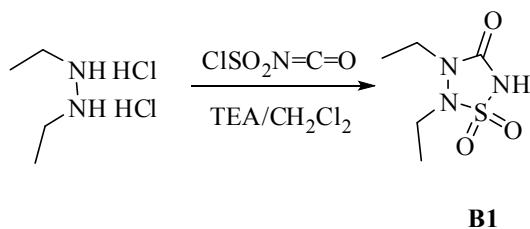
Table 4.1 Amine Inputs



4.2 Synthesis of Inhibitors

4.2.1 Synthesis of 2,3-Diethyl 1, 2, 3, 5-Thiatriazolidin-3-One 1,1-Dioxide B1

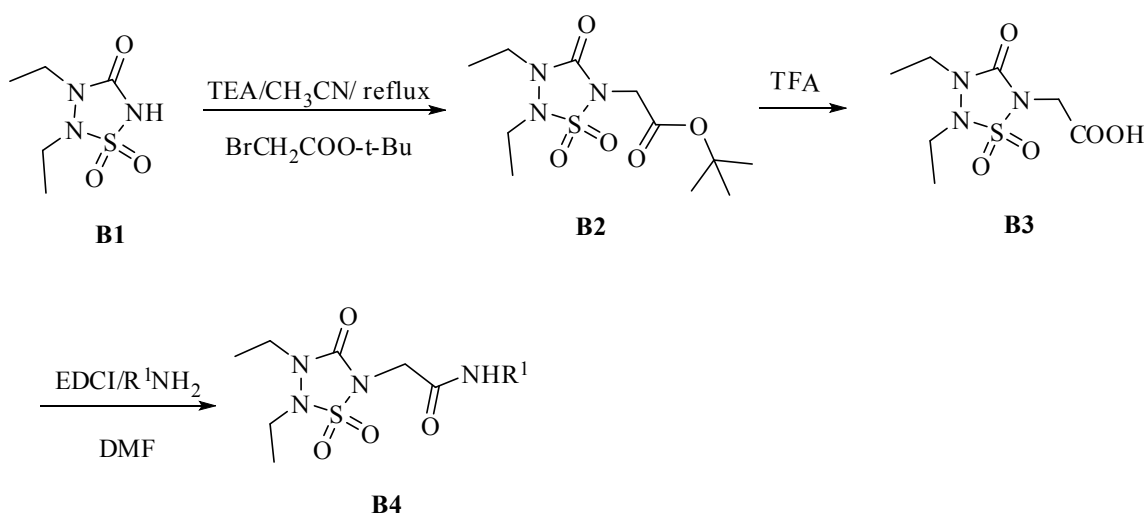
The heterocyclic scaffold **B1** was assembled in one step by condensing commercially available 1, 2-diethyl hydrazine dihydrochloride with N-chlorosulfonyl isocyanate in the presence of excess triethylamine (TEA) (Scheme 4.1).



Scheme 4.1 Synthesis of template B1

4.2.2 Synthesis of Compound B4 and B7

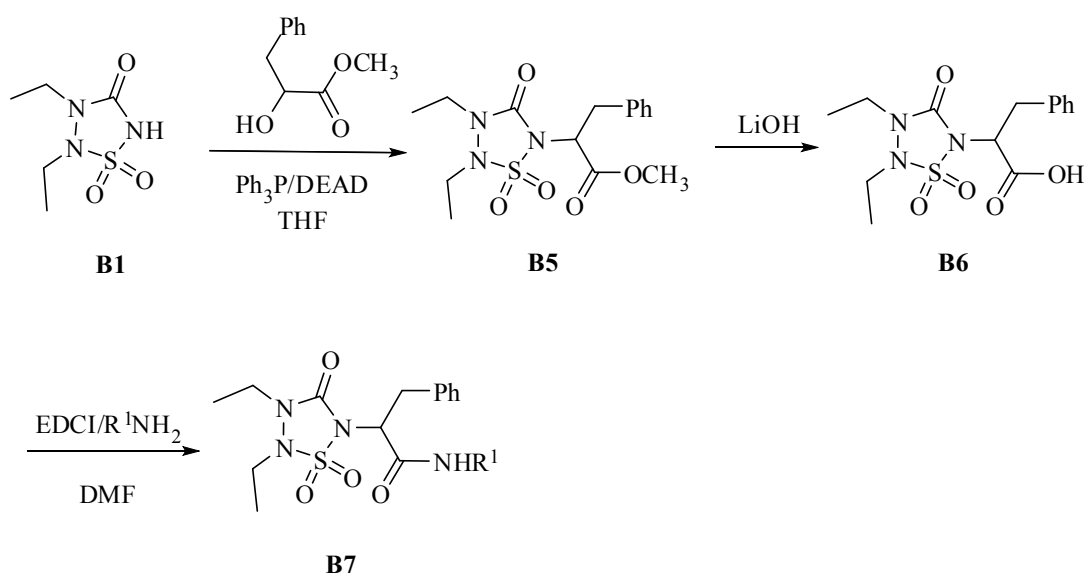
Treatment of the resulting 2, 3-diethyl 1, 2, 3, 5-thiatriazolidin-3-one 1,1-dioxide intermediate **B1** with TEA followed by the addition of t-butyl bromoacetate yielded the corresponding t-butyl ester **B2** which was readily deblocked using trifluoroacetic acid (TFA) to give the corresponding acid **B3**. The acid was then coupled to an array of structurally-diverse amines (Table 4.1) to yield compounds **B4a-i** (Scheme 4.2, Table 4.2).



Scheme 4.2 Synthesis of Compound III

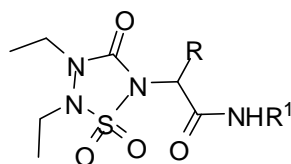
For the pathway **a** in Figure 4.2, we speculated that a derivative of amide **III** having a lysine side chain on the α carbon could potentially provide a favorable ion-ion interaction with Asp 51 (see Figure 4.6 for Pr 3 active site). However, Mitsunobu reaction of **B1** with the α -hydroxyester of Cbz-L-lysine failed to give the expected product. S_N2 reaction between compound **B1** and α -bromoester of Cbz-L-lysine was also not successful. Fortunately, Mitsunobu reaction with the α -hydroxyester of DL-phenylalanine was successful and made possible the synthesis of a wide range of derivatives of **B7** and their subsequent use in the exploration of the

S2'-S3' subsites (Scheme 4.3). The α -hydroxyester of DL-phenylalanine was prepared according to the procedure described by Shin et al [241]. Briefly, treatment of (DL)-phenylalanine with NaNO_2 in 2.5 N H_2SO_4 yielded the corresponding α -hydroxy acid which was subsequently converted to (DL)-3-phenyl-2-hydroxy-propionic acid methyl ester via treatment of the cesium salt with iodomethane in DMF. Mitsunobu reaction of the aforementioned intermediate **B1** with (DL) 3-phenyl-2-hydroxy-propionic acid methyl ester followed by hydrolysis afforded acid **B6**



Scheme 4.3 Synthesis of Compound III

which was coupled with a diverse set of amine inputs to give compounds **B7a~e** (Scheme 4.3, Table 4.2).

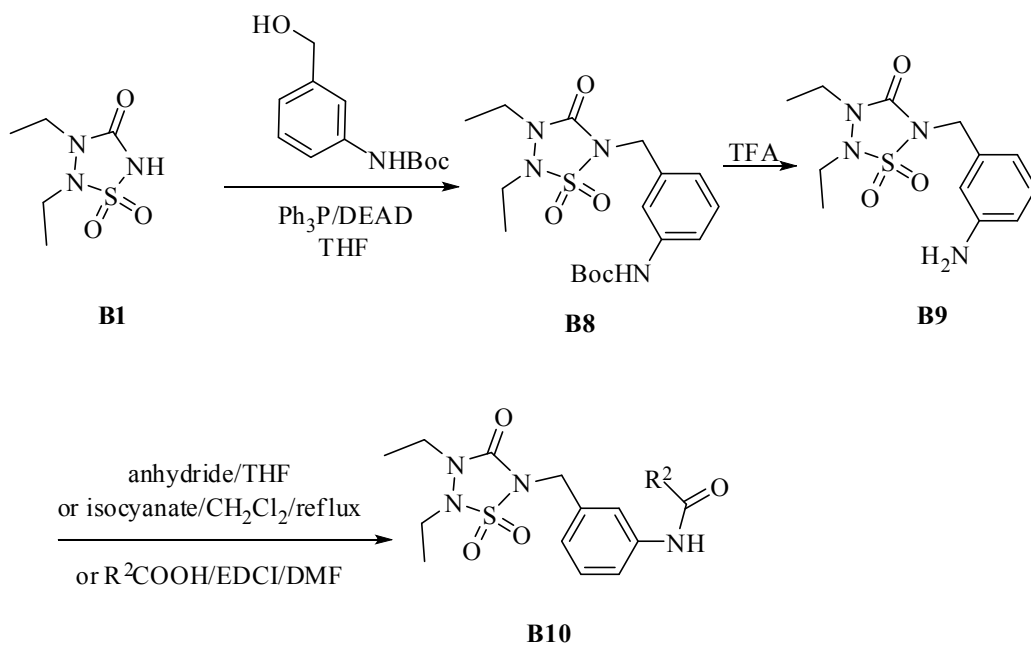
Table 4.2 Amide Derivatives

Entry	R	R ¹
B4a	H	phenyl
B4b	H	benzyl
B4c	H	phenethyl
B4d	H	2,2-diphenylethyl
B4e	H	2-(2-methoxyphenyl)ethyl
B4f	H	4-morpholinophenyl
B4g	H	benzo[d][1,3]dioxol-5-yl
B4h	H	3-phenoxyphenyl
B4i	H	2-morpholinoethyl
B7a	bzl	2-(2-methoxyphenyl)ethyl
B7b	bzl	4-morpholinophenyl
B7c	bzl	benzo[d][1,3]dioxol-5-yl
B7d	bzl	2-aminophenyl
B7e	bzl	2-(isobutoxycarbonylamino)phenyl

*Compounds B7a-e are DL isomers

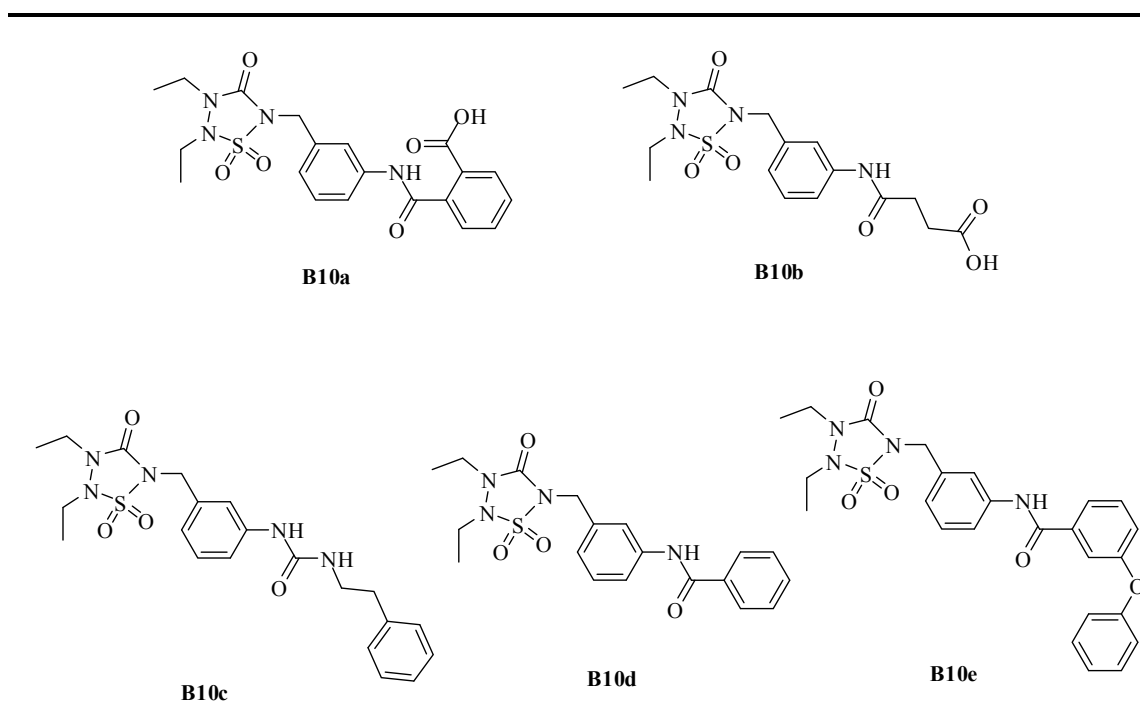
4.2.3 Synthesis of Compounds B10a~e

Alkylation of 2,3-diethyl 1,2,3,5-thiadiazolidin-3-one 1,1-dioxide **B1** with N-Boc-m-aminobenzyl alcohol under Mitsunobu reaction conditions, followed by deprotection of the Boc group using TFA, yielded the corresponding aromatic amine which was further elaborated to yield compounds **B10a~e** (Scheme 4.4). The compounds are summarized in Table 4.3.



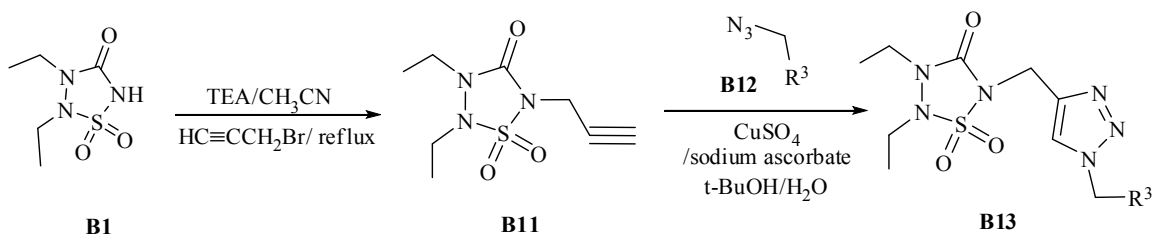
Scheme 4.4 Synthesis of Compound III

Table 4.3 List of Compounds B10a~e

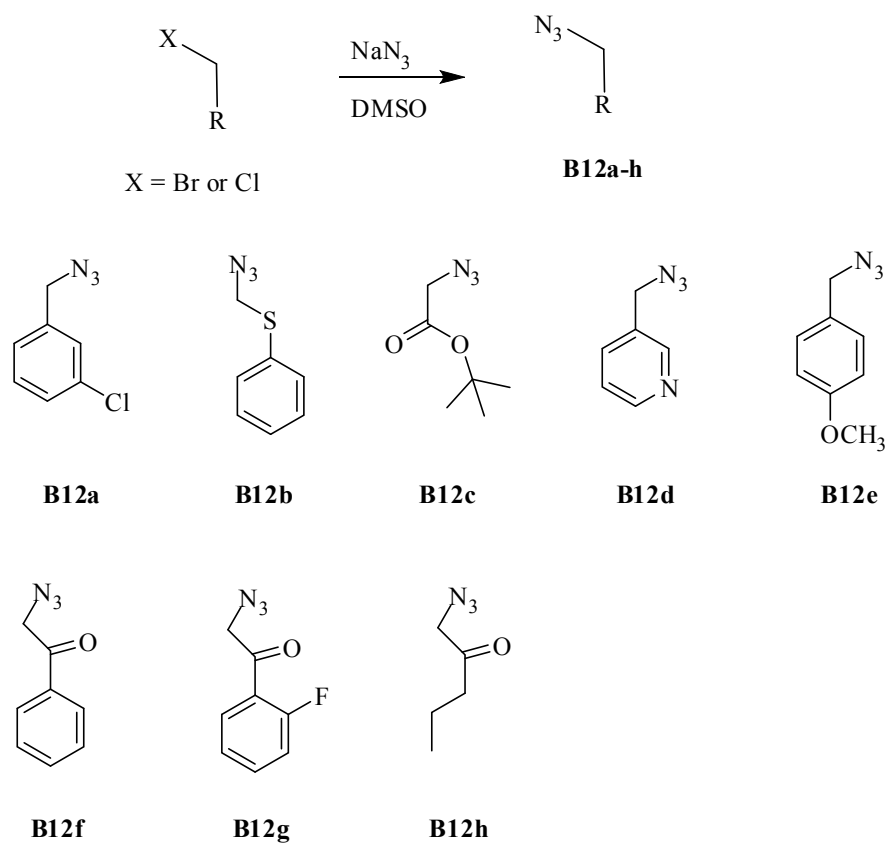


4.2.4 Synthesis of Compounds B13a~i

Click chemistry [242] is a very powerful tool for generating 5-member heterocyclic compounds. Specifically, for preparing a triazole ring, alkynes and azides are required. The most practical method for attaching a triazole ring is to alkylate compound **B1** with propargyl bromide which is then coupled with a variety of azides (Scheme 4.5). Most of the desired azides were readily prepared from the corresponding bromides which are either commercially available or synthesized according to literature procedures [243] (Scheme 4.6). The triazole compounds are summarized in Table 4.4 (note that compound **B13d** is generated from **B13c** using acid catalyzed hydrolysis by TFA).



Scheme 4.5 Synthesis of Triazole Compound III



Scheme 4.6 Synthesized Triazole Library

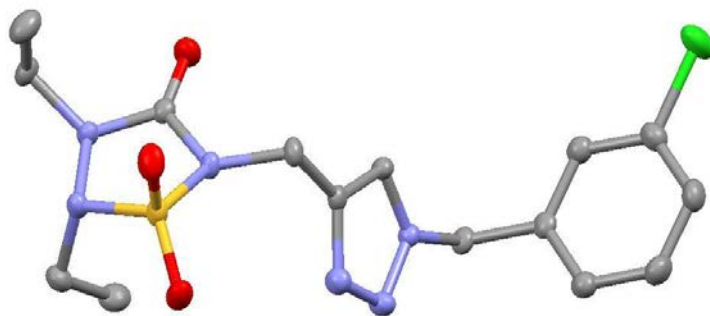
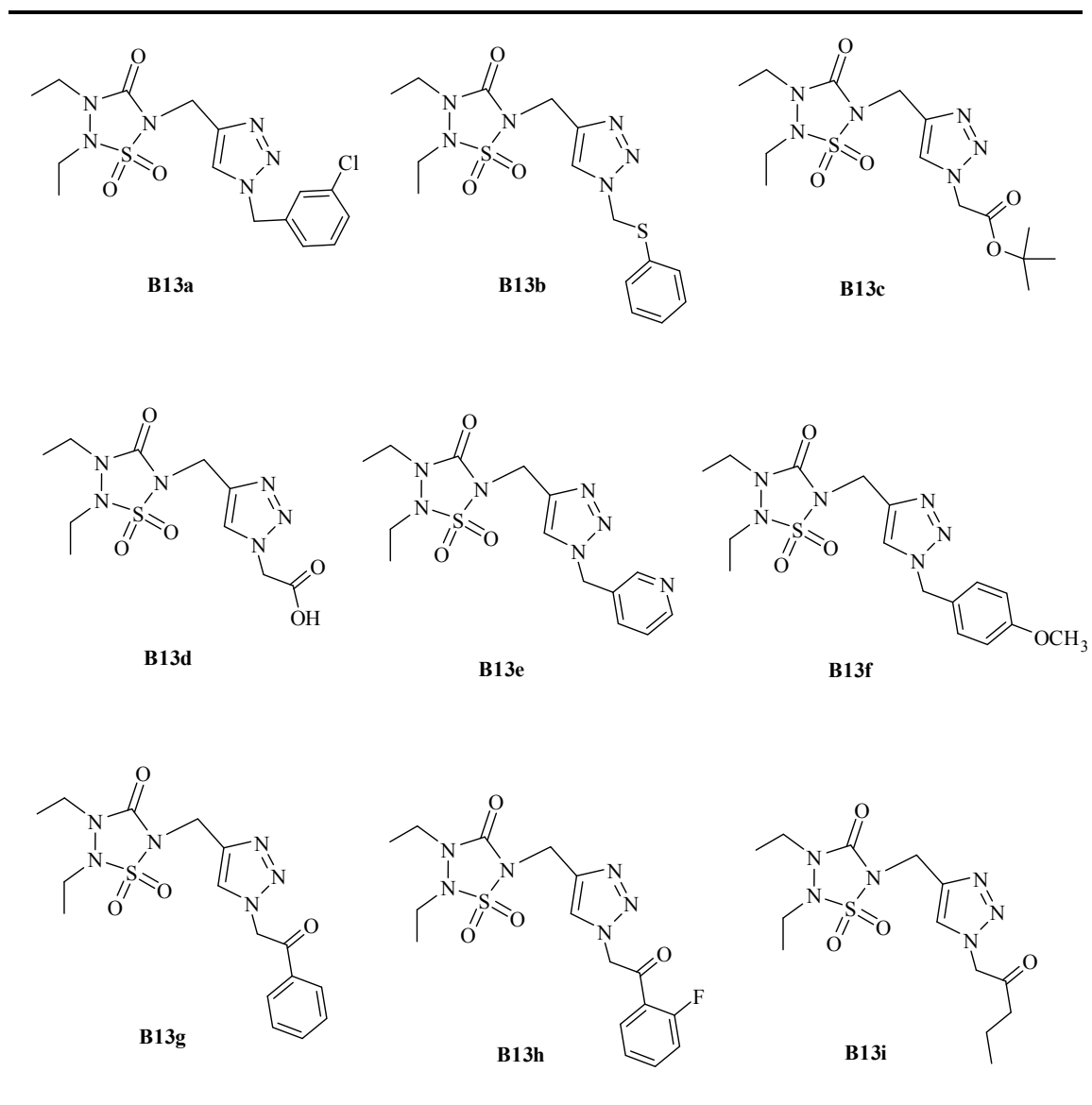


Figure 4.3 Mercury [244] Drawing of Compound B13a, showing the 50% thermal ellipsoids. Hydrogen atoms have been omitted for clarity.

Table 4.4 Summary of Triazole Compounds



In order to confirm the triazole ring formation, the X-ray crystal structure of a representative member of this class of compounds (compound **B13a**) was determined (shown in Figure 4.3).

4.2.5 Synthesis of Potential Transition State Analogs B13k-m

The molecular modeling studies (page 120) showed that the ketone carbonyl of **B13g** is hydrogen bonded to the side chain hydroxyl of the catalytic Ser195 residue. We reasoned that the introduction of strongly electron-withdrawing substituents into the phenyl ring or replacement of the phenyl ring by a heteroaromatic 5 or 6-membered ring would enhance the electrophilicity of the carbonyl carbon transforming **B13g** into a potential transition state inhibitor [245] of Pr 3 (Figure 4.4). Thus, structural variants of **B13k**, **B13m** with a 2,6-difluorophenyl or a thiazole group were synthesized. The azide precursors of compounds **B13k** and **B13m** could not be prepared directly from the corresponding α -bromoacetyl compounds; consequently an alternative method was used. This involved α -bromination followed by reduction and treatment with base to form the corresponding epoxide which was sequentially subjected to ring opening, click chemistry and oxidation with pyridinium chlorochromate (PCC) (Scheme 4.7).

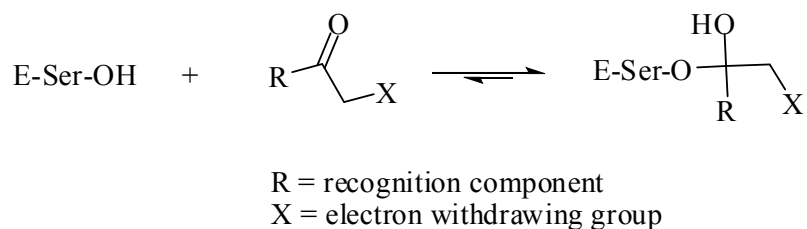
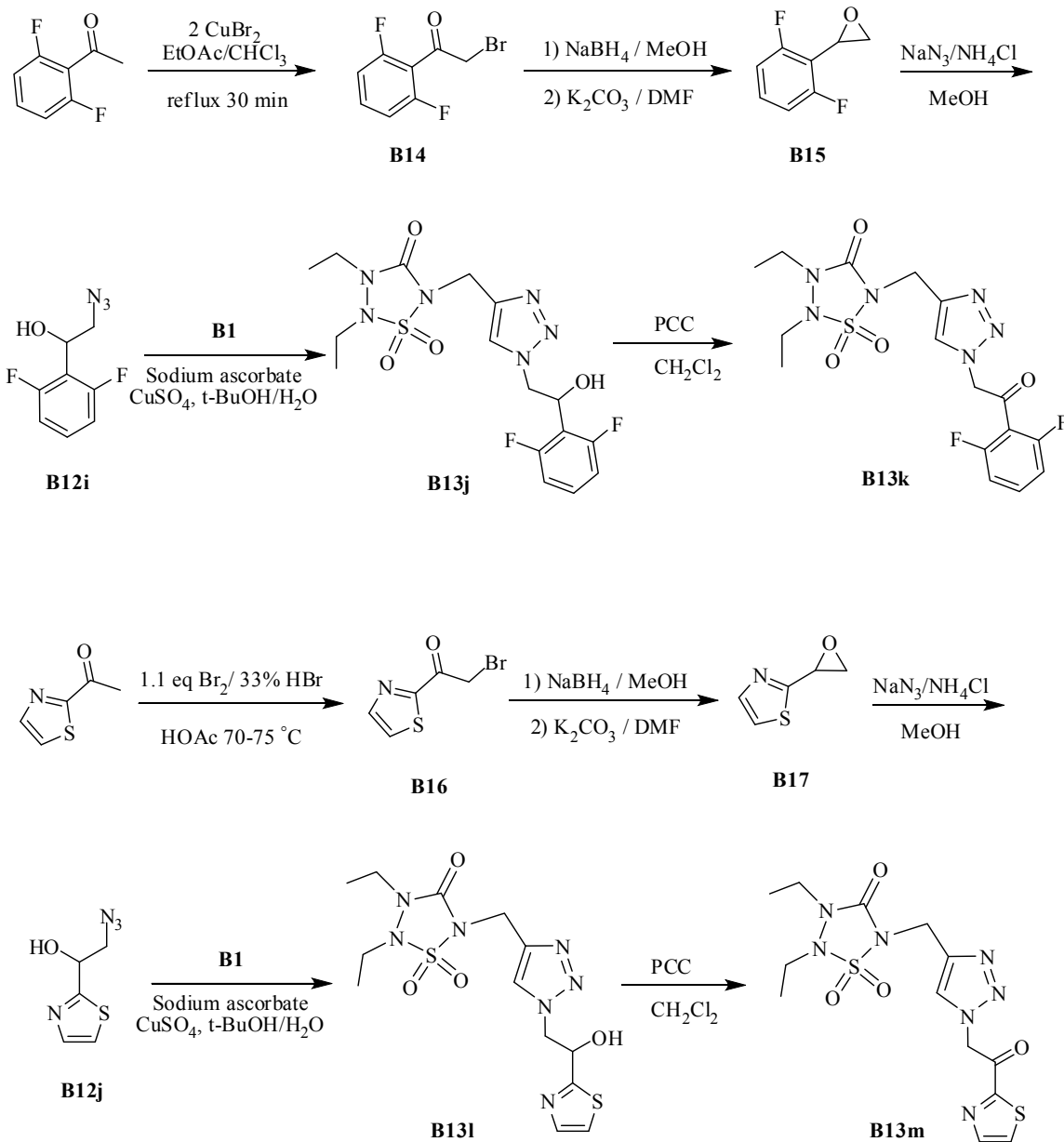


Figure 4.4 General Mechanism of Transition State Inhibitors.



Scheme 4.7 Synthesis of Triazole Compound III

4.3 Results and Discussion

4.3.1 Biochemical Studies

The inhibitory activity of compounds **B4a-i**, **B7a-h**, **B10a-e**, and **B13a-m** toward HNE

and Pr 3 was determined. It was found to range from 0 to 38% for HNE and 0 to 37% for Pr 3 under the conditions that the inhibitor-enzyme ratio was 500 for compound with a chiral center and 250 for compounds with no chiral center. Most of the inhibitors showed low inhibition towards both HNE and Pr 3, therefore only several selected compounds from each class are shown in Figure 4.5. The most active Pr 3 inhibitor **B13g** was confirmed in triplicates and it showed constant instant inhibition about 37%, but was devoid of inhibitory activity toward HNE. Construction of Dixon plot was attempted but the experiment failed because of precipitation of **B13g**. The binding constant K_i of the most active compound against Pr 3 was estimated using Michaelis-Menten equation:

$$V = (V_{\max} * [S]) / (K_m + [S])$$

where the substrate of Pr3 is Boc-Ala-Ala-Nva-SBzl ($K_{cat}/k_m = 1.06 \times 10^6 \text{ M}^{-1}\text{s}^{-1}$, $K_m = 63 \text{ }\mu\text{M}$) [246], suggesting that compound **B13g** is a low micromolar inhibitor against Pr 3. According to the molecular modeling docking result, several modifications were made to improve the potency of the inhibitor. Specifically, the phenyl ring of **B13g** was replaced with an *n*-propyl group according to the S1 pocket preferences of HNE and Pr 3, resulting in compound **B13i**. Also the phenyl ring was replaced with two electron-withdrawing rings which can potentially lead to transition state inhibitors, yielding compounds **B13k**, **B13m**. Unfortunately these compounds showed no significant inhibition towards either HNE or Pr 3. The fact that **B13g** showed no inhibition against HNE but shows consistent inhibition toward Pr 3 suggests that the design of transition state inhibitors of Pr 3 based on this template may provide a fruitful avenue of investigation for the development of potent and selective inhibitors of Pr 3.

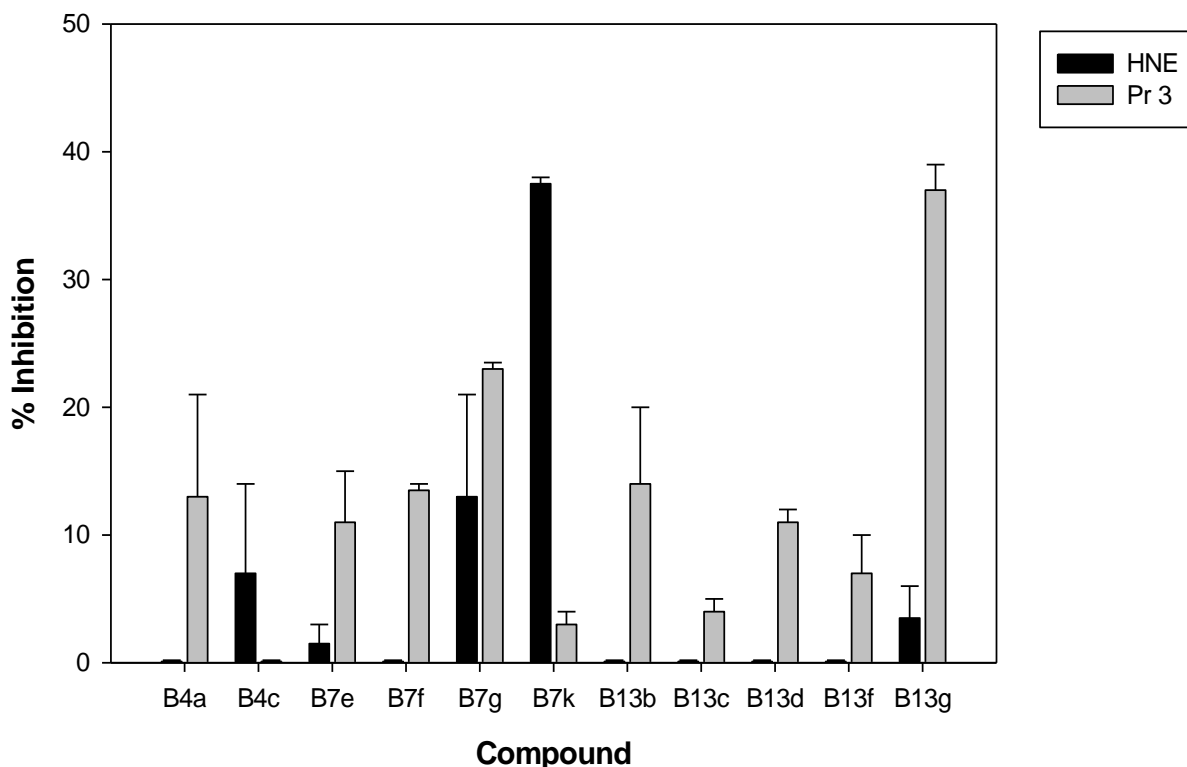


Figure 4.5 Inhibitory Activity of Selected Compounds Against Human Neutrophil Elastase and Proteinase 3. (The rest of the compounds are not showed here due to the low inhibition)

4.3.2 Molecular Modeling Studies

The most active compound **B13g** was docked to dock into Pr 3 active site (pdb code: 1FUJ) [238] using SYBYL 8.0. Molecular modeling studies suggested that **B13g** fits into the Pr 3 active site well and engages in multiple interactions with the enzyme, including the following: a) the phenyl ring binds to a hydrophobic pocket defined by Ile190, Phe192; b) the triazole ring appears to accept H-bonds from both the backbone Val216 NH and from the Lys99 side chain; c) the heterocyclic carbonyl O is well positioned to H-bond with the Lys99 side chain; d) one of the sulfamide O's is capable of H-bonding with the backbone NH of Ile217; e) the two ethyl groups interact with the second hydrophobic pocket, defined by sidechains of Phe215, Ile217 and

Trp218 (Figure 4.6; the docked structures is derived from computational studies). Quite unexpectedly, inhibitor **B13g** was predicted to bind to the active site in a reverse mode, namely, with the phenyl ring occupying the S1 pocket and the rest of the molecule projecting toward the S' subsites.

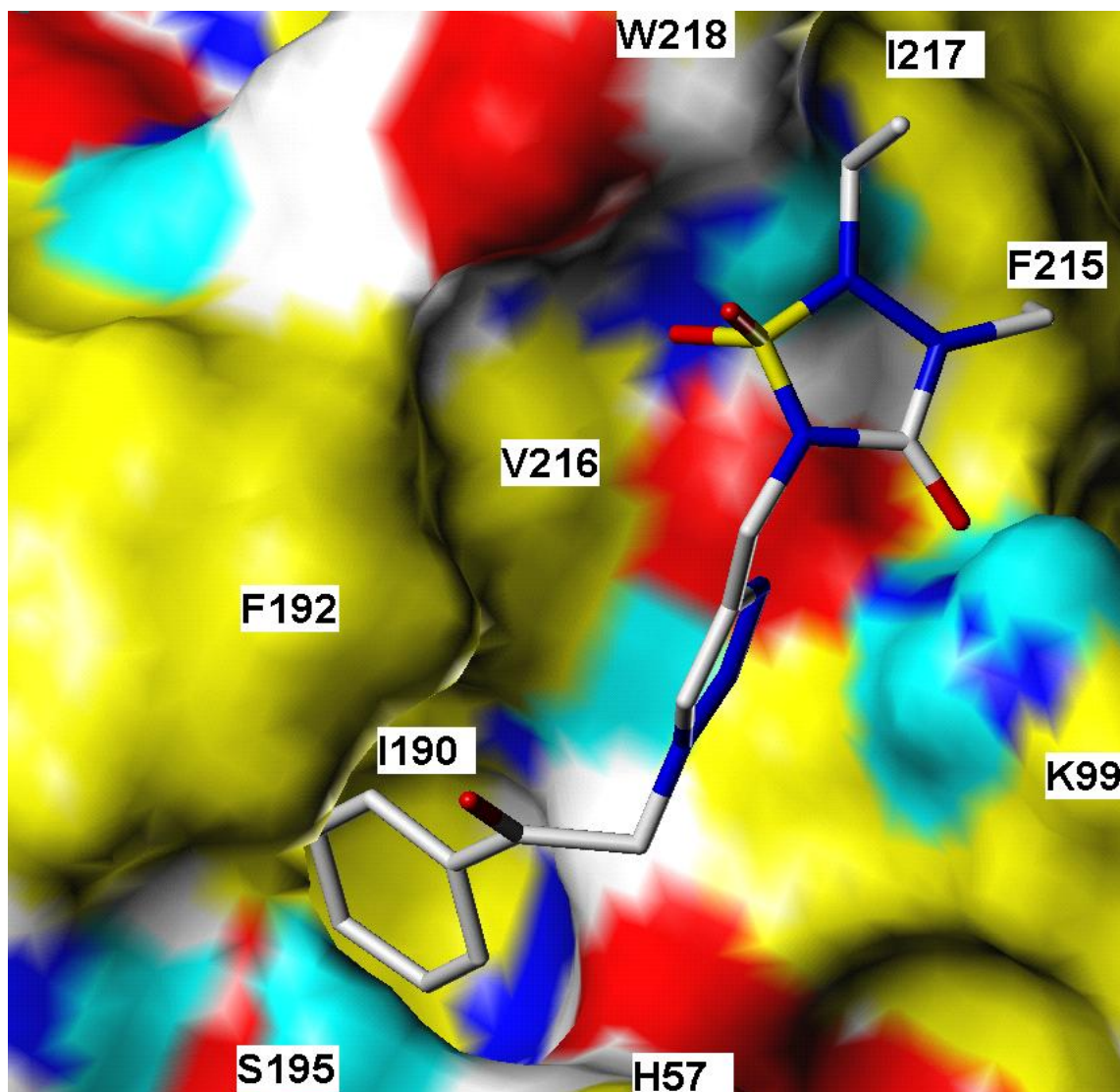


Figure 4.6 Molecular Simulation of Compound B13g Bound to Pr3 Active Site. The structure was generated from molecular simulation. Ligand rendered as CPK-colored sticks. Receptor surface colors correspond to: yellow = nonpolar, white = polar alkylys, blue = polar N, cyan = polar H, red = O.

Based on Figure 4.6, replacement of the phenyl ring by an n-propyl chain (as in compound **B13i**) would show better activity against Pr 3 since a smaller aliphatic chain is more favorable. Also, replacement of the phenyl ring which occupies the S1 pocket with an electron-withdrawing group would yield in potential transition state analogs, thus enhancing the P3 inhibition.

4.4 Experimental

4.4.1 Synthesis

General

The ^1H spectra were recorded on a Varian XL-300 or XL-400 NMR spectrometer. A Hewlett-Packard diode array UV-vis spectrophotometer was used in the in vitro evaluation of the inhibitors. Human neutrophil elastase, proteinase 3 and Boc-Ala-Ala-Nva thiobenzyl ester were purchased from Elastin Products Company, Owensville, MO. Methoxysuccinyl Ala-Ala-Pro-Val p-nitroanilide and 5,5'-dithio-bis(2-nitrobenzoic acid) were purchased from Sigma Chemicals, St. Louis, MO. Melting points were determined on a Mel-Temp apparatus and are uncorrected. Reagents and solvents were purchased from various chemical suppliers (Aldrich, Acros Organics, TCI America, and Bachem). Silica gel (230–450 mesh) used for flash chromatography was purchased from Sorbent Technologies (Atlanta, GA). Thin layer chromatography was performed using Analtech silica gel plates. The TLC plates were visualized using iodine and/or UV light. The high resolution mass spectra were performed by the Mass Spectrometry Lab at the University of Kansas, Lawrence, KS.

Representative Synthesis

2, 3-Diethyl 1, 2, 3, 5-thiatriazolidin-3-one 1, 1-dioxide B1. 1, 2-Diethylhydrazine dihydrochloride (33.0 g; 187 mmol) suspended in dry methylene chloride (300 mL) was cooled in an ice-bath under N₂ and treated with triethylamine (76.0 g; 747 mmol). After stirring for 20 minutes, a solution of N-chlorosulfonyl isocyanate (27.0 g; 187 mmol) in dry methylene chloride (100 mL) was added dropwise. The reaction mixture was stirred overnight at room temperature. The solvent was removed and 6M HCl (150 mL) was added. The aqueous solution was extracted with ethyl acetate (3×200 mL) and the combined organic extracts were dried over anhydrous sodium sulfate. The drying agent was filtered and the solvent was removed, and then the crude product was purified by flash chromatography (silica gel/ethyl acetate/hexanes) to give compound **B1** as a white solid (12.0 g; 33% yield), mp 64-66 °C. ¹H NMR (CDCl₃): δ 1.25-1.31 (m, 6H), 3.39-3.45 (q, 2H), 3.58-3.64 (q, 2H).

2, 2-Diethyl-5-carboxymethyl-1, 2, 3, 5-thiatriazolidin-3-one 1, 1-dioxide t-butyl ester B2. To a solution of compound **B1** (14 g; 72.5 mmol) in dry N, N-dimethyl-formamide (70 mL) kept in an ice bath was added sodium hydride (60%, w/w; 4.5 g; 112 mmol) and the reaction mixture was stirred for 15 minutes before adding t-butyl bromoacetate (18.5 g; 92.7 mmol). The reaction mixture was refluxed overnight with stirring. The solvent was removed *in vacuo* and the crude product was purified by flash chromatography (silica gel/ethyl acetate/hexanes) to give compound **B2** as a colorless oil (17.7g; 79% yield). ¹H NMR (CDCl₃): δ 1.22-1.28 (t, 3H), 1.28-1.34 (t, 3H), 1.47 (s, 9H), 3.39-3.44 (q, 2H), 3.60-3.65 (q, 2H), 4.10 (s, 2H).

2,2-Diethyl-5-carboxymethyl-1,2,3,5-thiatriazolidin-3-one 1, 1-dioxide B3. To a solution of Compound **B2** (3.34 g; 10.9 mmol) in dry methylene chloride (3 mL) was added trifluoroacetic acid (15 mL) and the reaction was stirred at room temperature for 1 h. The solvent and

trifluoroacetic acid were removed and the residue was re-dissolved in ethyl acetate (200 mL). The organic solution was washed with saturated sodium bicarbonate (3×40 mL) and then brine (40 mL). The organic layer was dried over anhydrous sodium sulfate. The drying agent was filtered and the solvent was removed to give compound **B3** as colorless oil (2.74 g; 100% yield). ¹H NMR (CDCl₃): δ 1.22-1.32 (m, 6H), 3.38-3.43 (q, 2H), 3.60-3.65 (q, 2H), 4.25 (s, 2H).

General coupling procedure for preparation of compounds B4a-i. A solution of acid **3** (2.4 mmol) in dry N, N-dimethylformamide (5 mL) was treated with 1-[3-(dimethylamino)-propyl]-3-ethylcarbodiimide hydrochloride (0.51g; 2.64 mmol), followed by the addition of amine (2.4 mmol) from Table 1. The reaction mixture was stirred at room temperature overnight. The solvent was removed *in vacuo* and the residue was taken up with ethyl acetate (30 mL). The organic layer was washed sequentially with 5% HCl (3×10 mL), saturated NaHCO₃ (3× 10 mL), and then brine (10 mL). The organic layer was dried over anhydrous sodium sulfate. The drying agent was filtered and the solvent removed on the rotary evaporator. The crude product was purified by flash chromatography (silica gel/ ethyl acetate/ hexanes) to give pure amide product (**B4a-i**).

Compound B4a. White solid (52% yield), mp 108-110 °C. ¹H NMR (CDCl₃): δ 1.22-1.28 (t, 3H), 1.29-1.35 (t, 3H), 3.42-3.48 (q, 2H), 3.62-3.68 (q, 2H), 4.25 (s, 2H), 7.10-7.50 (m, 5H), 8.08 (s, 1H); HRMS (ESI) calculated for C₁₃H₁₈N₄O₄SNa [M+Na]⁺ 349.0946, found 349.0936.

Compound B4b. White solid (53% yield), mp 62-63 °C. ¹H NMR (CDCl₃): δ 1.18-1.25 (m, 6H), 3.34-3.42 (q, 2H), 3.58-3.66 (q, 2H), 4.20 (s, 2H), 4.46-4.50 (d, 2H), 6.28 (s, 1H), 7.22-7.36 (m, 5H); HRMS (ESI) calculated for C₁₄H₂₁N₄O₄S [M+H]⁺ 341.1284, found 341.1295; C₁₄H₂₀N₄O₄SNa [M+Na]⁺ 363.1103, found 363.1090.

Compound B4c. White solid (20% yield), mp 91-92 °C. ¹H NMR (CDCl₃): δ 1.18-1.25 (m, 6H), 2.80-2.85 (t, 2H), 3.22-3.28 (q, 2H), 3.56-3.63 (m, 4H), 4.10 (s, 2H), 5.98 (s, 1H), 7.18-7.32 (m, 5H); HRMS (ESI) calculated for C₁₅H₂₃N₄O₄S [M+H]⁺ 355.1440, found 355.1451; C₁₅H₂₂N₄O₄SNa [M+Na]⁺ 377.1259, found 377.1255.

Compound B4d. Oil (51% yield). ¹H NMR (CDCl₃): δ 1.10-1.18 (m, 6H), 3.02-3.08 (q, 2H), 3.52-3.58 (q, 2H), 3.92-3.96 (m, 2H), 4.08 (s, 2H), 4.10-4.18 (m, 1H), 5.96 (s, 1H), 7.20-7.32 (m, 10H); HRMS (ESI) calculated for C₂₁H₂₆N₄O₄SNa [M+Na]⁺ 453.1572, found 453.1575.

Compound B4e. Oil (39% yield). ¹H NMR (CDCl₃): δ 1.20-1.26 (m, 6H), 2.80-2.85 (t, 2H), 3.28-3.33 (q, 2H), 3.50-3.58 (q, 2H), 3.58-3.66 (q, 2H), 3.80 (s, 3H), 4.06 (s, 2H), 6.20 (s, 1H), 6.82-6.88 (m, 2H), 7.08-7.11 (m, 1H), 7.17-7.21 (m, 1H); HRMS (ESI) calculated for C₁₆H₂₄N₄O₅SNa [M+Na]⁺ 407.1365, found 407.1355.

Compound B4f. Yellow solid (32% yield), mp 135-137 °C. ¹H NMR (CDCl₃): δ 1.22-1.36 (m, 6H), 3.08-3.12 (t, 4H), 3.40-3.48 (q, 2H), 3.52-3.60 (q, 2H), 3.82-3.86 (t, 4H), 4.24 (s, 2H), 6.82-6.86 (d, 2H), 7.34-7.38 (d, 2H), 7.72 (s, 1H); HRMS (ESI) calculated for C₁₇H₂₆N₅O₅S [M+H]⁺ 412.1655, found 412.1643.

Compound B4g. Brown solid (35% yield), mp 83-85 °C. ¹H NMR (CDCl₃): δ 1.22-1.36 (m, 6H), 3.40-3.46 (q, 2H), 3.52-3.58 (q, 2H), 4.10 (s, 2H), 5.90 (s, 2H), 6.65-6.78 (dd, 2H), 7.10 (s, 1H), 8.22 (s, 1H); HRMS (ESI) calculated for C₁₄H₁₉N₄O₆S [M+H]⁺ 371.1025, found 371.0984; C₁₄H₁₈N₄O₆SNa [M+Na]⁺ 393.0845, found 393.0847.

Compound B4h. Oil (62% yield). ¹H NMR (CDCl₃): δ 1.22-1.36 (m, 6H), 3.42-3.48 (q, 2H), 3.62-3.68 (q, 2H), 4.25 (s, 2H), 6.74-7.37 (m, 9H), 7.95 (s, 1H); HRMS (ESI) calculated for C₁₉H₂₂N₄O₅SNa [M+Na]⁺ 441.1209, found 441.1206.

Compound B4i. Oil (45% yield). ¹H NMR (CDCl₃): δ 1.23-1.30 (t, 3H), 1.30-1.37 (t, 3H),

2.42-2.52 (m, 6H), 3.37-3.46 (m, 4H), 3.63-3.74 (m, 6H), 4.18 (s, 2H), 6.61 (s, 1H); HRMS (ESI) calculated for $C_{13}H_{26}N_5O_5S$ $[M+H]^+$ 364.1655, found 364.1635; $C_{13}H_{25}N_5O_5SNa$ $[M+Na]^+$ 386.1474, found 386.1490.

(DL)Methyl 2-(2,3-diethyl-1,1-dioxido-4-oxo-1,2,3,5-thiatriazolidin-5-yl)-3-phenylpropanoate B5. To a stirred solution of compound **B1** (9.95 g; 55.2 mmol) and (DL) 3-phenyl-2-hydroxy propanoic acid methyl ester (10.6 g; 55.2 mmol) in dry tetrahydrofuran was added triphenyl phosphine (28.96 g; 110.4 mmol), followed by the dropwise addition of a solution of diethyl azodicarboxylate (97%; 19.9 g; 110.4 mmol) in dry tetrahydrofuran (30 mL). The reaction was stirred at room temperature overnight and the resulting precipitate was filtered off. The filtrate was evaporated to give the crude product which was purified by flash chromatography (silica gel/ ethyl acetate/ hexanes) to give compound **B5** as a colorless oil (3.2 g; 16% yield). 1H NMR ($CDCl_3$): δ 1.00-1.06 (t, 3H), 1.16-1.22 (t, 3H), 2.82-3.08 (m, 2H), 3.40-3.75 (m, 4H), 3.80 (s, 3H), 4.63-4.70 (m, 1H), 7.20-7.32 (m, 5H).

(DL) 2-(2,3-diethyl-1,1-dioxido-4-oxo-1,2,3,5-thiatriazolidin-5-yl)-3-phenyl-propanoic acid B6. A solution of compound **B5** (3.74 g; 10.5 mmol) in 1,4-dioxane (40 mL) was treated with 17.5 mL 6N potassium hydroxide solution at room temperature for 0.5 hr. The pH was adjusted to 7 by the addition of 5% hydrochloride solution and then the solvent was removed. The residue was acidified to pH 2 and extracted with ethyl acetate (3×50 mL). The combined organic extracts were dried over anhydrous sodium sulfate. The drying agent was filtered and the solvent was removed. The crude product was purified by flash chromatography (silica gel/ethyl acetate/hexanes) to give compound **B6** as a colorless oil (2.4 g; 59% yield). 1H NMR ($CDCl_3$): δ 1.00-1.06 (t, 3H), 1.16-1.22 (t, 3H), 2.76-2.86 (m, 1H), 2.94-3.04 (m, 1H), 3.39-3.75 (m, 4H), 4.65-4.73 (m, 1H), 7.20-7.32 (m, 5H).

Synthesis of Amides 7a-e. The same coupling procedures were used as described above.

Compound B7a. Oil (15% yield). ^1H NMR (CDCl_3): δ 0.92-0.98 (t, 3H), 1.12-1.18 (t, 3H), 2.50-2.61 (m, 1H), 2.72-2.84 (m, 3H), 3.36-3.75 (m, 6H), 3.81 (s, 3H), 4.47-4.55 (m, 1H), 6.50 (s, 1H), 6.80-7.30 (m, 9H); HRMS (ESI) calculated for $\text{C}_{23}\text{H}_{30}\text{N}_4\text{O}_5\text{SNa}$ $[\text{M}+\text{Na}]^+$ 497.1835, found 497.1835.

Compound B7b. White solid (23% yield), mp 155-156 °C. ^1H NMR (CDCl_3): δ 0.92-0.98 (t, 3H), 1.12-1.18 (t, 3H), 2.60-2.68 (m, 1H), 2.85-2.94 (m, 1H), 3.08-3.12 (m, 4H), 3.38-3.78 (m, 4H), 3.91-3.95 (m, 4H), 4.62-4.68 (m, 1H), 6.81-6.85 (d, 2H), 7.20-7.35 (m, 5H), 7.36-7.40 (d, 2H), 8.25 (s, 1H); HRMS (ESI) calculated for $\text{C}_{24}\text{H}_{32}\text{N}_5\text{O}_5\text{S}$ $[\text{M}+\text{H}]^+$ 502.2124, found 502.2101; $\text{C}_{24}\text{H}_{31}\text{N}_5\text{O}_5\text{SNa}$ $[\text{M}+\text{Na}]^+$ 524.1944, found 524.1939.

Compound B7c. Brown solid (14% yield), mp 100-101 °C. ^1H NMR (CDCl_3): δ 0.94-1.00 (t, 3H), 1.16-1.20 (t, 3H), 2.60-2.68 (m, 1H), 2.86-2.94 (m, 1H), 3.38-3.77 (m, 4H), 4.62-4.68 (m, 1H), 5.93 (s, 2H), 6.68-6.78 (m, 2H), 7.18-7.30 (m, 6H), 8.32 (s, 1H); HRMS (ESI) calculated for $\text{C}_{21}\text{H}_{24}\text{N}_4\text{O}_6\text{SNa}$ $[\text{M}+\text{Na}]^+$ 483.1314, found 483.1306.

Compound B7d. White solid (33% yield), mp 128-130 °C. ^1H NMR (CDCl_3): δ 0.94-1.00 (t, 3H), 1.16-1.20 (t, 3H), 2.60-2.75 (m, 1H), 2.85-3.00 (m, 1H), 3.37-3.80 (m, 4H), 3.78 (bs, 2H), 4.69-4.77 (m, 1H), 6.68-7.34 (m, 9H), 7.90 (s, 1H); HRMS (ESI) calculated for $\text{C}_{20}\text{H}_{26}\text{N}_5\text{O}_4\text{S}$ $[\text{M}+\text{H}]^+$ 432.1706, found 432.1698; $\text{C}_{20}\text{H}_{25}\text{N}_5\text{O}_4\text{SNa}$ $[\text{M}+\text{Na}]^+$ 454.1525, found 454.1506.

Compound B7e. White solid (8% yield), mp 113-115 °C. ^1H NMR (CDCl_3): δ 0.94-1.02 (m, 9H), 1.16-1.20 (t, 3H), 1.90-2.01 (m, 1H), 2.69-2.80 (m, 1H), 2.89-3.00 (m, 1H), 3.40-3.80 (m, 4H), 3.92-3.96 (d, 2H), 4.68-4.74 (m, 1H), 7.00 (s, 1H), 7.04-7.32 (m, 9H), 8.20 (s, 1H); HRMS (ESI) calculated for $\text{C}_{25}\text{H}_{33}\text{N}_5\text{O}_6\text{SNa}$ $[\text{M}+\text{Na}]^+$ 554.2049, found 554.2053.

Synthesis of compound B8. To a stirred solution of compound **B1** (0.77 g; 4 mmol) and 3-N-Boc amino benzyl alcohol (0.90 g; 4 mmol) in dry tetrahydrofuran (10 mL) was added triphenyl phosphine (2.12 g; 8 mmol) followed by the dropwise addition of a solution of diethyl azodicarboxylate (1.44 g; 8 mmol) in dry tetrahydrofuran (5 mL). The reaction was stirred at room temperature overnight. The solvent was removed under vacuum and the residue was taken up with ethyl acetate (40 mL), and then washed with water (20 mL). The organic layer was dried over anhydrous sodium sulfate. The solvent was evaporated and the crude product was purified by flash chromatography (silica gel/ethyl acetate/hexanes) to give compound **B8** as colorless oil (0.49 g; 30% yield). ¹H NMR (CDCl₃): δ 1.12-1.30 (m, 6H), 1.50 (s, 9H), 3.25-3.40 (q, 2H), 3.50-3.65 (q, 2H), 4.60 (s, 2H), 6.72 (s, 1H), 6.98-7.40 (m, 4H).

Synthesis of compound B9. To a solution of compound **B8** (0.47 g; 1.18 mmol) was added trifluoroacetic acid (5 mL) and the reaction was stirred at room temperature for 1 h. Trifluoroacetic acid was removed under vacuum and the residue was redissolved in 20 mL methylene chloride. The solvent was removed and the crude product was purified by flash chromatography (silica gel/ ethyl acetate/ hexanes) to give compound **B9** as a colorless oil (0.30 g; 85% yield). ¹H NMR (CDCl₃): δ 1.16-1.24 (m, 6H), 3.26-3.36 (q, 2H), 3.54-3.64 (q, 2H), 4.58 (s, 2H), 5.25 (bs, 2H), 6.98-7.30 (m, 4H).

Synthesis of compounds B10a-b. A solution of free amine **B9** (0.4 mmol) in dry methylene chloride (3 mL) kept in an ice-bath was treated with phthalic or succinic anhydride (0.4 mmol) and then the reaction mixture was refluxed for 1 h. The solvent was removed and the crude product was purified by flash chromatography (silica gel/ ethyl acetate/ hexanes) to give the corresponding product (**B10a-b**).

Compound B10a. White solid (70% yield), mp 134-136 °C. ¹H NMR (DMSO-D₆): δ 1.10-1.20

(m, 6H), 3.32-3.40 (q, 2H), 3.55-3.63 (q, 2H), 4.64 (s, 2H), 7.02-7.70 (m, 7H), 7.72 (s, 1H), 7.88-7.90 (m, 1H), 10.40 (s, 1H); HRMS (ESI) calculated for $C_{20}H_{22}N_4O_6SNa$ $[M+Na]^+$ 469.1158, found 469.1161.

Compound B10b. White solid (85% yield), mp 109-111 °C. 1H NMR (DMSO- D_6): δ 1.18-1.26 (m, 6H), 2.64-2.72 (t, 2H), 2.72-2.80 (t, 2H), 3.31-3.37 (q, 2H), 3.58-3.64 (q, 2H), 4.60 (s, 2H), 7.08-7.62 (m, 4H), 7.95 (s, 1H); HRMS (ESI) calculated for $C_{16}H_{22}N_4O_6SNa$ $[M+Na]^+$ 421.1158, found 421.1139.

Compound B10c. A solution of compound **B9** (0.37 g; 0.81 mmol) and phenethyl isocyanate (0.18 g; 1.21 mmol) in dry methylene chloride (3 mL) was refluxed for 1 h. The solvent was removed under vacuum and ethyl acetate (80 mL) was added. The organic layer was washed with 5% HCl (20 mL) and dried over anhydrous sodium sulfate. The drying agent was filtered and the solvent was removed. The crude product was purified by flash chromatography (silica gel/ ethyl acetate/ hexanes) to give compound **B10c** as colorless oil (0.15 g; 42% yield). 1H NMR ($CDCl_3$): δ 1.16-1.24 (m, 6H), 2.75-2.80 (t, 2H), 3.26-3.34 (q, 2H), 3.42-3.48 (q, 2H), 3.56-3.62 (q, 2H), 4.55 (s, 2H), 5.23 (s, 1H), 7.00-7.28 (m, 10H); HRMS (ESI) calculated for $C_{21}H_{27}N_5O_4SNa$ $[M+Na]^+$ 468.1681, found 468.1679.

Compounds 10d-e. Amides **13d-e** were prepared from **12** and appropriate acids using a same coupling procedure described above.

Compound B10d. Oil (76% yield). 1H NMR ($CDCl_3$): δ 1.20-1.30 (m, 6H), 3.30-3.38 (q, 2H), 3.57-3.65 (q, 2H), 4.80 (s, 2H), 7.12-7.85 (m, 9H), 8.00 (s, 1H); HRMS (ESI) calculated for $C_{19}H_{22}N_4O_4SNa$ $[M+Na]^+$ 425.1259, found 425.1272.

Compound B10e. Oil (10% yield). 1H NMR ($CDCl_3$): δ 1.20-1.28 (m, 6H), 3.30-3.38 (q, 2H), 3.57-3.65 (q, 2H), 4.60 (s, 2H), 7.00-7.64 (m, 13H), 7.86(s, 1H); HRMS (ESI) calculated for

$C_{25}H_{26}N_4O_5SNa$ $[M+Na]^+$ 517.1522, found 517.1527.

Compound B11. Compound **B1** (1.93 g; 10 mmol) was dissolved in 20 mL dry acetonitrile and triethylamine (1.01g; 10 mmol) was added, followed by propargyl bromide (1.19 g; 10 mmol). The resulting mixture was refluxed overnight. The solvent was removed, and the residue was dissolved in 40 mL ethyl acetate. The organic solution was washed with 5% HCl (3 x 20 mL), 5% saturated $NaHCO_3$ (3 x 20 mL) and then brine (20 mL). The organic layer was dried over anhydrous sodium sulfate. The drying agent was filtered off and the filtrate was evaporated under vacuum to give compound **B11** as a yellow oil (1.26 g; 54% yield). 1H NMR ($CDCl_3$): δ 1.20-1.32 (m, 6H), 2.38-2.40 (t, 1H), 3.36-3.42 (q, 2H), 3.60-3.66(q, 2H), 4.26-4.29 (d, 2H).

General procedure for preparation of azide B12a-h: To a solution of NaN_3 (1.44 g; 22 mmol) in 20 mL DMSO was added appropriate commercial or self-prepared halide (20 mmol), and the reaction was stirred at room temperature for overnight. The reaction mixture was added 70 mL H_2O under a water bath, and then extracted with 3 x 50 mL of diethyl ether. The combined organic layers were washed with 2 x 50 mL brine and dried over anhydrous sodium sulfate. Removal of solvent gave a pure product.

Compound B12a. Oil (100% yield). 1H NMR ($CDCl_3$): 4.35 (s, 2H), 7.20-7.38 (m, 4H).

Compound B12b. Oil (98% yield). 1H NMR ($CDCl_3$): 4.56 (s, 2H), 7.29-7.56 (m, 5H).

Compound B12c. Oil (99% yield). 1H NMR ($CDCl_3$): 1.51 (s, 9H), 3.77 (s, 2H).

Compound B12d. Oil (90% yield). 1H NMR ($CDCl_3$): 4.40 (s, 2H), 7.33-7.39 (m, 1H), 7.67-7.82 (m, 1H), 8.53-8.63 (m, 2H).

Compound B12e. Oil (98% yield). 1H NMR ($CDCl_3$): 3.81 (s, 3H), 4.25 (s, 2H), 6.88-6.94 (d, 2H), 7.23-7.29 (d, 2H).

Compound B12f. Oil (95% yield). 1H NMR ($CDCl_3$): 4.58 (s, 2H), 7.45-7.68 (m, 3H), 7.92-7.96

(m, 2H).

Compound B12g. Oil (92% yield). ¹H NMR (CDCl₃): 4.52 (s, 2H), 7.10-7.30 (m, 2H), 7.57-7.64 (m, 1H), 7.97-8.02 (m, 1H).

Compound B12h. Oil (76% yield). ¹H NMR (CDCl₃): 0.90-1.00 (t, 3H), 1.62-1.70 (q, 2H), 2.39-2.47 (t, 2H), 3.93 (s, 2H).

Azides **B12i-j** were prepared using the following procedure [243d]: Epoxide **B15** or **B17** (2.63 mmol) was dissolved in 15 mL methanol and then sodium azide (0.60 g; 9 mmol) and ammonium chloride (0.36 g; 6.6 mmol) were added. The resulting mixture was refluxed for 15 h. The solvent was removed and 15 mL of water was added. The aqueous solution was extracted with 2 x 15 mL ethyl acetate, and the combined organic layers were dried over anhydrous sodium sulfate. The drying agent was filtered and the filtrate was pumped to dryness, yielding a pure product.

Compound B12i. Oil (96% yield). ¹H NMR (CDCl₃): 3.49-3.55 (m, 1H), 3.77-3.85 (m, 3H), 5.09-5.15 (m, 1H), 6.89-7.00 (m, 2H), 7.24-7.40 (m, 1H).

Compound B12j. Oil (64% yield). ¹H NMR (CDCl₃): 3.63-3.80 (m, 2H), 4.72 (bs, 1H), 5.17-5.21 (m, 1H), 7.37-7.39 (d, 1H), 7.76-7.78 (d, 1H).

General alkyne-azide cycloaddition of compounds B13a-c, B13e-j and B13l. To a solution of **II** (1.8 mmol) and appropriate azide (1.8 mmol) in 5 mL of 1:1 t-BuOH and H₂O solution were added sodium ascorbate (0.04 g; 0.18 mmol) and copper sulfate pentahydrate (0.005 g; 0.018 mmol). The reaction mixture was stirred at room temperature overnight. The solvent was removed and the residue was taken up with ethyl acetate (30 mL) (any insoluble impurities were filtered off). The organic solution was washed with water (2 x 20 mL) and then dried over anhydrous sodium sulfate. The drying agent was filtered and the solvent was removed. The

residue was purified by flash chromatography (silica gel/ ethyl acetate/ hexanes) to give pure compounds **B13a-c**, **B13e-j** and **B13l**.

Compound B13a. White solid (75% yield), mp 83-84 °C. ¹H NMR (CDCl₃): 1.18-1.22 (t, 6H), 3.28-3.36 (q, 2H), 3.55-3.63 (q, 2H), 4.80 (s, 2H), 5.52 (s, 2H), 7.09-7.14 (t, 1H), 7.21 (s, 1H), 7.28-7.30 (d, 2H), 7.70 (s, 1H); HRMS (ESI) calculated for C₁₅H₂₀ClN₆O₃S [M+H]⁺ 399.1006, found 399.1016; C₁₅H₁₉ClN₆O₃SNa [M+Na]⁺ 421.0826, found 421.0824.

Compound B13b. Oil (63% yield). ¹H NMR (CDCl₃): 1.20-1.25 (t, 6H), 3.30-3.38 (q, 2H), 3.58-3.66 (q, 2H), 4.80 (s, 2H), 5.60 (s, 2H), 7.28 (s, 5H), 7.64 (s, 1H); HRMS (ESI) calculated for C₁₅H₂₁N₆O₃S₂ [M+H]⁺ 397.1117, found 397.1137; C₁₅H₂₀N₆O₃S₂Na [M+Na]⁺ 419.0936, found 419.0932.

Compound B13c. White solid (52% yield), mp 96-97 °C. ¹H NMR (CDCl₃): 1.20-1.24 (t, 6H), 1.46 (s, 9H), 3.30-3.38 (q, 2H), 3.58-3.66 (q, 2H), 4.82 (s, 2H), 5.06 (s, 2H), 7.78 (s, 1H); HRMS (ESI) calculated for C₁₄H₂₄N₆O₅SNa [M+Na]⁺ 411.1427, found 411.1440.

Compound B13e. White solid (63% yield), mp 85-86 °C. ¹H NMR (CDCl₃): 1.20-1.24 (m, 6H), 3.30-3.40 (q, 2H), 3.55-3.65 (q, 2H), 4.80 (s, 2H), 5.59 (s, 2H), 7.29-7.34 (m, 1H), 7.55-7.59 (m, 1H), 7.63 (s, 1H), 8.59-8.62 (m, 2H); HRMS (ESI) calculated for C₁₄H₂₀N₇O₃S [M+H]⁺ 366.1348, found 366.1354.

Compound B13f. White solid (66% yield), mp 71-72 °C. ¹H NMR (CDCl₃): 1.18-1.22 (t, 6H), 3.28-3.36 (q, 2H), 3.55-3.63 (q, 2H), 3.80 (s, 3H), 4.78 (s, 2H), 5.43 (s, 2H), 6.85-6.89 (d, 2H), 7.18-7.22 (d, 2H), 7.51 (s, 1H); HRMS (ESI) calculated for C₁₆H₂₂N₆O₄SNa [M+Na]⁺ 417.1321, found 417.1321.

Compound B13g. White solid (86% yield), mp 107-109 °C. ¹H NMR (CDCl₃): 1.20-1.26 (t, 6H), 3.34-3.40 (q, 2H), 3.60-3.66 (q, 2H), 4.86 (s, 2H), 5.85 (s, 2H), 7.52-7.60 (t, 2H), 7.64-7.72

(t, 1H), 7.82 (s, 1H), 7.98-8.02 (d, 2H); HRMS (ESI) calculated for C₁₆H₂₀N₆O₄SNa [M+Na]⁺ 415.1164, found 415.1164.

Compound B13h. Oil (34% yield). ¹H NMR (CDCl₃): 1.20-1.28 (t, 6H), 3.32-3.39 (q, 2H), 3.58-3.65 (q, 2H), 4.85 (s, 2H), 5.79-5.83 (d, 2H), 7.20-7.37 (m, 2H), 7.62-7.70 (m, 1H), 7.80 (s, 1H), 7.95-8.02 (m, 1H); HRMS (ESI) calculated for C₁₆H₁₉FN₆O₄SNa [M+Na]⁺ 433.1070, found 433.1049.

Compound B13i. Oil (76% yield). ¹H NMR (CDCl₃): 0.92-0.98 (t, 3H), 1.20-1.25 (t, 6H), 1.60-1.74 (m, 2H), 2.43-2.49 (t, 2H), 3.32-3.40 (q, 2H), 3.59-3.67 (q, 2H), 4.93 (s, 2H), 5.20 (s, 2H), 7.73 (s, 1H); HRMS (ESI) calculated for C₁₃H₂₂N₆O₄SNa [M+Na]⁺ 381.1321, found 381.1327.

Compound B13j. White solid (77% yield), mp 127-129 °C. ¹H NMR (CDCl₃): 1.16-1.22 (t, 6H), 3.28-3.35 (q, 2H), 3.55-3.62 (q, 2H), 4.16-4.22 (m, 1H), 4.68-4.74 (m, 1H), 4.77 (s, 2H), 6.06-6.13 (m, 1H), 6.89-6.97 (t, 2H), 7.28-7.40 (m, 1H), 7.73 (s, 1H); HRMS (ESI) calculated for C₁₆H₂₀F₂N₆O₄SNa [M+Na]⁺ 435.1133, found 453.1134.

Compound B13l. Oil (77% yield). ¹H NMR (CDCl₃): 1.19-1.25 (t, 6H), 3.28-3.36 (q, 2H), 3.55-3.63 (q, 2H), 4.60-4.71 (m, 1H), 4.75 (s, 2H), 4.96-5.04 (m, 1H), 5.43-5.51 (m, 1H), 5.56-5.61 (d, 1H), 7.34-7.36 (d, 1H), 7.73-7.76 (d, 2H); HRMS (ESI) calculated for C₁₃H₁₉N₇O₄S₂Na [M+Na]⁺ 424.0838, found 424.0827.

Compound B13k, 13m: To a suspension of pyridinium chlorochromate (PCC, 0.53g; 2.5 mmol) in 5 mL methylene chloride was added compound **B13j** or **13l** (1mmol) and the reaction was stirred at room temperature for 3 days. The supernatant was decanted and the gummy residue was washed with 10 mL of methylene chloride. The combined organic solutions were concentrated and the residue was purified using flash chromatography (silica gel/ ethyl acetate/ hexanes) to give pure compound **B13k** or **13m**.

Compound B13k. Oil (28% yield). ^1H NMR (CDCl_3): 1.20-1.26 (t, 6H), 3.32-3.40 (q, 2H), 3.59-3.67 (q, 2H), 4.86 (s, 2H), 5.70 (s, 2H), 7.01-7.08 (t, 2H), 7.51-7.60 (m, 1H), 7.81 (s, 1H); HRMS (ESI) calculated for $\text{C}_{16}\text{H}_{18}\text{F}_2\text{N}_6\text{O}_4\text{SNa}$ $[\text{M}+\text{Na}]^+$ 451.0976, found 451.0964.

Compound B13m. Oil (8% yield). ^1H NMR (CDCl_3): 1.20-1.26 (t, 6H), 3.32-3.40 (q, 2H), 3.59-3.67 (q, 2H), 4.87 (s, 2H), 6.03 (s, 2H), 7.82-7.84 (m, 2H), 8.15-8.15 (d, 1H); HRMS (ESI) calculated for $\text{C}_{13}\text{H}_{17}\text{N}_7\text{O}_4\text{S}_2\text{Na}$ $[\text{M}+\text{Na}]^+$ 422.0681, found 422.0686.

Compound B13d: Compound **B13c** (0.11g; 0.28 mmol) was added 3 mL 4M HCl in dry 1,4-dioxane, and the reaction was stirred at room temperature for 2 h. The solvent was removed and the residue was washed with 1 mL chloroform, leaving the pure product **13d** as a white solid (0.09 g; 97% yield), mp 145-147 °C. ^1H NMR (CD_3OD): 1.18-1.22 (m, 6H), 3.30-3.40 (q, 2H), 3.60-3.70 (q, 2H), 4.80 (s, 2H), 5.26 (s, 2H), 8.03 (s, 1H); HRMS (ESI) calculated for $\text{C}_{10}\text{H}_{16}\text{N}_6\text{O}_5\text{SNa}$ $[\text{M}+\text{Na}]^+$ 355.0801, found 355.0802.

Synthesis of compound B14: Copper (II) bromide (4.46 g; 20 mmol) was ground and placed into a RB flask, ethyl acetate (10 mL) was added and the mixture was brought to boiling. 2', 6'-difluoroacetylphenone (1.72 g; 11 mmol) in 10 mL chloroform was added through the top of the condenser. The reaction started immediately and the mixture was refluxed for 30 min whereupon a large amount of amber precipitate formed and gas release ceased. The reaction mixture was cooled down, 10 mL H_2O was added and stirred for 1 min. The precipitate was filtered and the filtrate was extracted with 30 mL ethyl acetate. The organic layer was washed with brine (2 x 20 mL) and dried over anhydrous sodium sulfate. The drying agent was filtered off and the filtrate was concentrated to dryness to give compound **B14** as a colorless oil (2.35g; 100% yield). ^1H NMR (CDCl_3): 4.39 (s, 2H), 6.95-7.05 (m, 2H), 7.42-7.55 (m, 1H).

Synthesis of compound B15: Compound **B14** (2.35 g; 10 mmol) was dissolved in 30 mL

methanol and sodium borohydride (0.40 g; 10 mmol) was added at 0 °C in small portions. The reaction was then stirred for 1 h at 0 °C. Two milliliters of 12 N sulfuric acid and 10 mL water were added and the reaction was stirred for 2 min before the solvent was removed. The residue was dissolved in 40 mL ethyl acetate, and the organic solution was washed with 30 mL water. The organic layer was separated and dried over anhydrous sodium sulfate. The drying agent was filtered and the filtrate was pumped to dryness. The residue was dissolved in 10 mL DMF, and solid potassium carbonate (3.45 g; 25 mmol) was added. The resulting mixture was stirred at room temperature overnight. Water (15 mL) was added and the solution was extracted ethyl acetate (2 x 40 mL). The combined organic layers were washed with brine (2 x 30 mL) and dried over anhydrous sodium sulfate. The drying agent was filtered off and the filtrate was concentrated to give pure compound **B15** (0.82 g; 53% yield) as a colorless oil. ¹H NMR (CDCl₃): 3.14-3.18 (m, 1H), 3.32-3.36 (m, 1H), 4.01-4.04 (m, 1H), 6.82-6.95 (m, 2H), 7.21-7.33 (m, 1H).

Synthesis of compound B16: 2-Acetylthiazole (1.27 g; 10 mmol) was dissolved in 8 mL glacial acetic acid, 33% HBr in acetic acid (2.5 mL; ~10 mmol) was added and the resulting mixture was placed in an ice-bath. Bromine (0.57 mL; 11 mmol) was added and then the reaction was allowed to warm to 70-75 °C for 2 h with stirring. The disappearance of reddish color indicated the reaction has completed. The reaction mixture was cooled to room temperature, and the precipitate was filtered and washed with 15 mL ethyl acetate. The filter cake was transferred into a round-bottom flask, 20 mL of water was added and pH was adjusted to ~ 10 using 6 N NaOH. The oily product was extracted with ethyl acetate (2 x 30 mL) and the combined organic layers were dried over anhydrous sodium sulfate. The drying agent was filtered and the filtrate was concentrated to dryness, yielding a pure compound **B16** (1.63 g; 79% yield) as a reddish oil.

^1H NMR (CDCl_3): 4.73 (s, 2H), 7.78-7.80 (d, 1H), 8.05-8.07 (d, 1H).

Compound **B17** was prepared using the same procedure as compound **B15**.

Compound B17: oil (63% yield). ^1H NMR (CDCl_3): 3.01-3.05 (m, 1H), 3.24-3.28 (m, 1H), 4.28-4.32 (m, 1H), 7.32-7.34 (d, 1H), 7.77-7.79 (d, 1H).

4.4.2 Enzyme Assays and Inhibition Studies

Human Neutrophil Proteinase 3

Twenty microliters of 32.0 mM 5, 5'-dithio-bis(2-nitrobenzoic acid) in dimethyl sulfoxide and 10 μL of 3.45 μM human proteinase 3 in 0.1 M phosphate buffer /pH 6.50 (final enzyme concentration: 34.5 nM) were added to a cuvette containing a solution of 940 μL 0.1 M HEPES buffer/0.5 M NaCl/pH 7.25, 10 μL 862.5 μM inhibitor in dimethyl sulfoxide (final inhibitor concentration: 8.62 μM) and 20 μL 12.98 mM Boc-Ala-Ala-NVa-SBzl (final substrate concentration: 259.6 μM) at 25 $^\circ\text{C}$. The change in absorbance was monitored at 410 nM for 2 minutes. A control (hydrolysis run) was also run under the same conditions by adding 5, 5'-dithio-bis(2-nitrobenzoic acid) in dimethyl sulfoxide and 10 μL of 3.45 μM solution of human proteinase 3 in 0.1 M phosphate buffer/pH 6.50 (final enzyme concentration: 34.5 nM) to a cuvette containing a solution of 940 μL 0.1 M HEPES buffer/0.5 M NaCl/pH 7.25, 10 μL dimethyl sulfoxide and 20 μL 12.98 mM Boc-Ala-Ala-NVa-SBzl (final substrate concentration: 259.6 μM). The change in absorbance was monitored at 410 nM for 2 minutes. The percent inhibition of Pr 3 was determined using $\% \text{ inhibition} = (1-v/v_0) \times 100$ and is the average of duplicate or triplicate determinations.

Human Neutrophil Elastase

Ten microliters of 7.0 μM human elastase in 0.05 mM sodium acetate buffer/0.5 M NaCl/pH 5.50 (final enzyme concentration: 70 nM) was added to a cuvette containing a solution of 970 μL 0.1 M HEPES buffer /0.5 M NaCl/pH 7.25, 10 μL of 3.5 mM solution of inhibitor in dimethyl sulfoxide (final inhibitor concentration: 35 μM) and 10 μL of 70 mM methoxysuccinyl-Ala-Ala-Pro-Val *p*-nitroaniline (final substrate concentration: 700 μM) at 25 °C. The change in absorbance was monitored at 410 nM for 2 minutes. A control (hydrolysis run) was also run under the same conditions by adding 10 μL of a 7.0 μM solution of human elastase (final enzyme concentration: 70 nM) to a cuvette containing 970 μL 0.1 M HEPES buffer/0.5 M NaCl/pH 7.25, 10 μL DMSO and 10 μL of 70 mM methoxysuccinyl-Ala-Ala-Pro-Val *p*-nitroaniline (final substrate concentration: 700 μM). The change in absorbance was monitored at 410 nM for 2 minutes. The percent inhibition of HNE was determined using $\% \text{ inhibition} = (1 - v/v_0) \times 100$ and is the average of duplicate or triplicate determinations.

4.4.3 Computational Method

Molecular docking simulation was performed using the SURFLEX program [247]. The structure of Compound **B13g** was constructed in SYBYL [231] and was structurally optimized to default convergence thresholds using the Tripos Force Field [232] and Gasteiger–Marsili partial atomic charges [233]. A receptor model was prepared for Pr 3 using the 1FUJ crystal structure. This structure was protonated in SYBYL according to pH = 7.0 protonation states, stripped of all water molecules and bound ligands, and electrostatically represented with Gasteiger–Marsili charges.

4.4.4 X-ray Crystallography

A crystal was affixed to a nylon cryoloop using oil (Paratone-n, Exxon) and mounted in the cold stream of a Bruker Kappa-Apex-II area-detector diffractometer. The temperature at the crystal was maintained at 150 K using a Cryostream 700EX low-temperature apparatus (Oxford Cryosystems). The unit cell was determined from the setting angles of the reflections collected in 36 frames of data. Data were measured using graphite mono-chromated molybdenum K_{α} radiation ($\lambda = 0.71073 \text{ \AA}$) collimated to a 0.6 mm diameter and a CCD detector at a distance of 50 mm from the crystal with a combination of phi and omega scans. A scan width of 0.5 degrees and scan time of 10 seconds were employed. Data collection, reduction, structure solution, and refinement were performed using the Bruker Apex2 suite (v2.0-2) [248]. All available reflections to $2\theta_{\max} = 52^{\circ}$ were harvested and corrected for Lorentz and polarization factors with Bruker SAINT (v6.45) [249]. Reflections were then corrected for absorption, interframe scaling, and other systematic errors with SADABS 2004/1 [250]. The structure was solved (direct methods) and refined (full-matrix least-squares against F^2) with the Bruker SHELXTL package (v6.14-1) [251]. All non-hydrogen atoms were refined using anisotropic thermal parameters. Hydrogen atoms were included at idealized positions and were not refined. Pertinent details are given in Table 4.5.

Table 4.5 X-ray Data Collection and Structure Solution Parameters for Compound B13a

molecular formula	C ₁₅ H ₁₉ ClN ₃ O ₆ S
fw	398.87
diffractometer	Bruker Kappa Apex II
radiation/ λ , Å	Mo K α /0.71073
temp, K	150
color, habit	colorless, needle
crystal system	Monoclinic
space group	P2 ₁ /n
crystal size(mm ³)	0.17 x 0.25 x 0.69
<i>a</i> , Å	10.2729(12)
<i>b</i> , Å	8.4972(9)
<i>c</i> , Å	41.227(5)
β , deg	94.384(6)
<i>V</i> , Å ³	3588.2(7)
<i>Z</i>	8
calcd density(g cm ⁻¹)	1.477
octants collected	$\pm h, \pm k, \pm l$
Max. <i>h</i> , <i>k</i> , <i>l</i>	12, 10, 50
Θ range ()	2.45-26.00
μ , mm ⁻¹	0.359
rflns/unique (<i>R</i> _{int})	80192/7069 (0.0270)
obs,[$>2\sigma$]/params	7069/473
<i>R</i> _{obs} , <i>R</i> _{all}	0.0326/0.0383
GOF	1.083
ρ_{\max}/ρ_{\min} , e Å ⁻³	0.333, -0.466

CHAPTER 5

1,2,5-THIADIAZOLIDINE 1,1-DIOXIDE-BASED COPD-RELATED PROTEASE INHIBITORS

5.1 Inhibitor Design Rationale

Mechanism-based inhibitors of serine proteases based on 1,2,5-thiadiazolidin-3-one 1,1-dioxide (structure (I), Figure 5.1) have demonstrated that these compounds are highly effective inhibitors of these enzymes. Both molecular simulation studies and X-ray crystallography studies suggested that the hydrophobic P₁ residue nestled in the S1 pocket of HNE and the carbonyl group of the heterocyclic ring is attacked by the active site serine (Ser195) during the enzyme inactivation [217]. Based on these facts, we reasoned that replacement of the C=O group by a CH₂ group would generate a 1,2,5-thiadiazolidine 1,1-dioxide (cyclosulfamide) and transform (I) into a new class of non-covalent inhibitors (IV) (Figure 5.1) [252]. The non-covalent inhibitor IV is predicted to bind to the HNE enzyme in the similar fashion, but the absence of carbonyl group would result in simple competitive inhibition. More importantly, HNE and Pr 3 have very similar substrate specificity but exhibit significant differences in the S' subsites, specifically, the S' subsites of HNE are more hydrophobic whereas the S' subsites of Pr 3 are more polar. Therefore the variation of R of inhibitor IV could potentially be used to exploit the active sites of both HNE and Pr 3.

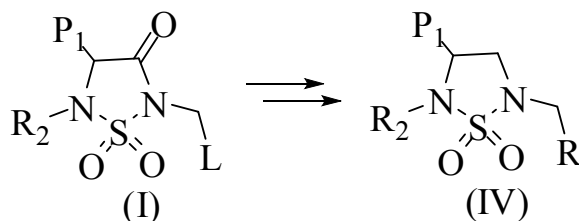


Figure 5.1 Design of Non-Covalent Inhibitor (IV)

A preliminary study of inhibitor IV using molecular modeling was first undertaken using AutoDock4. Considering the preferences of HNE and Pr 3, especially at S' subsites, two model compounds (shown in Figure 5.2 A, B) were docked into the HNE active site (pdb code: 1ppf) whereas two model compounds (shown in Figure 5.2 C, D) were docked into the Pr 3 active site (pdb code: 1fuj). The docking results are shown in Figure 5.3. Both non-covalent HNE inhibitor A and B bind to the HNE active site in similar fashion as the mechanism-based inhibitors **A15** and **A16** (chapter 3), respectively (shown in Figure 5.3 A, B). Specifically, the hydrophobic isobutyl residue is nestled into the S1 pocket and the rest of the molecule was accommodated in the hydrophobic S' subsites. Although they bind slightly differently at S' subsites from the mechanism-based inhibitors, the binding scores are similar or higher than compounds **A15**, **A16**. For Pr 3, inhibitor II can take the full advantage of polar interactions of Pr 3 active sites because the substitution will not be cleaved off as the mechanism-based inhibitor I. Depending on the Pr 3 S' subsite specificity, two more polar compounds **C**, **D** in Figure 5.2 were docked in Pr 3 active site and the docking results are shown in Figure 5.3 **C**, **D**. Clearly, both compounds make effective contacts with Pr 3 active site as following: a) both the isobutyl residues bind to the hydrophobic S1 pocket defined by Ile190, Phe192; b) for compound **C**, the heterocyclic sulfamide ring is positioned at the Pr 3 active site similarly as compound **A** and **B**, and the triazole with an amine group is oriented to either hydrogen binding to carboxylic acid group of Asp61 side chain or form even stronger ion-ion interaction with this carboxylic acid; c) unlike compound **C**, two heterocyclic rings of compound **D** are oriented to the S pockets driven by a hydrogen binding between acid oxygen and one NH of the Lys99 side chain amine group (an ion-ion interaction may be also possible in the charged state).

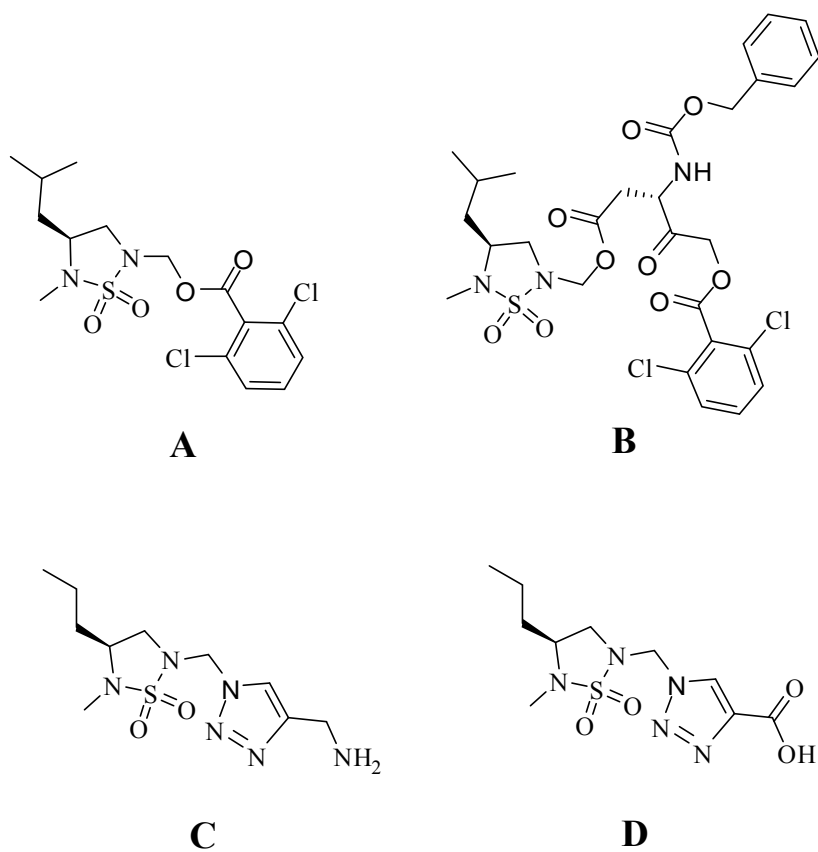


Figure 5.2 Predicted HNE/Pr 3 Non-covalent Inhibitors. Compound **A**, **B** are HNE inhibitors and compound **C**, **D** are Pr 3 inhibitors.

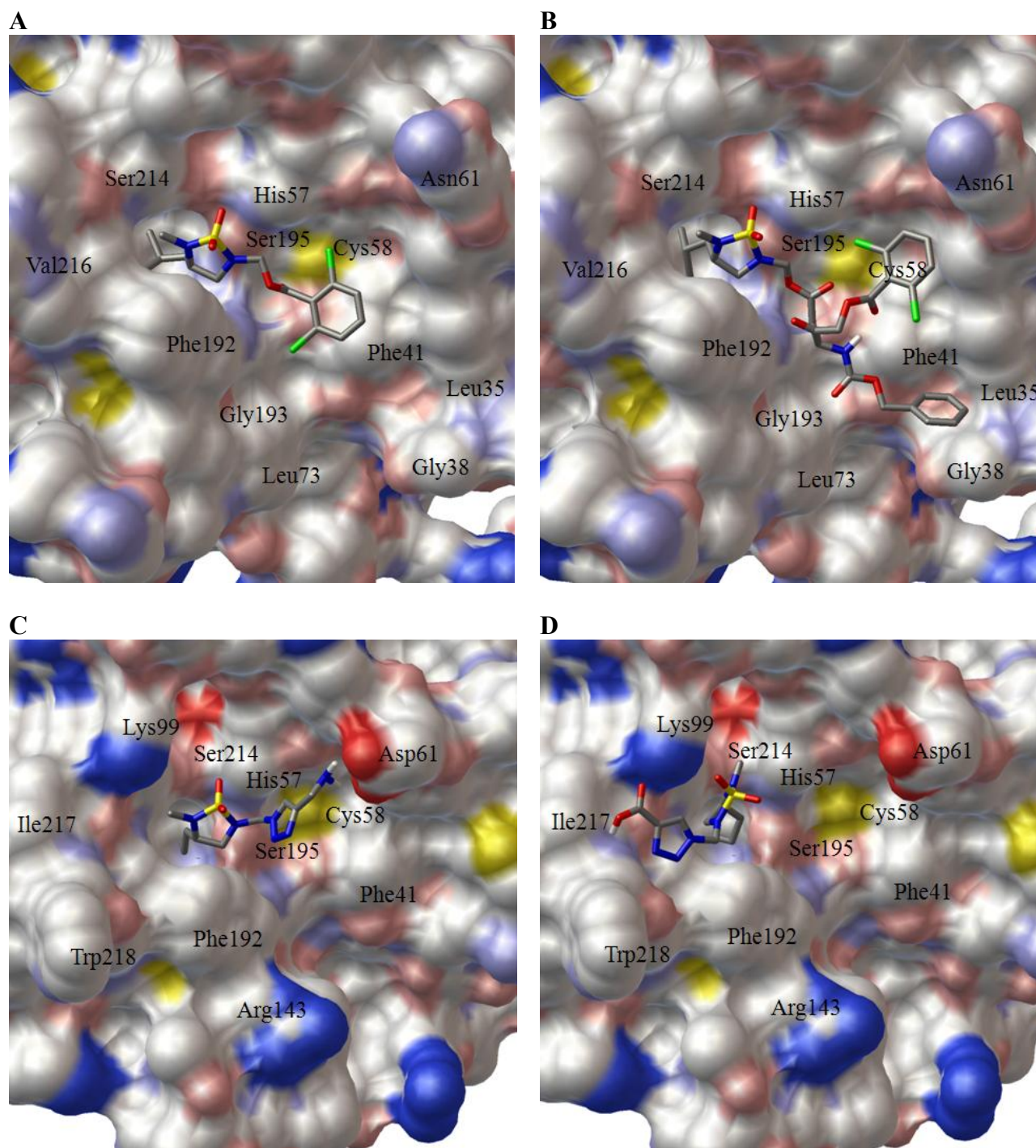
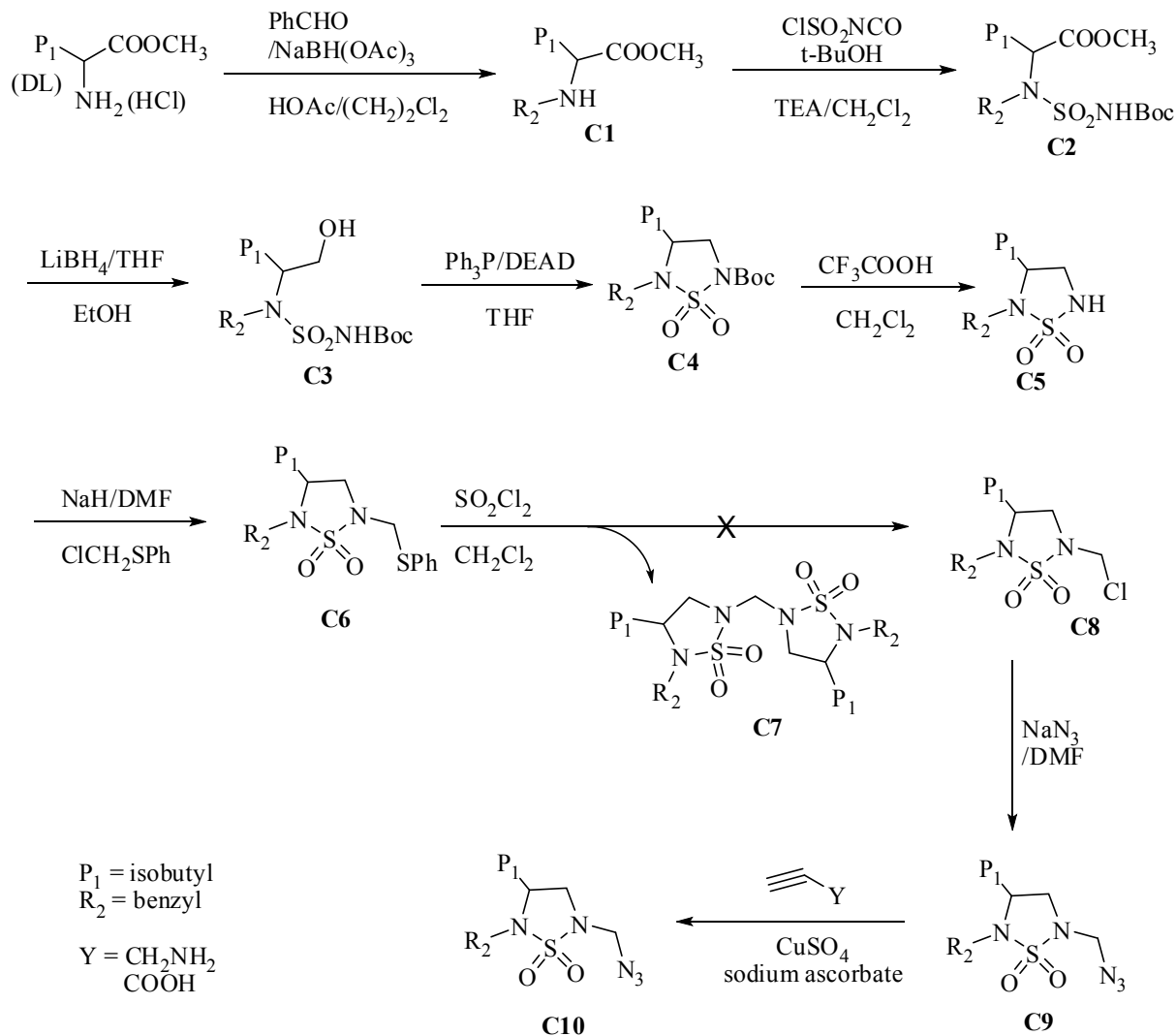


Figure 5.3 Non-covalent Inhibitors and HNE/Pr 3 Interactions. The structures are generated from molecular simulation using AutoDock4. Ligands rendered as CPK-colored sticks. Receptor surface colors correspond to: red = O, blue = polar N, cyan = polar O, light blue = amide NH, yellow = S, white = nonpolar. (A) compound **A** bound to the HNE active site, (B) compound **B** bound to the HNE active site, (C) compound **C** bound to the Pr 3 active site, (D) compound **D** bound to the Pr 3 active site.

5.2 Results and Discussion

5.2.1 Synthesis

The synthesis of 1,2,5-Thiadiazolidine 1,1-Dioxide-based non-covalent inhibitors is outlined in Scheme 5.1. Treatment of (DL) norvaline methyl ester hydrochloride with benzaldehyde followed by sodium triacetoxyborohydride in the presence of acetic acid yielded compound **C1**. The reaction of compound **C1** with freshly prepared tert-butyl chlorosulfonylcarbamate in the presence of TEA followed by reduction using lithium borohydride and Mitsunobu reaction with triphenylphosphine and diethyl azodicarboxylate (DEAD) yielded compound **C4**. The Boc protection was removed using TFA and N-phenylthiomethyl group was introduced by N-alkylation with chloromethyl phenyl sulfide in the presence of sodium hydride to give compound **C6**. Treatment of compound **C6** with sulfuryl chloride was expected to yield compound **C8**. Compound **C8** is a very important intermediate that can be used to exploit the prime subsites of both HNE and Pr 3. For example, inhibitors using alkylation of **C8** according to the HNE S' subsites preferences may potentially interact with HNE S' subsites. When the chlorine of **C8** can be replaced by an azide, the resulting azide product can be transformed into a triazole product (Pr 3 prefers polar groups at S' subsites) by click chemistry method. A polar amino or carboxylic acid group can be functionalized on the triazole ring if a propargyl amine or propiolic acid is used in click chemistry reaction. Unfortunately, treatment of compound **C6** with sulfuryl chloride yielded a complex mixture. Work up of this mixture and subsequent purification of the product by flash chromatography afforded a solid which did not exhibit the spectral characteristics of the expected N-chloromethyl compound **C7**. Instead, an unexpected dimeric product **C8** was obtained. The characterization of this compound and a postulated mechanism of its formation are shown below.



Scheme 5.1 Synthesis of HNE/Pr 3 Non-covalent Inhibitors

The structure of product **C7** was established on the basis of the following data: the molecular weight of the compound was determined by ESI-MS to be 549, corresponding to the molecular formula $\text{C}_{27}\text{H}_{40}\text{N}_4\text{O}_4\text{S}_2$, which was in agreement with the elementary analysis of the product. The structure of **C7** was established unambiguously via single crystal X-ray crystallography. An ORTEP [21] view (Figure 5.4) and X-ray crystal structure data (Table 5.1) are shown below [253].

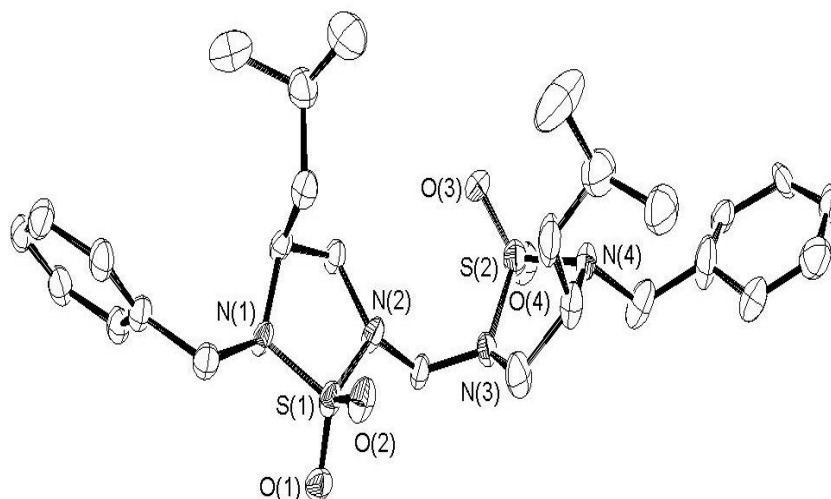


Figure 5.4 ORTEP Drawing of Compound C8 Showing the 30% Thermal Ellipsoids. H atoms have been omitted for clarity.

Table 5.1 Crystal Data and Structure Refinement Parameters for C8

Empirical formula	C ₂₇ H ₄₀ N ₄ O ₄ S ₂
Formula weight	548.75
Temperature	150 K
Diffractometer	Bruker Kappa APEX II
Radiation	Mo K α , 0.71073 Å
Crystal system	Monoclinic
Space group	C2/c
Unit cell dimensions	a = 40.714(7) Å b = 6.2300(9) Å c = 27.774(4) Å β = 124.547(9)°
Volume	5802.5(16) Å ³
Z	8
Density (calculated)	1.256 Mg/m ³
Absorption coefficient	0.222 mm ⁻¹
F(000)	2352
Crystal size	0.43 x 0.06 x 0.05 mm ³
Crystal habit	Needle
Crystal color	colorless
Θ range for data collection	2.04 to 26.00° -50 \leq h \leq 50
Limiting indices	-7 \leq k \leq 7 -34 \leq l \leq 34
Reflections collected/unique	50861/5705 [R(int) = 0.4278]
Completeness to θ = 26.00°	99.8 %
Refinement method	Full-matrix least-squares on F ²
Data / restraints / parameters	5705 / 0 / 367
Refinement threshold	I > 2 σ (I)
Data > threshold	1681
Goodness-of-fit on F2	1.021
Final R indices [I > 2 σ (I)]	R1 = 0.0896, wR2 = 0.1829
R indices (all data)	R1 = 0.3060, wR2 = 0.3004
Largest diff. peak and hole	0.491 and -0.400 e.Å ⁻³

A plausible mechanism depicting the formation of **C7** is outlined in Figure 5.5, line (a), whereby initial formation of a chlorosulfonium salt proceeds further along two pathways: one leading to an iminium ion (A) [254], and the other leading to a sulfur ylide (B), probably favored by the high acidity of the methylene hydrogens in the moiety $-N(SO_2N-)CH_2SClPh$. This ylide subsequently undergoes rearrangement to α -chlorosulfide (C) in a process that is reminiscent of the Pummerer rearrangement [255,256]. When (C) dissociates into an ion pair (both ions are stabilized by resonance), anion (D) undergoes a Michael-type reaction with iminium ion (A) to afford the unusual dimeric product **C7**. The equilibrium leading to (A) will likely be more favorable for formation of (A) than (B), and hence more favorable for (A) than for (C) and (D). However, capture of (D) by (A) to produce **C7** would shift the series of equilibria from (B) to (C) and (D), ultimately leading to **C7**.

It now becomes clear why such a dimeric product is not observed when the initial phenyl thiomethyl ether bears a carbonyl group at position 3 of the 1,2,5-thiadiazolidine 1,1-dioxide ring, but merely affords the chloromethyl derivative upon treatment with sulfuryl chloride (Figure 5.5, line (b)). The presence of a C=O group adjacent to nitrogen located at position 2 diminishes its nucleophilicity considerably (by virtue of being adjacent to a C=O group, as well as an SO₂ group), rendering path (a) in Figure 5.5 inoperative and blocking the formation of a dimer.

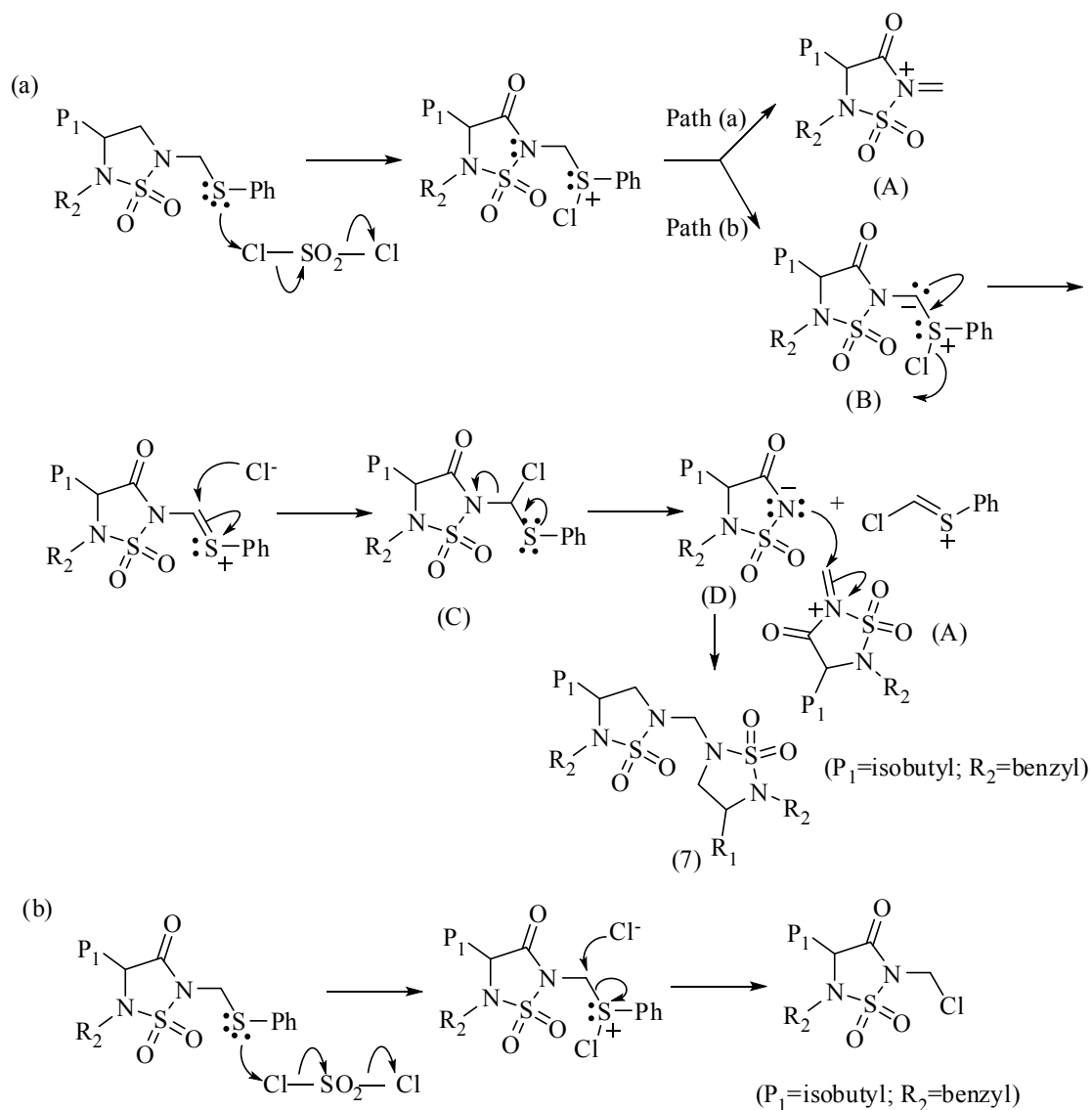
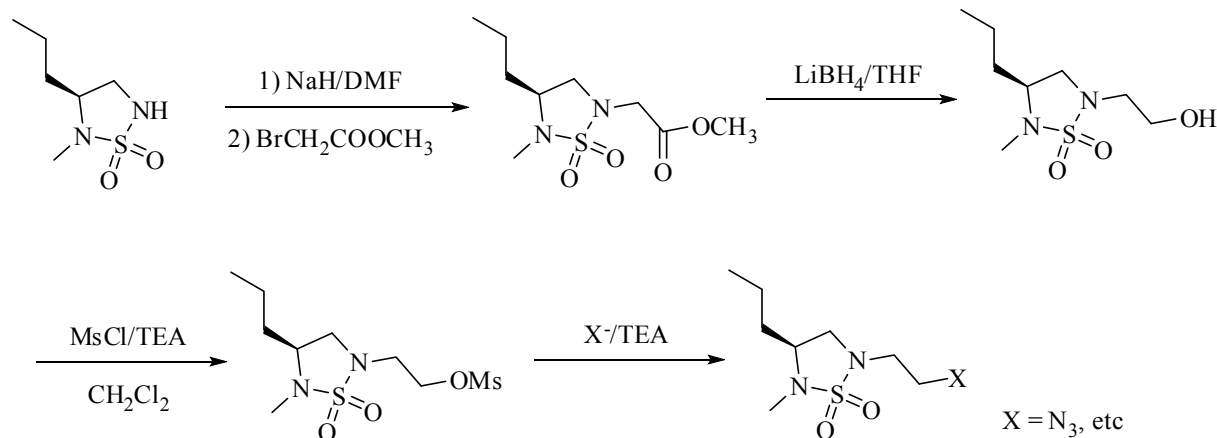


Figure 5.5 Postulated Mechanism for the Formation of Compound C8

5.3 Conclusions and Future Plans

The synthesis of desired inhibitor was unsuccessful due to the formation of dimeric compound **C8**. In the future, non-covalent inhibitors using the same heterocyclic scaffold can be sequentially prepared by the following reaction from compound **C6**: an alkylation with methyl bromoacetate, followed by reduction with lithium borohydride and mesylation with methanesulfonyl chloride. The product can be used for alkylation as originally planned such as,

replacing with an azide to make the Pr 3 non-covalent inhibitors (Scheme 5.2).



Scheme 5.2 Proposed Synthesis of Non-covalent Inhibitors.

5.4 Experimental

General

The ¹H NMR spectra were recorded on a Varian XL-300 or XL-400 NMR spectrometer. Melting points were determined on a Mel-Temp apparatus and are uncorrected. IR spectra were taken with a FT-IR-Avatar 360 spectrometer. MS spectra were recorded with Varian-1200L mass spectrometer. Elemental analysis data were obtained from Columbia Analytical Services (Tucson, AZ). Reagents and solvents were purchased from various chemical suppliers (Aldrich, Acros organics, TCI America, and Bachem). Silica gel (230-450 mesh) used for flash chromatography was purchased from Sorbent Technologies, Atlanta, GA. Thin layer chromatography was performed using Analtech silica gel plates. The TLC plates were visualized using iodine and/or UV light.

Methyl 2-(benzylamino)-4-methylpentanoate C1: DL-Leucine methyl ester hydrochloride (43.6 g; 240 mmol) was suspended in 250 mL 1,2-dichloroethane, and then benzaldehyde (30.8

g; 270 mmol) and acetic acid (19.2 g; 320 mmol) were added, followed by sodium triacetoxyborohydride (71.2 g; 335 mmol). The reaction was stirred at R.T. overnight. The reaction mixture was adjusted to pH 10 using 20% sodium hydroxide, and then two layers were separated. The aqueous layer was extracted with 2×100 mL diethyl ether and the organic layers were combined and dried over anhydrous sodium sulfate. Removal of solvent yielded a crude product, which was purified by flash chromatography (silica gel/ethyl acetate/hexanes) to give compound **C1** as a colorless oil (27.0 g, 48.6% yield). ir (neat): 3333 (NH), 1735 (C=O) cm^{-1} ; ^1H nmr (CDCl_3): δ 0.88 (dd, 6H, 2 CH_3 , $J=6.6, 19.8$ Hz), 1.48 (t, 2H, CH_2 , $J=7.5$ Hz), 3.31 (t, 1H, $\alpha\text{-H}$, $J=7.5$ Hz), 3.71 (dd, 2H, CH_2 , $J=12.9, 60$ Hz), 3.72 (s, 3H, OCH_3), 7.20-7.26 (m, 5H, phenyl protons); ms: m/z 258 (M^++Na , 27%), 236 (M^++1 , 53%), 176 ($\text{M}^+-\text{C}(\text{O})\text{OCH}_3$, 21%), 91 (phCH_2^+ , 100%). *Anal. Calcd.* for $\text{C}_{14}\text{H}_{21}\text{NO}_2$: C, 71.46; H, 8.99; N, 5.95. Found: C, 71.19; H, 9.28; N, 5.94.

Methyl 2-(benzyl(N-(tert-butoxycarbonyl)sulfamoyl)-amino)-4-methylpentanoate C2: A solution of N-chlorosulfonyl isocyanate (14.9 g; 103 mmol) in 130 mL dry methylene chloride cooled in an ice-bath was added dropwise a solution of t-butyl alcohol (7.72 g; 103 mmol) in 130 mL dry methylene chloride with stirring. After 15 min stirring, the resulting solution was added dropwise to a solution of compound **C1** (24.24 g; 103 mmol) and triethylamine (10.6 g; 103 mmol) in 130 mL dry methylene chloride under an ice-bath. The ice-bath was removed after the addition and the reaction stirred at R.T. for 6 h. The reaction mixture was washed with 150 mL brine and the organic layer was dried over anhydrous sodium sulfate. Removal of solvent yielded a crude product, which was purified by flash chromatography (silica gel/ethyl acetate/hexanes) to give compound **C2** as a white solid (31.0 g, 72.6% yield), mp 95-96 °C. ir (KBr pellet): 3355 (NH), 1740 (C=O) cm^{-1} ; ^1H nmr (CDCl_3): δ 0.68 (dd, 6H, 2 CH_3 , $J=6.0, 94.5$ Hz), 1.40-1.60 (m,

3H, CH & CH₂), 1.50 (s, 9H, t-Butyl protons), 3.70 (s, 3H, OCH₃), 4.65 (t, 1H, alpha-H, J=7.5 Hz), 4.71 (dd, 2H, CH₂, J=16.5, 122.1 Hz, CH₂), 7.25-7.45(m, 5H, phenyl protons); ms: m/z 437 (M⁺+Na, 100%), 381 (M⁺-OCH₃, 19%), 258 (M⁺-SO₂NHBoc+Na, 29%), 236 (M⁺-SO₂NHBoc+1, 46%), 91 (PhCH₂⁺, 19%). *Anal. Calcd.* for C₁₉H₃₀N₂O₆S: C, 55.05; H, 7.29; N, 6.76. Found: C, 55.13; H, 7.03; N, 6.62.

Tert-butyl N-benzyl-N-(1-hydroxy-4-methylpentan-2-yl)sulfamoylcarbamate C3: To a solution of compound **C2** (27.21 g; 65.5 mmol) in 100 mL dry THF was added dropwise a solution of 2 M lithium borohydride in THF (32.8 mL; 65.6 mmol), followed by the dropwise addition of 197 mL absolute ethanol. The reaction mixture was stirred at R.T. overnight. The reaction mixture was cooled in an ice-bath and neutralized to pH 4 using 5% aqueous HCl solution, and then the solvent was completely removed. 250 mL water was added and extracted with 3×300 mL ethyl acetate. The combined organic extracts were dried over anhydrous sodium sulfate. Removal of solvent yielded a crude product, which was purified by flash chromatography (silica gel/ethyl acetate/hexanes) to give compound **C3** as a white solid (22.0 g, 86.7% yield), mp 107-109 °C. ir (KBr pellet): 3217 (OH), 1733 (C=O) cm⁻¹; ¹H nmr (CDCl₃): δ 0.82 (dd, 6H, 2CH₃, J=6.3, 38.4 Hz), 1.05-1.35 (m, 2H, CH₂), 1.48 (s, 9H, t-Butyl protons), 1.56-1.65 (m, 1H, CH), 2.82 (t, 1H, OH, J=5.4 Hz), 3.55-3.70 (m, 2H, CH₂), 4.03-4.17 (m, 1H, CH), 4.50 (dd, 2H, CH₂, J=15.9, 29.7 Hz), 7.18-7.45(m, 5H, phenyl protons); ms: m/z 409 (M⁺+Na, 100%), 353 (M⁺-t-Butene+Na, 12%), 230 (M⁺-SO₂NHBoc+Na, 35%), 91 (PhCH₂⁺, 9%). *Anal. Calcd.* for C₁₈H₃₀N₂O₅S: C, 55.94; H, 7.82; N, 7.25. Found: C, 56.11; H, 8.12; N, 7.18.

Tert-butyl 5-benzyl-4-isobutyl-1,2,5-thiadiazolidine-2-carboxylate 1,1-dioxide C4: A solution of compound **C3** (21.54 g; 55.7 mmol) in 170 mL dry THF was treated with triphenyl

phosphine (29.22 g; 111.4 mmol) and diethyl azodicarboxylate (DEAD, 19.4 g; 111.4 mmol) with stirring at R.T. for 4 h. Removal of the solvent left a crude product, which was purified by flash chromatography (silica gel/ethyl acetate/hexanes) to give compound **C4** as a white solid (16.19 g, 79.0% yield), mp 81-82°. ir (KBr pellet): 1721 (C=O) cm^{-1} ; ^1H nmr (CDCl_3): δ 0.79 (dd, 6H, 2 CH_3 , $J=6.3, 14.4$ Hz), 1.35-1.60 (m, 3H, CH & CH_2), 1.56 (s, 9H, t-Butyl protons), 3.40-3.51 (m, 2H, CH_2), 3.80-3.88 (m, 1H, CH), 4.29 (dd, 2H, CH_2 , $J=15.3, 48.3$ Hz), 7.30-7.41 (m, 5H, phenyl protons); ms: m/z 391 ($\text{M}^+\text{+Na}$, 5%), 335 (M^+ - t-Butene +Na, 42%), 176 (M^+ - CH_2OH - SO_2NHBoc , 35%), 91 (PhCH_2^+ , 100%). *Anal. Calcd.* for $\text{C}_{18}\text{H}_{28}\text{N}_2\text{O}_4\text{S}$: C, 58.67; H, 7.66; N, 7.60. Found: C, 58.85; H, 7.75; N, 7.53.

2-Benzyl-3-isobutyl-1,2,5-thiadiazolidine 1,1-dioxide C5: A solution of compound **C4** (15.76 g; 42.8 mmol) in 40 mL dry methylene chloride was treated with trifluoroacetic acid (140 mL) at R.T. for 3 h. Removal of the solvent left a crude product, which was purified by flash chromatography (silica gel/ethyl acetate/hexanes) to give compound **C5** as a white solid (10.5 g, 91.5% yield), mp 60-62°. ir (KBr pellet): 3225 (NH) cm^{-1} ; ^1H NMR (CDCl_3) δ 0.80 (dd, 6H, 2 CH_3 , $J=6.3, 24.9$ Hz), 1.38-1.58 (m, 3H, CH & CH_2), 3.12-3.20 (m, 1H, one proton of CH_2), 3.40-3.50 (m, 1H, one proton of CH_2), 3.50-3.60 (m, 1H, CH), 4.28(s, 1H, NH), 4.29 (dd, 2H, CH_2 , $J=12.0, 45.6$), 7.25-7.42 (m, 5H, phenyl protons); ms: m/z 291 ($\text{M}^+\text{+Na}$, 100%), 91 (PhCH_2^+ , 20%). *Anal. Calcd.* for $\text{C}_{13}\text{H}_{20}\text{N}_2\text{O}_2\text{S}$: C, 58.18; H, 7.51; N, 10.44. Found: C, 58.09; H, 7.42; N, 10.20.

2-Benzyl-3-isobutyl-5-[(phenylsulfanyl)methyl]-1,2,5-thiadiazolidine 1,1-dioxide C6: A solution of compound **C5** (0.97 g; 3.6 mmol) in 4 mL dry DMF was cooled in an ice-bath, and then sodium hydride (0.23 g; 60% w/w; 5.8 mmol) was added with stirring. 10 min later, chloromethyl phenyl sulfide (0.80 g; 5.0 mmol) was added. The reaction was allowed to warm to

room temperature and stirred for 2 h. DMF was removed by oil pump under 40 °C. The residue was dissolved in 30 mL ethyl acetate and washed with 2×20 mL brine, and then the organic layer was dried over anhydrous sodium sulfate. Removal of the solvent left a crude product, which was purified by flash chromatography (silica gel/ethyl acetate/hexanes) to give compound **C6** as a colorless oil (1.18 g, 84.0% yield). ¹H nmr (CDCl₃): δ 0.75 (dd, 6H, 2CH₃, J=6.0, 20.7 Hz), 1.35-1.50 (m, 3H, CH & CH₂), 2.95 (dd, 1H, one proton of CH₂, J=7.2, 9.0 Hz), 3.32-3.43 (m, 1H, CH), 3.65 (m, 1H), 3.65 (dd, 1H, one proton of CH₂, J=7.2, 9.0 Hz), 4.38 (dd, 2H, CH₂, J=7.8, 15.0 Hz), 4.45 (dd, 2H, CH₂, J=13.8, 156.9 Hz), 7.23-7.53 (m, 10H, phenyl protons); ms: m/z 391 (M⁺+1, 78%), 281 (M⁺-PhSH, 100%). *Anal. Calcd.* for C₂₀H₂₆N₂O₂S₂: C, 61.50; H, 6.71; N, 7.17. Found: C, 61.34; H, 7.04; N, 7.16.

2,2'-Methylenebis(5-benzyl-4-isobutyl-1,2,5-thiadi-azolidine) 1,1,1',1'-tetraoxide C7: A solution of compound **C6** (1.18 g; 3.0 mmol) in 4 mL dry methylene chloride in an ice-bath was added a solution of sulfuryl chloride (0.82 g; 6.0 mmol) in 2 mL dry methylene chloride with stirring. The reaction was allowed to warm to R.T. and stirred for 2 h. The solvent was removed and the residue was purified by flash chromatography (silica gel/ethyl acetate/hexanes) to give compound **C7** as a white solid (0.15 g, 18.2% yield), mp 127-128°. ¹H nmr (CDCl₃): δ 0.79 (dd, 12H, 4CH₃, J=6.3, 24.0Hz), 1.40-1.58 (m, 6H, 2CH & 2CH₂), 3.25 (dd, 2H, two protons of 2CH₂, J=6.3, 9.6 Hz), 3.38-3.48 (m, 2H, 2CH), 3.72 (dd, 2H, two protons of 2CH₂, J=6.9, 9.6 Hz), 4.26 (dd, 4H, 2CH₂, J=14.7, 62.1 Hz), 4.60 (s, 2H, bridge CH₂), 7.25-7.41(m, 10H, phenyl protons); ms: m/z 549 (M⁺+1, 76%), 281 (M⁺-5, 100%), 91 (PhCH₂⁺, 24%). *Anal. Calcd.* for C₂₇H₄₀N₄O₄S₂: C, 59.09; H, 7.35; N, 10.21. Found: C, 59.54; H, 7.12; N, 10.26.

CHAPTER 6

POTENTIAL WEST NILE VIRUS/DENGUE NS2B-NS3 PROTEASE INHIBITORS BASED ON THE 1-OXO-1, 2, 3, 4-TETRAHYDROISOQUINOLINE AND 1-OXO-1, 2- DIHYDROISOQUINOLINE SCAFFOLDS

6.1 Inhibitor Design Rationale

The biochemical rationale underlying the use of the 1-Oxo-1,2,3,4-tetrahydroisoquinoline scaffold in the design of serine protease inhibitors rested on the following considerations: (a) previous studies related to the steric course and specificity of α -chymotrypsin-catalyzed reactions have shown that D-1-Oxo-1,2,3,4-tetrahydroisoquinoline 3-carboxymethyl ester (Figure 6.1(V)) behaves as a relatively efficient substrate of the enzyme, indicating that the heterocyclic scaffold is capable of binding productively to the active site of the enzyme [257]; (b) WNV NS2B-NS3pro has a chymotrypsin-like fold and a prototypical catalytic triad, with the active site located at the interface of the N- and C-terminal lobes; (c) we reasoned that an entity such as (VI) (Figure 6.1) that embodied a recognition element (1-Oxo-1, 2, 3, 4-tetrahydroisoquinoline scaffold) and a suitably-positioned serine trap may function as a non-peptidyl transition state inhibitor of the viral protease (Figure 6.1(b)) [252]. Of particular interest were the α -ketoamide derivatives (structure (VI), Z = CONHR), since judicious changes in the nature of the R group could potentially lead to the exploitation of additional favorable binding interactions.

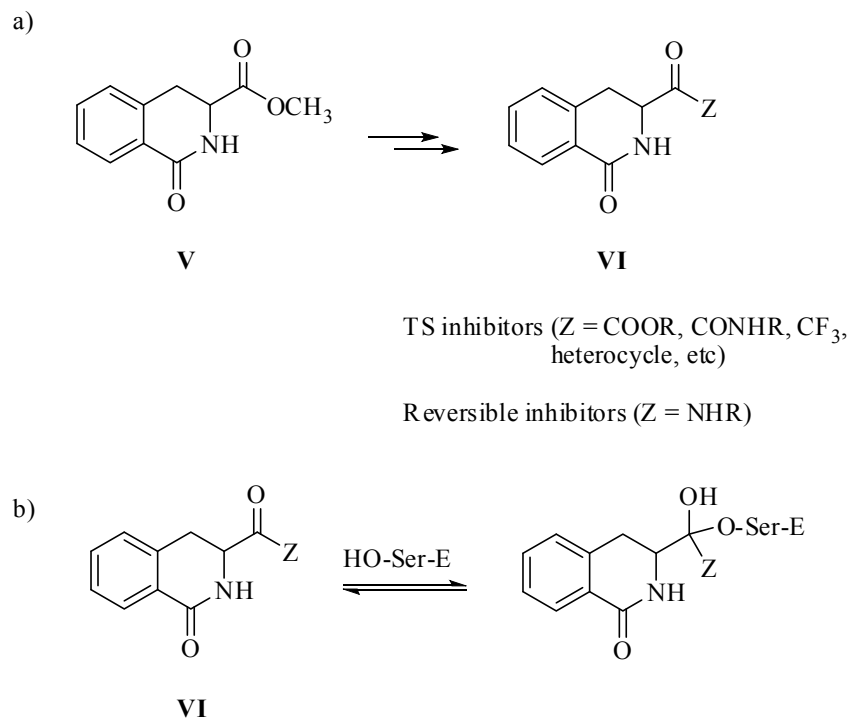
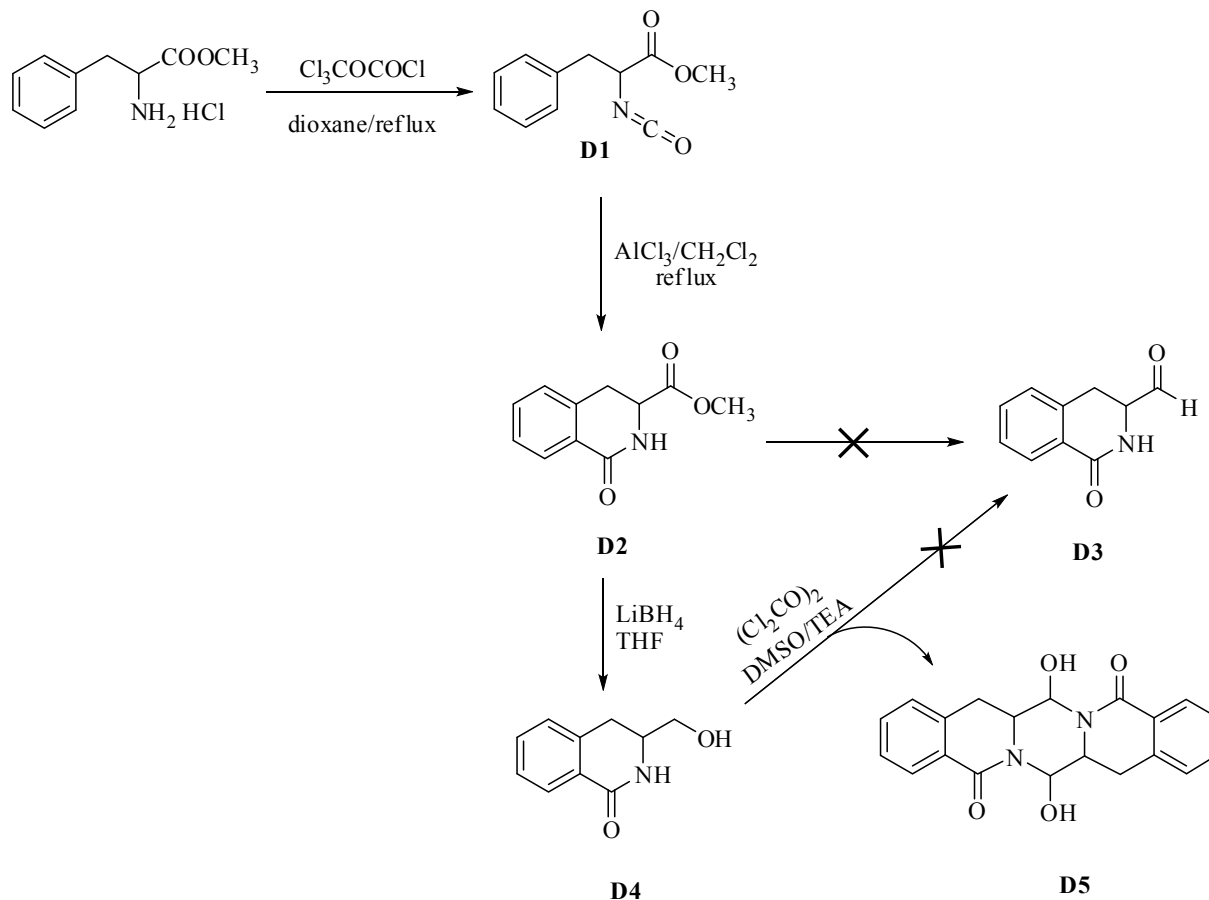


Figure 6.1 WNV/DENV NS2B-NS3 Protease Inhibitor Design. (a) Design of transition state inhibitors VI based on the 1-Oxo-1, 2, 3, 4-tetrahydroisoquinoline scaffold; (b) Postulated mechanism of action of VI.

6.2 Results and Discussions

6.2.1 Synthesis

The synthesis of inhibitor VI is shown in Scheme 6.1-6.3. The 1-Oxo-1,2,3,4-tetrahydroisoquinoline scaffold **D2** was readily prepared via the treatment of (DL) phenylalanine methyl ester hydrochloride salt with chloromethyl chloroformate followed by cyclization with aluminum chloride. We initially set out to prepare aldehyde **D3** from compound **D2** (Scheme 6.1) since it would serve as a suitable intermediate for synthesizing the desired transition state inhibitors. Thus, when compound **D2** was treated with diisobutylaluminium hydride (DIBAL) [258]



Scheme 6.1 Synthesis of 1-Oxo-1,2,3,4-Tetrahydro-Isoquinoline Scaffold

only the starting material was recovered. An alternative method for making **D3**, also unsuccessful, involved the treatment of **D2** with iodotrimethylsilane in methylene chloride to give the corresponding trimethylsilyl ether ($\text{RCOOSi}(\text{CH}_3)_3$) which was then treated with DIBAL, as described in the literature [259]. Lithium aluminum hydride reduction of ester **D2** in the presence of diethylamine [260] failed to give **D3** and gave instead the corresponding alcohol. A second approach toward the synthesis of **D3** was pursued which involved reduction of **D2** (LiBH_4/THF) to give alcohol **D4** followed by treatment with pyridinium chlorochromate in methylene chloride [261]. NMR analysis of the complex reaction mixture showed the absence of any aldehyde, despite complete consumption of the starting alcohol. Swern oxidation of **D4** yielded a white solid the structure of which was established by X-ray crystallography to be that

of compound **D5** (X-ray crystal structure is shown in Figure 6.2 and the crystal data and structure refinement parameters are listed in Table 6.1).

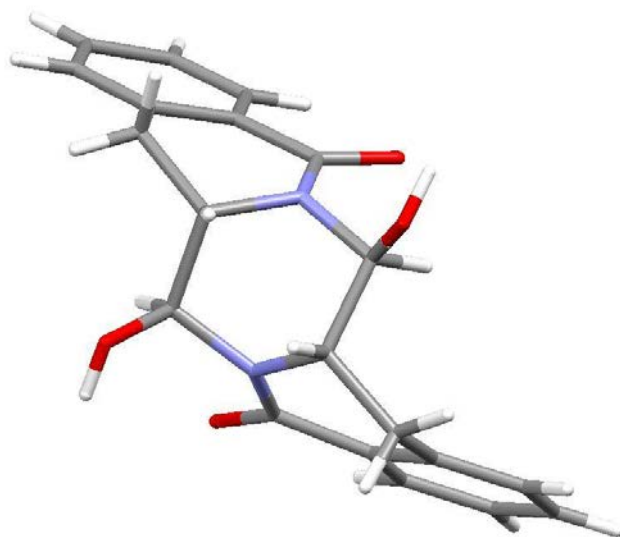


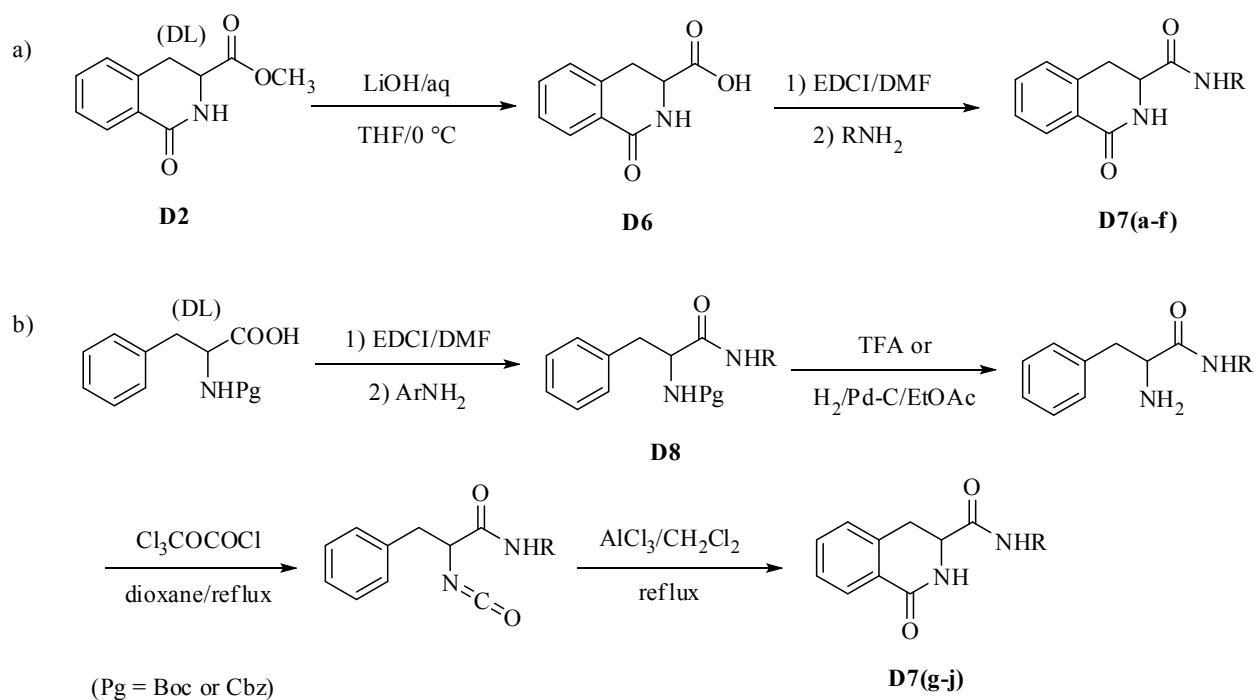
Figure 6.2 Mercury Drawing of Compound **D5**.

Table 6.1 Crystal Data And Structure Refinement Parameters for **D5**

Empirical formula	C ₂₀ H ₂₀ N ₂ O ₅	Crystal size	0.33 x 0.14 x 0.05 mm ³
Formula weight	368.38	θ range for data collection	3.51 to 26.00°
Temperature	296(2) K	Index ranges	-13 ≤ h ≤ 13
Wavelength	0.71073 Å		-16 ≤ k ≤ 16
Crystal system	Monoclinic		-15 ≤ l ≤ 15
Space group	P2(1)/n	Reflections collected /unique	30136
Unit cell dimensions	a = 11.0019(7) Å b = 13.1759(8) Å c = 12.6798(8) Å α = 90° β = 105.731(4)° γ = 90°	Independent reflections	3476 [R(int) = 0.0934]
		Completeness to θ = 26.00°	99.8 %
		Absorption correction	None
		Max. and min. transmission	0.9953 and 0.9675
		Refinement method	Full-matrix least-squares on F ²
		Data / restraints / parameters	3476 / 0 / 252
Volume	1769.22(19) Å ³	Goodness-of-fit on F ²	1.009
Z	4	Final R indices [I > 2σ(I)]	R1 = 0.0437, wR2 = 0.0946
Density (calculated)	1.383 Mg/m ³	R indices (all data)	R1 = 0.0869, wR2 = 0.1149
Absorption coefficient	0.100 mm ⁻¹	Largest diff. peak and hole	0.200 and -0.223 e.Å ⁻³
F(000)	776		

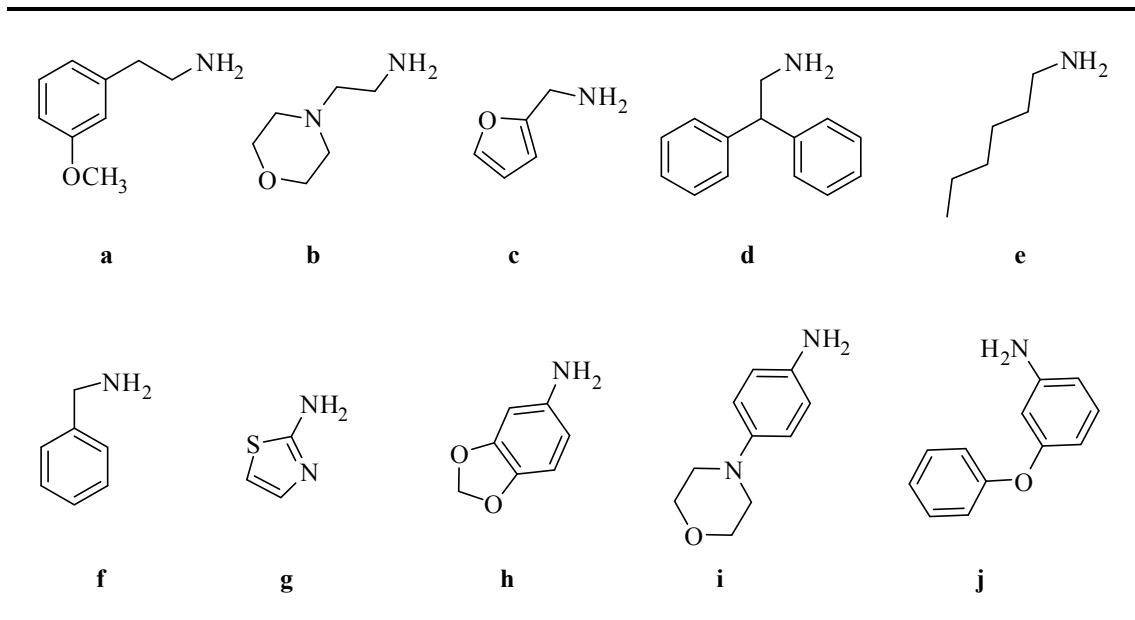
It is evident that aldehyde **D3** is formed which then dimerizes to **D5** under the reaction

conditions. Further attempts to generate variants of **VI**, such as the direct formation of **VI** with $Z = \text{heterocycle}$ [262], were also unsuccessful and necessitated a change in strategy that entailed the solution-phase generation of a library of compounds based on the 1-Oxo-1, 2, 3, 4-tetrahydroisoquinoline scaffold that could potentially function as reversible competitive inhibitors of the enzyme. Thus, the synthesis of compounds **D7(a-f)** proceeded uneventfully when aliphatic amines were used (Scheme 6.2 (a)), however, an alternative superior route was utilized in the synthesis of compounds **D7(g-j)** derived from aromatic amines (Scheme 6.2 (b)). A fairly diverse set of amine inputs (Table 6.2) was utilized for optimal space exploration. Inhibitors **D7(a-j)** are summarized in Table 6.3.



Scheme 6.2 Synthesis of Reversible Inhibitor VI

Table 6.2 Amine Inputs

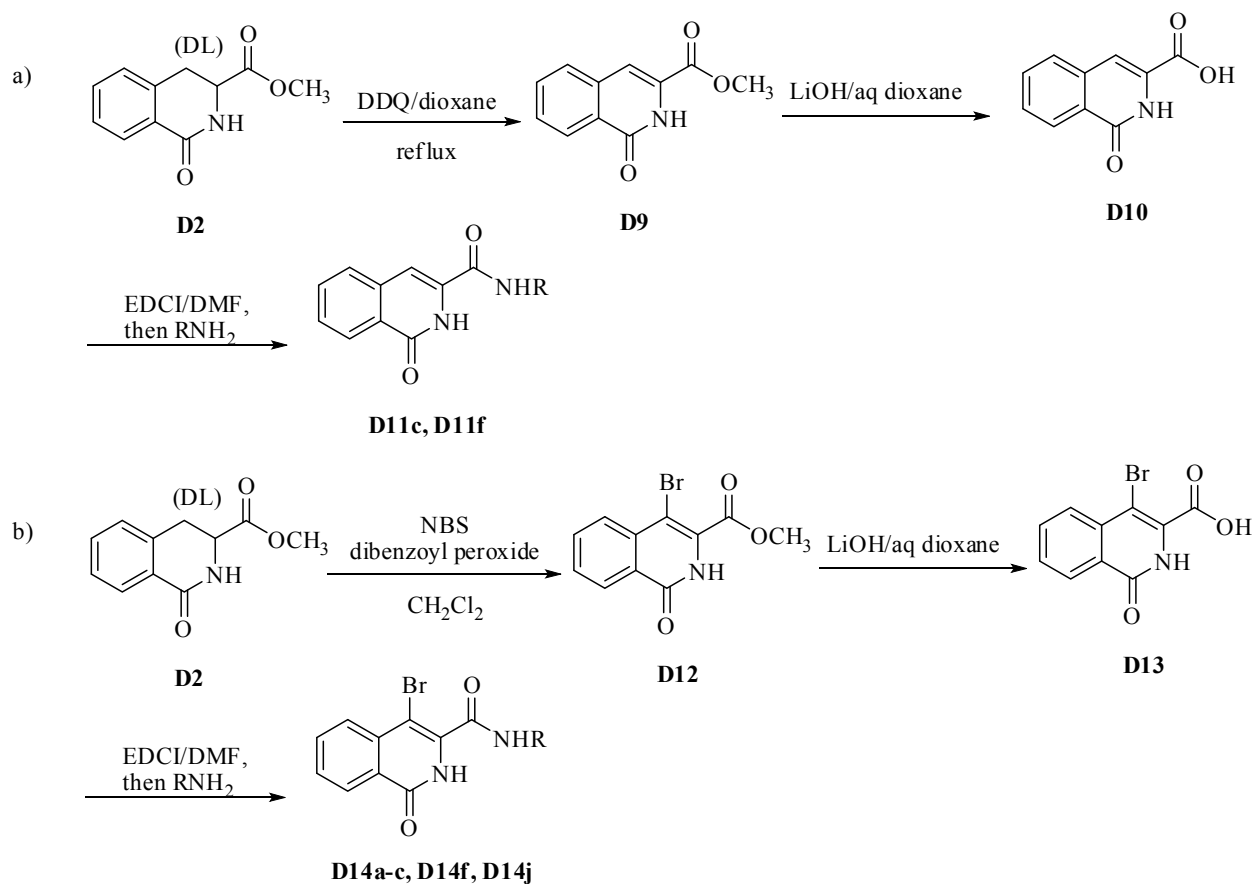


6.2.2 Biochemical Studies

All the compounds were screened against WNV and DENV NS2B-NS3 proteases. With the exception of compound **D7g** (~25% inhibition at 50 μ M inhibitor concentration), the rest of the compounds were devoid of any inhibitory activity against WNV and DENV NS2B-NS3 protease, suggesting that these compounds do not engage in multiple binding interactions with the target enzyme. This series of compounds were inactive against a representative panel of serine proteases, including bovine α -chymotrypsin, human neutrophil elastase, cathepsin G, and human skin chymase [208,263]. Intriguingly, compounds **D7f** and **D7h** were found to inhibit bovine trypsin (42% and 22% inhibition, respectively, at a 50 μ M inhibitor concentration).

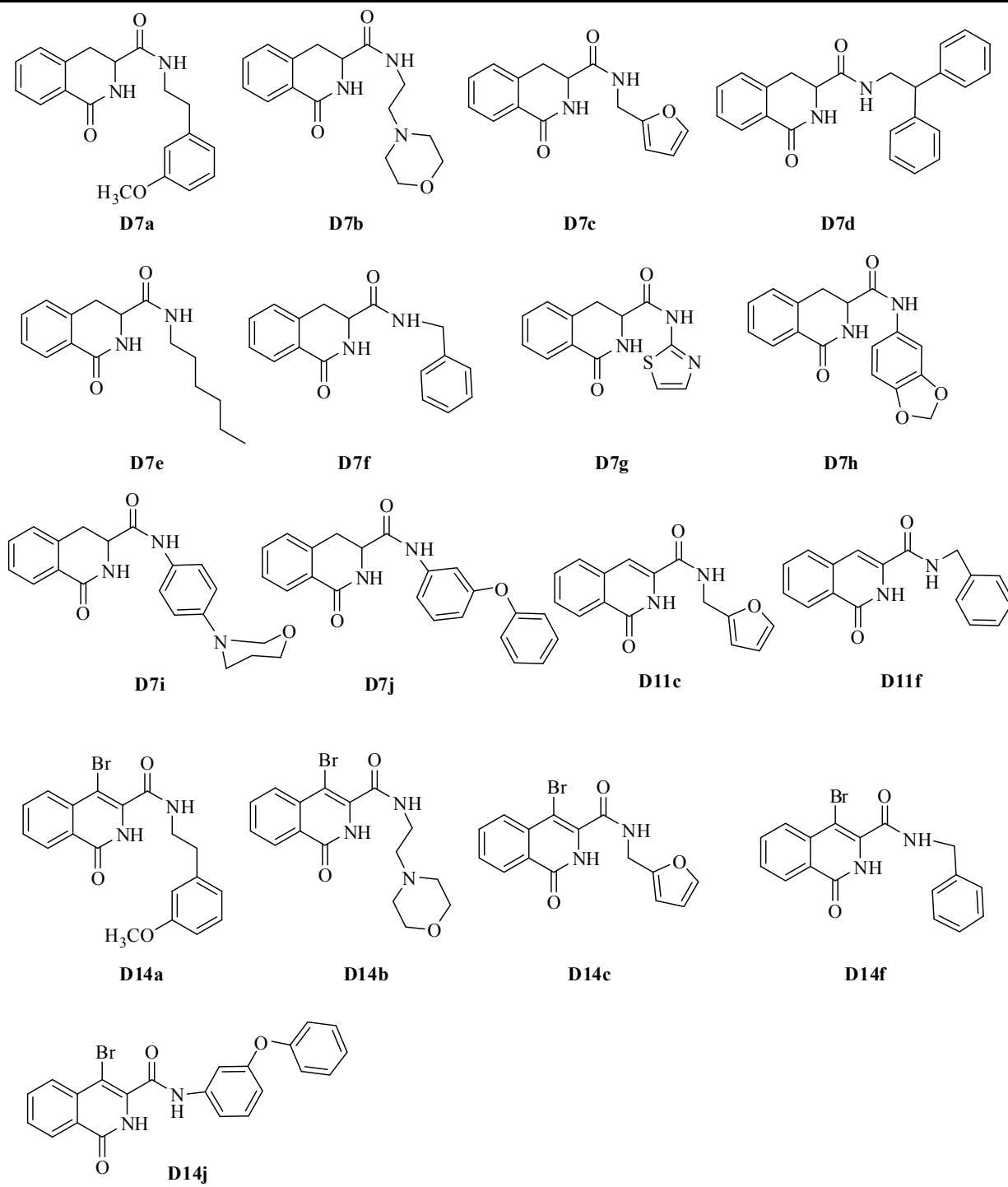
The exploratory studies cited above suggested that the non-planar component in **VI** might be inimical to binding, consequently a focused library of compounds (**D11c**, **D11f**, **D14a-c**, **D14f**, **D14j**) was generated based on the 1-oxo-1, 2-dihydroisoquinoline scaffold and its bromo variant

using Scheme 6.3 (Table 6.2). Screening of these libraries resulted in the identification of a hit (compound **D14j**) that was a fair inhibitor of WNV protease (IC_{50} 30 μ M).



Scheme 6.3 Synthesis of 1-Oxo-1,2-dihydroisoquinoline Based Inhibitors

Table 6.3 Summary of Inhibitors VI



6.2.3 Molecular Modeling Studies

The enzyme-inhibitor interactions between WNV NS2B-NS3 protease and the hit **D14j** were studied using AutoDock4 [230]. The binding of energy-minimized compound **D14j** to the active site of the enzyme is illustrated in **Figure 6.3**. The aromatic portion of the bromoisoquinoline moiety forms a π -stacking interaction with Tyr161 and engages in end-on hydrophobic interactions with Tyr150. The amide on the bromoisoquinoline group hydrogen bonds with the hydroxyl side chain of the catalytic Ser135, namely, the carbonyl oxygen on bromoisoquinoline serves as a hydrogen acceptor from the Ser135 proton and the amide proton serve as hydrogen bond donor to the Ser135 hydroxyl oxygen. The amide proton on the linker between the bromoisoquinoline and the (m-phenoxy)phenyl is predicted to hydrogen bond with the backbone carbonyl of Gly151. The first aromatic ring in the (m-phenoxy)phenyl group is solvent exposed and is not predicted to participate in any significant favorable interactions. However, the second aromatic ring interacts with the side chain of Val72, with the mildly hydrophobic β carbons of His51 and Asp75, and has an end-on hydrophobic interaction with Trp50. Although the aromatic portion of the bromoisoquinoline moiety engages in π -stacking interactions and fits well within a very small cavity, it might be possible to improve the affinity for this cavity by noting that the end of the ring points toward highly polar species, such as the Asp129 side chain and the Tyr130 backbone. Furthermore, the first aromatic ring in the (m-phenoxy)phenyl component serves as a semi rigid spacer of ideal length for fostering the favorable interactions associated with the bromoisoquinoline ring and on the second aromatic ring in the m-phenoxy)phenyl component. Consequently, exploring other groups that maintain the same spacer distance and orientation may provide additional opportunities for affinity enhancement.

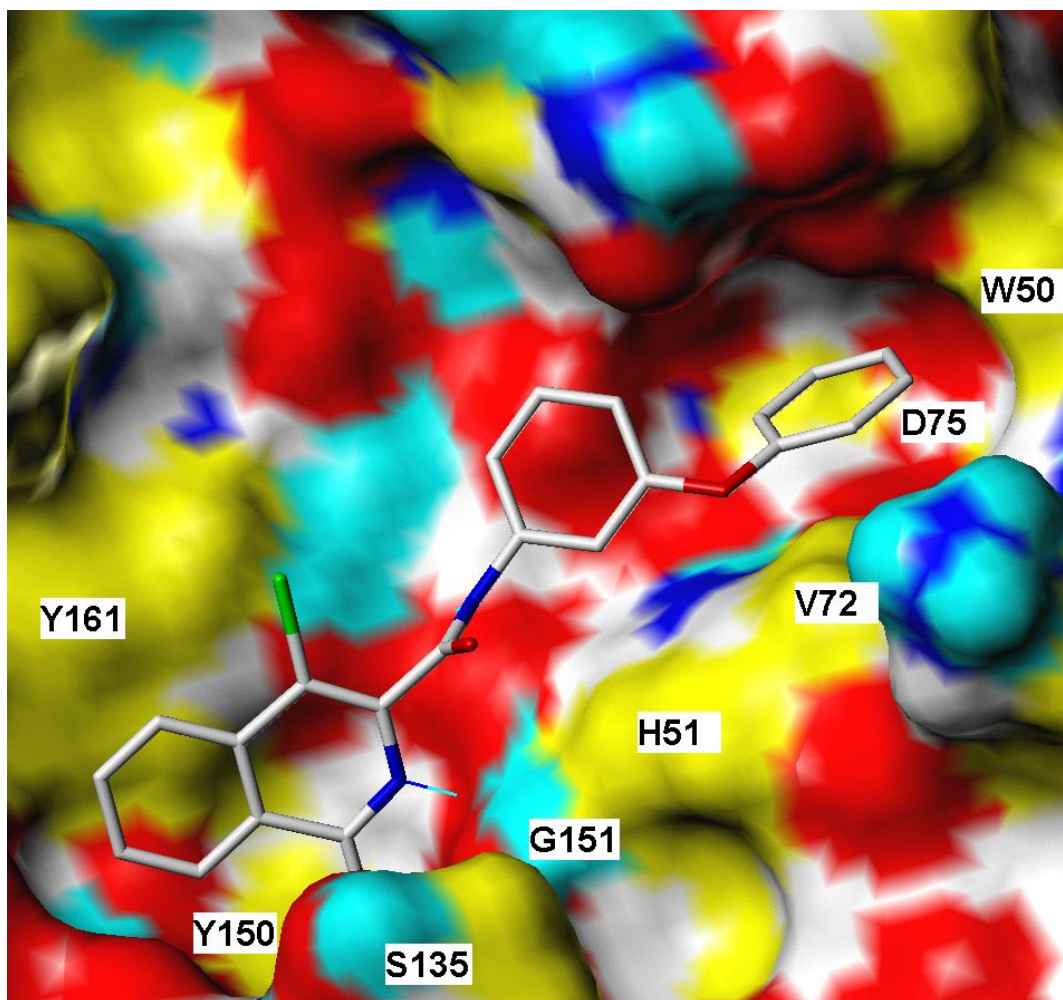


Figure 6.3 Predicted Binding of Energy-Minimized Compound D14j Docked to the Binding Site of WNV Protease. The enzyme surface is colored as follows: red polar O, blue = polar N, cyan = donatable H, white = mildly polar H/C, yellow = nonpolar H/C/S.

In summary, exploratory studies utilizing the 1-oxo-1, 2-dihydroisoquinoline scaffold have lead to the identification of an inhibitor of WNV protease suitable for further exploration.

6.3 Experimental

6.3.1 Synthesis

General

The ^1H NMR spectra were recorded on a Varian XL-300 or XL-400 NMR spectrometer. A Gemini EM microplate spectrofluorometer (Molecular Devices Corporation, Sunnyvale, CA) was used in the enzyme assays and inhibition studies. Melting points were determined on a Mel-Temp apparatus and are uncorrected. Reagents and solvents were purchased from various chemical suppliers (Aldrich, Acros Organics, TCI America, and Bachem). Silica gel (230-450 mesh) used for flash chromatography was purchased from Sorbent Technologies, Atlanta, GA. Thin layer chromatography was performed using Analtech silica gel plates. The TLC plates were visualized using iodine and/or UV light. WNV NS2B-NS3 protease was expressed in *E. coli* as described for Dengue virus-2 protease [264] and was purified as previously described [265]. Boc-Gly-Lys-Arg-AMC was purchased from Bachem.

Representative Synthesis

(RS)-Methyl 2-isocyanato-3-phenylpropanoate D1: DL-phenylalanine methyl ester hydrochloride (13.6g; 63 mmol) was placed in a round bottom flask and pumped under high vacuum overnight. 1,4-Dioxane (150 mL) was then added, followed by trichloromethyl chloroformate (10.5 mL; 88.5 mmol). The resulting mixture was refluxed gently overnight. The solvent was removed and the residue was distilled under reduced pressure to give the corresponding isocyanate **D1** as a colorless oil (12.9 g, 99% yield). ^1H NMR (CDCl_3) δ 2.99-3.08 (dd, 1H), 3.12-3.20 (dd, 1H), 3.81(s, 3H), 4.02-4.10 (q, 1H), 7.18-7.38 (m, 5H).

(RS)-Methyl 1-oxo-1,2,3,4-tetrahydroisoquinoline-3-carboxylate D2: To a solution of compound **D1** (12.9 g; 63 mmol) in dry methylene chloride (120 mL) was added AlCl_3 (16.8 g; 126 mmol) in small portions and the resulting mixture was refluxed for 2 h. The reaction mixture was allowed to cool to room temperature and then placed in an ice-water bath. Water (100 mL)

was slowly added and the mixture was stirred for 30 minutes. The two layers were separated and the organic layer was dried over anhydrous sodium sulfate. Removal of the solvent left a crude product which was purified by flash chromatography (silica gel/ ethyl acetate/ hexanes) to give compound **D2** as a white solid (9.2 g; 71% yield), mp 98-100 °C. ¹H NMR (CDCl₃) δ 3.18-3.27 (dd, 1H), 3.28-3.40 (dd, 1H), 3.80 (s, 3H), 4.40-4.46 (m, 1H), 6.65 (s, 1H), 7.20-7.52 (m, 3H), 8.05-8.12 (d, 1H).

(RS)-3-(Hydroxymethyl)-3,4-dihydroisoquinolin-1(2H)-one D4: To a solution of compound **D2** (4.1g; 20.0 mmol) in dry THF (20 mL) was added dropwise a solution of 2M LiBH₄ in THF (10 mL; 20.0 mmol), followed by the dropwise addition of 60 mL absolute ethanol. The reaction was stirred at room temperature overnight. The reaction mixture was cooled in an ice-bath and the pH was adjusted to 4 by adding 5% HCl. The solvent was removed and the residue was treated with water (60 mL) and extracted with ethyl acetate (3×50 mL). The combined organic extracts were dried over anhydrous sodium sulfate. Removal of the solvent left compound **D4** as a colorless oil (3.2 g, 90% yield). ¹H NMR (CDCl₃): δ 2.88-2.95 (d, 2H), 3.65-3.75 (dd, 1H), 3.80-3.90 (dd, 1H), 3.85-3.96 (m, 1H), 7.20-7.48 (m, 4H), 8.02-8.05 (d, 1H).

Dimeric compound D5: A solution of 2M oxalyl chloride in CH₂Cl₂ (2.75 mL, 5.5 mmol) and 12 mL CH₂Cl₂ were placed in a 50-mL three-neck round bottom flask equipped with a thermometer, a CaCl₂ drying tube and two pressure-equalizing dropping funnels containing DMSO (0.85 mL; 11 mmol) in 2.5 mL CH₂Cl₂ and compound **D4** (0.88 g; 5 mmol) in 5 mL CH₂Cl₂ and 1 mL DMSO, respectively. The DMSO solution was added to the stirred oxalyl chloride solution at -50~-60 °C. After stirring for 2 minutes, the solution containing compound **D4** was added over 5 minutes and the mixture was stirred for an additional 15 minutes. Triethylamine (3.5 mL; 25 mmol) was then added and the reaction mixture was stirred for 5

minutes and allowed to warm to room temperature for 3.5 h. Water (25 mL) was added and the two layers were separated. The aqueous layer was extracted once with CH₂Cl₂ (25 mL) and the combined organic extracts were washed with brine (25 mL) and dried over anhydrous sodium sulfate. Removal of the solvent left a crude product which was purified by flash chromatography (silica gel/ethyl acetate/hexanes) to give compound **D5** (150 mg; 8% yield) as a white solid, mp 154-156 °C. ¹H NMR (DMSO-D₆): δ 3.12-3.25 (dd, 2H), 3.38-3.50 (dd, 2H), 3.88-3.98 (t, 2H), 4.08 (s, 2H), 5.48-5.55 (d, 2H), 7.30-7.42 (m, 4H), 7.50-7.60 (t, 2H), 7.79-7.83 (d, 2H).

(RS)-1-oxo-1,2,3,4-tetrahydroisoquinoline-3-carboxylic acid D6: To a chilled solution of compound **D2** (3.0 g; 14.7 mmol) in 30 mL THF was added 15 mL of 1 M lithium hydroxide and the reaction mixture was stirred in an ice-bath for 30 minutes. The solvent was removed on the rotary evaporator and the residue treated with water (30 mL). The solution was extracted once with 50 mL ethyl acetate. The aqueous solution was acidified to pH 2, yielding a white precipitate which was collected by suction filtration and air dried to yield a white solid **D6** (2.1 g; 75% yield), mp 224-226 °C. ¹H NMR (CD₃OD) δ 3.22-3.36 (dd, 1H), 3.38-3.45 (dd, 1H), 4.37-4.42 (t, 1H), 7.30-7.55 (m, 3H), 7.95-8.00 (d, 1H).

General synthetic procedure for amide D7(a-f) formation

A solution of acid **D6** (0.38 g; 2 mmol) in dry N, N-dimethylformamide (5 mL) was treated with 1-[3-(dimethylamino) propyl]-3-ethylcarbodiimide hydrochloride (0.38 g; 2 mmol), followed by the appropriate amine (2 mmol). The reaction mixture was stirred at room temperature overnight. The solvent was removed in vacuo and ethyl acetate (50 mL) was added to the residue. The organic layer was washed with 5% aqueous HCl (2×10 mL), saturated aqueous NaHCO₃ (2 × 10 mL), and brine (10 mL). The organic layer was dried over anhydrous sodium sulfate, the solvent was removed on the rotovac, and the crude product was purified using flash chromatography

(silica gel/ethyl acetate/hexanes) to give the corresponding amide **D7**.

Compound D7a: White solid (10% yield), mp 124-126 °C. ¹H NMR (CDCl₃) δ 2.60-2.72 (t, 2H), 3.20-3.30 (dd, 1H), 3.25-3.55 (m, 3H), 3.72 (s, 3H), 4.20-4.25 (q, 1H), 6.52-6.72 (m, 3H), 7.02-7.50 (m, 5H), 7.58-7.61 (d, 1H), 7.92-7.98 (d, 1H).

Compound D7b: White solid (26% yield), mp 138-140 °C. ¹H NMR (CD₃OD) δ 2.28-2.52 (t, 6H), 3.20-3.38 (m, 4H), 3.55-3.65 (t, 4H), 3.72(s, 3H), 4.22-4.30 (t, 1H), 7.22-7.55 (m, 3H), 7.89-7.95 (d, 1H).

Compound D7c: White solid (57% yield), mp 157-158 °C. ¹H NMR (CDCl₃) δ 3.25-3.35 (dd, 1H), 3.40-3.46 (dd, 1H), 4.26-4.33 (m, 1H), 4.26-4.38 (dd, 1H), 4.40-4.52 (dd, 1H), 6.00-6.02 (d, 1H), 6.22-6.24(t, 1H), 6.55 (s, 2H), 7.20-7.55 (m, 4H), 7.99-8.02 (d, 1H).

Compound D7d: White solid (23% yield), mp 166-168 °C. ¹H NMR (CDCl₃) δ 3.10-3.22 (dd, 1H), 3.28-3.40 (dd, 1H), 3.65-3.80 (dd, 1H), 3.85-4.00 (dd, 1H), 4.00-4.12(t, 1H), 4.12-4.20 (q, 1H), 4.58 (s, 1H), 4.68 (s, 1H), 6.98-7.52 (m, 13H), 7.85-7.92 (d, 1H).

Compound D7e: White solid (24% yield), mp 99-101°C. ¹H NMR (CDCl₃) δ 0.75-0.82 (t, 3H), 1.09-1.20 (m, 2H), 1.30-1.41(m, 2H), 3.18-3.23 (m, 2H), 3.24-3.38 (dd, 1H), 3.38-3.52 (dd, 1H), 4.22-4.30 (q, 1H), 6.62 (s, 1H), 7.20-7.60 (m, 4H), 7.95-8.00 (d, 1H).

Compound D7f: White solid (20% yield), mp 165-167 °C. ¹H NMR (CDCl₃) δ 3.25-3.34 (dd, 1H), 3.42-3.51(dd, 1H), 4.22-4.30 (t, 1H), 4.28-4.35 (dd, 1H), 4.40-4.47(dd, 1H), 6.82 (s, 1H), 6.89-7.54 (m, 9H), 7.88-7.94 (d, 1H).

General procedure for N-Boc/N-Cbz phenylalanine and aromatic amine coupling reactions.

DL-N-Cbz-phenylalanine (or L-N-Boc-phenylalanine) (5 mmol) was dissolved in 10 mL DMF and 1-[3-(dimethylamino)propyl]-3-ethylcarbodiimide hydrochloride (0.96 g; 5 mmol) was

added, followed by the appropriate aromatic amine (5.5 mmol). The resulting mixture was stirred at room temperature overnight. Removal of the solvent on the rotary evaporator left a residue which was dissolved in 50 mL ethyl acetate. The ethyl acetate solution was washed with 5% aqueous HCl (3 × 25 mL), saturated aqueous NaHCO₃ (3×25 mL), and brine (25 mL). The organic layer was dried over anhydrous sodium sulfate and the solvent was removed on the rotovac to give pure product **D8**.

Compound D8a: White solid (63% yield), mp 88-90 °C. ¹H NMR (CDCl₃) δ 1.4 (s, 9H), 3.05-3.20 (m, 2H), 4.64-4.78 (m, 1H), 5.18 (s, 1H), 7.00-7.28 (m, 6H), 7.52-7.55 (d, 1H), 11.20 (s, 1H).

Compound D8b: White solid (48% yield), mp 145-147 °C. ¹H NMR (CDCl₃) δ 3.02-3.20 (m, 2H), 4.45-4.56 (q, 1H), 5.05 (s, 2H), 5.50 (s, 1H), 5.92 (s,2H), 6.52-6.70 (dd, 2H), 7.03 (s, 1H), 7.18-7.37 (m, 10H),7.55 (s, 1H).

Compound D8c: White solid (87% yield), mp 200-202 °C. ¹H NMR (CDCl₃) δ 3.05-3.22 (m, 6H), 3.80-3.90 (t, 4H), 4.45-4.56 (q, 1H), 5.08 (s, 2H), 5.48 (s, 1H), 6.78-6.82 (dd, 2H), 7.18-7.38 (m, 12H), 7.40 (s, 1H).

Compound D8d: White solid (100% yield), mp 132-134 °C. ¹H NMR (CDCl₃) δ 3.02-3.20 (m, 2H), 4.45-4.58 (m, 1H), 5.05 (s, 2H), 5.48 (s, 1H), 6.37-6.42 (m, 1H), 6.70-6.75 (m, 1H), 6.98-7.37 (m, 19H), 7.68 (s, 1H).

Synthesis of compound D7g: Compound **D8a** (1.14 g; 3.28 mmol) was dissolved in 15 mL trifluoroacetic acid at room temperature. The reaction mixture was stirred for 30 minutes and the trifluoroacetic acid was removed under vacuum. Water (5 mL) was added and the pH was adjusted to 9 using a saturated solution of sodium carbonate. The free amine was extracted with

50 mL ethyl acetate and the organic layer was dried using anhydrous sodium sulfate. Removal of the solvent left a colorless oil (0.6 g; 74% yield). The oil was dissolved in 10 mL 1,4-dioxane, and trichloromethyl chloroformate (0.4 mL; 3.4 mmol) was added. The resulting mixture was stirred at room temperature overnight. Removal of the solvent under vacuum left a residue which was dissolved in methylene chloride (20 mL). Aluminum chloride (0.64 g; 4.8 mmol) was added and the resulting mixture was refluxed for 1h. The reaction mixture was allowed to cool to room temperature and water (10 mL) was slowly added. The mixture was stirred for 30 minutes and then transferred to a separatory funnel. The organic layer was washed with water (2×15 mL) and dried over anhydrous sodium sulfate. Removal of the solvent gave pure product **D7g** as a gray solid (50 mg; 6% yield), mp 202-204 °C. ¹H NMR (CDCl₃) δ 2.92-3.01 (dd, 1H), 3.40-3.49 (dd, 1H), 4.40-4.48 (m, 1H), 5.58 (s, 1H), 7.20-7.38 (m, 6H), 7.76-7.78 (d, 1H).

Representative procedure for the synthesis of compounds D7h-j:

Compound **D8b** (1.0 g; 2.39 mmol) was dissolved in 50 mL ethyl acetate, then 10% palladium/carbon(0.33 g) wetted with 2 mL ethyl acetate was added. The mixture was placed on a Parr hydrogenator, 20 psi hydrogen gas was applied and the mixture was shaken for 3 h. The reaction mixture was gravity filtered and the filtrate was evaporated to give a brown oil (0.5g; 74% yield). The oil was dissolved in 8 mL 1, 4-dioxane and trichloromethyl chloroformate (0.3 mL; 2.5 mmol) was added. The resulting mixture was stirred at room temperature overnight. The solvent was removed under vacuum and the residue was taken up with methylene chloride (15 mL). Aluminum chloride (0.48 g; 3.6 mmol) was added and the resulting mixture was refluxed for 1 h and allowed to cool to room temperature. After water (15 mL) was slowly added, the reaction mixture was stirred for 30 minutes and then transferred to a separatory funnel. The organic layer was washed with water (2×15 mL) and dried over anhydrous sodium sulfate.

Removal of the solvent left a crude product which was purified by flash chromatography (silica gel/ ethyl acetate/ hexanes) to give compound **7h** as a white solid (120 mg; 16% yield), mp 120-2 °C. ¹H NMR (CDCl₃) δ 3.02-3.22 (m, 2H), 4.35-4.40 (m, 1H), 5.95 (s, 2H), 6.50-6.59 (m, 2H), 6.79-6.83 (d, 1H), 6.88 (s, 1H), 7.20-7.35 (m, 5H).

Compound D7i: White solid (5% yield), mp 166-168 °C. ¹H NMR (CDCl₃) δ 3.01-3.35 (m, 6H), 3.80-3.90 (t, 4H), 4.37-4.41(m, 1H), 6.04 (s, 1H), 6.89-6.95 (dd, 2H), 7.02-7.08 (dd, 2H), 7.22-7.38 (m, 5H).

Compound D7j: White solid (7% yield), mp 93-95 °C. ¹H NMR(CDCl₃) δ 3.02-3.10 (dd, 1H), 3.24-3.30 (dd, 1H), 4.38-4.40 (m, 1H), 6.22 (s, 1H), 6.82-7.40 (m, 14H).

Methyl 1-oxo-1,2-dihydroisoquinoline-3-carboxylate D9: To a solution of 1-Oxo-1,2,3,4-tetrahydroisoquinoline 3-carboxy-methyl ester **D2** (13.61g; 66 mmol) in 200 mL 1, 4-dioxane was added 2,3-dichloro-5,6-dicyanobenzoquinone (DDQ) (16.0g; 70.5 mmol) and then the mixture was refluxed overnight. After the reaction completion, the solvent was removed. The residue was taken up with 200 mL ethyl acetate and the organic layer was washed with 5% NaOH (2×50mL), and then dried over anhydrous sodium sulfate. The drying agent was filtered and the filtrate was evaporated. The crude product was purified using flash chromatography (silica gel/ethyl acetate/hexanes) to give compound **D9** as a white solid (3.0 g; 22% yield), mp 154-155 °C. ¹H NMR (CDCl₃) δ 3.92 (s, 3H), 7.52-7.68 (m, 4H), 8.37-8.41 (m, 1H), 9.12 (s, 1H).

1-Oxo-1,2-dihydroisoquinoline-3-carboxylic acid D10. To a solution of ester **D9** (5 mmol) in 10 mL dioxane was added 1M lithium hydroxide (10 mL), and the reaction mixture was stirred at room temperature for 1 h. The solvent was removed on the rotary evaporator and the residue was treated with 20 mL water and acidified to pH 2, forming a precipitate. The precipitate was

collected by suction filtration and washed with 20 mL ethyl acetate to give the corresponding acid as a white solid (80% yield), mp 230-2. ¹H NMR (DMSO-D₆) δ 7.40 (s, 1H), 7.60-7.68 (t, 1H), 7.75-7.83 (t, 1H), 7.83-7.88 (d, 1H), 8.20-8.25 (d, 1H), 11.80 (s, 1H).

Methyl 4-bromo-1-oxo-1,2-dihydroisoquinoline-3-carboxylate D12: To a solution of 1-Oxo-1,2,3,4-tetrahydroisoquinoline 3-carboxy-methyl ester **D2** (3.56 g; 17.4 mmol) in 175 mL methylene chloride were added N-bromosuccinimide (NBS) (6.26 g; 35.2 mmol) and benzyl peroxide (0.20 g; 0.8 mmol), and the reaction was refluxed for 24 h. The reaction was cooled down to room temperature and then washed with saturated NaHCO₃ (3 x 80 mL) and brine (80 mL). The organic layer was dried over anhydrous sodium sulfate. The drying agent was filtered and the filtrate was concentrated. The crude product was precipitated in 30 mL ethyl acetate and filtered, yielding compound **D12** as a white solid (2.84 g; 57% yield), mp 186-187 °C. ¹H NMR (CDCl₃) δ 4.05 (s, 3H), 7.65-7.71 (t, 1H), 7.82-7.88 (t, 1H), 8.25-8.30 (d, 1H), 8.43-8.48 (d, 1H), 9.45 (s, 1H).

4-Bromo-1-oxo-1,2-dihydroisoquinoline-3-carboxylic acid D13 was obtained using the same procedure as **D10**. White solid (64% yield), mp >260 °C. ¹H NMR (DMSO-D₆) δ 7.65-7.73 (t, 1H), 7.84-8.00 (m, 2H), 8.20-8.30 (d, 1H), 11.80 (s, 1H).

General coupling reaction procedure for compounds D11c, D11f, D14a-c, D14f and D14j.

A solution of compound **D9** or **D13** (2 mmol) in 5 mL dry N, N-dimethylformamide (DMF) was treated with 1-[3-(dimethylamino)propyl]-3-ethylcarbodiimide hydrochloride (EDCI) (0.38 g; 2 mmol), followed by the appropriate amine (2 mmol). The reaction mixture was stirred at room temperature overnight. The solvent was removed under vacuum and the residue was added ethyl acetate (30 mL). The organic layer was washed with 5% aqueous HCl (3×10 mL), saturated aqueous NaHCO₃ (3×10 mL), and brine (10 mL). The organic layer was dried over anhydrous

sodium sulfate. The drying agent was filtered and the solvent was removed. The crude product was purified by flash chromatography (silica gel/ethyl acetate/hexanes) to give compound **D11c**, **D11f**, **D14a-c**, **D14f** or **D14j**.

Compound D11c: White solid (10% yield), mp 138-140 °C. ¹H NMR (DMSO-D₆) δ 4.48 (s, 2H), 6.34-6.36 (m, 1H), 6.60-6.62 (m, 1H), 7.35 (s, 1H), 7.57-7.80 (m, 4H), 8.20-8.24 (d, 1H).

Compound D11f: White solid (15% yield), mp 189-191 °C. ¹H NMR (CDCl₃) δ 4.68-4.73 (d, 2H), 7.20-8.08 (m, 10H), 10.88 (s, 1H).

Compound D14a: White solid (18% yield), mp 175-177 °C. ¹H NMR (CDCl₃) δ 2.95-3.00 (t, 2H), 3.82 (s, 3H), 3.80-3.86 (m, 2H), 6.80-6.89 (m, 3H), 7.23-7.30 (m, 1H), 7.60-7.67 (t, 1H), 7.67 (s, 1H), 7.76-7.83 (t, 1H), 8.02-8.05 (d, 1H), 8.43-8.46 (d, 1H), 9.78 (s, 1H).

Compound D14b: White solid (10% yield), mp 252-254 °C. ¹H NMR (DMSO-D₆) δ 3.05-3.15 (m, 4H), 3.70-3.80 (m, 4H), 6.92-7.00 (d, 2H), 7.52-7.60 (d, 2H), 7.60-7.68 (m, 1H), 7.84-7.96 (m, 2H), 8.23-8.28 (d, 1H), 10.82 (s, 1H), 12.17 (s, 1H).

Compound D14c: White solid (15% yield), mp 197-199 °C. ¹H NMR (CDCl₃) δ 4.68-4.73 (d, 2H), 6.37 (s, 2H), 7.41 (m, 1H), 7.60-7.68 (t, 1H), 7.74-7.82 (t, 1H), 8.00 (s, 1H), 8.02-8.08 (d, 1H), 8.40-8.46 (d, 1H), 9.90 (s, 1H).

Compound D14f: White solid (45% yield), mp 208-209 °C. ¹H NMR (DMSO-D₆) δ 4.45-4.52 (d, 2H), 7.23-8.27 (m, 9H), 9.28-9.37 (t, 1H), 12.10 (s, 1H).

Compound D14j: White solid (33% yield), mp 216-218 °C. ¹H NMR (DMSO-D₆) δ 6.78-8.42 (m, 13H), 10.50 (s, 1H), 11.72 (s, 1H).

6.3.2 Biochemical Studies

Protease assays [265]. All assays were performed in opaque 96-well plates. Reaction mixtures (100 μ L/assay) contained 200 mM TRIS buffer, pH 9.5, 13.5 mM NaCl, 30% glycerol, 0.025 μ M enzyme, and 100 μ M Boc-Gly-Lys-Arg-7-AMC. Enzyme incubations were at 25 $^{\circ}$ C for 30 minutes. The fluorescence of 7-amino-4-methyl coumarin (AMC) released from the cleavage of the substrate was monitored using excitation and emission wavelengths of 385 nm and 465 nm, respectively.

Protease inhibitor assays [265]. The protease inhibitor assays contained 200 mM TRIS buffer, pH 9.5, 13.5 mM NaCl, 30% glycerol, 0.025 μ M enzyme (2.5 pmol), 100 μ M Boc-Gly-Lys-Arg-7-AMC and 50 μ M inhibitor. The inhibitors were dissolved in DMSO and diluted in assay buffer. The DMSO concentration in the assay mix was maintained at 1%, including in the no-inhibitor control. The assay mixtures containing WNV protease with an inhibitor (or without the inhibitor as a control) were pre-incubated at room temperature for fifteen minutes. An aliquot of the substrate (100 μ M) was added and the incubation continued for an additional fifteen minutes. Fluorescence values were obtained using excitation and emission wavelengths of 385 nm and 465 nm, respectively. The percent inhibition of protease activity was determined using Microsoft Excel.

6.3.3 Molecular Modeling Studies

Molecular docking simulations were performed via the AutoDock4 program [230]. Compound **D14j** was constructed in SYBYL8.0 [231] and structurally optimized to default convergence thresholds using the Tripos Force Field [232] and Gasteiger-Marsili partial atomic

charges [28]. The active site model for WNV protease was prepared using the 2FP7 [195]. The structure was protonated in SYBYL8.0, stripped of all water molecules and bound ligands, and electrostatically represented with Gasteiger-Marsili charges. AutoDock simulations were performed using the Lamarckian Genetic Algorithms (GA) subroutine at default settings for GA population size, cross-over rate and mutation rate, and starting with fully-randomized ligand position, orientation and conformation. One hundred GA runs were performed for the ligand-enzyme pair.

CHAPTER 7

WEST NILE VIRUS/DENGUE VIRUS NS2B-NS3 PROTEASE INHIBITORS BASED ON THE 2-MERCAPTOQUINAZOLIN-4(3H)-ONE SCAFFOLD

7.1 Inhibitor Design Rationale

The design of 2-mercaptoquinazolin-4(3H)-one scaffold-derived inhibitors for West Nile virus and Dengue virus NS2B-NS3 proteases is based on the following considerations: 1) inhibitor **D14j** showed weak inhibition towards WNV NS2B-NS3 protease (Figure 7.1); 2) molecular modeling studies revealed that inhibitor **D14j** forms multiply interactions with the active site of WNV NS2B-NS3 protease including hydrogen bonding, π -stacking and hydrophobic interactions (the specific interactions are shown in 6.2.3); 3) molecular modeling studies also suggested that the second aromatic ring in the (m-phenoxy)phenyl component serves as a semi rigid linker of two aromatic rings which fit into two separated binding pockets and that the replacement of the terminal phenyl ring with a polar aromatic ring would enhance the binding affinity. Consequently, a similar but more synthetically tractable template, 2-mercaptoquinazolin-4(3H)-one, was used to couple with a set of structurally diverse and polar amines through a short amide linker (structure VII, Figure 7.1). A similar strategy, in terms of increasing inhibitor polarity, was employed including: 1) coupling reaction with sulfonamide could introduce two potential hydrogen bonding acceptor sulfonyl oxygens to the inhibitor VII; 2) the replacement of the middle phenyl ring with a triazole ring may result in extra hydrogen bonding without losing the hydrophobic interactions between the inhibitor aromatic ring and the pocket defined by Val72 and Trp50. Although the X-ray crystal structure of the DENV NS2B-NS3 protease-inhibitor complex has not reported, the high homology and X-ray crystal structures of both protease-cofactor complexes have shown a high similarity in their active sites. Therefore,

we reasoned that inhibitor **VII** that incorporates two polar aromatic rings via a short flexible spacer would be favorable for binding both NS2B-NS3 protease active sites. Compared to the reported peptide-based WNV NS2B-NS3 protease inhibitors, inhibitor **VII** is more chemically robust and drug-like and, consequently more capable in providing good pharmacokinetics and bioavailability.

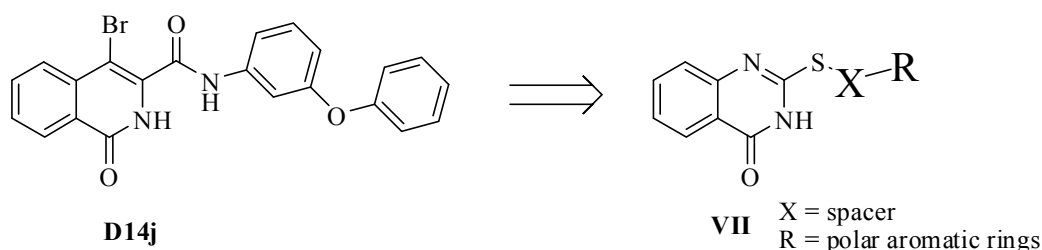


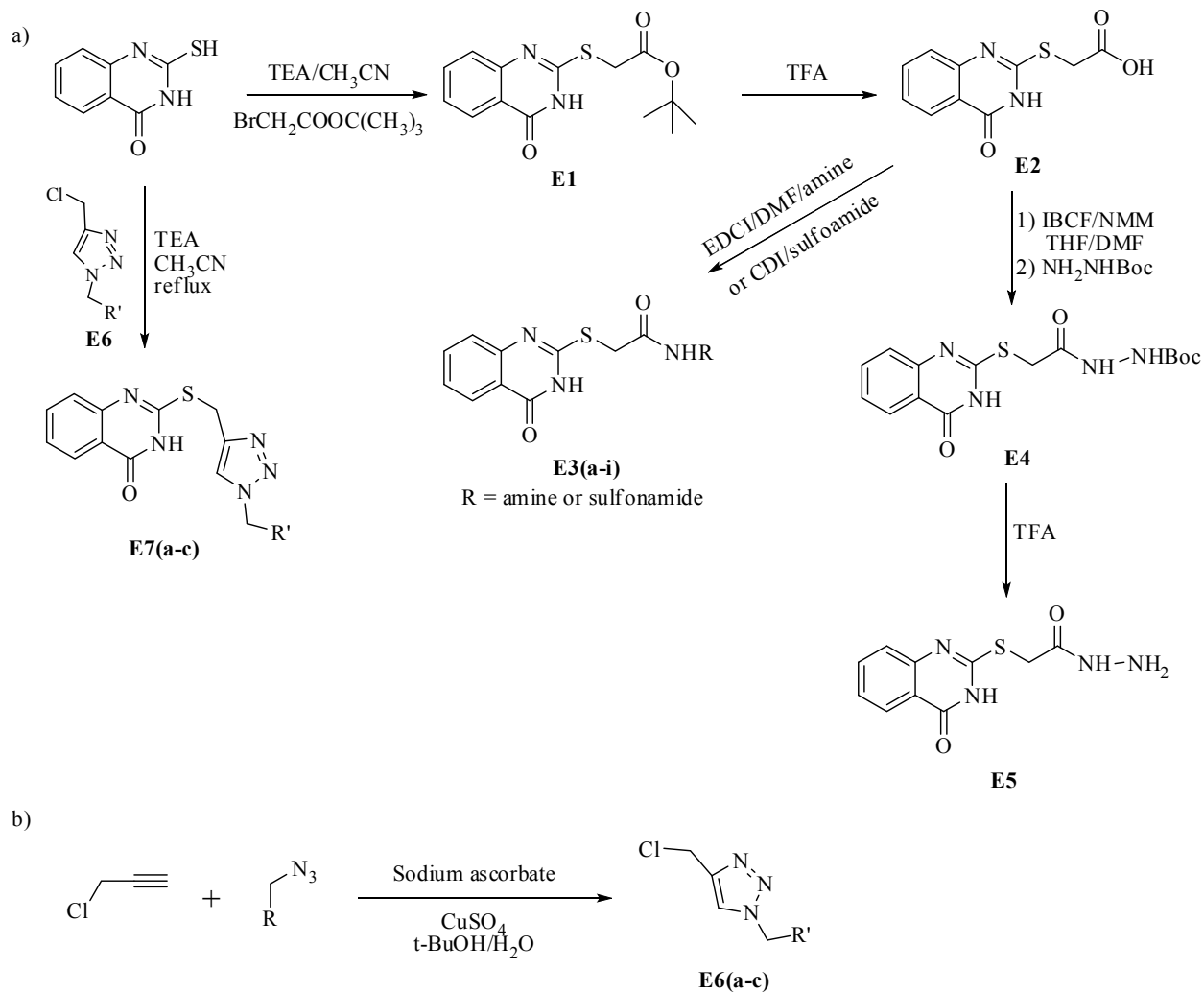
Figure 7.1 Design of Non-Covalent Inhibitors

7.2 Results and Discussions

7.2.1 Synthesis

The synthesis of inhibitor **VII** is shown in Scheme 7.1. The key intermediate **E2** was readily prepared by treatment of 2-mercaptoquinazolin-4(3H)-one with tert-butyl bromoacetate in the presence of TEA followed by the removal of Boc with TFA. The acid **E2** was then coupled with a range of structurally diverse amines, sulfonamides and carbazate, yielding compound **E3(a-i)** and **E4**. Removal of Boc protection for **E4** afforded compound **E5**. The triazole compounds **E7(a-c)** were initially planned to functionalize an alkyne group on the sulfur atom of 2-mercaptoquinazolin-4(3H)-one either by alkylation with propargyl bromide or Mitsunobu reaction with propargyl alcohol, however both reactions failed to give the desired alkyne product. Therefore triazoles **E6a-c** were first prepared using propargyl chloride and appropriate azides (shown in Scheme 7.1 b, azides were obtained in chapter 4), and the resulting triazole

intermediates **E6a-c** are listed in Table 7.1. Finally, 2-mercaptoquinazolin-4(3H)-one was alkylated with **E6a-c** to give the desired products **E7a-c**. A summary of 2-mercaptoquinazolin-4(3H)-one based inhibitors are listed in Table 7.2.



Scheme 7.1 Synthesis of WNV/DENV NS2B-NS3 Inhibitors

Table 7.1 Chloromethyl Triazole Inputs

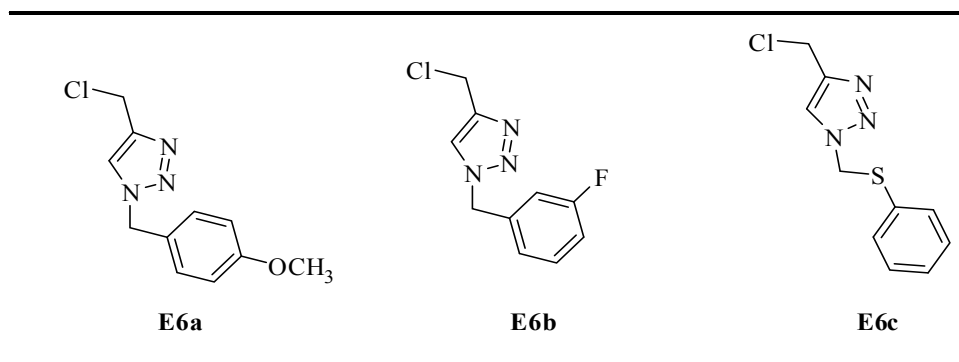
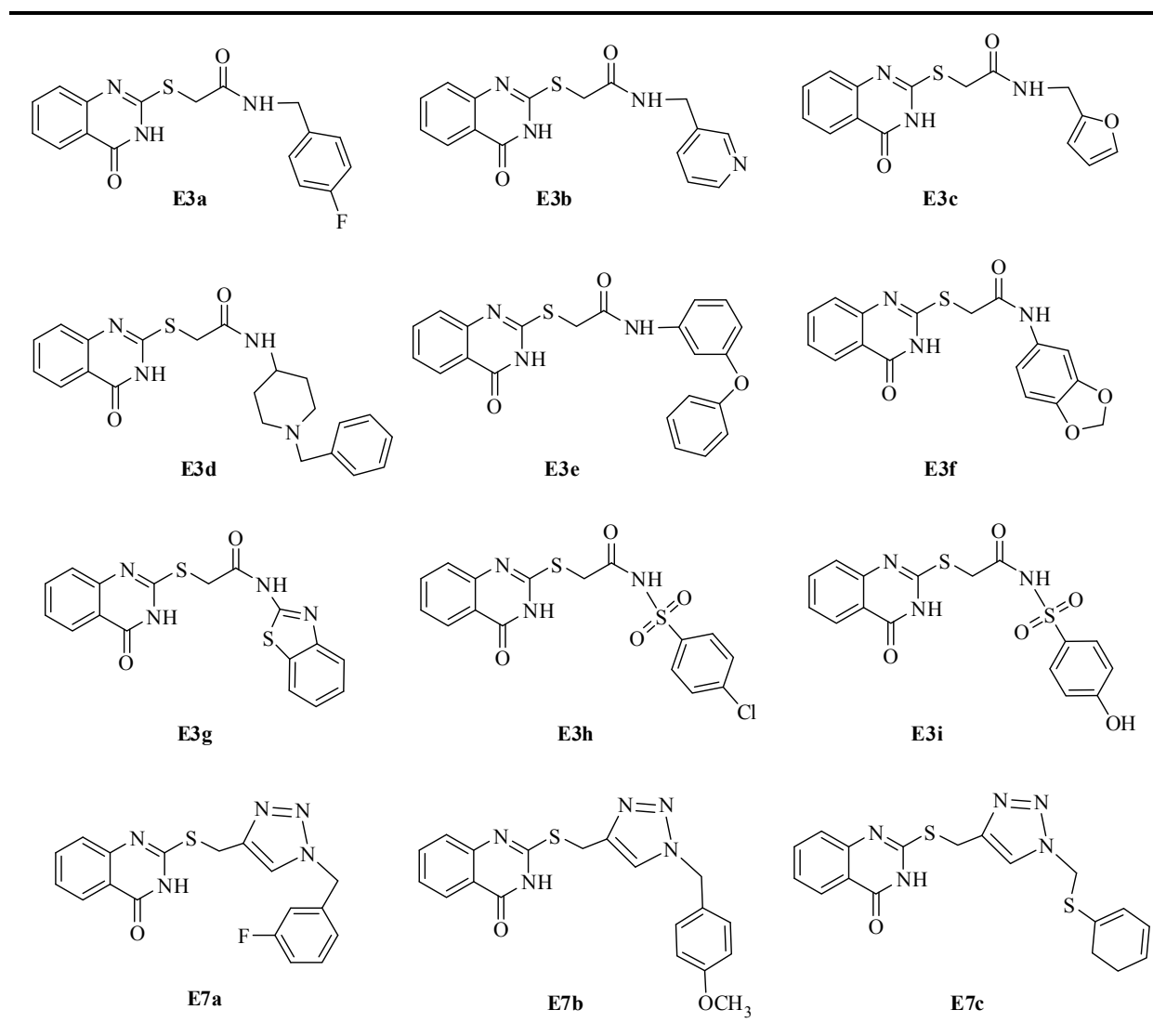


Table 7.2 2-Mercaptoquinazolin-4(3H)-One Scaffold Based Inhibitors



7.2.2 Biological Studies

All the inhibitors were screened against WNV and DENV NS2B-NS3 proteases at 50 μM concentration with Boc-Gly-Lys-Arg-7-AMC as the substrate. All the compounds with greater than 20% percent inhibition against WNV NS2B-NS3 protease are shown in **Figure 7.2** (Left) whereas their percent inhibition against DENV NS2B-NS3 protease are shown in **Figure 7.2** (Right). As expected, all the amide compounds except for **E3c** showed apparent inhibition against WNV NS2B-NS3 protease. Of these amide compounds, **E3d**, **E3e**, **E3g** showed greater than 40% inhibition, indicating approximate IC_{50} of 50-100 μM . The triazole compound **E7a** was found the similar activity as **E3e**, but the sulfonamides were devoid of any inhibitory activity against WNV NS2B-NS3 protease possibly due to the large size of sulfonyl group. Within these four most active compounds for WNV protease, two of them (**E3d**, **E3e**) were found to inhibit DENV NS2B-NS3 protease with about 40-50% when a 50 μM of inhibitor was used, and the

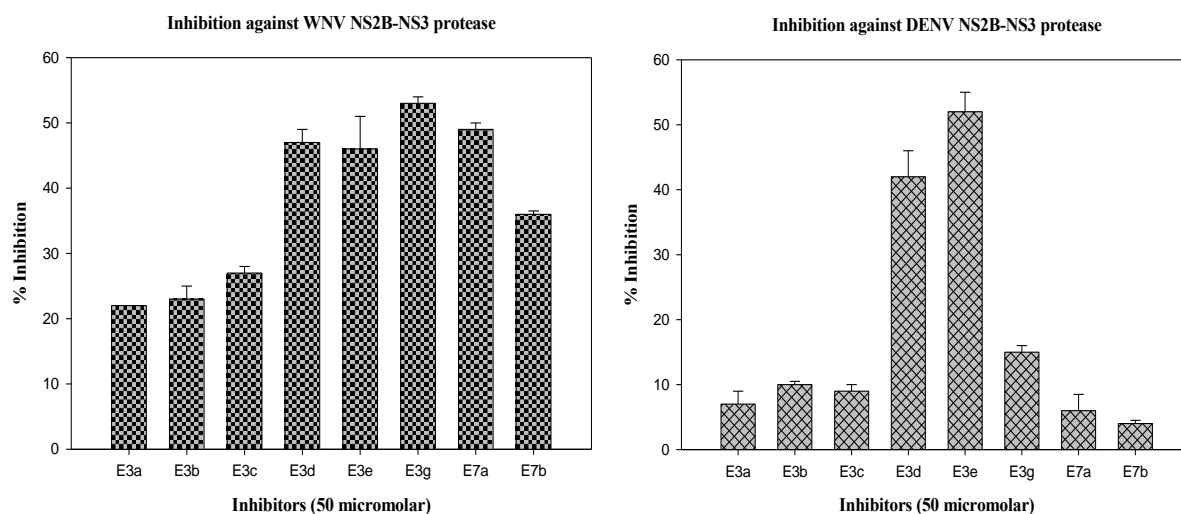


Figure 7.2 Percent Inhibition of Selected Inhibitor **E3** and **E7** against WNV and DENV NS2B-NS3 Proteases

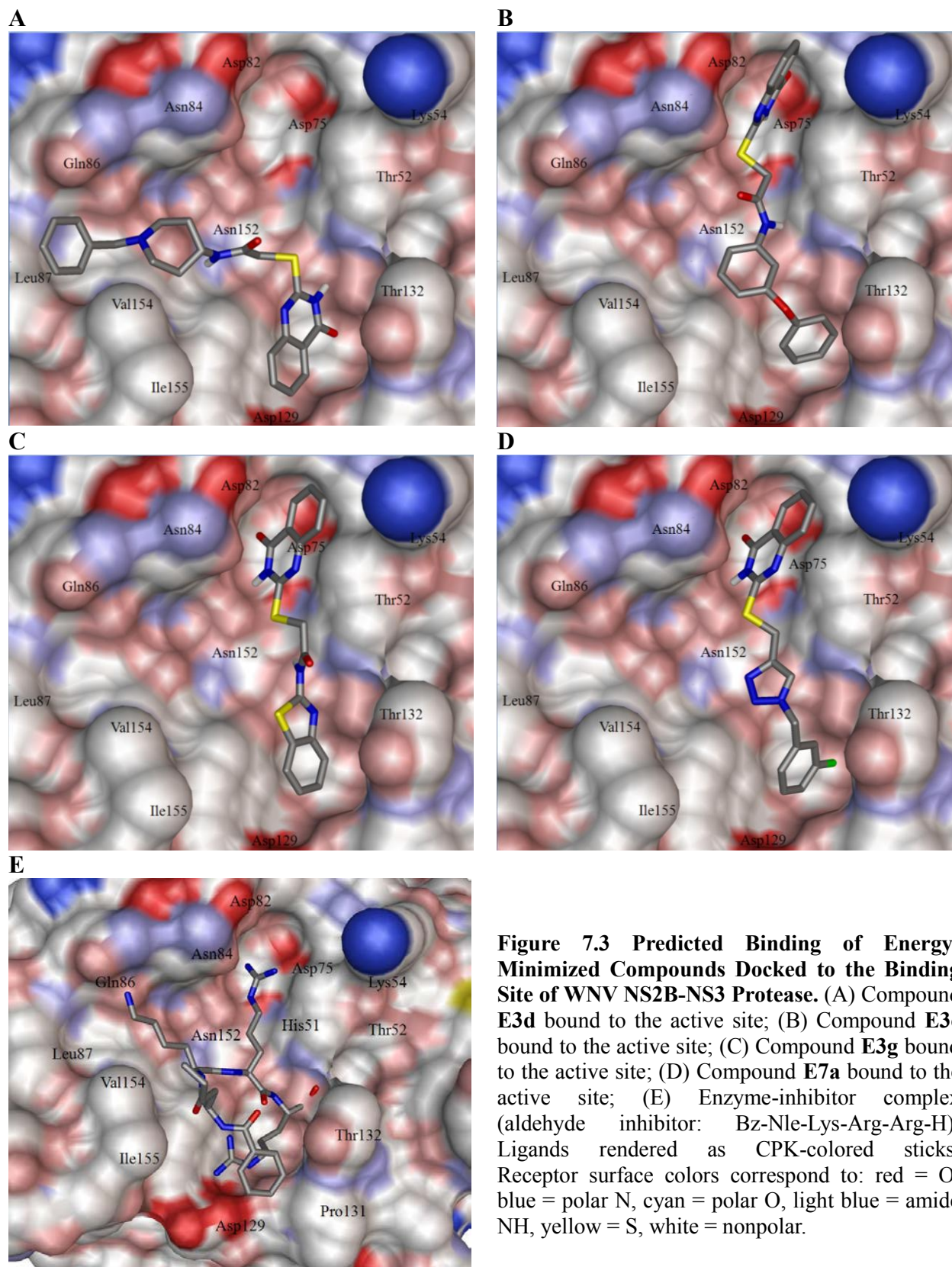
IC_{50} of **E3e** was found as 89 μM . The fact that many hits have been found in a fairly small library

suggests that variation of the spacer and introduction of more polar groups into inhibitor **VII** can enhance the inhibitory activity against both WNV and DENV NS2B-NS3 proteases.

7.2.3 Computational Studies

The four most active compounds **E3d**, **E3e**, **E3g** and **E7a** were docked into WNV NS2B-NS3 protease active site (pdb code: 2fp7) [195] and the docking results are shown in Figure 7.3. From the X-ray crystal structure of enzyme-inhibitor complex, the tetra-peptide aldehyde inhibitor was folded in a shape which extends its three basic residues to acidic residues of enzyme, affording strong binding affinity (shown in Figure 7.3 E). Interestingly, all four compounds **E3d**, **E3e**, **E3g** and **E7a** bind to the center of the “3-star shape” active site with the aromatic terminals occupying two of the three pockets. Of which, the heterocyclic ring of compound **E3d** binds to the same pocket of active site as **D14j**, a sulfur atom and flexible 6-member ring allowed the molecule to fit into a relatively shallow and hydrophobic pocket and a hydrogen bond between the NH hydrogen of heterocyclic ring and Ser135 amide oxygen. The rest of the three compounds bind to the active site in a similar fashion with the heterocyclic ring nestled in the most polar pocket and these molecules are stretched between two polar pockets. The amide NHs next to the aromatic rings of **E3e** and **E3g** are donating H to the amide oxygen of Gly151 whereas compound **E7a** uses the NH on the heterocyclic ring to form a hydrogen bond. The terminal phenyl rings bind to the opposite pocket either by π -stacking or hydrophobic interactions. It is clear that a strategy employing two polar aromatic rings linked by a flexible spacer does deliver WNV NS2B-NS3 protease inhibitors. Apparently, the introduction of another appropriate component to inhibitor **VII**, resulting an inhibitor occupying all three pockets like the aldehyde inhibitor, could potentially enhance the potency significantly.

As mentioned in Chapter 1, NS2B-NS3 proteases have two conformations, a productive and an unproductive conformation. The X-ray crystal structures of WNV NS2B-NS3 protease and inhibitor bound complexes (assuming at productive conformation) have been solved and employed here. Unfortunately, the X-ray crystal structure of enzyme-inhibitor of DENV NS2B-NS3 protease has not been reported thus. In the unproductive conformation of DENV NS2B-NS3 protease, the C-terminus of the cofactor NS2B which forms part of the active site, especially contributing the ion-ion interaction for P₂ residue, is separated from NS3 protease. The P₂ residue prefers a basic side chain as suggested by the substrate, however, compound **E3d** and **E3e** are predicted to bind to the active site using dipole-dipole interactions with the relatively polar pocket instead of ion-ion interactions with deprotonated carboxylic acid. Therefore, the unproductive conformation of DENV NS2B-NS3 protease was used for molecular docking with compounds **E3d** and **E3e**. The entire active site is Y-shaped with one shallow pocket isolated by a narrow valley and the other two pockets accommodating fairly linear structures. It appears that the sandwich pocket defined by Pro132 and Leu128 forms a strong hydrophobic interaction with the terminal phenyl ring for both compounds. The heterocyclic ring of compound **E3d** is positioned in the largest pocket with the NH on the ring hydrogen bonding to back bond oxygen of Ile36. Compound **E3e** is able to bend across the valley and the heterocyclic ring is interacting with the polar part of the pocket. It is possible that the isolation of two aromatic rings by a narrow and rigid valley limits the flexibility of the spacer, making the entire molecule more rigid, and therefore minimizes the entropy loss. Similarly, a three-branched molecule which can fit all three pockets maybe a promising and potent inhibitor of DENV NS2B-NS3 protease.



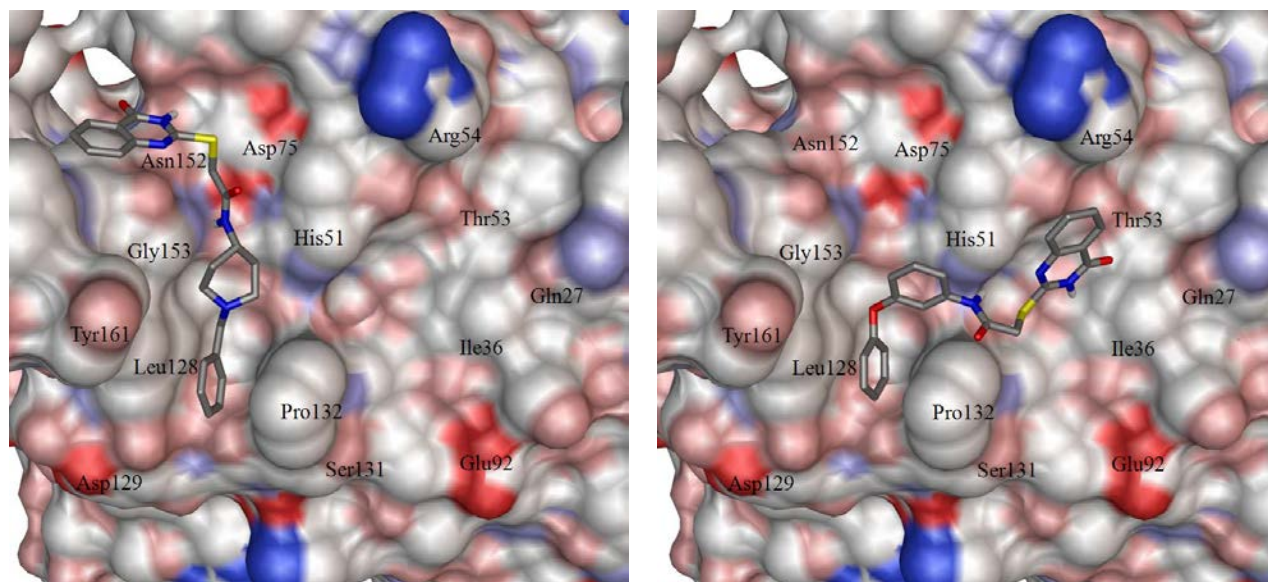


Figure 7.4 Predicted Binding of Energy-Minimized Compounds Docked to the Binding Site of DENV NS2B-NS3 Protease. Left: compound **E3d** bound to the active site; Right: compound **E3e** bound to the active site. Ligands rendered as CPK-colored sticks. Receptor surface colors correspond to: red = O, blue = polar N, cyan = polar O, light blue = amide NH, yellow = S, white = nonpolar.

7.3 Conclusions

A small focused library was synthesized and some of the compounds showed good inhibitory activity against both WNV and DENV NS2B-NS3 proteases. The initial hypothesis proved to be successful and the computational studies with compounds **E3d** and **E3e** suggested that additional polar interactions could potentially enhance the potency. The introduction of a third component to inhibitor **VII** is currently in progress and the preliminary results agree with the prediction. All of the compounds are chemically robust and are non-peptide inhibitors, which are likely to have good pharmacokinetics and oral bioavailability.

7.4 Experimental

7.4.1 Synthesis

General

The ^1H NMR spectra were recorded on a Varian XL-300 or XL-400 NMR spectrometer. A Gemini EM microplate spectrofluorometer (Molecular Devices Corporation, Sunnyvale, CA) was used in the enzyme assays and inhibition studies. Melting points were determined on a Mel-Temp apparatus and are uncorrected. Reagents and solvents were purchased from various chemical suppliers (Aldrich, Acros Organics, TCI America, and Bachem). Silica gel (230-450 mesh) used for flash chromatography was purchased from Sorbent Technologies, Atlanta, GA. Thin layer chromatography was performed using Analtech silica gel plates. The TLC plates were visualized using iodine and/or UV light. WNV and DENV NS2B-NS3 proteases were expressed in *E. coli* as described for Dengue virus-2 protease [264] and purified as previously described [265]. Boc-Gly-Lys-Arg-7-AMC was purchased from Bachem.

Representative synthesis

Methyl 2-(4-oxo-3,4-dihydroquinazolin-2-ylthio)acetate E1: To a solution of 2-Mercapto-4(3H)-quinazoline (8.91 g; 50 mmol) and tert-butyl bromoacetate (9.75 g; 50 mmol) in 150 mL acetonitrile was added triethylamine (12.1 g; 120 mmol). The resulting reaction mixture was refluxed for 20 h. The solvent was removed and the residue was taken up with 250 mL ethyl acetate and 150 mL water. The un-dissolved white precipitate was filtered and the organic layer was washed with additional 150 mL water. The organic layer was then dried over anhydrous sodium sulfate and the drying agent was filtered. The residue after the evaporation by vacuum evaporator was combined with the previous precipitate to give fairly pure **E1** as a white solid (14.6 g; 100% yield) m.p. 168-170 °C. ^1H NMR (CDCl_3) δ 1.43 (s, 9H), 3.96 (s, 2H), 7.28-7.45 (m, 2H), 7.69-7.80 (t, 1H), 8.01-8.04 (d, 1H), 12.75 (bs, 1H).

2-(4-Oxo-3,4-dihydroquinazolin-2-ylthio)acetic acid E2: Compound **E1** (14.6 g; 50 mmol) was placed in a 250 ml RB flask and 100 ml trifluoroacetic acid was added at room temperature.

The reaction was stirred for 4 h before trifluoroacetic acid was removed under vacuum. To the residue was added 400 ml water and cooled in an ice-water bath, forming a precipitate which was collected using vacuum filtration. The filtered cake was then dissolved using 250 ml 10% NaOH and the aqueous solution was extracted with 3×150 ml ethyl acetate. Then the aqueous solution was acidified to pH 2 using 6 N HCl under an ice-water bath. The precipitate from this acidic solution was filtered, yielding pure compound **E2** as a yellow solid (9.45 g; 80%) m.p. 209-211 °C. ¹H NMR (DMSO-D₆) δ 4.036 (s, 2H), 7.40-7.48 (m, 2H), 7.72-7.80 (t, 1H), 8.00-8.05 (d, 1H), 12.72 (s, 1H).

Representative synthesis of compound E3a-g:

Compound E3a: A solution of acid **E2** (0.47 g; 2 mmol) in 6 ml DMF was added EDCI (0.46 g; 2.4 mmol). Fifteen minutes later, 4-fluorobenzylamine (0.28 g; 2.2 mmol) was added and the resulting reaction mixture was stirred overnight. The solvent was removed and the residue was treated with 50 ml of water, forming a precipitate which was filtered and air dried to give compound **E3a** as a white solid (0.27 g; 39% yield) m.p. 213-215 °C. ¹H NMR (DMSO-D₆) δ 3.98 (s, 2H), 4.26 (s, 2H), 6.92-7.08 (m, 2H), 7.24-7.35 (m, 2H), 7.35-7.50 (m, 2H), 7.65-7.80 (m, 2H), 8.02-8.07 (d, 1H).

Compound E3b: Yellow solid (77% yield) m.p. 226-228 °C. ¹H NMR (DMSO-D₆) δ 3.99 (s, 2H), 4.33-4.38 (d, 2H), 7.18-7.23 (m, 1H), 7.38-7.45 (m, 2H), 7.60-7.66 (d, 1H), 7.68-7.79 (t, 1H), 8.00-8.05 (d, 1H), 8.38-8.42 (d, 1H), 8.46 (s, 1H), 8.77-8.83 (t, 1H).

Compound E3c: White solid (65% yield) m.p. 206-208 °C. ¹H NMR (DMSO-D₆) δ 4.00 (s, 2H), 4.29-4.33 (d, 2H), 6.22-6.24 (d, 1H), 6.37-6.39 (d, 1H), 7.39-7.47 (m, 2H), 7.56-7.57 (m, 1H), 7.73-7.80 (t, 1H), 8.00-8.03 (d, 1H), 8.96-8.75 (t, 1H), 12.63 (bs, 1H).

Compound E3d: White solid (65% yield) m.p. 193-195 °C. ¹H NMR (DMSO-D₆) δ 1.37-1.51

(m, 2H), 1.65-1.76 (m, 2H), 1.94-2.08 (m, 2H), 2.65-2.76 (m, 2H), 3.33 (s, 2H), 3.41 (s, 1H), 3.92 (s, 2H), 7.20-7.52 (m, 7H), 7.69-7.80 (m, 1H), 8.00-8.05 (d, 1H), 8.20-8.23 (d, 1H).

Compound E3e: Yellow solid (23% yield) m.p. 217-219 °C. ¹H NMR (DMSO-D₆) δ 4.66 (s, 2H), 6.16-6.39 (m, 1H), 6.96-7.18 (m, 3H), 7.31-7.60 (m, 5H), 7.72-7.82 (m, 2H), 8.00-8.16 (dd, 2H), 9.43-9.48 (d, 1H).

Compound E3f: Yellow solid (27% yield) m.p. 153-155 °C. ¹H NMR (DMSO-D₆) δ 4.67 (s, 2H), 5.98 (s, 2H), 6.68-7.02 (m, 2H), 7.39-7.58 (m, 3H), 7.72-7.80 (m, 2H), 8.00-8.15 (m, 2H).

Compound E3g: Pink solid (75% yield) m.p. 194-196 °C. ¹H NMR (DMSO-D₆) δ 4.35 (s, 2H), 7.29-7.60 (m, 4H), 7.60-7.81 (m, 2H), 7.89-8.04 (m, 2H), 12.84 (s, 1H).

Representative synthesis of compound E3h-i:

Compound E3h: To acid **E2** (0.47 g; 2 mmol) in dry THF (6 ml) was added dropwise a solution of CDI (0.34 g; 2 mmol) in dry THF (4 ml) at room temperature. The reaction mixture was stirred for 30 min and then refluxed for 30 min. 4-Chlorobenzene sulfonamide (0.38 g; 2 mmol) was added in one portion to the above solution when it was cooled to room temperature. 10 min later, a solution of DBU (0.30 g; 2 mmol) in dry THF (2 ml) was added dropwise to the above reaction mixture. The reaction was stirred at room temperature overnight. The solvent was removed and the residue was taken up with 20 ml ethyl acetate and 20 ml water. The aqueous layer was acidified to pH 3 after separation and the precipitate formed was collected using vacuum filtration, yielding the pure product **E3h** as an orange solid (0.30 g; 38% yield) m.p. 164-166 °C. ¹H NMR (DMSO-D₆) δ 4.68 (s, 2H), 7.40-7.50 (m, 3H), 7.63-7.78 (m, 2H), 7.91-7.96 (m, 1H), 8.00-8.05 (d, 1H), 8.18-8.23 (d, 1H), 9.53-9.55 (d, 1H).

Compound E3i: Yellow solid (42% yield) m.p. 156-158 °C. ¹H NMR (DMSO-D₆) δ 4.71 (s, 2H), 7.38-7.53 (m, 2H), 7.62-7.80 (m, 3H), 7.89-7.97 (t, 1H), 8.00-8.05 (d, 1H), 8.18-8.23 (d,

1H), 9.53-9.56 (d, 1H), 14.22 (bs, 1H).

Tert-butyl 2-(2-(4-oxo-3,4-dihydroquinazolin-2-ylthio)acetyl)hydrazinecarboxylate E4: A solution of acid **E2** (0.47 g; 2 mmol) in 6 ml THF and 3 ml DMF was added isobutyl chloroformate (0.28 g; 2.2 mmol) and N-methyl morpholine (NMM) (0.24 ml; 2.4 mmol) at 0 °C. 5 min later, tert-butyl carbazate (0.26 g; 2 mmol) was added and the resulting reaction mixture was stirred at 0 °C for 0.5 h and then room temperature for 2 h. The solvent was removed and the residue was stirred in a mixed solvent containing 20 ml ethyl acetate and 30 ml water for 20 min. The precipitate was filtered and air dried to give compound **E4** as a white solid (0.45 g; 64% yield) m.p. >260 °C. ¹H NMR (DMSO-D₆) δ 1.42 (s, 9H), 3.98 (s, 2H), 7.33-7.42 (t, 1H), 7.58-7.63 (d, 1H), 7.65-7.75 (t, 1H), 8.08-8.12 (d, 1H), 8.35 (s, 1H), 9.80 (s, 1H), 12.56 (s, 1H).

2-(4-Oxo-3,4-dihydroquinazolin-2-ylthio)acetohydrazide E5: To compound **E4** (0.38 g; 1.1 mmol) was added 6 ml trifluoroacetic acid at room temperature and the reaction was stirred for 1 h. Trifluoroacetic acid was removed and the residue was treated with 5 ml water, forming a precipitate. The precipitate was filtered and air dried to give compound **E5** as a green solid (0.14 g; 51% yield) m.p. 214-216 °C. ¹H NMR (DMSO-D₆) δ 4.03 (s, 1H), 7.40-7.48 (t, 1H), 7.48-7.58 (d, 1H), 7.72-7.80 (t, 1H), 8.00-8.08 (d, 1H), 10.42 (s, 1H), 12.76 (s, 1H).

Representative synthesis of compound E6a-c:

4-(Chloromethyl)-1-(4-methoxybenzyl)-1H-1,2,3-triazole E6a: Propargyl chloride (0.74 g; 10 mmol) and 3-fluorobenzyl azide (1.51 g; 10 mmol) were dissolved in 10 ml t-butanol and 10 ml water, then sodium ascorbate (0.20 g; 1.0 mmol) and copper(II) sulfate pentahydrate (0.025 g; 0.01 mmol) were added. The resulting reaction mixture was stirred at room temperature for 24 h. The solvent was removed and the residue was taken up with 30 ml ethyl acetate and 20 ml water.

The insoluble impurity was filtered and the separated organic layer was washed with 20 ml saturated sodium chloride. The organic solution was dried and the drying agent was filtered. The solvent was evaporated under vacuum and the crude product was purified by flash chromatography (silica gel/ethyl acetate/hexanes) to give pure product **E6a** as a colorless oil (0.56 g; 22%). ¹H NMR (CDCl₃) δ 4.71 (s, 2H), 5.56 (s, 2H), 6.84-7.00 (m, 1H), 7.02-7.13 (m, 1H), 7.19-7.26 (m, 1H), 7.40-7.53 (m, 1H), 8.24 (s, 1H).

4-(Chloromethyl)-1-(3-fluorobenzyl)-1H-1,2,3-triazole E6b: White solid (13 % yield) m.p. 92-94 °C. ¹H NMR (CDCl₃) δ 3.78 (s, 3H), 4.66 (s, 2H), 5.45 (s, 2H), 6.84-6.92 (d, 2H), 7.20-7.28 (d, 2H), 7.53 (s, 1H).

4-(Chloromethyl)-1-(phenylthiomethyl)-1H-1,2,3-triazole E6c: Oil (13% yield). ¹H NMR (CDCl₃) δ 4.63 (s, 2H), 5.60 (s, 2H), 7.20-7.35 (m, 5H), 7.60 (s, 1H).

Representative synthesis of compound E7a-c:

Compound E7a: To a mixture of 2-mercapto-4(3H)-quinazoline (0.39 g; 2.2 mmol) and compound **E6a** (0.50 g; 2.2 mmol) in 10 ml acetonitrile was added triethylamine (0.66 ml; 5.2 mmol) and the resulting mixture was refluxed overnight. The reaction mixture was diluted with 30 ml water and stirred for 10 min. The precipitate formed was filtered and air dried to give pure compound **E7a** as a white solid (0.60 g; 74% yield) m.p. 234-236 °C. ¹H NMR (DMSO-D₆) δ 4.52 (s, 2H), 5.60 (s, 2H), 7.00-7.20 (m, 2H), 7.28-7.61 (m, 4H), 7.69-7.80 (q, 1H), 8.00-8.05 (d, 1H), 8.20 (s, 1H), 12.62 (s, 1H).

Compound E7b: Gray solid (18% yield) m.p. 160-162 °C. ¹H NMR (DMSO-D₆) δ 3.79 (s, 3H), 4.53 (s, 2H), 5.41 (s, 2H), 6.80-6.85 (d, 2H), 7.17-7.22 (d, 2H), 7.36-7.41 (t, 1H), 7.47-7.52 (d, 1H), 7.64-7.73 (m, 2H), 8.10-8.16 (d, 1H), 12.32 (bs, 1H).

Compound E7c: Gray solid (18% yield) m.p. 169-171 °C. ¹H NMR (DMSO-D₆) δ 4.47 (s, 2H),

5.89 (s, 2H), 7.18-7.23 (d, 3H), 7.28-7.35 (t, 2H), 7.42-7.50 (t, 1H), 7.53-7.58 (d, 1H), 7.77-7.82 (t, 1H), 7.96 (s, 1H), 8.02-8.06 (d, 1H).

7.4.2 Biochemical Studies

Protease assays [265]. All assays were performed in opaque 96-well plates. Reaction mixtures (100 μ L/assay) contained 200 mM TRIS buffer, pH 9.5, 13.5 mM NaCl, 30% glycerol, 0.025 μ M enzyme, and 100 μ M Boc-Gly-Lys-Arg-7-AMC. Enzyme incubations were at 25 °C for 30 minutes. The fluorescence of 7-amino-4-methyl coumarin (AMC) released from the cleavage of the substrate was monitored using excitation and emission wavelengths of 385 nm and 465 nm, respectively.

Protease inhibitor assays [265]. The protease inhibitor assays contained 200 mM TRIS buffer, pH 9.5, 13.5 mM NaCl, 30% glycerol, 0.025 μ M enzyme (2.5 pmol), 100 μ M Boc-Gly-Lys-Arg-7-AMC and 50 μ M inhibitor. The inhibitors were dissolved in DMSO and diluted in assay buffer. The DMSO concentration in the assay mix was maintained at 1%, including in the no-inhibitor control. The assay mixtures containing WNV/DENV NS2B-NS3 protease with an inhibitor (or without the inhibitor as a control) were pre-incubated at room temperature for fifteen minutes. An aliquot of the substrate (100 μ M) was added and the incubation continued for an additional fifteen minutes. Fluorescence values were obtained using excitation and emission wavelengths of 385 nm and 465 nm, respectively. The percent inhibition of protease activity was determined using Microsoft Excel.

7.4.3 Computational Studies

Molecular docking simulations were performed via the AutoDock4 program [230]. All the compounds were constructed in SYBYL8.0 [231] and structurally optimized to default convergence thresholds using the Tripos Force Field [232] and Gasteiger-Marsili partial atomic charges [233]. The active site models for WNV and DENV NS2B-NS3 proteases were prepared using the 2FP7 and 2FOM, respectively [195]. The structures were protonated in AutoDock4, stripped of all water molecules and bound ligands, and electrostatically represented with Gasteiger-Marsili charges. AutoDock4 simulations were performed using the Lamarckian Genetic Algorithms (GA) subroutine at default settings for GA population size, cross-over rate and mutation rate, and starting with fully-randomized ligand position, orientation and conformation. One hundred GA runs were performed for the ligand-enzyme pair.

CHAPTER 8

CONCLUSIONS

Mammalian and viral proteases are involved in a multitude of physiological processes. The aberrant activity of mammalian proteases is the underlying cause of many diseases, including COPD. Furthermore, the activity of viral proteases is essential for the survival of viruses, as well as their infectivity and virulence. Consequently, mammalian and viral proteases are validated targets for the development of novel therapeutic agents and antiviral drugs.

This dissertation has described the design, synthesis and biochemical evaluation of COPD-related serine protease inhibitors and West Nile virus/Dengue virus NS2B-NS3 protease inhibitors using structure-based, computer-aided design, combinatorial chemistry and click chemistry synthetic methodologies.

A general strategy for constructing 1,2,5-thiadiazolidin-3-one 1,1 dioxide-based dual function inhibitors against COPD-related targets was established. The HNE/caspase-1 dual function inhibitor **A16** has been shown to exhibit time-dependent inhibition against HNE and caspase-1 *in vitro* using biochemical assays and HPLC methods. The proposed mechanism of enzyme inactivation was confirmed using both X-ray crystal structure and high resolution mass spectrometry. The fact that compound **A18** showed excellent inhibition towards HNE confirmed the profound effect of the pKa of leaving group and the lack of preference of HNE S' subsites. This should serve as a launching pad for future COPD-relevant dual function inhibitor design.

The 1,2,5-thiadiazolidin-3-one 1,1 dioxide scaffold was also modified in order to achieve reversible competitive inhibition. The first modification involves an amide-to-urea transformation and the resulting 1,2,3,5-thiatriazolidin-3-one 1,1-dioxide which was functionalized with a triazole substitution **B13** showed selective inhibition against Pr 3 over

HNE, confirming that the Pr 3 active site is more polar than HNE. Simple reversible competitive inhibitor **B13g** showed significant inhibition against Pr 3 and it could serve as potential launching pad for developing more potent reversible competitive inhibitors for Pr 3. The conversion involving a carbonyl-to-methylene transformation was unsuccessful, however an alternative synthesis was proposed. A mechanism was also proposed to explain the cause of the side reaction.

The 1-oxo-1, 2, 3, 4-tetrahydroisoquinoline and 1-oxo-1, 2-dihydroisoquinoline scaffolds were initially used for developing non-peptidyl inhibitors against WNV and DENV NS2B-NS3 proteases. Compound **D14j** was identified as a hit for WNV NS2B-NS3 protease. Based on the computational docking result of **D14j** with WNV NS2B-NS3 protease, a similar but synthetically more powerful template (2-mercaptoquinazolin-4(3H)-one) and more polar substitutions were used for optimization. Several hits were identified as WNV NS2B-NS3 protease inhibitors whereas two hits were identified as DENV NS2B-NS3 protease inhibitors during this optimization. The computational studies suggested that the introduction of an additional branch could potentially enhance the potency of the inhibitor for both WNV and DENV NS2B-NS3 proteases.

In summary, an array of novel inhibitors of mammalian and viral proteases have been reported.

REFERENCES

REFERENCES

- [1] Bugg, T. D. H. *Introduction to enzyme and coenzyme chemistry* 2nd ed., Blackwell Publishing, **2004**, pp 1-7.
- [2] Hedstrom, L. *Introduction: Protease*” *Chem. Rev.*, **2002**, *102*(12), 4429–4430.
- [3] (a) Abbenante, G.; Fairlie, D. P. *Protease inhibitors in the clinic*” *Medicinal Chemistry*, **2005**, *1*, 71-104; (b) [http: www.protease.net](http://www.protease.net) [cited 6 Jan 2010]
- [4] Powers, J. C.; Asgian, J. L.; Ekici, Ö. D.; James, K. E. *Irreversible inhibitors of Serine, Cysteine, and Threonine Proteases*” *Chem. Rev.*, **2002**, *102*, 4639-4750.
- [5] Bird P. I.; Trapani, J. A.; Villadangos, J. A. *Endolysosomal proteases and their inhibitors in immunity*” *Nat. Rev. Immunol.*, **2009**, *9*(12), 871-882.
- [6] Hochstrasser, M. *Introduction to Intracellular Protein Degradation*” *Chem. Rev.*, **2009**, *109*(4), 1479–1480.
- [7] Wolfe, M. S. *Intramembrane proteolysis*” *Chem. Rev.*, **2009**, *109*, 1599-1612.
- [8] Bakshi, P.; Margenthaler, E.; Laporte, V.; Crawford, F.; Mullan, M. *Novel role of CXCR2 in regulation of γ -Secretase activity*” *ACS Chem. Biol.*, **2008**, *3*(12), 777–789.
- [9] Allan, L. A.; Clarke, P. R. *Apoptosis and autophagy: Regulation of caspase-9 by phosphorylation*” *FEBS J.*, **2009**, *276*(21), 6063-6073.
- [10] (a) Greene, C. M.; McElvaney, N. G. *Proteases and antiproteases in chronic neutrophilic lung disease-relevance to drug discovery*” *Brit. J. Pharmacol.*, **2009**, *158*, 1048-1058; (b) Abbenante, G.; Fairlie, D. P. *Protease inhibitors in the clinic*” *Medicinal Chemistry*, **2005**, *1*, 71-104; (c) Shao, M. X.; Nadel, J. A. *Neutrophil Elastase Induces MUC5AC Mucin Production in Human Airway Epithelial Cells via a Cascade Involving Protein Kinase C, Reactive Oxygen Species, and TNF-Converting Enzyme*” *J. Immunol.*, **2005**, *175*, 4009-4016.
- [11] (a) Hu, N.; Westra, J.; Kallenberg, C. G. *Membrane-bound proteinase 3 and its receptors: relevance for the pathogenesis of Wegener's Granulomatosis*” *Autoimmun Rev.*, **2009**, *8*(6), 510-514; (b) Moosig, F.; Lamprecht, P.; Gross, W. L. *Wegener's granulomatosis: the current view*” *Clin. Rev. Allergy Immunol.*, **2008**, *35*(1-2), 19-21; (c) Korkmaz, B.; Moreau, T.; Gauthier, F. *Neutrophil elastase, proteinase 3 and cathepsin G: physicochemical properties, activity and physiopathological functions*” *Biochimie.*, **2008**, *90*, 227-242. (d) Duranton, J.; Bieth, J. G. *Inhibition of proteinase 3 by [alpha]1-antitrypsin in vitro predicts very fast inhibition in vivo*” *Am. J. Respir. Cell Mol. Biol.*, **2003**, *29*, 57-61; (e) Sugawara, S. *Immune functions of proteinase 3*” *Crit. Rev.*

Immunol., **2005**, 25(5), 343-360.

- [12] (a) Kudo, T.; Kigoshi, H.; Hagiwara, T.; Takino, T.; Yamazaki, M.; Yui, S. –Cathepsin G, a neutrophil protease, induces compact cell-cell adhesion in MCF-7 human breast cancer cells” *Mediators Inflamm.*, **2009**, DOI:10.1155/2009/850940; (b) Korkmaz, B.; Moreau, T.; Gauthier, F. –Neutrophil elastase, proteinase 3 and cathepsin G: physicochemical properties, activity and physiopathological functions” *Biochimie*. **2008**, 90(2), 227-242; (c) Pham, C. T. –Neutrophil serine proteases: specific regulators of inflammation” *Nat. Rev. Immunol.*, **2006**, 6(7), 541-550; (d) Guay, C.; Laviolette, M.; Tremblay, G. M. –Targeting serine proteases in asthma” *Curr. Top. Med. Chem.*, **2006**, 6(4), 393-402.
- [13] (a) D'Eliseo, D.; Pisu, P.; Romano, C.; Tubaro, A.; De Nunzio, C.; Morrone, S.; Santoni, A.; Stoppacciaro, A.; Velotti, F. –Granzyme B is expressed in urothelial carcinoma and promotes cancer cell invasion” *Int. J. Cancer.*, **2010**, PMID: 20027633; (b) Thomas, H. E.; Trapani, J. A.; Kay, T. W. –The role of perforin and granzymes in diabetes” *Cell Death Differ.*, **2010**, 17(4), 577-585; (c) Ikemoto, T.; Hojo, Y.; Kondo, H.; Takahashi, N.; Hirose, M.; Nishimura, Y.; Katsuki, T.; Shimada, K. –Plasma granzyme B as a predicting factor of coronary artery disease-Clinical significance in patients with chronic renal failure” *J. Cardiol.*, **2009**, 54(3), 409-415; (d) Boivin, W. A.; Cooper, D. M.; Hiebert, P. R.; Granville, D. J. –Intracellular versus extracellular granzyme B in immunity and disease: challenging the dogma” *Lab. Invest.*, **2009**, 89(11), 1195-1220.
- [14] (a) Di Cera, E. –Thrombin” *Mol. Aspects Med.* **2008**, 29(4), 203-254; (b) Martorell, L.; Martínez-González, J.; Rodríguez, C.; Gentile, M.; Calvayrac, O.; Badimon, L. –Thrombin and protease-activated receptors (PARs) in atherothrombosis” *Thromb. Haemost.*, **2008**, 99(2), 305-315; (c) Lecompte, T.; Toussaint-Hacquard, M.; Devignes, J. –Anticoagulants drugs direct trombin inhibitors” *Ann. Fr. Anesth. Reanim.*, **2009**, 28(9 Suppl), S3-7; (d) Franchini, M.; Mannucci, P. M. –A new era for anticoagulants” *Eur. J. Intern. Med.*, **2009**, 20(6), 562-568; (e) Levine, M. N. –New antithrombotic drugs: potential for use in oncology” *J. Clin. Oncol.*, **2009**, 27(29), 4912-4918.
- [15] (a) Borensztajn, K.; Peppelenbosch, M. P.; Spek, C. A. –Factor Xa: at the crossroads between coagulation and signaling in physiology and disease” *Trends Mol. Med.*, **2008**, 14(10), 429-440; (b) Krupiczkoj, M. A.; Scotton, C. J.; Chambers, R. C. –Coagulation signalling following tissue injury: focus on the role of factor Xa” *Int. J. Biochem. Cell. Biol.*, **2008**, 40(6-7), 1228-1237; (c) Steffel, J.; Lüscher, T. F. –Novel anticoagulants in clinical development: focus on factor Xa and direct thrombin inhibitors” *J. Cardiovasc. Med. (Hagerstown)*, **2009**, 10(8), 616-623; (d) Borris, L. C. –Rivaroxaban, a new, oral, direct factor Xa inhibitor for thromboprophylaxis after major joint arthroplasty” *Expert Opin. Pharmacother.*, **2009**, 10(6), 1083-1088.
- [16] (a) Kunamneni, A.; Ravuri, B. D.; Saisha, V.; Ellaiah, P.; Prabhakar, T. –Urokinase-a very popular cardiovascular agent” *Recent Pat. Cardiovasc. Drug Discov.*, **2008**, 3(1), 45-58; (b) Zhang, G.; Eddy, A. A. –Urokinase and its receptors in chronic kidney disease” *Front Biosci.*, **2008**, 13, 5462-5478; (c) Gharaee-Kermani, M.; Hu, B.; Phan, S. H.; Gyetko, M. R. –The role of urokinase in idiopathic pulmonary fibrosis and implication

- for therapy” *Expert Opin. Investig. Drugs.*, **2008**, *17*(6), 905-916; (d) Annecke, K.; Schmitt, M.; Euler, U.; Zerm, M.; Paepke, D.; Paepke, S.; von Minckwitz, G.; Thomssen, C.; Harbeck, N. –uPA and PAI-1 in breast cancer: review of their clinical utility and current validation in the prospective NNBC-3 trial” *Adv. Clin. Chem.*, **2008**, *45*, 31-45; (e) Tang, C. H.; Wei, Y. –The urokinase receptor and integrins in cancer progression” *Cell Mol. Life Sci.*, **2008**, *65*(12), 1916-1932.
- [17] (a) Matteucci, E.; Giampietro, O. –Dipeptidyl peptidase-4 (CD26): knowing the function before inhibiting the enzyme” *Curr. Med. Chem.*, **2009**, *16*(23), 2943-2951; (b) Verspohl, E. J. –Novel therapeutics for type 2 diabetes: incretin hormone mimetics (glucagon-like peptide-1 receptor agonists) and dipeptidyl peptidase-4 inhibitors” *Pharmacol. Ther.*, **2009**, *124*(1), 113-138; (c) Rungby, J. –Inhibition of dipeptidyl peptidase 4 by BI-1356, a new drug for the treatment of beta-cell failure in type 2 diabetes” *Expert Opin. Investig. Drugs.*, **2009**, *18*(6), 835-838; (d) Bohannon, N. –Overview of the gliptin class (dipeptidyl peptidase-4 inhibitors) in clinical practice” *Postgrad. Med.*, **2009**, *121*(1), 40-45; (e) Ahrén, B. –Emerging dipeptidyl peptidase-4 inhibitors for the treatment of diabetes” *Expert Opin. Emerg. Drugs.*, **2008**, *13*(4), 593-607.
- [18] (a) Matsumoto, C.; Hayashi, T.; Kitada, K.; Yamashita, C.; Miyamura, M.; Mori, T.; Ukimura, A.; Ohkita, M.; Jin, D. Takai, S.; Miyazaki, M.; Okada, Y.; Kitaura, Y.; Matsumura, Y. –Chymase Plays an Important Role in Left Ventricular Remodeling Induced by Intermittent Hypoxia in Mice” *Hypertension*, **2009**; *54*(1): 164-171. (b) Palaniyandi S. S.; Nagai, Y.; Watanabe, K.; Ma, M.; Veeraveedu P. T.; Prakash, P.; Kamal, K. A.; Abe, Y.; Yamaguchi, K.; Tachikawa, H.; Kodama, M.; Aizawa, Y. –Chymase Inhibition Reduces the Progression to Heart Failure After Autoimmune Myocarditis in Rats” *Exp. Biol. Med. (Maywood)*, **2007**, *232*(9), 1213-1221.
- [19] (a) Hallgren, J.; Pejler, G. –Biology of mast cell tryptase. An inflammatory mediator” *FEBS J.*, **2006**, *273*(9), 1871-1895; (b) Payne, V.; Kam, P. C. –Mast cell tryptase: a review of its physiology and clinical significance” *Anaesthesia*. 2004, *59*(7), 695-703; (c) Ennis, M. –New targets for modifying mast cell activation in asthma” *Curr. Allergy. Asthma. Rep.*, **2006**, *6*(3), 247-251.
- [20] (a) Uhland, K. –Matriptase and its putative role in cancer” *Cell. Mol. Life Sci.*, **2006**, *63*(24), 2968-2978; (b) List, K.; Bugge, T. H.; Szabo, R. –Matriptase: potent proteolysis on the cell surface” *Mol. Med.*, **2006**, *12*(1-3), 1-7.
- [21] (a) Pajonk, F.; McBride, W. H. –The Proteasome in Cancer Biology and Treatment” *Radiation Research*, **2001**, *156*(5), 447-459; (b) Tsukamoto, S.; Yokosawa, H. –Targeting the proteasome pathway” *Expert Opin. Ther. Targets.*, **2009**, *13*(5), 605-621; (c) Jung, T.; Catalgol, B.; Grune, T. –The proteasomal system” *Mol. Aspects Med.*, **2009**, *30*(4), 191-296; (d) D'Alessandro, A.; Pieroni, L.; Ronci, M.; D'Aguzzo, S.; Federici, G.; Urbani, A. –Proteasome inhibitors therapeutic strategies for cancer” *Recent Pat. Anticancer Drug Discov.*, **2009**, *4*(1), 73-82.
- [22] (a) Chowdhury, I.; Tharakan, B.; Bhat, G. K. –Caspases-An update” *Comparative*

- Biochemistry and Physiology*, Part B, 151, (2008) pp 10-27; (b) Talanian, R. V.; Brady, K. D.; Vryns, V. L. –Caspases as Targets for Anti-Inflammatory and Anti-Apoptotic Drug Discovery” *J. Med. Chem.*, **2000**, 43(18) 3351-3371; (c) Howley, B.; Fearnhead, H. O. –Caspases as therapeutic targets” *J. Cell. Mol. Med.*, **2008**, 12(5a), 1502-1516; (d) Nadiri, A.; Wolinski, M. K.; Saleh, M. –The inflammation caspases: Key players in the host response to pathogenic invasion and sepsis” *J. Immunol.*, **2006**, 177, 4239-4245.
- [23] (a) Zhao, Q.; Jia, Y.; Xiao, Y. –Cathepsin K: a therapeutic target for bone diseases” *Biochem. Biophys. Res. Commun.*, **2009**, 380(4), 721-723; (b) Le Gall, C.; Bonnelye, E.; Clézardin, P. –Cathepsin K inhibitors as treatment of bone metastasis” *Curr. Opin. Support Palliat. Care.*, **2008**, 2(3), 218-222; (c) Podgorski, I.; Linebaugh, B. E.; Sloane, B. F. –Cathepsin K in the bone microenvironment: link between obesity and prostate cancer?” *Biochem. Soc. Trans.*, **2007**, 35(Pt 4), 701-703; (d) Salminen-Mankonen, H. J.; Morko, J.; Vuorio, E. –Role of cathepsin K in normal joints and in the development of arthritis” *Curr. Drug Targets.*, **2007**, 8(2), 315-323.
- [24] (a) Gradman, A. H. –Evolving understanding of the renin-angiotensin-aldosterone system: pathophysiology and targets for therapeutic intervention” *Am. Heart. J.*, **2009**, 157(6 Suppl), S1-6; (b) Braga, M. F.; Leiter, L. A. –Role of renin-angiotensin system blockade in patients with diabetes mellitus” *Am. J. Cardiol.*, **2009**, 104(6), 835-839; (c) Bomback, A. S.; Toto, R. –Dual blockade of the renin-angiotensin-aldosterone system: beyond the ACE inhibitor and angiotensin-II receptor blocker combination” *Am. J. Hypertens.*, **2009**, 22(10), 1032-1040.
- [25] (a) Ersmark, K.; Samuelsson, B.; Hallberg, A. –Plasmeprins as potential targets for new antimalarial therapy” *Med. Res. Rev.*, **2006**, 26(5), 626-666; (b) Martins, T. M.; Novo, C.; do Rosário, V. E.; Domingos, A. –Aspartic proteases from *Plasmodium chabaudi*: a rodent model for human malaria” *Acta. Trop.*, **2003**, 89(1), 1-12.
- [26] (a) Vassar, R.; Kovacs, D. M.; Yan, R.; Wong, P. C. –The beta-secretase enzyme BACE in health and Alzheimer's disease: regulation, cell biology, function, and therapeutic potential” *J. Neurosci.*, **2009**, 29(41), 12787-12794; (b) Panza, F.; Solfrizzi, V.; Frisardi, V.; Capurso, C.; D'Introno, A.; Colacicco, A. M.; Vendemiale, G.; Capurso, A.; Imbimbo, B. P. –Disease-modifying approach to the treatment of Alzheimer's disease: from alpha-secretase activators to gamma-secretase inhibitors and modulators” *Drugs Aging.*, **2009**, 26(7), 537-555; (c) Willem, M.; Lammich, S.; Haass, C. –Function, regulation and therapeutic properties of beta-secretase (BACE1)” *Semin. Cell Dev. Biol.*, **2009**, 20(2), 175-182.
- [27] (a) Heeneman, S.; Sluimer, J. C.; Daemen, M. J. –Angiotensin-converting enzyme and vascular remodeling” *Circ. Res.*, **2007**, 101(5), 441-454; (b) Fogari, R.; Zoppi, A. –Antihypertensive drugs and fibrinolytic function” *Am. J. Hypertens.*, **2006**, 19(12), 1293-1299; (c) Zou, K.; Michikawa, M. –Angiotensin-converting enzyme as a potential target for treatment of Alzheimer's disease: inhibition or activation?” *Rev. Neurosci.*, **2008**, 19(4-5), 203-212.

- [28] (a) Oikonomidi, S.; Kostikas, K.; Tsilioni, I.; Tanou, K.; Gourgoulianis, K. I.; Kiropoulos, T. S. –Matrix metalloproteinases in respiratory diseases: from pathogenesis to potential clinical implications” *Curr. Med. Chem.*, **2009**, *16*(10), 1214-1228; (b) Butler G. S.; Overall, C. M. –Updated biological roles for matrix metalloproteinases and new 'intracellular' substrates revealed by degradomics” *Biochemistry*, **2009**, *48*(46), 10830-10845. (c) Roy, R.; Yang, J.; Moses, M. A. –Matrix metalloproteinases as novel biomarkers and potential therapeutic targets in human cancer” *J. Clin. Oncol.*, **2009**, *27*(31), 5287-5297; (d) Consolo, M.; Amoroso, A.; Spandidos, D. A.; Mazzarino, M. C. –Matrix metalloproteinases and their inhibitors as markers of inflammation and fibrosis in chronic liver disease (Review)” *Int. J. Mol. Med.*, **2009**, *24*(2), 143-152; (e) Marchant, D.; McManus, B. M. –Matrix metalloproteinases in the pathogenesis of viral heart disease” *Trends Cardiovasc. Med.*, **2009**, *19*(1), 21-26; (f) Vanlaere, I.; Libert, C. –Matrix metalloproteinases as drug targets in infections caused by gram-negative bacteria and in septic shock” *Clin. Microbiol. Rev.*, **2009**, *22*(2), 224-239; (g) Sárdy, M. –Role of matrix metalloproteinases in skin ageing” *Connect. Tissue Res.*, **2009**, *50*(2), 132-138; (h) Malemud, C. J. –Matrix metalloproteinases (MMPs) in health and disease: an overview” *Front Biosci.*, **2006**, *11*, 1696-1701.
- [29] (a) Kenny, P. A. –FACE: a new target in epidermal growth factor receptor dependent tumors” *Differentiation*. **2007**, *75*(9), 800-808; (b) Lovering, F.; Zhang, Y. –Therapeutic potential of TACE inhibitors in stroke” *Curr. Drug. Targets CNS Neurol. Disord.*, **2005**, *4*(2), 161-168; (c) Moss, M. L.; Jin, S. L.; Becherer, J. D.; Bickett, D. M.; Burkhart, W.; Chen, W. J.; Hassler, D.; Leesnitzer, M. T.; McGeehan, G.; Milla, M.; Moyer, M.; Rocque, W.; Seaton, T.; Schoenen, F.; Warner, J.; Willard, D. –Structural features and biochemical properties of TNF-alpha converting enzyme (TACE)” *J. Neuroimmunol.*, **1997**, *72*(2), 127-129.
- [30] Global Alert and Response. Weekly update: Pandemic (H1N1) 2009 - update 81. RUL: http://www.who.int/csr/don/2009_12_30/en/index.html [cited 6 Jan **2010**]
- [31] Elston, D. M. –Update on cutaneous manifestations of infectious diseases” *Med. Clin. North. Am.*, **2009**, *93* (6), 1283-1290.
- [32] Tong, L. –Viral proteases” *Chem. Rev.*, **2002**, *102*(12), 4609-4626.
- [33] (a) Bierman, W. F.; van Agtmael, M. A.; Nijhuis, M.; Danner, S. A.; Boucher, C. A. –HIV monotherapy with ritonavir-boosted protease inhibitors: a systematic review” *AIDS*, **2009**, *23*(3):279-291; (b) De Clercq, E. –Anti-HIV drugs: 25 compounds approved within 25 years after the discovery of HIV” *Int. J. Antimicrob. Agents.*, **2009**, *33*(4), 307-320; (c) Hughes, C. A.; Robinson, L.; Tseng, A.; MacArthur, R. D. –New antiretroviral drugs: a review of the efficacy, safety, pharmacokinetics, and resistance profile of tipranavir, darunavir, etravirine, rilpivirine, maraviroc, and raltegravir” *Expert Opin. Pharmacother.*, **2009**, *10*(15), 2445-2466; (d) Cane, P. A. –New developments in HIV drug resistance” *J. Antimicrob. Chemother.*, **2009**, *64*(Suppl 1), i37-40; (e) Fernández-Montero, J. V.; Barreiro, P.; Soriano, V. –HIV protease inhibitors: recent clinical trials and recommendations on use” *Expert Opin. Pharmacother.*, **2009**, *10*(10), 1615-1629.

- [34] (a) Paula, T.; Pablo, R.; Eugenia, V.; Pablo, B.; Sabino, P.; José, M.; Antonio, M.; Dolores, H. M.; Pablo, L.; Javier, G. S.; Vincente, S. –New drug targets for hepatitis C and other Flaviviridae viruses” *Infect. Disord. Drug Targets.*, **2009**, 9(2), 133-147; (b) Chen, K. X.; Njoroge, F. G. –A review of HCV protease inhibitors” *Curr. Opin. Investig. Drugs.*, **2009**, 10(8), 821-837; (c) Reiser, M.; Timm, J. –Serine protease inhibitors as anti-hepatitis C virus agents” *Expert Rev. Anti. Infect. Ther.*, **2009**, 7(5), 537-547; (d) Asselah, T.; Benhamou, Y.; Marcellin, P. –Protease and polymerase inhibitors for the treatment of hepatitis C” *Liver Int.*, **2009**, 29(Suppl 1), 57-67; (e) Mederacke, I.; Wedemeyer, H.; Manns, M. P. –Boceprevir, an NS3 serine protease inhibitor of hepatitis C virus, for the treatment of HCV infection” *Curr. Opin. Investig. Drugs.*, **2009**, 10(2), 181-189.
- [35] (a) Jain, R. P.; Vederas, J. C. –Structural variations in keto-glutamines for improved inhibition against hepatitis A virus 3C proteinase” *Bioorg. Med. Chem. Lett.*, **2004**, 14(14), 3655-3658; (b) Lall, M. S.; Ramtohl, Y. K.; James, M. N.; Vederas, J. C. –Serine and threonine beta-lactones: a new class of hepatitis A virus 3C cysteine proteinase inhibitors” *J. Org. Chem.*, **2002**, 67(5), 1536-1547.
- [36] (a) Tan, M.; Jiang, X. –Norovirus gastroenteritis, increased understanding and future antiviral options” *Curr. Opin. Investig. Drugs*, **2008**, 9(2), 146-151. (b) Scheffler, U.; Rudolph, W.; Gebhardt, J.; Rohayem, J. –Differential cleavage of the norovirus polyprotein precursor by two active forms of the viral protease” *J. Gen. Virol.*, **2007**, 88(Pt 7), 2013-2018.
- [37] (a) Brackney, D. E.; Foy, B. D.; Olson, K. E. –The effects of midgut serine proteases on dengue virus type 2 infectivity of *Aedes aegypti*” *Am. J. Trop. Med. Hyg.*, **2008**, 79(2), 267-274. (b) Melino, S.; Paci, M. –Progress for dengue virus diseases. Towards the NS2B-NS3pro inhibition for a therapeutic-based approach” *FEBS J.*, **2007**, 274(12), 2986-3002.
- [38] (a) Chappell, K. J.; Stoermer, M. J.; Fairlie, D. P.; Young, P. R. –West Nile Virus NS2B/NS3 protease as an antiviral target” *Curr. Med. Chem.*, **2008**, 15(27), 2771-2784. (b) Chappell, K.J.; Stoermer, M. J.; Fairlie, D. P.; Young, P. R. –Mutagenesis of the West Nile virus NS2B cofactor domain reveals two regions essential for protease activity” *J. Gen. Virol.*, **2008**, 89(Pt 4), 1010-1014. (c) Shiryaev, S. A.; Ratnikov, B. I.; Chekanov, A. V.; Sikora, S.; Rozanov, D. V.; Godzik, A.; Wang, J.; Smith, J. W.; Huang, Z.; Lindberg, I.; Samuel, M. A.; Diamond, M. S.; Strongin, A. Y. –Cleavage targets and the D-arginine-based inhibitors of the West Nile virus NS3 processing proteinase” *Biochem J.*, **2006**, 393(Pt 2), 503-511.
- [39] (a) Wanga, Q. M.; Chen, S. H. –Human rhinovirus 3C protease as a potential target for the development of antiviral agents” *Curr. Protein Pept. Sci.*, **2007**, 8(1), 19-27. (b) McKinlay, M. A. –Recent advances in the treatment of rhinovirus infections” *Curr. Opin. Pharmacol.*, **2001**, 1(5), 477-481.
- [40] Kawai, S. H.; Aubry, N.; Duceppe, J. S.; Llinàs-Brunet, M.; LaPlante, S. R. —

- Dimethylthiazolidine carboxylic acid as a rigid p3 unit in inhibitors of serine proteases: application to two targets” *Chem. Biol. Drug Des.*, **2009**, 74(5), 517-522.
- [41] (a) Meanwell, N. A.; Belema, M.; Carini, D. J.; D'Andrea, S. V.; Kadow, J. F.; Krystal, M.; Naidu, B. N.; Regueiro-Ren, A.; Scola, P. M.; Sit, S. Y.; Walker, M. A.; Wang, T.; Yeung, K. S. –Developments in antiviral drug design, discovery and development in 2004” *Curr. Drug Targets Infect. Disord.*, **2005**, 5(4), 307-400; (b) De Clercq, E. –Antiviral drugs in current clinical use” *J. Clin. Virol.*, **2004**, 30(2), 115-133.
- [42] Qiu, X.; Janson, C. A.; Culp, J. S.; Richardson, S. B.; Debouck, C.; Smith, W. W. Abdel-Meguid, S. S. –Crystal structure of varicella-zoster virus protease” *Proc. Natl. Acad. Sci., U S A.* **1997**, 94(7), 2874-2879.
- [43] Cudic, M.; Fields, G. B. –Extracellular proteases as targets for drug development” *Curr. Protein Pept. Sci.*, **2009**, 10(4), 297-307.
- [44] Tsukamoto, S.; Yokosawa, H –Targeting the proteasome pathway” *Expert. Opin. Ther. Targets*, **2009**, 13(5), 605-621.
- [45] Fingleton, B. –Matrix metalloproteinases as valid clinical targets” *Curr. Pharm. Des.*, **2007**, 13(3), 333-346.
- [46] Eder, J.; Hommel, U.; Cumin, F.; Martoglio, B.; Gerhartz, B. –Aspartic proteases in drug discovery” *Curr. Pharm. Des.*, **2007**, 13(3), 271-285.
- [47] Cornelis, S.; Kersse, K.; Festjens, n.; Lamkanfi, M.; Vandenabeele, p. –Inflammatory caspases: targets for novel therapies” *Curr. Pharm. Des.*, **2007**, 13(4), 367-385.
- [48] Hsu, J. T.; Wang, H. C.; Chen, G. W.; Shih, S. R. –Antiviral drug discovery targeting to viral proteases” *Curr. Pharm. Des.*, **2006**, 12(11), 1301-1314.
- [49] Kadaveru, K.; Vyas, J. Schiller, M. R. –Viral infection and human disease—insights from minimotifs” *Front Biosci.*, **2008**, 13, 6455-6471.
- [50] Raizada, M. K.; Ferreira, A. J. –ACE2: A new target for cardiovascular disease therapeutics” *J. Cardiovasc. Pharmacol.*, **2007**, 50, 112–119.
- [51] Dhillon, S. –Argatroban: a review of its use in the management of heparin-induced thrombocytopenia” *Am. J. Cardiovasc. Drugs*, **2009**, 9(4), 261-282.
- [52] Palalau, A. I.; Tahrani, A. A.; Piya, M. K.; Barnett, A. H. –DPP-4 inhibitors in clinical practice” *Postgrad. Med.*, **2009**, 121(6), 70-100.
- [53] Reeves, J. D.; Piefer, A. J. –Emerging drug targets for antiretroviral therapy” *Drugs*, **2005**, 65(13), 1747-1766.

- [54] (a) Rawlings, N. D. –A large and accurate collection of peptidase cleavages in the MEROPS database” *Database*, **2009**, DOI:10.1093/database/bap015; (b) Rawlings, N. D.; Morton, F. R.; Kok, C.Y.; Kong, J.; Barrett, A. J. –MEROPS: the peptidase database” *Nucleic Acids Res.*, **2008**, *36*, D320-D325.
- [55] Quesada, V.; Ordonez, G. R.; Sanchez, L. M.; Puente, X. S.; Lopez-Otin, C. –The Degradome database: mammalian proteases and diseases of proteolysis” *Nucleic Acids Res.*, **2009**; *37* (suppl_1), D239 - D243.
- [56] Schechter, I.; Berger, A. –On the size of the active site in proteases” *Biochem. Biophys. Res. Comm.*, **1967**, *27*, 157-162.
- [57] Hartley, B. S. –Proteolytic enzymes” *Annu Rev Biochem*, **1960**, *29*, 45-72.
- [58] Hedstrom, L. –Serine protease mechanism and specificity” *Chem. Rev.*, **2002**, *102*, 4501-4523.
- [59] NC-IUBMB (Nomenclature Committee of the International Union of Biochemistry and Molecular Biology) Enzyme Nomenclature 1992. –Recommendations of the Nomenclature Committee of the International Union of Biochemistry and Molecular Biology on the Nomenclature and Classification of Enzymes” **1992**, Academic Press. Orlando.
- [60] Rawlings, N. D.; Barrett, A. J. –Evolutionary families of peptidases” *Biochem. J.*, **1993** *290*, 205-218.
- [61] Barrett, A.J., Rawlings, N.D. & Woessner, J.F., eds. –Handbook of Proteolytic Enzymes” **2004**, Elsevier Press.
- [62] Jemal, A.; Ward, E.; Hao, Y. P.; Thun, M. –Trends in the leading causes of death in the United States, 1970-2002”. *The Journal of the American Medical Association*, **2005**, *294*, 1255–1259.
- [63] MacNee, W. –Pulmonary and systemic oxidant/antioxidant imbalance in chronic obstructive pulmonary disease” *Proc. Am. Thor. Soc.*, **2005**, *2*, 50-60.
- [64] Luppi, F.; Hiemstra, P. S. –Epithelial Responses to Oxidative Stress in Chronic Obstructive Pulmonary Disease” *Am. J. Respir. Crit. Care Med.*, **2007**, *175*, 527-531.
- [65] (a) Aoshiba, K.; Yokohori, N.; Nagai, A. –Alveolar wall apoptosis causes lung destruction and emphysematous changes” *Am. J. Respir. Cell Mol. Biol.*, **2003**, *28*, 555-562. (b) Tudor, R. M.; Petrache, I.; Elias, J. A.; Voelkel, N. F.; Henson, P. M. –Apoptosis and emphysema: the missing link” *Am. J. Respir. Cell Mol. Biol.*, **2003**, *28*, 551-554.
- [66] Demedts, I. K.; Demoor, T.; Bracke, K. R.; Joos, G. F.; Brusselle, G. G. –Role of apoptosis in the pathogenesis of COPD and pulmonary emphysema” *Respir. Res.*, **2006**, *7*, 53-62.

- [67] Rennard, S. I. –Inflammation and Repair Processes in Chronic Obstructive Pulmonary Disease” *Am. J Respir. Crit. Care Med.*, **2005**, *160*, S12-S16.
- [68] Abboud, R. T.; Vimalanathan, S. –Pathogenesis of COPD. Part I. The role of protease-antiprotease imbalance in emphysema” *Int. J. Tuberc. Lung Dis.*, **2008**, *12* (4), 361-367.
- [69] Stockley, R. A. –Neutrophils and protease/antiprotease imbalance” *Am. J. Respir. Crit. Care Med.*, **1999**, *260*, S49-S52.
- [70] Croxton, T. L.; Weinmann, G. G.; Senior, R. M.; Wise, R. A. –Clinical research in chronic obstructive pulmonary disease: needs and opportunities” *Am. J. Respir. Crit. Care Med.*, **2003**, *167*, 1142-1149.
- [71] Ciencewicki, J.; Trivedi, S.; Kleeberger, S. R. –Oxidants and the pathogenesis of lung diseases” *J. Allergy Clin. Immunol.*, **2008**, *122* (3), 456-470.
- [72] MacNee, W. –Oxidative stress and chronic obstructive pulmonary disease” *Eur. Respir. Monograph*, **2006**, *11*, 100-129.
- [73] Kelly, F. J.; Mudway, I. S. –Protein oxidation at the air-lung interface.” *Amino Acids*, **2003**, *25*, 375-396.
- [74] MacNee, W. ; Tuder, R. M. –New paradigms in the pathogenesis of chronic obstructive pulmonary disease I” *Proc. Am. Thorac. Soc.*, **2009**, *6*, 527-531.
- [75] Cavarra, E.; Lucattelli, M.; Gambelli, F.; Bartalesi, B.; Fineschi, S.; Szarka, A.; Giannerini, F.; Martorana, P. A.; Lungarella, G. –Human SLPI inactivation after cigarette smoke exposure in a new in vivo model of pulmonary oxidative stress” *Am. J. Physiol. Lung Cell Mol. Physiol.*, **2001**, *281*, L412-L417.
- [76] Shapiro, S. D. –Proteolysis in the lung” *Eur. Respir. J. Suppl.*, **2003**, *44*, 30s-32s.
- [77] Oikonomidi, S.; Kostikas, K.; Tsilioni, I.; Tanou, K.; Gourgoulisanis, K. I.; Kiropoulos, T. S. –Matrix metalloproteinases in respiratory diseases: from pathogenesis to potential clinical implications” *Curr. Med. Chem.*, **2009**, *16* (10), 1214-1228.
- [78] Anderson, D.; MacNee, W. –Targeted treatment in COPD: a multi-system approach for a multi-system disease” *International Journal of COPD*, **2009**, *4*, 321-335.
- [79] Segura-Valdez, L.; Pardo, A.; Gaxiola, M.; Uhal, B. D.; Becerril, C.; Selman, M. –Up-regulation of gelatinases A and B, collagenases 1 and 2, and increased parenchymal cell death in COPD” *Chest*, **2000**, *117*, 684-694.
- [80] Muzio, M.; Stockwell, B. R.; Stennicke, H. R.; Salvesen, G. S.; Dixit, V. M. –An induced proximity model for caspase-8 activation” *J. Biol. Chem.*, **1998**, *273*, 2926-2930.

- [81] Denault, J. B.; Salvesen, G. S. –Caspases: Keys in the ignition of cell death” *Chem. Rev.*, **2002**, *102*, 4489-4499.
- [82] Hirata, H.; Takahashi, A.; Kobayashi, S.; Yonehara, S.; Sawai, H.; Okazaki, T.; Yamamoto, K.; Sasada, M. –Caspases are activated in a branched protease cascade and control distinct downstream processes in Fas-induced apoptosis” *J. Exp. Med.*, **1998**, *187*, 587-600.
- [83] Li, P.; Nijhawan, D.; Budihardjo, I.; Srinivasula, S. M.; Ahmad, M.; Alnemri, E. S.; Wang, X. –Cytochrome c and dATP-dependent formation of Apaf-1/caspase-9 complex initiates an apoptotic protease cascade” *Cell*, **1997**, *91*, 479-489.
- [84] Liu, X.; Kim, C. N.; Yang, J.; Jemmerson, R.; Wang, X. –Induction of apoptotic program in cell-free extracts: requirement for dATP and cytochrome c” *Cell*, **1996**, *86*, 147-157.
- [85] Zou, H.; Henzel, W. J.; Liu, X.; Lutschg, A.; Wang, X. –Apaf-1, a human protein homologous to *C. elegans* CED-4, participates in cytochrome c-dependent activation of caspase-3” *Cell*, **1997**, *90*, 405-413.
- [86] Slee, E.A.; Harte, M. T.; Kluck, R. M.; Wolf, B. B.; Casiano, C. A.; Newmeyer, D. D.; Wang, H. G.; Reed, J. C.; Nicholson, D. W.; Alnemri, E. S.; Green, D. R.; Martin, S. J. –Ordering the cytochrome c-initiated caspase cascade: hierarchical activation of caspases-2, -3, -6, -7, -8, and -10 in a caspase-9-dependent manner” *J. Cell Biol.*, **1999**, *144*, 281-292.
- [87] Darmon, A. J.; Nicholson, D. W.; Bleackley, R. C. –Activation of the apoptotic protease CPP32 by cytotoxic T-cell-derived granzyme B” *Nature*, **1995**, *377*, 446-448.
- [88] Ngan, D. A.; Vickerman, S. V.; Granville, D. J.; Paul Man, S. F.; Sin, D. D. –The possible role of granzyme Bin the pathogenesis of chronic obstructive pulmonary disease” *Thor. Adv. Respir. Dis.*, **2009**, *3*(3), 113-129.
- [89] Eastman, A. –Survival factors, intracellular signal transduction, and the activation of endonucleases in apoptosis” *Semin. Cancer Biol.*, **1995**, *6*, 45-52.
- [90] Vandivier, R. W.; Fadok, V. A.; Hoffmann, P. R.; Bratton, D. L.; Penvari, C.; Brown, K. K.; Brain, J. D.; Accurso, F. J.; Henson, P. M. –Elastase-mediated phosphatidylserine receptor cleavage impairs apoptotic cell clearance in cystic fibrosis and bronchiectasis” *J. Clin. Invest.*, **2002**, *109*, 661-670.
- [91] Powell, W. C.; Fingleton, B.; Wilson, C. L.; Boothby, M.; Matrisian, L. M. –The metalloproteinase matrilysin proteolytically generates active soluble Fas ligand and potentiates epithelial cell apoptosis” *Curr. Biol.*, **1999**, *9*, 1441-1447.
- [92] Tuder, R. M.; Zhen, L.; Cho, C. Y.; Taraseviciene-Stewart, L.; Kasahara, Y.; Salvemini,

- D.; Voelkel, N. F.; Flores, S. C. "Oxidative stress and apoptosis interact and cause emphysema due to vascular endothelial growth factor receptor blockade" *Am. J. Respir. Cell Mol. Biol.*, **2003**, *29*, 88-97.
- [93] Rangasamy, T.; Cho, C. Y.; Thimmulappa, R. K.; Zhen, L.; Srisuma, S. S.; Kensler, T. W.; Yamamoto, M.; Petrache, I.; Tuder, R. M.; Biswal, S. "Genetic ablation of Nrf2 enhances susceptibility to cigarette smoke induced emphysema in mice" *J. Clin. Invest.* **2004**, *114*, 1248-1259.
- [94] Roth, M. "Pathogenesis of COPD. Part III. Inflammation in COPD" *Int. J. Tuberc. Lung Dis.*, **2008**, *12* (4), 375-380.
- [95] Rahman, I. "Oxidative stress, chromatin remodelling and gene transcription in inflammation and chronic lung diseases" *J. Biochem. Mol. Biol.*, **2003**, *36*, 95-109.
- [96] Chung, K. F.; Adcock, I. M. "Multifaceted mechanisms in COPD: inflammation, immunity, and tissue repair and destruction" *Eur. Respir. J.*, **2008**, *31*, 1334-1356.
- [97] Brown, W. M. "Treating COPD with PDE 4 inhibitors" *International Journal of COPD*, **2007**, *2* (4), 517-533.
- [98] Beavo, J. A.; Brunton, L. L. "Cyclic nucleotide research-still expanding after half a century" *Nat. Rev. Mol. Cell Biol.*, **2002**, *3*, 710-718.
- [99] Banner, K. H.; Press, N. J. "Dual PDE3/4 inhibitors as therapeutic agents for chronic obstructive pulmonary disease" *British Journal of Pharmacology*, **2009**, *157*, 892-906.
- [100] Torphy, T. J.; Page, C. "Phosphodiesterases: the journey towards therapeutics" *Trends Pharmacol. Sci.*, **2000**, *21*, 157-159.
- [101] Dyke, H. J.; Montana, J. G. "Update on the therapeutic potential of PDE4 inhibitors" *Expert Opin. Investig. Drug.*, **2002**, *11*, 1-13.
- [102] Dinarello, C. A. "Blocking IL-1 in systemic inflammation" *J. Exp. Med.*, **2005**, *201*, 1355-1359.
- [103] Arend, W. P.; Palmer, G.; Gabay, C. "IL-1, IL-18, and IL-33 families of cytokines" *Immunological Reviews*, **2008**, *223*, 20-38.
- [104] Dinarello, C. A. "Immunological and Inflammatory Functions of the Interleukin-1 Family" *Annu. Rev. Immunol.*, **2009**, *27*, 519-550.
- [105] Martinon, F.; Tschopp, J. "Inflammatory caspases and inflammasomes: master switches of inflammation" *Cell Death and Differentiation*, **2007**, *14*, 10-22.
- [106] Dinarello, C. A. "Interleukin 1 and interleukin 18 as mediators of inflammation and the

- aging process" *Am. J. Clin. Nutr.*, **2006**, 83 (suppl), 447S-455S.
- [107] Martinon, F.; Tschopp, J. "Inflammatory Caspases: Linking an Intracellular Innate Immune System to Autoinflammatory Diseases" *Cell*, **2004**, 117, 561-574.
- [108] Laurell, C-B.; Eriksson, S. "The electrophoretic alpha-1-globulin pattern of serum in alpha-1-antitrypsin deficiency" *Scand. J. Clin. Lab. Invest.*, **1963**, 15, 132-140.
- [109] Gross, P.; Pfitzer, E. A.; Tolker, E.; Babyak, M. A.; Kaschak, M. "Experimental emphysema. Its production with papain in normal and silicotic rats" *Arch. Environ. Health.*, **1965**, 11, 50-58.
- [110] Karlinsky, J. B.; Fredette, J.; Davidovits, G.; Catanese, A.; Snider, R.; Faris, B.; Snider, G. L.; Franzblau, C. "The balance of lung connective tissue elements in elastase-induced emphysema" *J. Lab. Clin. Med.*, **1983**, 1022, 151-162.
- [111] Senior, R. M.; Tegner, H.; Kuhn, C. III. "The induction of pulmonary emphysema with human leukocyte elastase" *ARRD*, **1977**, 116, 469-475.
- [112] Kao, R. C.; Wehner, N. G.; Skubitz, K. M.; Gray, B. H.; Hoidal, J. R. "Proteinase 3. A distinct human polymorphonuclear leukocyte proteinase that produces emphysema in hamsters" *JCI*, **1988**, 82, 1963-1973.
- [113] Owen, C. A. "Roles for proteinases in the pathogenesis of chronic obstructive pulmonary disease" *International Journal of COPD*, **2008**, 3 (2), 253-268.
- [114] Meyer-Hoffert, U. "Neutrophil-derived serine proteases modulate innate immune responses" *Front Biosci.*, **2009**, 14, 3409-3418
- [115] Korkmaz, B.; Moreau, T.; Gauthier, F. "Neutrophil elastase, proteinase 3 and cathepsin G: Physicochemical properties, activity and physiopathological functions" *Biochimie*, **2008**, 90, 227-242.
- [116] Salvesen, G.; Enghild, J. J. "Zymogen activation specificity and genomic structures of human neutrophil elastase and cathepsin G reveal a new branch of the chymotrypsinogen superfamily of serine proteinases" *Boimed. Biochim. Acta.*, **1991**, 50, 665-671.
- [117] Mackenzie, N. E.; Malthouse, J. P.; Scott, A. I. "Studying enzyme mechanism by ¹³C nuclear magnetic resonance" *Science*, **1984**, 225 (4665), 883-889.
- [118] Radisky, E. S.; Lee, J. M.; Lu, C. K.; Koshland, D. E. "Insights into the serine protease mechanism from atomic resolution structures of trypsin reaction intermediates" *PNAS*, **2006**, 103 (18), 6835- 6840.
- [119] Bethencourt, L; Nunez, O. "Serine Protease Mechanism-Based Mimics. Direct Evidence for a Transition State Bridge Proton in Stable Potentials" *J. Org. Chem.*, **2008**, 73, 2105-

2113.

- [120] Hedstrom, L. –Serine Protease Mechanism and Specificity” *Chem. Rev.*, **2002**, *102*, 4501-4523.
- [121] Lestienne, P.; Bieth, J. G. –Activation of human leukocyte elastase activity by excess substrate, hydrophobic solvents, and ionic strength” *J. Biol. Chem.* **1980**, *255*, 9289-9294.
- [122] Bode, W.; Wei, A. Z.; Huber, R.; Meyer, E.; Travis, J.; Neumann, S. –X-ray crystal structure of the complex of human leukocyte elastase (PMN elastase) and the third domain of the turkey ovomucoid inhibitor” *EMBO J.*, **1986**, *5*, 2453-2458.
- [123] Stein, R. L.; Strimpler, A. M. –Catalysis by human leukocyte elastase. Aminolysis of acyl-enzymes by amino acid amides and peptides” *Biochemistry*, **1987**, *26*, 2238-2242.
- [124] Korkmaz, B.; Hajjar, E.; Kalupov, T.; Reuter, N.; Brillard-Bourdet, M.; Moreau, T.; Juliano, L.; Gauthier, F. –Influence of charge distribution at the active site surface on the substrate specificity of human neutrophil protease 3 and elastase. A kinetic and molecular modeling analysis” *J. Biol. Chem.*, **2007**, *282*, 1989-1997.
- [125] Korkmaz, B.; Attucci, S.; Moreau, T.; Godat, E.; Juliano, L.; Gauthier, F. –Design and use of highly specific substrates of neutrophil elastase and proteinase 3” *Am. J. Respir. Cell Mol. Biol.*, **2004**, *30*, 801-807.
- [126] Rao, N. V.; Wehner, N. G.; Marshall, B. C.; Gray, W. R.; Gray, B. H.; Hoidal, J. R. –Characterization of proteinase-3 (PR-3), a neutrophil serine proteinase. Structural and functional properties” *J. Biol. Chem.* **1991**, *266*, 9540-9548.
- [127] Koehl, C.; Knight, C. G.; Bieth, J. G. –Compared action of neutrophil proteinase 3 and elastase on model substrates. Favorable effect of S'-P' interactions on proteinase 3 catalyses” *J. Biol. Chem.*, **2003**, *278*, 12609-12612.
- [128] Hajjar, E.; Korkmaz, B.; Gauthier, F.; Brandsdal, B. O.; Witko-Sarsat, V.; Reuter, N. –Inspection of the binding sites of proteinase 3 for the design of a highly specific substrate” *J. Med. Chem.*, **2006**, *49*, 1248-1260.
- [129] Hof, P.; Mayr, I.; Huber, R.; Korzus, E.; Potempa, J.; Travis, J.; Powers, J. C.; Bode, W. –The 1.8 Å crystal structure of human cathepsin G in complex with Suc-Val-Pro-PheP-(OPh)₂: a Janus-faced proteinase with two opposite specificities” *EMBO J.*, **1996**, *15*, 5481-5491.
- [130] Tanaka, T.; Minematsu, Y.; Reilly, C. F.; Travis, J.; Powers, J. C. –Human leukocyte cathepsin G. Subsite mapping with 4-nitroanilides, chemical modification, and effect of possible cofactors” *Biochemistry*, **1985**, *24*, 2040-2047.

- [131] Attucci, S.; Korkmaz, B.; Juliano, L.; Hazouard, E.; Girardin, C.; Brillard-Bourdet, M.; Rehault, S.; Anthonioz, P.; Gauthier, F. –Measurement of free and membrane-bound cathepsin G in human neutrophils using new sensitive fluorogenic substrates” *Biochem. J.*, **2002**, *366*, 965-970.
- [132] Rehault, S.; Brillard-Bourdet, M.; Juliano, M. A.; Juliano, L.; Gauthier, F.; Moreau, T. –New, Sensitive fluorogenic substrates for human cathepsin G based on the sequence of serpin-reactive site loops” *J. Biol. Chem.*, **1999**, *274*, 13810-13817.
- [133] Segal, D. M.; Powers, J. C.; Cohen, G. H.; Davies, D. R.; Wilcox, P. E. –Substrate binding site in bovine chymotrypsin A-gamma. A crystallographic study using peptide chloromethyl ketones as site-specific inhibitors” *Biochemistry*, **1971**, *10*, 3728-3738.
- [134] Schrijver, G.; Schalkwijk, J.; Robben, J. C.; Assmann, K.J.; Koene, R. A. –Antiglomerular basement membrane nephritis in beige mice. Deficiency of leukocytic neutral proteinases prevents the induction of albuminuria in the heterologous phase” *J. Exp. Med.*, **1989**, *169*, 1435-1448.
- [135] Liu, Z.; Shapiro, S. D.; Zhou, X.; Twining, S. S.; Senior, R. M.; Giudice, G. J.; Fairley, J. A.; Diaz, L. A. –A critical role for neutrophil elastase in experimental bullous pemphigoid” *J. Clin. Invest.*, **2000**, *105*, 113-123.
- [136] Janoff, A.; Sloan, B.; Weinbaum, G.; Damiano V, Sandhaus, R. A.; Elias, J.; Kimbel, P. –Experimental emphysema induced with purified human neutrophil elastase: tissue localization of the instilled protease” *Am. Rev. Respir. Dis.*, **1977**, *115*, 461-478.
- [137] Gadek, J. E.; Fells, G. A.; Crystal, R. G. –Cigarette smoking induces functional antiprotease deficiency in the lower respiratory tract of humans” *Science*, **1979**, *206*, 1315-1316.
- [138] Carp, H.; Miller, F.; Hoidal, J. R.; Janoff, A. –Potential mechanism of emphysema: alpha 1-proteinase inhibitor recovered from lungs of cigarette smokers contains oxidized methionine and has decreased elastase inhibitory capacity” *Proc. Natl. Acad. Sci. USA*, **1982**, *79*, 2041-2045.
- [139] Geraghty, P.; Rogan, M. P.; Greene, C. M.; Boxio, R. M.; Poiriert, T.; O’Mahony, M.; Belaouaj, A.; O’Neill, S. J.; Taggart, C. C.; McElvaney, N. G. –Neutrophil elastase up-regulates cathepsin B and matrix metalloproteinase-2 expression” *J. Immunol.*, **2007**, *178*, 5871-5878.
- [140] Imai, K.; Yokohama, Y.; Nakanishi, I.; Ohuchi, E.; Fujii, Y.; Nakai, N.; Okada, Y. –Matrix metalloproteinase 7 (matrilysin) from human rectal carcinoma cells. Activation of the precursor, interaction with other matrix metalloproteinases and enzymic properties” *J. Biol. Chem.*, **1995**, *270*, 6691-6697.
- [141] Ferry, G.; Lonchamp, M.; Pennel, L.; de Nanteuil, G.; Canet, E.; Tucker, G. C.

- Activation of MMP-9 by neutrophil elastase in an in vivo model of acute lung injury” *FEBS Lett.*, **1997**, *402*, 111-115.
- [142] Shamamian, P.; Schwartz, J. D.; Pocock, B. J.; Monea, S.; Whiting, D.; Marcus, S. G.; Mignatti, P. –Activation of progelatinase A (MMP-2) by neutrophil elastase, cathepsin G, and proteinase-3: a role for inflammatory cells in tumor invasion and angiogenesis” *J. Cell Physiol.*, **2001**, *189*(2), 197-206.
- [143] Jenne, D. E.; Tschopp, J.; Ludemann, J.; Utecht, B.; Gross, W. L. –Wegener’s autoantigen decoded” *Nature*, **1990**, *346*, 520.
- [144] Rarok, A. A.; Limburg, P.C.; Kallenberg, C. G. –Neutrophil-activating potential of antineutrophil cytoplasm autoantibodies” *J. Leukoc. Biol.*, **2003**, *74*, 3-15.
- [145] Esnault, V. L.; Testa, A.; Audrain, M.; Roge, C.; Hamidou, M.; Barrier, J. H.; Sesboue, R.; Martin, J. P.; Lesavre, P. –Alpha 1-antitrypsin genetic polymorphism in ANCA-positive systemic vasculitis” *Kidney Int.*, **1993**, *43*, 1329-1332.
- [146] Segelmark, M.; Elzouki, A. N.; Wieslander, J.; Eriksson, S. –The PiZ gene of alpha 1-antitrypsin as a determinant of outcome in PR3-ANCA-positive vasculitis” *Kidney Int.*, **1995**, *48*, 844-850.
- [147] Pederzoli, M.; Kantari, C.; Gausson, V.; Moriceau, S.; Witko-Sarsat, V. –Proteinase-3 induces procaspase-3 activation in the absence of apoptosis: potential role of this compartmentalized activation of membrane-associated procaspase-3 in neutrophils” *J. Immunol.*, **2005**, *174*, 6381- 6390.
- [148] Preston, G. A.; Zarella, C. S.; Pendergraft 3rd, W. F.; Rudolph, E. H.; Yang, J. J.; Sekura, S. B.; Jennette, J. C.; Falk, R. J. –Novel effects of neutrophil-derived proteinase 3 and elastase on the vascular endothelium involve in vivo cleavage of NF-kappaB and proapoptotic changes in JNK, ERK, and p38 MAPK signaling pathways” *J. Am. Soc. Nephrol.*, **2002**, *13*, 2840-2849.
- [149] Dublet, B.; Ruello, A.; Pederzoli, M.; Hajjar, E.; Courbebaisse, M.; Canteloup, S.; Reuter, N.; Witko-Sarsat, V. –Cleavage of p21/WAF1/CIP1 by Proteinase 3 modulates differentiation of a monocytic cell line. Molecular analysis of the cleavage site” *J. Biol. Chem.*, **2005**, *280*, 30242-30253.
- [150] Witko-Sarsat, V.; Canteloup, S.; Durant, S.; Desdouets, C.; Chabernaude, R.; Lemarchand, P.; Descamps-Latscha, B. –Cleavage of p21waf1 by proteinase-3, a myeloid-specific serine protease, potentiates cell proliferation” *J. Biol. Chem.*, **2002**, *277*, 47338-47347.
- [151] Bank, U.; Ansorge, S. –More than destructive: neutrophil derived serine proteases in cytokine bioactivity control” *J. Leukoc. Biol.*, **2001**, *69*, 197-206.
- [152] Shimoda, N.; Fukazawa, N.; Nonomura, K.; Fairchild, R. L. –Cathepsin G Is Required for

- Sustained Inflammation and Tissue Injury after Reperfusion of Ischemic Kidneys” *Am. J. Pathol.*, **2007**, *170*(3), 930-940.
- [153] Stefansson, S.; Yepes, M.; Gorlatova, N.; Day, D. E.; Moore, E. G.; Zabaleta, A.; McMahon, G. A.; Lawrence, D. A. –Mutants of plasminogen activator inhibitor-1 designed to inhibit neutrophil elastase and cathepsin G are more effective in vivo than their endogenous inhibitors” *J. Biol. Chem.*, **2004**, *279*(29), 29981-29987.
- [154] Ermolieff, J.; Boudier, C.; Laine, A.; Meyer, B.; Bieth, J. G. –Heparin protects cathepsin G against inhibition by protein proteinase inhibitors” *J. Biol. Chem.*, **1994**, *269*, 29502-29508.
- [155] Durantou, J.; Boudier, C.; Belorgey, D.; Mellet, P.; Bieth, J. G. –DNA Strongly Impairs the Inhibition of Cathepsin G by α 1-Antichymotrypsin and α 1-Proteinase Inhibitor” *J. Biol. Chem.*, **2000**, *275*, 3787-3792.
- [156] Durantou, J.; Belorgey, D.; Carrere, J.; Donato, L.; Moritz, T.; and Bieth, J. G. –Effect of DNase on the activity of neutrophil elastase, cathepsin G and proteinase 3 in the presence of DNA” *FEBS Lett.*, **2000**, *473*, 154-156.
- [157] Romero, V.; Andrade, F. –Non-apoptotic functions of granzymes” *Tissue Antigens*, **2008**, *71*, 409-416.
- [158] Buzza, M. S.; Bird, P. I. –Extracellular granzymes: current perspectives” *Biol. Chem.*, **2006**, *387*, 827-837.
- [159] Chowdhury, D.; Lieberman, J. –Death by a thousand cuts: granzyme pathways of programmed cell death” *Annu. Rev. Immunol.*, **2008**, *26*, 389-420.
- [160] Bots, M.; Van Bostelen, L.; Rademaker, M. T.; Offringa, R.; Medema, J. P. –Serpins prevent granzyme-induced death in a species-specific manner” *Immunol. Cell. Biol.*, **2006**, *84*, 79-86.
- [161] Buzza, M.S.; Hirst, C. E.; Bird, C. H.; Hosking, P.; McKendrick, J.; Bird, P. I. –The granzyme B inhibitor, PI-9, is present in endothelial and mesothelial cells, suggesting that it protects bystander cells during immune responses” *Cell Immunol.*, **2001**, *210*, 21-29.
- [162] Buzza, M.S.; Zamurs, L.; Sun, J.; Bird, C. H.; Smith, A. I.; Trapani, J. A.; Froelich, C. J.; Nice, E. C.; Bird, P. I. –Extracellular matrix remodeling by human granzyme B via cleavage of vitronectin, fibronectin, and laminin” *J. Biol. Chem.*, **2005**, *280*, 23549-23558.
- [163] Froelich, C. J.; Pardo, J.; Simon, M. M. –Granule-associated serine proteases: granzymes might not just be killer proteases” *Trends Immunol.*, **2009**, *30*: 117-123.
- [164] Choy, J. C.; Hung, V. H.; Hunter, A. L.; Cheung, P. K.; Motyka, B.; Goping, I. S.;

- Sawchuk, T.; Bleackley, R. C.; Podor, T. J.; McManus, B. M.; Granville, D. J. –Granzyme B induces smooth muscle cell apoptosis in the absence of perforin: involvement of extracellular matrix degradation” *Arterioscler. Thromb. Vasc. Biol.*, **2004**, *24*, 2245-2250.
- [165] Garbacki, N.; Di Valentin, E.; Piette, J.; Cataldo, D.; Crahay, C.; Colige, A. –Matrix metalloproteinase 12 silencing: a therapeutic approach to treat pathological lung tissue remodeling?” *Pulm. Pharmacol. Ther.*, **2009**, *22*(4), 267-278.
- [166] Elkington, P. T.; Friedland, J. S. –Matrix metalloproteinases in destructive pulmonary pathology” *Thorax.*, **2006**, *61*(3), 259-266.
- [167] Lagente, V.; Le Qument, C.; Boichot, E. –Macrophage metalloelastase (MMP-12) as a target for inflammatory respiratory diseases” *Expert Opin. Ther. Targets.*, **2009**, *13*(3), 287-295.
- [168] Shapiro, S. D. –Matrix metalloproteinase degradation of extracellular matrix: biological consequences” *Curr. Opin. Cell Biol.*, **1998**, *10*, 602-608.
- [169] Tetley, T. D. –Macrophages and the pathogenesis of COPD” *Chest*, **2002**, *121*, 156S-159S.
- [170] Russell, R. E.; Thorley, A.; Culpitt, S. V.; Dodd, S.; Donnelly, L. E.; Demattos, C.; Fitzgerald, M.; Barnes, P. J. –Alveolar macrophage-mediated elastolysis: roles of matrix metalloproteinases, cysteine, and serine proteases” *Am. J. Physiol. Lung Cell Mol. Physiol.*, **2002**, *283*, L867-L873.
- [171] Hautamaki, R. D.; Kobayashi, D. K.; Senior, R. M.; Shapiro, S. D. –Requirement for macrophage elastase for cigarette smoke-induced emphysema in mice” *Science*, **1997**, *277*, 2002-2004.
- [172] Churg, A.; Zay, K.; Shay, S.; Xie, C.; Shapiro, S. D.; Hendricks, R.; Wright, J. L. –Acute cigarette smoke induced connective tissue breakdown requires both neutrophils and macrophage metalloelastase in mice” *Am. J. Respir. Cell Mol. Biol.*, **2002**, *27*, 368-374.
- [173] Bertini, I.; Calderone, V.; Fragai, M.; Luchinat, C.; Mangani, S.; Terni, B. –X-ray structures of binary and tertiary enzyme-product-inhibitor complexes of matrix metalloproteinases” *Angew. Chem. Int. Ed. Engl.*, **2003**, *42*, 2673-2676.
- [174] Aleshin, A. E.; Shiryayev, S. A.; Strongin, A. Y.; Liddington, R. C. –Structural evidence for regulation and specificity of flaviviral proteases and evolution of the Flaviviridae fold” *Protein Sci.* **2007**, *16*(5), 795-806.
- [175] Hayes, C. G. –West Nile Virus: Uganda, 1937, to New York City, 1999” *Ann. N. Y. Acad. Sci.*, **2001**, *951*, 25–37.
- [176] <http://www.cdc.gov/ncidod/dvbid/westnile/surv&control.htm> [cited 6 Feb 2010]

- [177] Pertersen, L. R.; Marfin, A. A.; Gubler, D. J. –West Nile virus” *JAMA*, **2003**, *290*, 524-528.
- [178] Sampath, A.; Padmanabhan, R. –Molecular targets for flavivirus drug discovery” *Antiviral Res.*, **2009**, *81*(1), 6-15.
- [179] Stevens, A. J.; Gahan, M. E.; Mahalingam, S.; Keller, P. A. –The Medicinal Chemistry of Dengue Fever” *J. Med. Chem.*, **2009**, *52*, 7911-7926.
- [180] Henchal, E. A.; Putnak, J. R. –The Dengue Viruses” *Clin. Microbiol. Rev.*, **1990**, *3*, 376-396.
- [181] Van der Meulen, K. M.; Pensaert, M. B.; Nauwynck, H. J. –West Nile virus in the vertebrate world” *Arch. Virol.*, **2005**, *150*, 637-657.
- [182] Webster, D. P.; Farrar, J.; Rowland-Jones, S. –Progress towards a dengue vaccine” *Lancet Infect Dis.*, **2009**, *9*(11), 678-687.
- [183] Lindenbach, B. D.; Thiel, H. J.; Rice, C. M. –Flaviviridae: The Viruses and Their Replication” *Fields Virology*, **2007**, 5th Ed, pp: 1101-1152.
- [184] Lescar, J.; Luo, D.; Xu, T.; Sampath, A.; Lim, S. P.; Canard, B.; Vasudevan, S. G. –Towards the design of antiviral inhibitors against flaviviruses: The case for the multifunctional NS3 protein from Dengue virus as a target” *Antiviral Res.*, **2008**, *80*, 94-101.
- [185] Chambers, T. J.; Nestorowicz, A.; Amberg, S. M.; Rice, C. M. –Mutagenesis of the yellow fever virus NS2B protein: effects on proteolytic processing, NS2B–NS3 complex formation, and viral replication” *J. Virol.*, **1993**, *67*, 6797-6807.
- [186] Radichev, I.; Shiryaev, S. A.; Aleshin, A. E.; Ratnikov, B. I.; Smith, J. W.; Liddington, R. C.; Strongin, A. Y. –Structure-based mutagenesis identifies important novel determinants of the NS2B cofactor of the West Nile virus two-component NS2B-NS3 proteinase” *J. Gen. Virol.*, **2008**, *89*, 636-641.
- [187] Nall, T. A.; Chappell, K. J.; Stoermer, M. J.; Fang, N.; Tyndall, J. D. A.; Young, P. R.; Fairlie, D. P. –Enzymatic Characterization and Homology Model of a Catalytically Active Recombinant West Nile Virus NS3 Protease” *J. Biol. Chem.*, **2004**, *279*(47), 48535-48542.
- [188] Shiryaev, S. A.; Kozlov, I. A.; Ratnikov, B. I.; Smith, J. W.; Lebl, M.; Strongin, A. Y. –Cleavage preference distinguishes the two-component NS2B–NS3 serine proteinases of Dengue and West Nile viruses” *Biochem. J.*, **2007**, *401*(Pt 3), 743–752.
- [189] Knox, J. E.; Ma, N. L.; Yin, Z.; Patel, S. J.; Wang, W. L.; Chan, W. L.; Ranga Rao, K. R.;

- Wang, G.; Ngew, X.; Patel, V.; Beer, D.; Lim, S. P.; Vasudevan, S. G.; Keller, T. H. –Peptide inhibitors of West Nile NS3 protease: SAR study of tetrapeptide aldehyde inhibitors” *J. Med. Chem.*, **2006**, *49*(22), 6585–6590.
- [190] Bode, W.; Wei, A. Z.; Huber, R.; Meyer, E.; Travis, J.; Neumann, S. –X-ray crystal structure of the complex of human leukocyte elastase (PMN elastase) and the third domain of the turkey ovomucoid inhibitor” *EMBOJ*, **1986**, *5*(10), 2453-2458.
- [191] (a) Tucker, T. J.; Lumma, W. C.; Mulichak, A. M.; Chen, Z.; Naylor-Olsen, A. M.; Lewis, S. D.; Lucas, R.; Freidinger, R. M.; Kuo, L. C. –Design of highly potent noncovalent thrombin inhibitors that utilize a novel lipophilic binding pocket in the thrombin active site” *J. Med. Chem.*, **1997**, *40*(6), 830-832; (b) Tucker, T. J.; Lumma, W. C.; Lewis, S. D.; Gardell, S. J.; Lucas, B. J.; Baskin, E. P.; Woltmann, R.; Lynch, J. J.; Lyle, E. A.; Appleby, S. D.; Chen, I. W.; Dancheck, K. B.; Vacca, J. P. –Potent noncovalent thrombin inhibitors that utilize the unique amino acid D-dicyclohexylalanine in the P3 position. Implications on oral bioavailability and antithrombotic efficacy” *J. Med. Chem.*, **1997**, *40*(11), 1565-1569.
- [192] (a) Ohbayashi, H. –Current synthetic inhibitors of human neutrophil elastase in 2005” *Expert Opin. Ther. Patents*, **2005**, *15*(7), 759-771; (b) Thongyoo, P.; Bonomelli, C.; Leatherbarrow, R. J.; Tate, E. W. –Potent Inhibitors of β -Tryptase and Human Leukocyte Elastase Based on the McoTI-II Scaffold” *J. Med. Chem.*, **2009**, *52*, 6197–6200.
- [193] (a) Tomlinson, S. M.; Malmstrom, R. D.; Watowich, S. J. –New Approaches to Structure-Based Discovery of Dengue Protease Inhibitors” *Infectious Disorders-Drug Targets*, **2009**, *9*(3), 327-343; (b) Tomlinson, S. M.; Malmstrom, R. D.; Russo, A.; Mueller, N.; Pang, Y. P.; Watowich, S. J. –Structure-based discovery of Dengue virus protease inhibitors” *Antiviral Research*, **2009**, *82*, 110-114.
- [194] (a) Wolfenden, R. –Transition state analogous for enzyme catalysis” *Nature*, **1969**, *223*, 704-705; (b) Wolfenden, R. –Analog approaches to the structure of the transition state in enzyme reactions” *Acc. Chem. Res.*, **1972**, *5*, 10-18.
- [195] Erbel, P.; Schiering, N.; D'Arcy, A.; Renatus, M.; Kroemer, M.; Lim, S. P.; Yin, Z.; Keller, T. H.; Vasudevan, S. G.; Hommel, U. –Structural basis for the activation of flaviviral NS3 proteases from dengue and West Nile virus” *Nat. Struct. Mol. Biol.*, **2006**, *13*(4), 372-373.
- [196] Inoue, Y.; Omodani, T.; Shiratake, R.; Okazaki, H.; Kuromiya, A.; Kubo, T.; Sato, F. –Development of a highly water-soluble peptide-based human neutrophil elastase inhibitor; AE-3763 for treatment of acute organ injury” *Bioorg. Med. Chem.*, **2009**, *7*(21), 7477-7486.
- [197] Angelastro, M. R.; Baugh, L. E.; Bey, P.; Burkhart, J. P.; Chen, T. M.; Durham, S. L.; Hare, C. M.; Huber, E. W.; Janusz, M. J.; Koehl, J. R.; Marquart, S. M.; Peet, N. P. –Inhibition of human neutrophil elastase with peptidyl electrophilic ketones. 2. Orally

- active PG-Val-Pro-Val pentafluoroethyl ketones" *J. Med. Chem.*, **1994**, 37(26), 4538-4553.
- [198] Takahashi, L. H.; Radhakrishnan, R.; Rosenfield, R. E., Jr.; Meyer, E. F., Jr.; Trainor, D. A. –Crystal Structure of the Covalent Complex Formed by a Peptidyl α,α -Difluoro- α -keto Amide with Porcine Pancreatic Elastase at 1.78-Å Resolution" *J. Am. Chem. Soc.*, **1989**, *111*, 3368-3374.
- [199] Mehdi, S.; Angelastro, M. R.; Burkhardt, J. P.; Kochl, J. R.; Peet, N. P.; Bey, P. –The inhibitions of human neutrophil elastase and cathepsin G by peptidyl 1,2-dicarbonyl derivatives" *Biochem. Biophys. Res. Commun.*, **1990**, *166*, 595–600.
- [200] Kettner, C. A.; Shenvi, A. B. –Inhibition of the Serine Proteases Leukocyte Elastase, Pancreatic Elastase, CathepsinG, and Chymotrypsin by Peptide Boronic Acids" *J. Biol. Chem.*, **1984**, *259*(24), 15106-15114.
- [201] Bursavich, M. G.; Rich, D. H. –Designing Non-Peptide Peptidomimetics in the 21st Century: Inhibitors Targeting Conformational Ensembles" *J. Med. Chem.*, **2002**, *45*(3), 541-558.
- [202] Petroková, H.; Dusková, J.; Dohnálek, J.; Skálová, T.; Vondrácková-Buchtelová, E.; Soucek, M.; Konvalinka, J.; Brynda, J.; Fábry, M.; Sedláček, J.; Hasek, J. –Role of hydroxyl group and R/S configuration of isostere in binding properties of HIV-1 protease inhibitors" *Eur. J. Biochem.*, **2004**, *271*, 4451–4461.
- [203] Venkatraman, S.; Velazquez, F.; Wu, W.; Blackman, M.; Chen, K. X.; Bogen, S.; Nair, L.; Tong, X.; Chase, R.; Hart, A.; Agrawal, S.; Pichardo, J.; Prongay, A.; Cheng, K. C.; Girijavallabhan, V.; Piwinski, J.; Shih, N. Y.; Njoroge, F. G. –Discovery and structure-activity relationship of P1-P3 ketoamide derived macrocyclic inhibitors of hepatitis C virus NS3 protease" *J. Med. Chem.*, **2009**, *52*(2), 336-346.
- [204] (a) Morrison, J. F.; Walsh C. T. –The behavior and significance of slow-binding enzyme inhibitors" *Adv. Enzymol. Relat. Areas Mol. Biol.* 1988, *61*, 201-203; (b) Venäläinen, J. I.; Juvonen, R. O.; Garcia-Horsman, J. A.; Wallén, E. A.; Christiaans, J. A.; Jarho, E. M.; Gynther, J.; Männistö, P. T. –Slow-binding inhibitors of prolyl oligopeptidase with different functional groups at the P1 site" *Biochem. J.*, **2004**, *382*, 1003–1008
- [205] Copeland, R. A. –Evaluation of enzyme inhibitors in drug discovery" Wiley-Interscience, **2005**, pp 145-146.
- [206] (a) Krantz, A. –A classification of enzyme inhibitors" *Bioorg. Med. Chem. Lett.*, **1992**, *2*, 1327–1334; (b) Pratt, R. F. "On the definition and classification of mechanism-based enzyme inhibitors" *Bioorg. Med. Chem. Lett.*, **1992**, *11*, 1323–1326.
- [207] Silverman, R. B. –Mechanism-Based Enzyme Inactivation" *Chemistry and Enzymology*, CRC Press, Boca Raton, FL, **1988**, pp 3-30.

- [208] Huang, W.; Yamamoto, Y.; Li, Y.; Dou, D.; Alliston, K. R.; Hanzlik, R. P.; Williams, T. D.; Groutas, W. C. –X-ray snapshot of the mechanism of inactivation of human neutrophil elastase by 1,2,5-thiadiazolidin-3-one 1,1-dioxide derivatives” *J. Med. Chem.*, **2008**, *51*, 2003-2008.
- [209] Groutas, W. C.; Stanga, M. A.; Brubaker, M. J. –¹³C NMR evidence for an enzyme-induced Lossen rearrangement in the mechanism-based inactivation of chymotrypsin by 3-benzyl-N-[(methylsulfonyl)oxy]succinimide” *J. Am. Chem. Soc.*, **1989**, *111*, 1931-1932.
- [210] Gelb, M. H.; Abeles, R. H. –Substituted Isatoic Anhydrides: Selective Inactivators of Trypsin-like Serine Proteases” *J. Med. Chem.*, **1986**, *29*, 585-589.
- [211] Böttcher, T.; Sieber, S. A. –Lactones as Specific Inhibitors of ClpP Attenuate the Production of Extracellular Virulence Factors of *Staphylococcus aureus*” *J. Am. Chem. Soc.*, **2008**, *130*, 14400–14401.
- [212] Copp, L. J.; Krantz, A.; Spencer, R. W. –Kinetics and mechanism of human leukocyte elastase inactivation by ynenol lactones” *Biochemistry*, **1987**, *26*(1), 169-178.
- [213] Doherty, J. B.; Ashe, B. M.; Argenbright, L. W.; Barker, P. L.; Bonney, R. J.; Chandler, G. O.; Dahlgren, M. E.; Dorn, C. P.; Finke, P. E.; Firestone, R. A.; Fletcher, D.; Hagmann, W. K.; Mumford, R.; Ogrady, L.; Maycock, A. L.; Pisano, J. M.; Shah, S. K.; Thompson, K. R.; Zimmerman, M. –Cephalosporin Antibiotics Can Be Modified To Inhibit Human-Leukocyte Elastase” *Nature*, **1986**, *322*, 192–194.
- [214] Doherty, J. B.; Shah, S. K.; Finke, P. E.; Dorn, C. P., Jr.; Hagmann, W. K.; Hale, J. J.; Kissinger, A. L.; Thompson, K. R.; Brause, K.; Chandler, G. O.; Knight, W. B.; Maycock, A. L.; Ashe, B. M.; Weston, H.; Gale, P.; Mumford, R. A.; Andersen, O. F.; Williams, H. R.; Nolan, T. E.; Frankenfield, D. L.; Underwood, D.; Vyas, K. P.; Kari, P. H.; Dahlgren, M. E.; Mao, J.; Fletcher, D. S.; Dellea, P. S.; Hand, K. M.; Osinga, D. G.; Peterson, L. B.; Williams, D. T.; Metzger, J. M.; Bonney, R. J.; Humes, J. L.; Pacholok, S. P.; Hanlon, W. A.; Opas, E.; Stolk, J.; Davies, P. –Chemical, Biochemical, Pharmacokinetic, and Biological Properties of L-680,833: A Potent, Orally Active Monocyclic β -Lactam Inhibitor of Human Polymorphonuclear Leukocyte elastase” *Proc. Nat. Acad. Sci. U.S.A.*, **1993**, *90*, 8727–8731.
- [215] Subramanyam, C.; Bell, m. r.; Carabateas, P.; Court, J. J.; Dority, J. A. Jr.; Ferguson, E.; Gordon, R.; Hlasta, D. J.; Kumar, V.; Saindanet, M. –2,6-Disubstituted Aryl Carboxylic Acids, Leaving Groups –Par Excellence” for Benzisothiazolone Inhibitors of Human Leukocyte Elastase” *J. Med. Chem.*, **1994**, *37*(17), 2623-2626.
- [216] Kuang, R.; Epp, J. B.; Ruan, S.; Chong, L. S.; Venkataraman, R.; Tu, J.; He, S.; Truong, T. M.; Groutas, W. C. –Utilization of the 1,2,5-thiadiazolidin-3-one 1,1 dioxide scaffold in the design of potent inhibitors of serine proteases: SAR studies using carboxylates” *Bioorg. Med. Chem.*, **2000**, *8*(5), 1005-1016.

- [217] Groutas, W. C.; Kuang, R.; Venkataraman, R.; Epp, J. B.; Ruan, S.; Prakash, O. –Structure-based design of a general class of mechanism-based inhibitors of the serine proteinases employing a novel amino acid-derived heterocyclic scaffold” *Biochemistry*, **1997**, *36*, 4739-4750.
- [218] Iijima, K.; Katada, J.; Yasuda, E.; Uno, I.; Hayashi, Y. –N-[2,2-Dimethyl-3-(N-(4-cyanobenzoyl)amino)nonanoyl]-L-phenylalanine Ethyl Ester as a Stable Ester-Type Inhibitor of Chymotrypsin-like Serine Proteases: Structural Requirements for Potent Inhibition of r-Chymotrypsin” *J. Med. Chem.*, **1999**, *42*, 312-323.
- [219] Powers, J. C.; Boone, R.; Carroll, D. L.; Gupton, B. F.; Kam, C. M.; Nishino, N.; Sakamoto, M.; Tuhy, P. M. –Reaction of azapeptides with human leukocyte elastase and porcine pancreatic elastase. New inhibitors and active site titrants” *J. Biol. Chem.*, **1984**, *259*(7), 4288-4294.
- [220] Herbert, J. M.; Frehel, D.; Rosso, M. P.; Seban, E.; Castet, C.; Pepin, O.; Maffrand, J. P.; Le Fur, G. –Biochemical and pharmacological activities of SR 26831, a potent and selective elastase inhibitor” *J. Pharmacol. Exp. Ther.*, **1992**, *260*(2), 809-816.
- [221] Lipinski, C. A.; Lombardo, F.; Dominy, B. W.; Feeney, P. J. –Experimental and computational approaches to estimate solubility and permeability in drug discovery and development settings” *Adv. Drug Delivery Rev.*, **1997**, *23*, 3-25.
- [222] He, S.; Kuang, R.; Venkataraman, R.; Tu, J.; Truong, T. M.; Chan, H. K.; Groutas, W. C. –Potent inhibition of Serine Proteases by heterocyclic sulfide derivatives of 1,2,5-thiadiazolidin-3-one 1,1 dioxide” *Bioorg. Med. Chem.*, **2000**, *8*, 1713-1717.
- [223] Dolle, R. E.; Hoyer, D.; Prasad, C. V.; Schmidt, S. J.; Helaszek, C. T.; Miller, R. E.; Ator, M. A. –P1 aspartate-based peptide alpha-((2,6-dichlorobenzoyl)oxy)methyl ketones as potent time-dependent inhibitors of interleukin-1 beta-converting enzyme” *J. Med. Chem.*, **1994**, *37*(5), 563–564.
- [224] Loser, R.; Abbenante, G.; Madala, P. K.; Halili, M.; Le, G. T.; Fairlie, D. P. –Noncovalent Tripeptidyl Benzyl- and Cyclohexyl-Amine Inhibitors of the Cysteine Protease Caspase-1” *J. Med. Chem.*, **2010**, *53*, 2651-2655.
- [225] Talanian, R. V.; Brady, K. D.; Cryns, V. L. –Caspases as targets for anti-inflammatory and anti-apoptotic drug discovery” *J. Med. Chem.*, **2000**, *43*(18), 3351-3371.
- [226] Hanessian, S.; Moitessier, N.; Gauchet, C.; Viau, M. –N-Aryl sulfonyl homocysteine hydroxamate inhibitors of matrix metalloproteinases: further probing of the S1, S1', and S2' pockets” *J. Med. Chem.*, **2001**, *44*(19), 3066-3073.
- [227] Nuti, E.; Panelli, L.; Casalini, F.; Avramova, S. I.; Orlandini, E.; Santamaria, S.; Nencetti, S.; Tuccinardi, T.; Martinelli, A.; Cercignani, G.; D'Amelio, N.; Maiocchi, A.; Uggeri, F.;

- Rossello, A. –Design, synthesis, biological evaluation, and NMR studies of a new series of arylsulfones as selective and potent matrix metalloproteinase-12 inhibitors” *J. Med. Chem.*, **2009**, 52(20), 6347-6361.
- [228] Norman, P. –Selective MMP-12 inhibitors: WO-2008057254” *Expert Opin. Ther. Pat.*, **2009**, 19(7), 1029-1034.
- [229] Holmes, I. P.; Gaines, S.; Watson, S. P.; Lorthioir, O.; Walker, A.; Baddeley, S. J.; Herbert, S.; Egan, D.; Convery, M. A.; Singh, O. M.; Gross, J. W.; Strelow, J. M.; Smith, R. H.; Amour, A. J.; Brown, D.; Martin, S. L. –The identification of beta-hydroxy carboxylic acids as selective MMP-12 inhibitors” *Bioorg. Med. Chem. Lett.*, **2009**, 19, 5760-5763.
- [230] Morris, G. M.; Huey, R.; Lindstrom, W.; Sanner, M. F.; Belew, R. K.; Goodsell, D. S.; Olson, A. J. –AutoDock4 and AutoDockTools4: Automated docking with selective receptor flexibility” *J. Comput. Chem.*, **2009**, 30(16), 2785-2791.
- [231] SYBYL, Tripos Associates, St. Louis, MO, 2008.
- [232] Clark, M.; Cramer, R. D. III; Van Opdenbosch, N. –Validation of the general purpose tripos 5.2 force field” *J. Comput. Chem.*, **1989**, 10(8), 982-1012.
- [233] Gasteiger, J.; Marsili, M. –A new model for calculating atomic charges in molecules” *Tetrahedron Lett.* **1978**, 19, 3181-3184.
- [234] Bohm, H. J.; Flohr, A.; Stahl, M. *Drug Discovery Today*, **2008**, 1, 227-233.
- [235] Zhao, H. –Scaffold selection and scaffold hopping in lead generation: a medicinal chemistry perspective” *Drug Discovery Today*, **2007**, 12, 149-155.
- [236] Gante, J. –Azapeptides” *Synthesis*, **1989**, 6, 405-413.
- [237] (a) Brubaker, M. J.; Groutas, W. C.; Hoidal, J. R.; Rao, N. V. –Human neutrophil proteinase 3: mapping of the substrate binding site using peptidyl thiobenzyl esters” *Biochem. Biophys. Res. Commun.*, **1992**, 188, 1318-1324; (b) Kam, C. M.; Kerrigan, J. E.; Dolman, K. M.; Goldschmeding, R.; Von dem Borne, A. E.; Powers, J. C. –Substrate and inhibitor studies on proteinase 3” *FEBS Lett.*, **1992**, 297(1-2), 119-123; (c) Wysocka, M.; Lesner, A.; Guzow, K.; Mackiewicz, L.; Legowska, A.; Wiczak, W.; Rolka, K. –Design of selective substrates of proteinase 3 using combinatorial chemistry methods” *Anal. Biochem.*, **2008**, 378, 208-215.
- [238] Fujinaga, M.; Chernaia, M. M.; Halenbeck, R.; Koths, K.; James, M. N. G. –The crystal structure of PR3, a neutrophil serine proteinase antigen of Wegener's granulomatosis antibodies” *J. Mol. Biol.*, **1996**, 261, 267-278.
- [239] Koehl, C.; Knight, C. G.; Bieth, J. G. –Compared action of neutrophil proteinase 3 and

- elastase on model substrates. Favorable effect of S'-P' interactions on proteinase 3 catalysts" *J. Biol. Chem.*, **2003**, *278*, 12609-12612.
- [240] (a) Korkmaz, B.; Moreau, T.; Gauthier, F. –Neutrophil elastase, proteinase 3 and cathepsin G: physicochemical properties, activity and physiopathological functions" *Biochimie*, **2008**, *90*, 227-242. (b) Hajjar, E.; Korkmaz, B.; Gauthier, F.; Brandsdal, B. O.; Witko-Sarsat, V.; Reuter, N. –Inspection of the binding sites of proteinase3 for the design of a highly specific substrate" *J. Med. Chem.*, **2006**, *49*, 1248-1260. (c) Korkmaz, B.; Attucci, S.; Hazouard, E.; Ferrandiere, M.; Jourdan, M. L.; Brillard-Bourdet, M.; Juliano, L.; Gauthier, F. –Discriminating between the activities of human neutrophil elastase and proteinase 3 using serpin-derived fluorogenic substrates" *J. Biol. Chem.*, **2002**, *277*, 39074-39081. (d) Korkmaz, B.; Attucci, S.; Moreau, T.; Godat, E.; Juliano, L.; Gauthier, F. –Design and use of highly specific substrates of neutrophil elastase and proteinase 3" *Am. J. Respir. Cell Mol. Biol.*, **2004**, *30*(6), 801-807.
- [241] Shin, I.; Lee, M. R.; Lee, J.; Jung, M.; Lee, W.; Yoon, J. –Synthesis of optically active phthaloyl D-aminoxy acids from L-amino acids or L-hydroxy acids as building blocks for the preparation of aminoxy peptides" *J. Org. Chem.*, **2000**, *65*, 7667-7675.
- [242] Kolb, H. C.; Finn, M. G.; Sharpless, K. B. –Click Chemistry: Diverse Chemical Function from a Few Good Reactions" *Angew. Chemie.*, **2001**, *40*(11), 2004-2021.
- [243] (a) Bryant, M. W.; Smith, R. A. J.; Wong, L. –Alkyne Formation in the Reaction of α -Bromo Ketones with Arylsulfonylhydrazines" *Aust. J. Chem.*, **1982**, *35*, 2529-2540; (b) King, L. C.; Strum, G. K. –Selective Bromination with Copper(II) Bromide" *J. Org. Chem.*, **1964**, *29*, 3459-3461; (c) Keith, J. M.; Leslie, A. G.; Barbier, A. J.; Wilson, S. J.; Boggs, J. D.; Lord, B.; Mazur, C.; Aluisio, L.; Lovenberg, T. W.; Carruthers, N. I. –Pyrrolidino-tetrahydroisoquinolines Bearing Pendant Heterocycles as Potent Dual H3 Antagonist and Serotonin Transporter Inhibitors" *Bioorg. Med. Chem. Lett.*, **2007**, *17*, 4374-4377; (d) Giraud, F.; Logé, C.; Pagniez, F.; Crepin, D.; Le Pape, P.; Le Borgne, M. –Design, synthesis, and evaluation of 1-(N-benzylamino)-2-phenyl-3-(1H-1,2,4-triazol-1-yl)propan-2-ols as antifungal agents" *Bioorg. Med. Chem. Lett.*, **2008**, *18*(6), 1820-1824.
- [244] Macrae, C. F.; Bruno, I. J.; Chisholm, J. A.; Edgington, P. R.; McCabe, P.; Pidcock, E.; Rodriguez-Monge, L.; Taylor, R.; van de Streek, J.; Wood, P. A. –Mercury CSD2.0-New features for the visualization and investigation of crystal structures" *J. Appl. Crystallogr.*, **2008**, *41*, 466-470.
- [245] Garfinkle, J.; Ezzili, C.; Rayl, T. J.; Hochstatter, D. G.; Hwang, I.; Boger, D. L. –Optimization of the central heterocycle of α -ketoheterocycle inhibitors of fatty acid amide hydrolase" *J. Med. Chem.*, **2008**, *51*, 4392-4303.
- [246] (a) Kam, C. M.; Kerrigan, J. E.; Dolman, K. M.; Goldschmeding, R.; Von dem Borne, A. E.; Powers, J. C. –Substrate and inhibitor studies on proteinase 3" *FEBS* **1992**, *297*, 119-123. (b) Dolman, K. M.; van de Wiel, B. A.; Kam, C. M.; Kerrigan, J. E.; Hack, C. E.; von dem Borne, A. E.; Powers, J. C.; Goldschmeding R. –Proteinase 3: substrate specificity

- and possible pathogenetic effect of Wegener's granulomatosis autoantibodies (c-ANCA) by dysregulation of the enzyme" *Adv. Exp. Med. Biol.*, **1993**, 336, 55-60.
- [247] Jain, A. N. –Surflex: fully automatic flexible molecular docking using a molecular similarity-based search engine" *J. Med. Chem.*, 2003, 46, 499.
- [248] APEX2 User Manual, Bruker AXS, Madison (USA), 2005.
- [249] SAINT Software Reference Manual, Version 4, Bruker AXS, Madison (USA), 1994-1996.
- [250] Sheldrick, G., SADABS (Version 2.03), University of Göttingen, Germany, 2002.
- [251] SHELXTL, Reference Manual, Version 5.1, Bruker AXS, Madison (USA), 1997.
- [252] Zhong, J.; Groutas, W. C. –Recent developments in the design of mechanism-based and alternate substrate inhibitors of serine proteases" *Curr. Top. Med. Chem.*, **2004**, 4, 1203-1216.
- [253] The crystal structure shows disorder in one of the benzene rings. An alternate position for C(25), C(26), and C(27) was modeled with 47% occupancy. The majority component is shown in Figure 5.4. CCDC 683843 contains the supplementary crystallographic data for this structure. These data can be obtained free of charge from the Cambridge Crystallographic Data Centre via www.ccdc.cam.ac.uk/data_request/cif.
- [254] The same ion was observed as the parent ion in the ESI-MS of compound C7.
- [255] De Lucchi, O.; Miotti, U.; Modena, G. –Organic Reactions" **1991**, 40, pp 157-405.
- [256] Dilworth, B. M.; McKerverey, M. A. –Organic synthesis with α -chlorosulfides" *Tetrahedron*, **1986**, 42, 3731-3752.
- [257] Hein, G. E.; Niemann, C. –Steric Course and Specificity of alpha-Chymotrypsin-catalyzed Reactions. I" *J. Am. Chem. Soc.*, **1962**, 84, 4487-4494.
- [258] Zakharkin, L. I.; Khorlina, I. M. –Reduction of esters of carboxylic acids into aldehydes with diisobutylaluminum hydride" *Tetrahedron Lett.*, **1962**, 3, 619-620.
- [259] Chandrasekhar, S.; Kumar, M. S.; Muralidhar, B. –One Pot Conversion of Carboxylic Acids to Aldehydes with DIBAL-H" *Tetrahedron Lett.*, **1998**, 39(8), 909-910.
- [260] Cha, J. S.; Kwon, S. S. –Manganese (III)-Based Oxidative Free Radical Cyclizations. 5. Termination of Polycyclization by Oxidative β -HydrideE limination" *J. Org. Chem.*, **1987**, 52, 5487-5489.
- [261] Mancuso, A. J.; Huang, S-L.; Swern, D. –Oxidation of Long-chain and Related Alcohols

- to Carbonyls by Dimethyl Sulfoxide –Activated” by Oxalyl Chloride” *J. Org. Chem.*, **1978**, *43*, 2480-2482.
- [262] Boger, D. L.; Miyauchi, H.; Du, W.; Hardouin, C.; Fecik, R. A.; Cheng, H.; Hwang, I.; Hedrick, M. P.; Leung, D.; Acevedo, O.; Guimaraes, C. R. W. Jorgensen, W. L.; Cravatt, B. F. –Discovery of a potent, selective, and efficacious class of reversible alpha-ketoheterocycle inhibitors of fatty acid amide hydrolase effective as analgesics” *J. Med. Chem.*, **2005**, *48*, 1849-1856.
- [263] (a) Li, Y.; Yang, Q.; Dou, D.; Alliston, K. R.; Groutas, W. C. –Inactivation of human neutrophil elastase by 1,2,5-thiadiazolidin-3-one 1,1 dioxido-based sulfonamides” *Bioorg. Med. Chem.*, **2008**, *16*, 692-698; (b) Lai, Z.; Gan, X.; Wei, L.; Alliston, K. R.; Yu, H.; Li, Y. H.; Groutas, W. C. –Potent inhibition of human leukocyte elastase by 1,2,5-thiadiazolidin-3-one 1,1 dioxido-based sulfonamide derivatives” *Arch. Biochem. Biophys.*, **2004**, *429*, 191-197; (c) Zhong, J.; Gan, X.; Alliston, K. R.; Lai, Z.; Yu, H.; Groutas, C. S.; Wong, T.; Groutas, W. C. –Potential protease inhibitors based on a functionalized cyclic sulfamide scaffold” *J. Comb. Chem.*, **2004**, *6*, 556-563; (d) Kuang, R.; Epp, J. B.; Ruan, S.; Yu, H.; Huang P.; He, S.; Tu, J.; Schechter, N. M.; Turbov, J.; Froleich, C. J.; Groutas, W. C. –A General Inhibitor Scaffold for Serine Proteases with a (Chymo)trypsin-Like Fold: Solution-Phase Construction and Evaluation of the First Series of Libraries of Mechanism-Based Inhibitors” *J. Am. Chem. Soc.*, **1999**, *121*, 8128-8129.
- [264] Yusof, R. S.; Clum, M.; Wetzel, H.; Murthy, M.; Padmanabhan, R. –Purified NS2B/NS3 Serine Protease of Dengue Virus Type 2 Exhibits Cofactor NS2B Dependence for Cleavage of Substrates with Dibasic Amino Acids in Vitro” *J. Biol. Chem.*, **2000**, *265*, 9963-9969.
- [265] Mueller, N. H.; Yon, C.; Ganesh, V. K.; Padmanabhan, R. –Characterization of the West Nile virus protease substrate specificity and inhibitors” *Int. J. Biochem. Cell Biol.*, **2007**, *39*, 606-614.